Investigating mechanisms of TDP-43 toxicity in cellular models of amyotrophic lateral sclerosis



Emily Carroll

Magdalen College

Nuffield Department of Clinical Neurosciences

University of Oxford

Supervised by Professor Kevin Talbot

Submitted for the degree of *Doctor of Philosophy*

August 2022

Abstract

Amyotrophic lateral sclerosis (ALS) is a fatal, neurodegenerative disorder for which there is currently no cure. TDP-43 cytoplasmic mislocalisation and aggregation are the pathological hallmarks of the disease, and mutations in the gene encoding TDP-43, *TARDBP*, have been observed in a small number of ALS cases. Given this, it is hoped that modelling *TARDBP* mutations may provide early mechanistic insight into the disease process. Here, I examine the effects of the pathogenic TDP-43^{M337V} mutation on cellular phenotypes in an mESC-MN model of ALS. In TDP-43^{M337V} mESC-MNs, I observed reduced viability, both in unstressed and oxidative stressed conditions, and impaired stress granule formation in response to oxidative stress compared to TDP-43^{WT} controls. Interestingly, these changes were observed without evidence of TDP-43 cytoplasmic mislocalisation in TDP-43^{M337V} mESC-MNs when compared to TDP-43^{WT} controls. Increasing culture duration did not significantly alter synaptic protein expression or exacerbate phenotypes observed at earlier time points. Analysis of cellular energy metabolism revealed significantly reduced glycolysis in TDP-43^{M337V} mESC-MNs compared to TDP-43^{WT} controls in response to oxidative stress. Following oxidative stress, treatment with terazosin, which has previously been shown to significantly improve viability in our TDP-43^{M337V} mESC-MNs, significantly increased glycolysis whilst reducing mitochondrial respiration in TDP-43^{M337V} mESC-MNs. Finally, analysis of axonal transport in unstressed conditions using live imaging microscopy, revealed significantly impaired bi-directional transport of mitochondria and signalling endosomes in TDP-43^{M337V} mESC-MNs compared to TDP-43^{WT} controls. Overall, this work identifies relevant, ALS-associated phenotypes in the TDP-43^{M337V} mESC-MN model, which provides a valuable high-throughput system for investigating disease mechanisms and screening potential therapeutic compounds.

Effects of Covid-19 pandemic

Due to the Covid-19 pandemic the department was closed for 4 months in 2019, from the end of March until the end of July, preventing the continuation of experiments during this period.

Declaration

This thesis is the result of entirely my own work except where otherwise indicated. It has not been submitted, either partially or in full, for any other qualification at this University or any other institution. I have clearly indicated the presence of all material arising from other sources, including any diagrams, charts, tables or graphs. I have acknowledged appropriately any assistance I have received in addition to that provided by my supervisors. This thesis does not exceed the prescribed word limit as indicated by the relevant Degree Committee.

Acknowledgements

First and foremost, I would like express my sincere gratitude to Professor Kevin Talbot for his support over the last 4 years. I've thoroughly enjoyed being a member of the Talbot group, which has given me the opportunity to work at the forefront of ALS research and attend and present at national and international conferences. I'd also like to thank the Oxford-MRC Doctoral Training Partnership for funding this work, and the Oxford Neuroscience 4-year DTP organising committee for offering me a place on the programme.

I'm extremely grateful to my secondary supervisors, Dr David Gordon and Dr Ana Candalija, for their help and guidance throughout the DPhil. I was able to work on the mESC-MN model thanks to David, who established the mESC-MN differentiation protocol in our group and kindly shared his expertise with me. And thanks to Ana, who went above and beyond when she continued to hold remote meetings with me, despite leaving the lab and moving back to Spain. Special thanks must also go to Dr Jakub Scaber for his support and insight, particularly over the last year. By sharing his axonal transport analysis script, Jakub has saved me countless hours of troubleshooting and laborious analysis. Thanks also to Dr Ruxandra Dafinca, for her time and patience when teaching me how to use the Seahorse XF Analyzer. Thanks to my fellow DPhil students, especially Björn, Yan and Lucy from the Talbot group and Antigoni from the Tofaris group. Your friendship has immensely enriched my experience in the lab and I couldn't have asked for better colleagues to work alongside.

Outside of the lab, I'm grateful to everyone that has made my time at Oxford so memorable. I made some great friendships through my college, Magdalen, which will forever remain a special place for me. Through the universities cross-country (OUCCC), athletics (OUAC) and

triathlon (OUTriC) clubs, I met some lovely and inspiring people, whom I thoroughly enjoyed training and competing alongside and which provided a welcome distraction from ‘my cells’. Finally, I’d like to dedicate this thesis to my parents, Peter and Jane, and my sister, Annie, who have been a source of unwavering support and encouragement over the years.

Publications arising from this work

H. Chaytow, **E. Carroll**, D. Gordon, Y.T. Huang, D. van der Hoorn, T. Becker, C.G. Becker, K.M.E. Faller, K. Talbot, T.H. Gillingwater. (2022). "Repurposing a PGK1-targeting therapy to protect motor neurons in ALS". *EBioMedicine*, 104202. DOI: http://doi.org/10.1016/j.ebiom.2022.104202.

R. Dafinca, C.T. Bitrian, **E. Carroll**, J. Scaber, M. Labow, K. Talbot. "TDP-43 mutations cause disruption in retrograde axonal transport and mitochondrial bioenergetics". (Manuscript in preparation).

Table of contents

Abstract *2*

Effects of Covid-19 pandemic *3*

Declaration *4*

Acknowledgements *5*

Publications arising from this work *7*

Table of contents *8*

List of Figures *14*

List of Tables *17*

Abbreviations *18*

CHAPTER 1 Introduction **21**

1.1. Amyotrophic lateral sclerosis (ALS) 21

1.1.1. ALS is primarily a disorder of the motor system that lies on a spectrum with frontotemporal dementia 21

1.1.2. ALS is incurable 22

1.1.3. Epidemiology and prevalence of ALS 25

1.2. Aetiology of ALS 26

1.2.1. ALS results from degeneration and loss of motor neurons 26

1.2.2. Cytoplasmic inclusions are the pathological hallmark of ALS/FTD 27

1.2.3. Genetic aetiology 29

1.2.4. The role of oxidative stress in ALS pathogenesis 33

1.2.5. Multi-step hypothesis of ALS 35

1.3. TDP-43 in ALS 37

1.3.1. TDP-43 structure 37

1.3.2. Physiological functions of TDP-43 38

1.3.3. Evidence of TDP-43 pathogenicity in ALS 40

1.3.3.1. TDP-43 mislocalisation and aggregation 40

1.3.3.2. TARDBP mutations 42

1.3.3.3. Post-translational modifications 42

1.3.3.4. TDP-43 cleavage and C-terminal fragments 43

1.4. TDP-43 and the pathophysiology of ALS 44

1.4.1. Altered RNA splicing, cryptic exon inclusion and disrupted TDP-43 autoregulation 45

1.4.2. Altered stress granule dynamics 46

1.4.3. Mitochondrial dysfunction 48

1.4.4. Disruption of the axonal transcriptome, growth and transport 49

1.4.5. Disrupted protein-protein interactions 51

1.5. Approaches for studying TDP-43 pathogenicity in ALS 52

1.5.1. Mouse models 52

1.5.1.1. TDP-43 depletion 52

1.5.1.2. Overexpression of wild-type and mutant TDP-43 53

1.5.1.3. Physiologically relevant expression models 56

1.5.2. Stem cell models of *TARDBP* mutations 58

1.5.2.1. mESC-MN models 58

1.5.2.2. iPSC-MNs 60

1.6. Aims 61

CHAPTER 2 Methods 63

2.1. An *in vitro* model for studying the TDP-43^{M337V} mutation 63

2.1.1. Transgenic model for studying the effects of the TDP-43^{M337V} mutation 63

2.1.2. Differentiation of mESCs to motor neurons 63

2.2. Analysis of protein expression 65

2.2.1. Protein extraction 65

2.2.2. Mitochondrial isolation 65

2.2.3. Western blotting 66

2.2.4. Immunofluorescence 68

2.3. Analysis of mRNA expression 69

2.3.1. RNA extraction 69

2.3.2. cDNA preparation 70

2.3.3. Quantitative reverse transcription PCR 71

2.4. Network analysis 72

2.4.1. RNA sequencing 72

2.4.2. Analysis of TDP-43 interactome data 72

2.5. Live Cell Assays 73

2.5.1. MTS Assay 73

2.5.2. Seahorse XF Extracellular Flux Assays 73

2.5.3. CyQuant® Cell Proliferation Assay 76

2.6. Microscopy 77

2.6.1. Confocal microscopy of fixed samples 77

2.6.2. Live cell microscopy 78

2.7. Statistical analysis 79

CHAPTER 3 Investigating the effects of increased culture duration on cellular phenotypes in mESC-MNs 81

3.1. Introduction and aims 81

3.1.1. A physiologically relevant model for studying the effects of TDP-43 mutations 81

3.1.2. Unmasking of phenotypes in cellular models with ageing 82

3.1.3. Aims 83

3.2. Results 84

3.2.1. mESCs differentiate to motor neurons and express the exogenous *TARDBP* BAC construct 84

3.2.2. Increasing culture duration does not significantly increase the expression of synaptic markers in mESC-MNs 90

3.2.3. Investigating the effects of increasing culture duration on TDP-43 mislocalisation in mESC-MNs 93

3.2.4. Investigating the effects of increasing culture duration on stress granule formation in mESC-MNs 99

3.2.5. Investigating co-localisation of TDP-43 and stress granules in mESC-MNs 102

3.2.6. Investigating the effects of increasing culture duration on cellular viability in mESC-MNs 106

3.3. Conclusions 109

CHAPTER 4 Investigating the effects of the TDP-43^{M337V} mutation on cellular energy metabolism in mESC-MNs 115

4.1. Introduction and aims 115

4.1.1. An overview of energy production within the CNS 115

4.1.2. Systemic and cellular metabolic dysregulation is a feature of ALS 118

4.1.3. Aims 119
4.2. Results 122
4.2.1. Altered expression of glycolytic enzymes and mitochondrial proteins in mice, iPSC-MNs and mESC-MNs expressing TDP-43^{M337V} 122
4.2.2. TDP-43^{M337V} and oxidative stress alter interactions with glycolytic and mitochondrial proteins in mESC-MNs 129
4.2.3. Basal and compensatory glycolysis are significantly reduced in TDP-43^{M337V} mESC-MNs following oxidative stress 134
4.2.4. Analysis of mitochondrial bioenergetics in mESC-MNs: mitochondrial membrane potential, oxidative phosphorylation and the effects of terazosin 140
4.3. Conclusions 147
CHAPTER 5 Investigating the effects of the TDP-43^{M337V} mutation on axonal transport in mESC-motor neurons 154
5.1. Introduction and aims 154
5.1.1. TDP-43 and impaired axonal transport in ALS 154
5.1.2. Aims 156
5.2. Results 157
5.2.1. TDP-43^{M337V} mESC-MNs show significant impairments to bi-directional mitochondrial transport 157
5.2.2. TDP-43^{M337V} mESC-MNs show a significant reduction in retrograde signalling 164
5.2.3. TDP-43^{M337V} iPSC-MNs show dysregulated expression of transcripts relating to anterograde and retrograde transport 169
5.2.4. Expression of motor protein subunits is not significantly altered in TDP-43^{M337V} mESC-MNs 174

5.3. Conclusions 176

CHAPTER 6 Conclusions 182

6.1. Summary of thesis findings 182

6.2. Relevant models provide insight into TDP-43 pathogenicity in ALS 184

6.3. The role of TDP-43 mislocalisation and aggregation in ALS pathogenesis 186

6.4. Selective vulnerability of motor neurons in ALS 187

6.5. The heterogeneity of ALS creates challenges in diagnosis and treatment 189

6.6. Drug repurposing in ALS 190

6.7. Closing remarks 192

REFERENCES ***193***

List of Figures

Figure 1.1 TDP-43 pathological inclusions in spinal motor neurons from ALS patients (Ansorge et al., 2009)..... 28

Figure 1.2: ALS pathology (adapted from Ling et al., 2013)..... 29

Figure 1.3 Genetics of ALS (adapted from Renton et al., 2014)..... 33

Figure 1.4 The pathophysiology of ALS..... 36

Figure 1.5 TDP-43 protein structure (from Prasad et al., 2019)..... 38

Figure 2.1 Stress granule quantification and co-localisation analysis in FIJI/ImageJ..... 78

Figure 3.1 Differentiation of mESCs to form motor neurons. 85

Figure 3.2 Expression of motor neuron markers in mESC-MNs. 86

Figure 3.3 mESC-MNs express exogenous human TDP-43 and endogenous mouse TDP-43. 88

Figure 3.4 TDP-43 expression in mESC-MNs..... 89

Figure 3.5 mESC-MNs express synaptic markers in vitro..... 92

Figure 3.6 mESC-MNs do not demonstrate TDP-43 mislocalisation. 95

Figure 3.7 mESC-MNs do not demonstrate GFP-TDP-43 mislocalisation. 98

Figure 3.8 Increasing culture duration leads to reduced stress granule size in mESC-MNs. 101

Figure 3.9 TDP-43 co-localisation with stress granules DIV 3..... 104

Figure 3.10 TDP-43 co-localisation with stress granules DIV 9..... 105

Figure 3.11 TDP-43^{M337V} mESC-MNs demonstrate impaired viability relative to TDP-43^{WT} motor neurons..... 108

Figure 4.1 Pathways of ATP production. 117

Figure 4.2 Upregulation of glycolysis may be neuroprotective in ALS (by Dr Helena Chaytow and Dr David Gordon) 121

Figure 4.3 Increased expression of glycolytic enzymes in iPSC-MNs carrying the TDP-43^{M337V} pathogenic mutation. 124

Figure 4.4 Dysregulated expression of mitochondrial proteins by the TDP-43^{M337V} mutation in iPSC-MNs. 125

Figure 4.5 Expression of glycolytic enzymes in mESC-MNs. 127

Figure 4.6 Increased expression of COX5A in TDP-43^{M337V} mESC-MNs. 128

Figure 4.7 TDP-43^{M337V} interactome reveals dysregulated interaction with electron transport chain components. 131

Figure 4.8 Co-localisation of ATPB and TDP-43 in TDP-43^{M337V} mESC-MNs. 133

Figure 4.9 Mitochondrial fractionation in TDP-43^{WT} and TDP-43^{M337V} mESC-MNs. 134

Figure 4.10 Seahorse Glycolytic Rate Assay (Adapted from Agilent). 136

Figure 4.11 The TDP-43^{M337V} mutation does not significantly alter glycolysis in unstressed conditions. 138

Figure 4.12 The TDP-43^{M337V} mutation significantly impairs glycolysis following oxidative stress, which is rescued by terazosin treatment. 139

Figure 4.13 MitoTracker intensity is significantly increased in TDP-43^{M337V} mESC-MNs relative to controls in unstressed conditions 141

..... 144

Figure 4.14 Seahorse Mito Stress Test (adapted from Agilent). 144

Figure 4.15 The TDP-43^{M337V} mutation does not significantly alter mitochondrial respiration in unstressed conditions. 145

Figure 4.16 The TDP-43^{M337V} mutation significantly impairs spare respiratory capacity following oxidative stress and treatment with terazosin significantly reduces mitochondrial respiration. 146

Figure 5.1 Analysis of axonal transport in mESC-MNs using microfluidic chambers. 158

Figure 5.2 Processes extending through channels stain for axonal markers. 159

Figure 5.3 Mitochondria move bi-directionally in mESC-MNs. 161

Figure 5.4 Anterograde mitochondrial transport in mESC-MNs. 162

Figure 5.5 Retrograde mitochondrial transport in mESC-MNs. 163

Figure 5.6 Bi-directional of CTB in mESC-MNs. 166

Figure 5.7 CTB retrograde transport is reduced in TDP-43^{M337V} mESC-MNs. 167

Figure 5.8 CTB anterograde transport is reduced in TDP-43^{M337V} mESC-MNs. 168

Figure 5.9 TDP-43^{M337V} mouse shows dysregulated expression of transcripts relating to retrograde transport but not anterograde transport compared to TDP-43^{WT} controls. 171

Figure 5.10 TDP-43^{M337V} iPSC-MNs show dysregulated expression of transcripts relating to anterograde transport. 172

Figure 5.11 TDP-43^{M337V} iPSC-MNs show dysregulated expression of transcripts relating to retrograde transport. 173

Figure 5.12 Expression of axonal transport components in mESC-MNs carrying the TDP-43^{M337V} mutation. 175

Figure 6.1 Summary of thesis findings. 183

List of Tables

Table 1.1 Genes associated with ALS (adapted from Mejzini et al., 2019). 30

Table 2.1 mESC media composition. 64

Table 2.2 ADFNK media composition. 65

Table 2.3 Primary antibodies used for immunoblotting and immunocytochemistry. 67

Table 2.4 Preparation of cDNA master mix. 70

Table 2.5 cDNA conversion protocol. 71

Table 2.6 Primers for qRT-PCR 71

Table 2.7 Mito Stress Test compound preparation. 75

Table 2.8 Glycolytic Rate Assay compound preparation 76

Abbreviations

ALS	Amyotrophic lateral sclerosis
ALSFRS	ALS functional rating scale
ATP	Adenosine triphosphate
ATPB	ATP synthase subunit B
BAC	Bacterial artificial chromosome
cDNA	Complimentary DNA
CE	Cryptic exon
ChAT	Choline Acetyltransferase
CNS	Central nervous system
COX5A	Cytochrome C oxidase subunit 5A
CSF	Cerebrospinal fluid
CTB	Cholera toxin subunit B
CTD	C-terminal domain
C9orf72	Chromosome 9 open reading frame 72
DIV	Days *in vitro*
DNA	Deoxyribonucleic acid
DPRs	Dipeptide repeat proteins
fALS	Familial ALS
FDA	Food and drug administration
FTD	Frontotemporal dementia
FUS	Fused in sarcoma
GFP	Green fluorescent protein
G3BP	Ras-GAP SH3 domain binding protein

HEK	Human embryonic kidney
HIV-1	Human immunodeficiency virus 1
iPSC-MN	Human induced pluripotent stem cell-derived motor neuron
kDa	Kilodalton
LMN	Lower motor neuron
MND	Motor neuron disease
M337V	Methionine-to-valine substitution at position 337
mESC-MN	Mouse embryonic stem cell-derived motor neuron
MN	Motor neuron
mRNA	Messenger RNA
miRNA	Micro RNA
$NaAsO_2$	Sodium arsenite
NES	Nuclear export signal
NLS	Nuclear localisation signal
NTg	Non-transgenic
PLS	Primary lateral sclerosis
PMA	Primary muscular atrophy
PMEFs	Primary mouse embryonic fibroblasts
PrP	Prion promoter
RA	Retinoic acid
RAN	Repeat-associated non-ATG
RNA	Ribonucleic acid
RNP	Ribonucleoprotein
ROS	Reactive oxygen species
RRM1 and 2	RNA recognition motifs 1 and 2

SAG	Smoothened agonist
sALS	Sporadic ALS
SOD1	Superoxide dismutase 1
TDP-43	TAR DNA binding protein 43
UMN	Upper motor neuron
WB	Western immunoblot
WT	Wild-type
YPet	Yellow fluorescent protein

CHAPTER 1 Introduction

1.1. Amyotrophic lateral sclerosis (ALS)

1.1.1. ALS is primarily a disorder of the motor system that lies on a spectrum with frontotemporal dementia

First described by Jean Martin Charcot in 1869, amyotrophic lateral sclerosis (ALS) is the most common form of adult-onset motor neuron disease (MND). ALS derives its name from the Greek 'amyotrophia', meaning lacking muscle nourishment, and 'skleros' which refers to sclerosis of the lateral columns of the spinal cord. Named after its distinctive neuropathology, ALS results from the degeneration of motor neurons in the motor cortex and spinal cord leading to spasticity, muscle denervation, muscle atrophy and progressive paralysis (McDermott & Shaw, 2008).

Clinical diagnosis of ALS is based on the observation of painless, progressive loss of function with evidence of upper motor neuron (UMN) and lower motor neuron (LMN) dysfunction. Symptoms typically start focally before spreading to other regions and causing more wide-spread symptoms. ALS is a clinically heterogeneous disorder, with significant variability in the presence of UMN and LMN signs observed between individuals. Whilst the majority of patients experience both UMN and LMN dysfunction, rarer forms of purely UMN involvement or LMN involvement are observed and classified as primary lateral sclerosis (PLS) and primary muscular atrophy (PMA) respectively (Grad et al., 2017). Patients with limb onset disease, which accounts for approximately ~70% of patients, typically present with cramping and

muscle stiffness followed by muscle weakness affecting the arms and legs. Approximately ~25% of patients present with bulbar onset disease, where initial symptoms include slow and slurred speech (dysarthria) and difficulty in chewing or swallowing (dysphagia) (Caroscio et al., 1987; Mitchell & Borasio, 2007). Respiratory onset disease is uncommon (<3% of cases) and shows male predominance, with symptoms including camptocormia or dropped head, persistent and widespread fasciculations and significant weight loss whilst limb mobility is generally well preserved (Gautier et al., 2010).

It is becoming increasingly evident that ALS is not solely a disorder of the motor system. Neuropsychological testing reveals that approximately 50% of ALS patients suffer from some form of cognitive impairment. These deficits most frequently affect behaviour and executive function, however deficits in language such as reduced verbal fluency have also been reported (Abrahams et al., 2000; Goldstein & Abrahams, 2013). The degree of cognitive decline is highly variable, with the majority of patients developing symptoms too mild to reach the threshold for clinical diagnosis. However, 10-15% of patients develop severe cognitive changes consistent with formal diagnostic criteria for frontotemporal dementia (FTD) (Goldstein & Abrahams, 2013). Furthermore, motor deficits associated with ALS have been well described in some FTD patients (Lomen-Hoerth et al., 2002; Mitsuyama & Takamiya, 1979). These observations demonstrate that dysregulation in ALS may extend beyond the corticomotorneuronal network to encompass additional brain regions.

1.1.2. ALS is incurable

ALS is a fatal disease for which there is currently no cure. While a small percentage of patients have slow progressing disease and survive for 10 years or more, the median survival time is 20 months from diagnosis or 30 months from symptom onset (Westeneng et al., 2018). Prediction

of individual prognosis is challenging and often based on a complex set of factors including clinical presentation and genetics. Bulbar onset disease, a short diagnostic delay, rapid functional decline, significant weight loss, co-occurrence with FTD and older age at symptom onset are all associated with shorter survival (Ferguson & Elman, 2007; Gordon et al., 2013). Tracheostomy can be performed to support breathing and consequently extend survival, but pharmacological interventions that meaningfully halt or slow disease progression remain elusive (Vianello et al., 2011).

In 1996, riluzole became the first approved treatment for ALS and remains the principal treatment offered to patients. Riluzole is a neuroprotective agent that blocks glutamatergic neurotransmission, thereby reducing excitotoxicity in the CNS. In double-blind placebo-controlled clinical trials, treatment with riluzole was found to improve survival by 2-6 months and/or delay time until tracheostomy or mechanical ventilation interventions (Bensimon et al., 1994; Lacomblez et al., 1996; Miller et al., 2012). A later retrospective study has provided further support for riluzole, whereby treatment was shown to slow the progression of disease compared to untreated controls (Riviere et al., 1998). Riluzole is thought to exert its disease modifying and pro-survival effects in the advanced stages of the disease (stage 4) (Fang et al., 2018). However, the mechanisms through which riluzole exerts its neuroprotective effects remain unclear, as other glutamate antagonists (lamotrigine and dextromethorphan) did not demonstrate efficacy in clinical trials (Gredal et al., 1997; Ryberg et al., 2003). Moreover, questions remain about the efficacy of riluzole and its cost-effectiveness as a therapeutic, given its marginal benefits and high cost (Messori et al., 1999).

After the approval of riluzole it was almost 20 years until edaravone, branded as ‘Radicava’, received FDA approval for the treatment of ALS in Japan in 2015, and later in the United States

in 2017 (Cruz, 2018). Edaravone is a free radical scavenger that is theorized to decrease the effects of oxidative stress. In a preliminary open-label trial involving 20 patients, six months of edaravone treatment was found to significantly reduce functional decline in patients compared to that observed over the preceding six months. In the majority of patients, this was accompanied by a reduction in CSF levels of the oxidative stress marker 3-nitrotyrosine (Yoshino & Kimura, 2006). However, in a later large-scale trial involving 206 patients, treatment with edaravone for 24 weeks did not significantly alter ALSFRS score compared with placebo treatment (Abe et al., 2014). This was further supported by a later small-scale trial, whereby edaravone treatment did not significantly alter ALSFRS score in patients with more advanced disease (Writing Group On Behalf Of The Edaravone Als 18 Study, 2017). Yet, subsequent post-hoc analysis of the large-scale trial revealed reduced decline in specific subsets of patients, presenting with shorter disease duration and milder symptoms (Takahashi et al., 2017). Based on these observations, a further Phase 3 trial with 137 patients was conducted with strict inclusion criteria, designed to select only those patients most likely to benefit from edaravone. A slowed decline in ALSFRS score was observed in those treated with edaravone compared with placebo controls (Writing & Edaravone, 2017). This slowed decline was maintained at 48 weeks in the 123 patients who completed the open-label extended treatment period of the trial (Shefner et al., 2020). However, approval for edaravone in Europe was declined by the European Medicines Agency in 2019, on the basis of insufficient evidence of long-term efficacy and a lack of confidence that the benefits of edaravone observed in Japanese cohorts would be translated across broader European patient populations (EMA review document (CHMP/290284/2019)). Two studies have since reported the long-term effects of edaravone, in retrospective studies of a small number of patients, which suggest slower progression and improved prognosis following treatment (Houzen et al., 2021; Okada et al., 2018). Yet, in the most recent study, intravenous treatment with edaravone plus riluzole

provided no additional disease-modifying benefits compared with riluzole treatment alone (Witzel et al., 2022).

Given remaining questions surrounding the clinical utility of riluzole and edaravone, the search for more efficacious treatments that meaningfully alter the course of the disease is on-going. Progress in identifying novel compounds for the treatment of ALS has been slow and success at clinical trials limited. The reasons for this are multi-fold and are due, for the most part, to the complex and multi-faceted nature of ALS as a disease. The diverse clinical presentation of ALS makes diagnosis difficult and coupled with prognostic, pathological and genetic heterogeneity it has been argued that characterising ALS as one disease is over simplistic (Turner, Hardiman, et al., 2013). The lack of effective biomarkers that are specific to ALS also poses a challenge, as these could be used to aid diagnosis, patient stratification into various sub-groups for clinical trials and the early provision of treatment (Turner, Bowser, et al., 2013; Verber et al., 2019). Finally, the complex pathophysiological mechanisms that underlie the disease are still not well understood, in part due to the lack of effective cellular and animal models to study disease processes (Katyal & Govindarajan, 2017). To improve success of drug discovery in ALS, a greater understanding of the pathophysiology of ALS, the temporal order of events and development of effective biomarkers will be critical.

1.1.3. Epidemiology and prevalence of ALS

ALS is a rare disorder, with a global incidence between 0.6 and 3.8 per 100 000 person-years (Benjaminsen et al., 2018; Jun et al., 2019; Leighton et al., 2019; Longinetti et al., 2018; Palese et al., 2019; Turgut et al., 2019; Zhou et al., 2018). A slightly higher incidence of ALS is observed in Europe, ranging from 2.1 to 3.8 per 100 000 person-years (Benjaminsen et al., 2018; Leighton et al., 2019; Longinetti et al., 2018; Palese et al., 2019; Rose et al., 2019). A

comparatively lower incidence has been observed in Asia, where the incidence was reported as 0.8 and 1.2 per 100 000 person-years in South Korea and China respectively (Jun et al., 2019; Zhou et al., 2018). The prevalence of ALS has been reported in recent population-based studies as between 4.1 and 8.4 per 100 000 persons (Benjaminsen et al., 2018; Leighton et al., 2019; Longinetti et al., 2018; Palese et al., 2019; Rose et al., 2019). Increases in ALS incidence and prevalence have been reported in Europe and the United States (Leighton et al., 2019; Mehta et al., 2018; Nelson et al., 2018). Most strikingly, a 36% increase in ALS incidence was reported over a 25-year period in Scotland, which was attributed to better ascertainment of neurological services across Scotland (Leighton et al., 2019). Irrespective of the cause, observations of increasing ALS incidence and prevalence underscore the need for greater allocation of resources into ALS research and patient care. ALS shows slighter greater male predominance, with the male-to-female ratio typically reported as between 1 and 2 (Benjaminsen et al., 2018; Ingre et al., 2015; Jun et al., 2019; Leighton et al., 2019; Palese et al., 2019; Turgut et al., 2019; Zhou et al., 2018). Although in one study, the male-to-female ratio was reported as high as 2.9 (Luna et al., 2019). The mean age of onset in Europe is 64 (Westeneng et al., 2018), with cases of familial ALS typically presenting with an earlier age of onset compared with sporadic forms of the disease (Camu et al., 1999; Juneja et al., 1997).

1.2. Aetiology of ALS

1.2.1. ALS results from degeneration and loss of motor neurons

Neuropathological analysis of post-mortem tissue has provided further insight into structural changes underlying motor system dysfunction in ALS. In the majority of ALS brains, no gross abnormalities are identified at the macroscopic level, however subtle changes are indicative of neurodegeneration. Atrophy of the anterior nerve roots of the spinal cord is often demonstrated,

as well as atrophy of the precentral gyrus in some patients (Ellison, 2012). In patients with co-morbid FTD, atrophy of the frontal and/or temporal cortex might be observed (Abrahams et al., 2005; Chang et al., 2005; Murphy et al., 2007). A reduction in white matter is also observed, most notably in the corticospinal tract (Kassubek et al., 2005; Roccatagliata et al., 2009). Analysis at the microscopic level, reveals degeneration and loss of large motor neurons in the anterior horn of the spinal cord and lower cranial motor nuclei in the brainstem (Nihei et al., 1993). Degeneration and loss of Betz cells, the large pyramidal neurons located in layer five of the primary motor cortex, is also observed (Hammer et al., 1979). Neuronal loss is accompanied by neuroinflammation, with large numbers of activated microglia and astrocytes observed in degenerating areas (McGeer & McGeer, 2002).

1.2.2. Cytoplasmic inclusions are the pathological hallmark of ALS/FTD

A key feature of degenerating neurons in ALS is the presence of intraneuronal cytoplasmic inclusions. These inclusions are of varying morphologies ranging from spherical Lewy body-like inclusions to skeins of thread-like structures. Ubiquitin-positive skein-like inclusions in the cytoplasm of anterior horn neurons were first identified through the work of Leigh *et al* and Lowe *et al* in the late 1980's (Leigh et al., 1988; Leigh et al., 1991; Lowe et al., 1988). Similar inclusions were later reported in cases of ALS with FTD (Okamoto et al., 1991; Okamoto et al., 1992; Wightman et al., 1992). In a landmark study, hyperphosphorylated forms of the protein TDP-43 (TAR DNA binding protein 43 kDa) were identified as a major component of these neuronal cytoplasmic inclusions (Neumann et al., 2006). The redistribution of TDP-43 from a predominantly nuclear location to form insoluble ubiquitinated aggregates in the cytoplasm has become a key neuropathological marker of ALS (Figure 1.1). Such inclusions are observed in motor neurons and glia of the brain and spinal cord in 97% of ALS cases (sporadic and familial) (Arai et al., 2006; Neumann et al., 2006). The exceptions to this are in

patients carrying FUS and SOD1 mutations, in which neuronal cytoplasmic inclusions consist predominantly of FUS and SOD1 proteins respectively (Kwiatkowski et al., 2009; Mackenzie et al., 2007; Vance et al., 2009). In addition to TDP-43 proteinopathy, C9ORF72-associated ALS is further characterised by RNA foci of G_4C_2 hexanucleotide repeats and sequestered RNA binding proteins, as well as cellular deposits of dipeptide-repeat proteins (DPRs) that form through repeat-associated non-ATG (RAN) translation (Ash et al., 2013; Haeusler et al., 2016; Mackenzie et al., 2014). Bunina bodies may also be present, which are small eosinophilic intraneuronal inclusions that were first described by Bunina in 1962 in two cases of familial ALS (Bunina, 1962). Pathological findings have further strengthened clinical observations linking ALS and FTD. ALS and FTD are both characterised as TDP-43 proteinopathies, as neuronal TDP-43 positive cytoplasmic inclusions are found in 97% and 45% of ALS and FTD cases respectively (Ling et al., 2013). Furthermore, neuronal cytoplasmic inclusions positive for the RNA binding protein fused in sarcoma (FUS) are found in ~1% of ALS and ~10% of FTD cases (Ling et al., 2013; Neumann et al., 2006) (Figure 1.2).

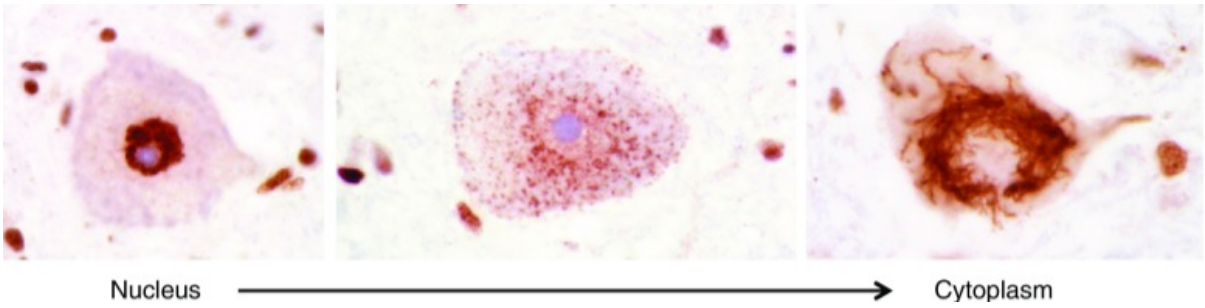


Figure 1.1 TDP-43 pathological inclusions in spinal motor neurons from ALS patients (Ansorge et al., 2009). TDP-43 mislocalises to the cytoplasm from its normally nuclear location and forms cytoplasmic aggregates.

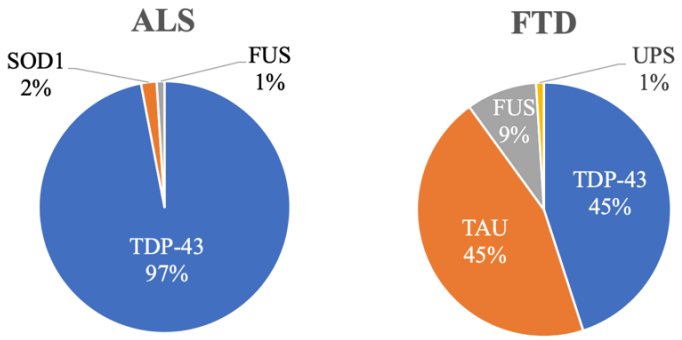


Figure 1.2: ALS pathology (adapted from Ling et al., 2013). Predominant protein species identified in pathological inclusions in ALS and FTD.

1.2.3. Genetic aetiology

The genetic profile of ALS is complex. The majority of ALS cases (90%) arise sporadically in the population without any known familial links (sALS), whereas the remaining 10% of cases are attributed to inherited genetic variants (fALS) (Renton et al., 2014). In 1993, mutations in the gene superoxide dismutase 1 (*SOD1*) were the first mutations found to cause fALS (Rosen et al., 1993). There was a long delay until the discovery of mutations in two other genes associated with ALS; TAR DNA binding protein (*TARDBP*), which encodes TDP-43, and fused in sarcoma (*FUS*) (Kwiatkowski et al., 2009; Sreedharan et al., 2008; Vance et al., 2009). These findings supported pathological observations, providing a direct link between ALS and disrupted SOD1, TDP-43 and FUS function. Since then, the pace of gene discovery has increased rapidly, aided significantly by advances in sequencing and genotyping technologies. To date, a number of mutations in more than 20 genes have been associated with ALS (Table 1.1).

It is clear that ALS is not a single gene disorder, yet some mutations are more prevalent in the population than others. Hexanucleotide (GGGGCC) repeat expansion in the gene *C9ORF72* was first described in 2011 (DeJesus-Hernandez et al., 2011; Renton et al., 2011). Present in

the non-coding region of the gene, this repeat expansion accounts for the largest percentage of ALS cases; ~40% of fALS and ~7% of sALS (Gromicho et al., 2018; Majounie et al., 2012). Mutations in *SOD1* are the second most common mutation in fALS patients, accounting for ~12% of cases but only accounting for ~1% of sporadic cases (Chio et al., 2008). Mutations in *TARDBP* and *FUS* genes each account for ~4-5% of fALS cases and ~1-2% of sALS (Chio et al., 2012; Kwiatkowski et al., 2009; Vance et al., 2009) (Figure 1.3). The remaining mutations currently known are much less prevalent in the population, accounting for <5% of fALS cases and a smaller percentage of sporadic disease (Renton et al., 2014).

Given the clinical and pathological overlap between ALS and FTD, it is perhaps not surprising that ALS and FTD also demonstrate a significant degree of genetic overlap. The most common mutation associated with familial and sporadic ALS, hexanucleotide repeat expansion of *C9ORF72,* also accounts for approximately ~25% of familial FTD. This genetic overlap can account for the majority of similarities observed clinically between these two seemingly distinct disorders (Majounie et al., 2012). However, hereditary studies have also identified links between mutations in ubiquilin 2 and ALS/ALS-FTD, showing a dominant, chromosome-X linked inheritance pattern (Deng et al., 2011).

Table 1.1 Genes associated with ALS (adapted from Mejzini et al., 2019).

Roles	Gene	Protein	Functions
RNA processing	TARDBP	TAR DNA- Binding Protein, 43 kDa	Splicing regulation, RNA transport, miRNA biogenesis
	FUS	Fused in sarcoma	Splicing regulation, RNA transport, maintenance of

			genomic integrity, miRNA processing
	ANG	Angiogenin	RNA processing, neurite outgrowth, vascularisation, stress granule formation
	ATXN2	Ataxin 2	RNA processing (interacts with TDP-43), endocytosis, modulates mTOR signalling
	hnRNPa1	Heterogeneous nuclear ribonucleoprotein A1	mRNA processing, splicing and transport
	hnRNPA2B1	Heterogeneous nuclear ribonucleoproteins A2/B1	mRNA processing, splicing and transport
Protein trafficking and degradation	C9ORF72	Guanine nucleotide exchange C9orf72	Transcription, splicing regulation, endosomal trafficking, autophagy
	VAPB	Vesicle-associated membrane protein-associated protein B/C	Vesicle trafficking
	UBQLN2	Ubiquilin-2	Protein degradation via the UPS
	SQSTM1	Sequestosome-1 (p62)	Protein degradation via the UPS and autophagy
	OPTN	Optineurin	Golgi maintenance, membrane trafficking autophagy
	TBK1	Tank Binding Kinase 1	Autophagy, innate immunity signalling
	VCP	Valosin Containing Protein	Protein degradation via UPS, autophagy, membrane fusion

Cytoskeleton and axonal dynamics	DCTN1	Dynactin subunit 1	Axonogenesis, microtubule anchoring, ER to Golgi transport, vesicle transport, cilia formation, spindle formation
	Profilin 1	Profilin 1	Cytoskeletal signalling, regulates actin polymerisation
	SPG11	Spatacsin	Cytoskeletal stability, regulating synaptic vesicle transport
	TUBA4A	Tubulin α-4A chain	Component of microtubules
	NEFH	Neurofilament heavy polypeptide	Maintenance of neuronal calibre, intracellular transport
	PRPH	Peripherin	Cytoskeletal protein, neurite elongation, axonal regeneration
	NEK1	NIMA (Never in Mitosis Gene A)-Related Kinase 1	Cilia formation, DNA-damage response, microtubule stability, neuronal morphology, axonal polarity
Mitochondria	CHCHD10	Coiled-Coil-Helix-Coiled-Coil-Helix Domain Containing 10	Mitochondrial protein, cristae morphology, oxidative phosphorylation
	C19ORF12	Protein C19orf12	Mitochondrial protein
Oxidative stress	SOD1	Superoxide dismutase 1 [Cu-Zn]	Cytosolic antioxidant

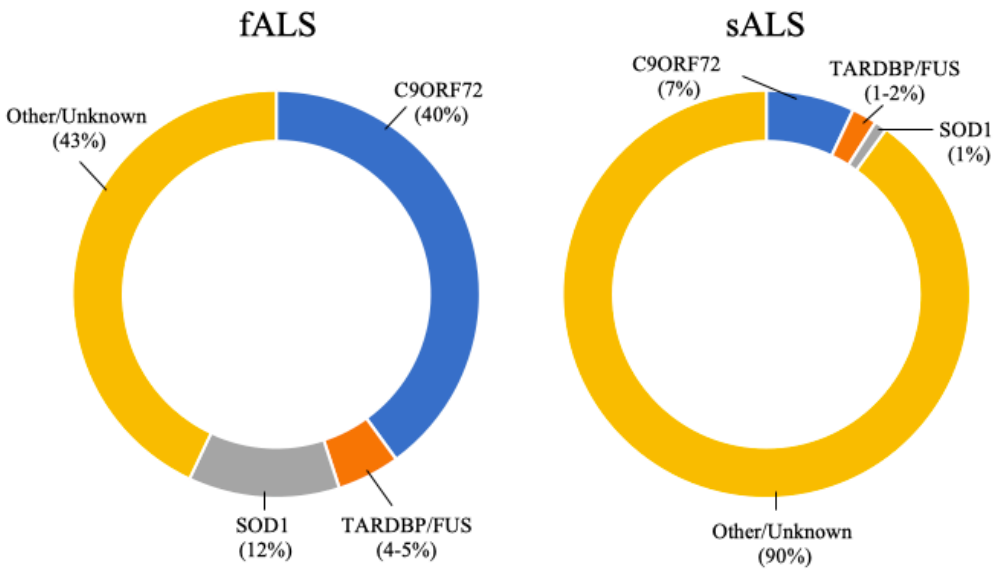


Figure 1.3 Genetics of ALS (adapted from Renton et al., 2014). Proportion of ALS explained by mutations in *C9ORF72*, *SOD1*, *TARDBP* and *FUS*.

1.2.4. The role of oxidative stress in ALS pathogenesis

Oxidative stress is one of the converging pathways for many neurodegenerative disorders including ALS. Yet whether oxidative stress is a direct cause of pathogenesis or merely a consequence of disease has been widely debated. Oxidative stress results from an imbalance in the production of reactive oxygen species (ROS) and the removal of these species by antioxidants (Barber & Shaw, 2010). Cellular ROS are formed as the by-product of aerobic metabolism and arise mostly due to the leakage of electrons from the mitochondrial respiratory chain. This leakage results in the incomplete reduction of oxygen during oxidative phosphorylation and leads to the production of superoxide radical anions and hydrogen peroxide (H_2O_2) (Coyle & Puttfarcken, 1993). Superoxide and H_2O_2 are themselves weak oxidants, but undergo further reactions to produce peroxynitrite and hydroxyl radicals respectively, which are highly reactive oxidising agents capable of inducing protein, lipid and DNA damage (Beckman et al., 1993; Pryor & Squadrito, 1995). Damage includes altering

protein conformation, disrupting cellular membrane dynamics and changes in DNA and RNA species (Barber & Shaw, 2010; Shaw et al., 1995).

The discovery of mutations in the gene encoding antioxidant SOD1, which accounts for ~20% of fALS cases, provide evidence for a mechanistic link between oxidative stress and ALS pathogenesis (Renton et al., 2014; Rosen et al., 1993). Studies in ALS post-mortem tissue have further implicated oxidative stress as a key pathophysiological mechanism in ALS. Protein carbonyl levels, a biomarker of oxidative stress, are elevated in the spinal cord and motor cortex of sporadic ALS patients (Ferrante et al., 1997; Shaw et al., 1995). Increased 3-nitrotyrosine levels, a marker for oxidative damage mediated by perioxynitrite, were reported in spinal cord motor neurons of SOD1-associated fALS and sALS patients (Abe et al., 1995; Beal et al., 1997). A transcriptomic study performed by Tam and colleagues in 2019, further supported these biological findings. The transcriptomes for 148 ALS post-mortem frontal cortex samples, including the motor cortex, were stratified using machine learning algorithms into distinct molecular subtypes. The largest cluster, identified in 61% of post-mortem samples, demonstrated elevated expression of genes associated with oxidative and proteotoxic stress compared to control samples (Tam et al., 2019). In addition to post-mortem analysis, which marks end stage disease, studies using patient CSF have implicated oxidative stress as a pathophysiological mechanism occurring earlier in disease. CSF samples from sALS and fALS (SOD1) patients have demonstrated elevated levels of 8-OHDg, an oxidized nucleoside of DNA and a marker of oxidative stress (Bogdanov et al., 2000; Ihara et al., 2005). Elevated levels of the lipid peroxidation marker, 4-hydroxynonenal, have also been reported in CSF samples from ALS patients (Simpson et al., 2004; Smith et al., 1998). Furthermore, increased levels of ascorbate free radicals, a further marker of oxidative stress resulting from the oxidation of ascorbate, have been detected in sALS and fALS patient CSF (Ihara et al., 2005).

In mouse models of ALS, preventing oxidative stress appears to alleviate TDP-43-ALS associated phenotypes. The neuronal over-expression of *Oxr1*, an oxidation resistance gene, was shown to prevent TDP-43^{M337V} mislocalisation in primary motor neurons, and improve neuromuscular defects and survival *in vivo* (Williamson et al., 2019). Collectively, these studies suggest that oxidative stress may play a central role in ALS pathogenesis.

1.2.5. Multi-step hypothesis of ALS

The pathophysiology of ALS is immensely complex, with multiple intrinsic and extrinsic factors thought to contribute to the onset and progression of neurodegeneration (Figure 1.4). Similar to cancer, ALS onset typically occurs later in life. Even in cases of fALS, individuals are capable of tolerating pathological mutations for 40-60 years before symptoms transpire (Camu et al., 1999; Juneja et al., 1997). The disease bears further similarities with cancer, given its rapid progression, selective targeting of a specific cell type and pleiotropy, whereby the same gene mutation can lead to different phenotypes between individuals (Al-Chalabi et al., 2014). For example, individuals carrying the *C9ORF72* hexanucleotide repeat expansion may remain unaffected throughout life or go on to develop ALS, FTD, joint ALS/FTD or in some cases neuropsychiatric disease (Byrne et al., 2013). Given these overlapping epidemiological features, the multi-stage theory, which was originally developed for cancer, has been proposed as a viable framework for ALS (Armitage & Doll, 1954). The multi-step hypothesis of ALS proposes that neurodegeneration arises as the result of multiple pathological 'hits'. One such 'hit' may be the presence of a germline pathogenic mutation, but additional factors would still be required to initiate the neurodegenerative process. The accumulation of pathological 'hits' would take time, which may provide an explanation for the adult-onset of ALS. Furthermore, this theory would explain why some individuals carrying pathogenic mutations never go on to develop the disease. Through such models it has been proposed that six sequential molecular

steps are required to trigger disease onset (Al-Chalabi et al., 2014). Whilst more than 20 genes have now been linked to ALS, additional risk factors that may constitute pathological steps in the multi-step model remain unclear. These may include intrinsic pathophysiological mechanisms such as oxidative stress, which is associated with normal aging and neurodegeneration (Liguori et al., 2018). Others may involve extrinsic exposures and lifestyle factors such as cyanotoxins, smoking, heavy metals, pesticides and chemicals, trauma, working in the armed forces and high levels of physical activity (Armon, 2009; Coffman et al., 2005; Horner et al., 2003; Julian et al., 2021; Nelson et al., 2000; Pupillo et al., 2018; Scarmeas et al., 2002; Spencer et al., 1987; Sutedja et al., 2009). However, the contribution of these factors is controversial and may be subject to recall and observation bias in retrospective studies. Nevertheless, it is likely that a complex interplay between genetic and environmental factors contributes to the aetiology of ALS.

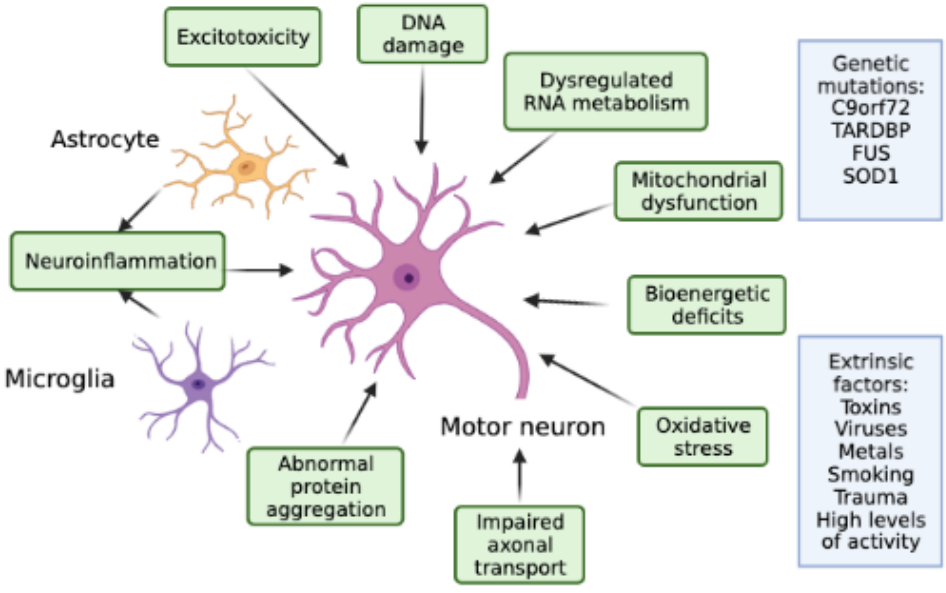


Figure 1.4 The pathophysiology of ALS. Created in *Biorender.com*.

1.3. TDP-43 in ALS

1.3.1. TDP-43 structure

TDP-43 is a 43 kDa protein formed of 414 amino acids, encoded by the gene *TARDBP* located on chromosome 1. TDP-43 consists of multiple functional domains including an N-terminal domain, a nuclear localisation signal (NLS), two RNA recognition motifs (RRM1 and RRM2), a nuclear export signal (NES) and a C-terminal domain. Whilst 3D structures of the N-terminal, C-terminal and RRM domains are now becoming available, complete structural determination of the full-length protein has proved a challenge due to the intrinsically disordered nature of the protein (Prasad et al., 2019).

The N-terminal domain plays a critical role in TDP-43 oligomerization, which is essential for TDP-43 splicing activity and is also thought to contribute to phase separation *via* liquid drop formation; a process involved in the formation of stress granules (Afroz et al., 2017; Molliex et al., 2015; Wang et al., 2018). Some studies have argued that N-terminal dimerization increases TDP-43's propensity to aggregate (Tsoi et al., 2017; Zhang et al., 2013). Conversely, others have suggested that N-terminal dimerization protects against TDP-43 aggregation (Afroz et al., 2017; Jiang et al., 2017). The nuclear localisation signal (NLS) is found in the linking section between the NTD and the RRM1 domain. Importin α mediates TDP-43 nuclear import, through directly binding to the NLS. The NLS is essential in directing TDP-43 to the nucleus, as mutations in this region induce nuclear TDP-43 depletion and aggregate formation (Nishimura et al., 2010; Winton et al., 2008). RRM1 and RRM2 are comprised of five β-sheets and two α-helices. They are involved in binding with cognate RNA/DNA molecules and have a high specificity for UG/TG-rich sequences (Kuo et al., 2014; Lukavsky et al., 2013). Until recently, TDP-43 was thought to contain a nuclear export signal (NES) within RRM2, that

binds the nuclear export factor exportin-1 (XPO1/CRM1) to shuttle TDP-43 from the nucleus into the cytoplasm (Ayala et al., 2008; Winton et al., 2008). However, the involvement of NES remains controversial, as further studies found that the TDP-43 NES sequence showed weak affinity for XPO1 (Pinarbasi et al., 2018), and inhibition or overexpression of XPO1 did not significantly alter TDP-43 cytoplasmic mislocalisation (Archbold et al., 2018; Ederle et al., 2018; Pinarbasi et al., 2018). The C-terminal domain (CTD) is a low-complexity intrinsically disordered prion-like domain, comprised of a glycine rich region and a glutamine/asparagine rich region (Q/N) (King et al., 2012). The CTD is essential for protein-protein interactions and has been specifically implicated in the pathological behaviour of TDP-43, as the majority of disease-associated mutations are located in this domain (Mackenzie & Rademakers, 2008) (Figure 1.5).

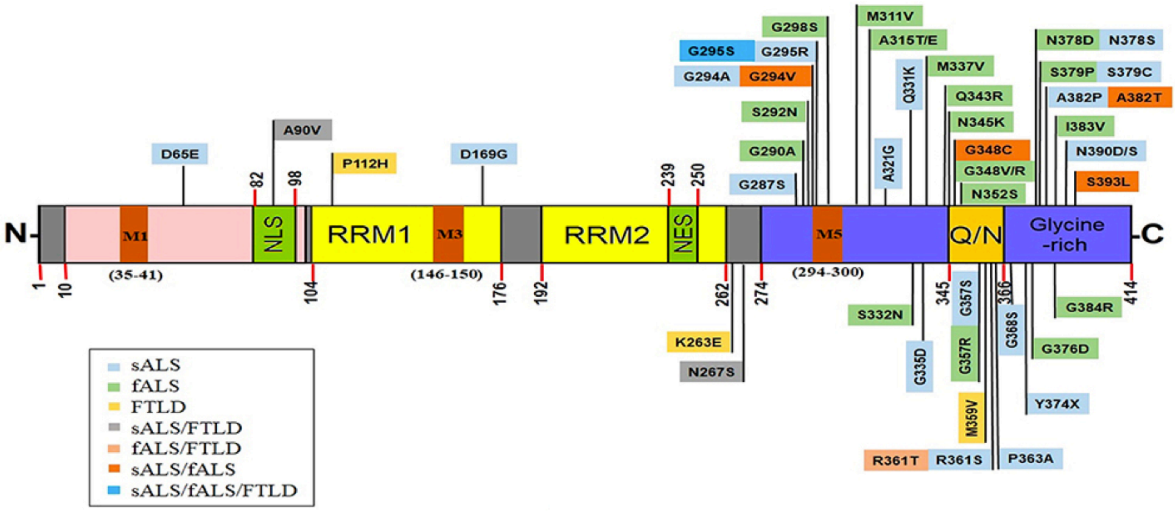


Figure 1.5 TDP-43 protein structure (from Prasad et al., 2019). The location of TDP-43 mutations associated with sporadic ALS (sALS), familial ALS (fALS), and frontotemporal dementia (FTD) are shown. 'N' identifies the N-terminal domain, which has roles in TDP-43 oligomerisation. 'C' identifies the C-terminal domain, which is required for protein-protein interactions and contains a glycine-rich region and a glutamine/asparagine rich region (Q/N). The RNA-recognition motifs, shown as 'RRM1' and 'RRM2', are crucial for DNA and RNA binding. The TDP-43 nuclear localisation signal (NLS) is located adjacent to RRM1 and the nuclear export signal (NES) lies within RRM2.

1.3.2. Physiological functions of TDP-43

TDP-43 is a highly conserved RNA binding protein that is ubiquitously expressed (Ayala et al., 2005). First discovered in 1995 as a modulator of HIV-1 expression, TDP-43 has since been shown to play an important role in multiple aspects of RNA metabolism and the regulation of gene transcription (Lagier-Tourenne et al., 2010; Ou et al., 1995; Ratti & Buratti, 2016). TDP-43 is involved in the repression of gene expression through transcriptional regulation and has additional roles in RNA processing, ranging from splicing to mRNA stability and transport (Buratti & Baralle, 2001; Coyne et al., 2017; Ling et al., 2013).

Under physiological conditions, the majority of TDP-43 is nuclear, while a small proportion is continuously shuttled between the nucleus and cytoplasm. In the nucleus, TDP-43 regulates the splicing of its own *TARDBP* mRNA transcripts and other genes including Cystic Fibrosis transmembrane conductance regulator (*CFTR*), *FUS*, Synuclein Alpha (*SCNA*), Huntingtin (*HTT*), amyloid precursor protein (*APP*) and microtubule-associated protein tau (*MAPT)* (Y. M. Ayala et al., 2011; Buratti & Baralle, 2001; Gu et al., 2017; Polymenidou et al., 2012; Polymenidou et al., 2011). TDP-43 is also thought to repress splicing of non-conserved cryptic exons, which are generated following the activation of cryptic splice sites. These sites normally lie dormant as they are not recognised by splicing machinery (Ling et al., 2015; Tan et al., 2016). In the cytoplasm under stress conditions, TDP-43 controls mRNA stability, translation, and nucleocytoplasmic transport by forming cytoplasmic ribonucleoprotein complexes, termed stress granules (Zhao et al., 2018). Stress granules are membrane-less complexes < 5μm in size, that form in response to cellular stressors including oxidative stress, heat-shock, viral infection and chemical stressors (Anderson & Kedersha, 2009; Aulas & Vande Velde, 2015). Their formation is thought to be a protective response to conserve energy, by limiting the translation of mRNAs not necessary for cellular survival (Lindquist, 1981). Stress granules sequester RNA binding proteins and translationally stalled RNAs until the stressor is removed,

whereby stress granules dissolve and normal cellular function resumes (Anderson & Kedersha, 2009). TDP-43 has been shown to assemble into stress granules and is involved in both the formation and maintenance of stress granules. TDP-43 regulates the expression of G3BP and TIA-1, which are key stress granule nucleating proteins (McDonald et al., 2011). In the cytoplasm, TDP-43 also associates with RNA molecules to produce ribonucleoprotein (RNP) granules, which associate with microtubules for long-range transport of mRNA (Alami et al., 2014). Furthermore, in primary motor neurons, TDP-43 has been shown to localise within and be transported along motor neuron axons and may play a role in regulating axonal outgrowth (Fallini et al., 2012). TDP-43 also has roles in miRNA biogenesis, small non-coding RNAs that regulate gene expression. TDP-43 acts in the nucleus to promote the production of miRNAs through interactions with the Drosha complex, as well as influencing miRNA processing in the cytoplasm through its interactions with the Dicer complex (Kawahara & Mieda-Sato, 2012).

1.3.3. Evidence of TDP-43 pathogenicity in ALS

The pathological hallmark of ALS is the presence of ubiquitinated, hyperphosphorylated cytoplasmic inclusions in motor neurons, enriched for TDP-43 (Arai et al., 2006; Neumann et al., 2006). Since this discovery, various studies have sought to determine the characteristics of pathological TDP-43 and their relative contribution to toxicity in ALS. In addition to TDP-43 mislocalisation and aggregation, research has uncovered a number of mutations in the gene encoding TDP-43, together with post-translational modifications and protein fragmentation that may underlie TDP-43 pathological behaviour. Here I briefly examine the evidence for toxicity associated with each of these features.

1.3.3.1. TDP-43 mislocalisation and aggregation

Since the discovery of TDP-43 positive inclusions in ALS, there has been significant speculation as to whether TDP-43 mislocalisation and cytoplasmic aggregation are significant drivers of pathogenesis in ALS, or merely an inconsequential feature of end-stage disease. To study the effects of TDP-43 mislocalisation, a number of models with targeted mutation of the NLS have been developed, which demonstrate robust TDP-43 mislocalisation (Barmada et al., 2010; Igaz et al., 2011; Sasaguri et al., 2016; Urushitani et al., 2010; Walker et al., 2015; Winton et al., 2008). In such models, TDP-43 mislocalisation is associated with toxicity, motor neuron loss and functional decline (Barmada et al., 2010; Igaz et al., 2011; Sasaguri et al., 2016; Walker et al., 2015). One study confirmed that toxicity was directly associated with mislocalisation, as preventing TDP-43 mislocalisation using a doxycycline-suppressible system in mice resulted in phenotypic rescue (Walker et al., 2015). Whilst TDP-43 aggregates were observed in some models (Sasaguri et al., 2016; Winton et al., 2008), the vast majority rarely developed TDP-43 aggregates, suggesting that toxicity induced by TDP-43 may arise due to its mislocalisation rather than aggregation (Barmada et al., 2010; Igaz et al., 2011; Urushitani et al., 2010; Walker et al., 2015). However, TDP-43 aggregates arising from TDP-43-ΔNLS expression have been shown to exacerbate TDP-43 mislocalisation through sequestering endogenous nuclear TDP-43 (Winton et al., 2008). These findings were corroborated in a later study that reported sequestration of wild-type nuclear TDP-43 by TDP-43-ΔNLS cytoplasmic aggregates in primary neurons. This sequestration was accompanied by a decrease neurite outgrowth, that was rescued through preventing TDP-43 aggregation, suggesting aggregation may be driving this toxicity (Zhang et al., 2013). Similar sequestration of nuclear TDP-43 by aggregated TDP-43 in the cytosol, was also observed in NSC34 cells overexpressing human wild-type TDP-43 (Cascella et al., 2016). Taken together, these studies suggest that TDP-43 mislocalisation is sufficient to induce neurotoxicity, and that TDP-43 cytoplasmic aggregation may exacerbate TDP-43 depletion from the nucleus. The

redistribution and aggregation of TDP-43 disrupts normal TDP-43 function, through both nuclear loss-of-function and toxic cytoplasmic gain-of-function mechanisms, which will be discussed later.

1.3.3.2. TARDBP mutations

Mutations in *TARDBP* are a rare cause of ALS, estimated to account for ~4% fALS and ~1.5% of sporadic disease (Mackenzie et al., 2010). The majority of *TARDBP* mutations are missense mutations located in exon 6 which encodes the glycine-rich CTD of TDP-43 (Kabashi et al., 2008; Rutherford et al., 2008; Sreedharan et al., 2008; Van Deerlin et al., 2008). The most prevalent mutations in this region are A382T and M337V, however numerous models are available for studying a vast number of *TARDBP* mutations (Buratti, 2015). C-terminal *TARDBP* mutations have been shown to enhance TDP-43 mislocalisation, aggregation and toxicity. In a yeast cell model, several ALS-linked *TARDBP* mutations including Q331K, M337V, Q343R, N345K, R361S and N390D were found to increase the number of TDP-43 aggregates and enhance toxicity *in vitro* and *in vivo* (Johnson et al., 2009). In primary rat cortical neurons expression of mutant TDP-43 was associated with increased cytoplasmic mislocalisation of TDP-43 and neuronal toxicity. In this study, TDP-43 mislocalisation itself was sufficient to induce cell death without the occurrence of inclusion bodies (Barmada et al., 2010). Expression of mutant TDP-43 (M337V and Q331K) also demonstrates greater propensity to fragment relative to wild type protein in Chinese hamster ovary cells, and was associated with neural apoptosis and developmental delay in chick embryos (Sreedharan et al., 2008). It is clear from such studies that mutations in *TARDBP* are pathogenic and sufficient to induce neuronal toxicity.

1.3.3.3. Post-translational modifications

Several post-translational modifications have been associated with pathological TDP-43 in ALS, including acetylation, cysteine oxidation and SUMOylation, however the most extensively studied modifications are ubiquitination and phosphorylation (Arai et al., 2006; Neumann et al., 2006). TDP-43 contains numerous phosphorylation sites including ser-379, ser-403 and ser-404, however the best studied are ser409 and ser410 (Hasegawa et al., 2008; Inukai et al., 2008; Neumann et al., 2009). Phosphorylation is performed by casein kinases, CK1 and CK2, and appears to precede ubiquitination (Hasegawa et al., 2008). Whilst TDP-43 phosphorylation is not a pre-requisite for mislocalisation and aggregation (Iguchi et al., 2012), phosphorylation by a hyperactive form of casein kinase 1 has been shown to promote the mislocalisation and cytoplasmic accumulation of phosphorylated TDP-43 in neuroblastoma SH-SY5Y cells (Nonaka et al., 2016). Ubiquitin is a small signalling molecule that tags proteins for degradation by the ubiquitin-proteasome system (UPS). TDP-43 is tagged by polyubiquitinated chains that are predominantly linked *via* the ubiquitin lysines, K-48 and K-63, which has been shown to facilitate cytosolic accumulation of TDP-43 into inclusions (Hebron et al., 2013; Tan et al., 2008).

1.3.3.4. TDP-43 cleavage and C-terminal fragments

In addition to full-length TDP-43, pathological aggregates from ALS patients have also been shown to contain 25 and 35 kDa C-terminal fragments (Neumann et al., 2006). C-terminal fragments are generated *via* the aberrant proteolytic cleavage of TDP-43 by caspase and calpain proteases (Yamashita et al., 2012; Zhang et al., 2007). These fragments are thought to be highly toxic, as overexpression of C-terminal fragments *in vitro* has been shown to drive the formation of toxic, insoluble, ubiquitinated and hyperphosphorylated cytoplasmic inclusions (Igaz et al., 2009; Xiao et al., 2015; Zhang et al., 2009). Similar phenotypes were observed in primary motor neurons where TDP-35 expression resulted in cytoplasmic aggregates and motor neuron

death (Xiao et al., 2015). Moreover, expression of a 35 kDa N-terminally truncated species of TDP-43 was shown to sequester full-length TDP-43 from the nucleus to form cytoplasmic aggregates (Xiao et al., 2015). However, these truncated species have also been suggested to act in a protective capacity, through preventing necrotic cell death by promoting the clearance of TDP-43 (Li et al., 2015; Suzuki et al., 2011). Interestingly, C-terminal fragments are not reported consistently throughout the central nervous system. Enrichment is most commonly reported in brain-derived TDP-43 as opposed to spinal cord inclusions, suggesting differences in the composition of inclusions arising from the brain and spinal cords of ALS and FTD patients (Igaz et al., 2008).

1.4. TDP-43 and the pathophysiology of ALS

The pathophysiology of ALS is immensely complex, with multiple mechanisms thought to contribute to neurodegeneration, including impaired proteostasis, altered RNA metabolism and stress granule dynamics, disrupted DNA repair, nucleocytoplasmic transport defects, glutamate excitotoxicity, impaired axonal transport, mitochondrial dysfunction, vesicular transport defects, neuroinflammation and oligodendrocyte dysfunction. A detailed review of these mechanisms is beyond the scope of this thesis, but their contribution to ALS pathophysiology is extensively reviewed elsewhere (Hardiman et al., 2017). Here, I focus on the mechanisms by which pathological TDP-43 contributes to the pathophysiology of ALS. The cytoplasmic redistribution of TDP-43 observed in ALS, is associated with a concomitant loss of nuclear TDP-43. Given this, hypotheses surrounding the mechanisms of TDP-43 pathogenicity in ALS have focussed on two primary schools of thought; nuclear loss-of-function versus toxic cytoplasmic gain-of-function. In the following section I discuss the interplay between TDP-43 and the pathophysiology of ALS, specifically examining the effects of TDP-43 dysfunction on

RNA splicing and TDP-43 autoregulation, stress granule formation, mitochondrial function, axonal function and protein-protein interactions.

1.4.1. Altered RNA splicing, cryptic exon inclusion and disrupted TDP-43 autoregulation

TDP-43 plays an important role in multiple aspects of RNA metabolism including splicing and RNA stability. Given this, it is not surprising that dysregulation of TDP-43 has been shown to induce wide-spread disruption of RNA metabolism and gene expression. In a seminal study, TDP-43 depletion in mouse brains was found to generate close to 1,000 altered splicing events and dysregulate the expression of over 500 genes (Polymenidou et al., 2011). In a subsequent study, expression of ALS-linked *TARDBP* mutations (Q331K and M337V) induced age-dependent, progressive motor axon degeneration and motor neuron death in mice, accompanied by aberrant RNA splicing events. These changes were specific to the expression of mutant TDP-43, which were not seen in mice expression human wild-type TDP-43. Importantly, neurodegeneration in these mice was found to occur without loss of nuclear TDP-43 or the accumulation of insoluble or aggregated forms of TDP-43, suggesting dysregulation of RNA splicing may be central to the toxicity induced by mutant forms of TDP-43 (Arnold et al., 2013). A more recent study has suggested that loss of nuclear TDP-43 causes cellular vulnerability through disrupting the splicing of the RNA-binding protein, HNRNPA1. In HeLa cells, TDP-43 was found to bind to and modulate the splicing of HNRNPA1 pre-mRNA. Depletion of nuclear TDP-43 led to increased inclusion of a particular exon within the HNRNPA1 transcript, that resulted in increased levels of a particular isoform of hnRNP protein, hnRNP A1B, which demonstrates greater fibrilization and aggregation propensity. This particular isoform was found to drive aggregate formation and impair survival in CB3

cells, relative to the hnRNP A1A isoform (Deshaies et al., 2018). This study highlights how loss of nuclear TDP-43 contributes to cellular vulnerability and the formation of pathological inclusions through aberrant RNA splicing. Splicing defects can also lead to the inclusion of cryptic exons (CE); non-intronic sequences that are erroneously included in mature RNAs. Their inclusion frequently results in premature stop codons and transcript degradation, or premature polyadenylation. CE's in the microtubule-associated protein, stathmin 2 (*STMN2*), and the synaptic protein *UNC13A* have been observed following TDP-43 depletion, leading to subsequent downregulation of these proteins (Brown et al., 2022; Ma et al., 2022; Melamed et al., 2019).

There is also evidence that aberrant regulation of TDP-43 itself may contribute to pathogenesis. TDP-43 autoregulates its own synthesis through binding the 3'UTR sequences in its own mRNA, which promotes RNA instability (Y. M. Ayala et al., 2011; Polymenidou et al., 2011). Disruption to TDP-43 autoregulation and a resulting increase in the expression of TDP-43, has been associated with cognitive dysfunction and aberrant RNA splicing in a *TARDBP* knock-in mouse model (White et al., 2018). Taken together, these studies demonstrate that depletion of TDP-43 or expression of mutant forms of TDP-43 leads to wide-spread dysregulation of RNA homeostasis, through disruption of RNA splicing, TDP-43 autoregulation and gene expression. Disruption to the splicing of specific targets, for example HNRNPA1, and/or disruption to TDP-43 autoregulation may induce downstream aggregate formation and subsequent toxicity.

1.4.2. Altered stress granule dynamics

Stress granules are membrane-less organelles containing non-translating mRNA-protein complexes (mRNPs) that form in response to cellular stress. Their formation is considered a primarily protective response, through limiting ROS production and associated apoptosis.

Stress granule formation may also conserve energy by limiting the translation of messenger RNA's not necessary for cellular survival. Following removal of the stressors, stress granules disassemble and normal cellular translation resumes (Dewey et al., 2012; Takahashi et al., 2013).

ALS-linked mutations in TDP-43 have been shown to influence stress granule dynamics, including assembly, size and disassembly (Dewey et al., 2011; Gordon et al., 2019; Liu-Yesucevitz et al., 2010; McDonald et al., 2011). For example, Dewey *et al* reported progressively larger stress granules in HEK cells expressing G348C mutant TDP-43 (Dewey et al., 2011). In contrast, mutant TDP-43^{M337V}, in mouse primary motor neurons and mESC-MNs, have been shown to reduce the percentage of motor neurons positive for stress granules and reduce the size of these stress granules in response to oxidative stress (Gordon et al., 2019). Reduced stress granule numbers have also been observed in skin fibroblasts derived from ALS patients carrying *TARDBP* mutations compared to patient controls (Romano et al., 2020).

TDP-43 has also been shown to localise to stress granules following certain cellular stressors including oxidative stress, osmotic stress, proteasomal inhibition, heat shock and ER stress (Colombrita et al., 2009; Dewey et al., 2011; Freibaum et al., 2010; Gordon et al., 2019; Liu-Yesucevitz et al., 2010; McDonald et al., 2011; Meyerowitz et al., 2011). Moreover TDP-43 inclusions in brain tissue from ALS and FTD patients has been found to co-stain for stress granule markers including TIA-1 and eIF3 (Liu-Yesucevitz et al., 2010). These observations led to the hypothesis that aberrant stress granule dynamics seed the formation of pathological TDP-43 aggregates. However, co-staining between TDP-43 and stress granules is not universally reported, suggesting that stress granules do not require incorporation of TDP-43 and that TDP-43 positive stress granules only form under certain conditions (V. Ayala et al.,

2011; Dewey et al., 2011). Moreover, TDP-43 has also been shown to form aggregates independent of stress granules, suggesting multiple mechanisms may underlie TDP-43 aggregate formation and associated toxicity. Rather than preceding TDP-43 aggregation directly, stress granules have been suggested to facilitate TDP-43 aggregation indirectly. One proposed mechanism is that stress granules sequester and perturb the function of HDAC6, a proteostasis factor crucial for misfolded and aggregated protein clearance, thus impeding the removal of TDP-43 aggregates (Chen & Cohen, 2019).

1.4.3. Mitochondrial dysfunction

Aberrant interactions between TDP-43 and mitochondria are thought to underlie an additional mechanism of toxicity in ALS. TDP-43 routinely interacts with mitochondria under normal conditions, yet it has been hypothesised that pathological forms of TDP-43 may disrupt mitochondrial function through aberrant interactions with mitochondria. In support of this, TDP-43 has been shown to co-localise with mitochondria in mouse motor neurons, which is enhanced by expression of mutant TDP-43^{M337V} and TDP-43^{Q331K} (Wang et al., 2013). Pathological forms of TDP-43 have also been shown to accumulate in mitochondria in patient-derived tissue samples and in primary human fibroblasts expressing ALS-associated *TARDBP* mutations. This observed localisation of TDP-43 to mitochondria was found to be toxic, as preventing co-localisation protected against neurotoxicity (W. Wang et al., 2016). However, co-localisation between mutant TDP-43 and mitochondria is not universally reported. TDP-43 did not localise to mitochondria in patient-derived fibroblasts with TDP-43 mutations (A382T), despite observations of reduced mitochondrial membrane potential, suggesting alternative mechanisms may underlie mitochondrial abnormalities (Onesto et al., 2016). An alternative hypothesis is that pathological TDP-43 alters the translation of proteins relating to mitochondrial function, leading to global mitochondrial imbalance. In a recent study,

aggregated TDP-43 was shown to bind to and sequester specific microRNAs and proteins, leading to increased levels of some proteins while depleting others. A significant proportion of the functionally depleted gene products were nuclear-encoded mitochondrial proteins. Dysregulated expression of these proteins was found to induce global mitochondrial imbalance, which was associated with significant increases in ROS production that exacerbate oxidative stress (Zuo et al., 2021). These findings suggest that mutant forms of TDP-43 can induce mitochondrial dysfunction through toxic gain-of-function mechanisms. However, there is also evidence linking loss of TDP-43 function with mitochondrial dysregulation. In a TDP-43 knockdown mouse model, RNA sequencing of the axonal compartment revealed dysregulation of multiple transcripts related to mitochondrial function. Notably, downregulation of transcripts relating to complex II (SDHD), complex III (UQCRQ), complex IV (COX5A and COX5B) and ATP synthase (ATP5B) were observed in TDP-43 depleted motor neurons. TDP-43 knockdown was also associated with a reduction in the number of intact mitochondria and reduced mitochondrial membrane potential compared to controls (Briese et al., 2020). Collectively, these studies indicate disturbances to mitochondrial function are a shared pathological phenotype observed across various models of TDP-43 proteinopathy. Moreover, that both loss-of-function and gain-of-function mechanisms can contribute to TDP-43 toxicity in the context of mitochondrial dysfunction.

1.4.4. Disruption of the axonal transcriptome, growth and transport

TDP-43 is frequently found in axons, where it serves several important roles including the transport of mRNAs, regulation of axon outgrowth and local protein synthesis (Alami et al., 2014; Briese et al., 2020; Fallini et al., 2012; Nagano et al., 2020). In addition to the formation of cytoplasmic TDP-43 aggregates in close proximity to the cell soma, aggregates have also been observed in axons and dendrites of neurons (Alami et al., 2014; Fallini et al., 2012). Loss

of TDP-43 has been shown to affect several pathways associated with axon health. Depletion of TDP-43 in primary motor neurons impairs axon growth and is accompanied by transcriptome alterations within axons, including downregulation of several transcripts encoding components of the cytoskeleton (Nefl, Tubb2a, Tuba1b) (Briese et al., 2020). Conversely, accumulation of TDP-43 within axons has been shown to inhibit local protein synthesis. In iPSC-MNs, derived from ALS patients carrying the *C9ORF72* hexanucleotide repeat expansion, TDP-43 accumulation within axons was found to induce the formation of RNA and G3B1 containing RNP-condensates in axons, which interfere with axonal and pre-synaptic protein synthesis (Altman et al, 2021). Expression of mutant TDP-43 has also been shown to disrupt axonal transport, a function critical to the maintenance of neuronal health and survival. TDP-43 forms cytoplasmic mRNP granules, which are transported bi-directionally along axons and facilitate delivery of mRNA to synaptic terminals. Mutant TDP-43 has been shown to impair the transport of mRNP granules *in vitro* and *in vivo* in *Drosophila* models, mouse cortical neurons and iPSC-MNs derived from ALS patients carrying *TARDBP* mutations (Alami et al., 2014). Impaired transport of signalling endosomes has also been observed in mouse models expressing mutant TDP-43^{M337V} (Sleigh et al., 2020), and impaired mitochondrial transport has been reported in iPSC-MNs expressing *TARDBP* mutations (Alami et al., 2014; Fazal et al., 2021). One study confirmed a direct link between the expression of *TARDBP* mutation and mitochondrial transport deficits, as correcting the mutation via CRISPR/Cas-9 gene editing reversed the observed mitochondrial transport deficits (Fazal et al., 2021). These studies suggest TDP-43 has important cytoplasmic functions in regulating axonal health and maintaining axonal transport. Disruption to TDP-43 function, through downregulation or expression of TDP-43 mutations leads to altered protein synthesis within the axonal compartment, impaired axon growth and disrupted axonal transport.

1.4.5. Disrupted protein-protein interactions

The vast majority of *TARDBP* mutations identified to date are found in the C-terminal region of TDP-43 (Kabashi et al., 2008; Rutherford et al., 2008; Sreedharan et al., 2008; Van Deerlin et al., 2008), a structural domain critical for its interaction with other proteins. These interactions are important for the regulation of various cellular processes including alternative splicing, translation and mediating liquid-liquid phase transitions, the latter an important process that underlies stress granule dynamics (V. Ayala et al., 2011; Buratti, 2015; Buratti & Baralle, 2010; Li et al., 2018; Ling et al., 2013). Given this, altered interactions between TDP-43 and its protein binding partners may disrupt cellular homeostasis and contribute to pathogenesis.

To date, several studies have examined the TDP-43 interactome in wild-type and TDP-43 mutant models (Blokhuis et al., 2016; Feneberg et al., 2020; Freibaum et al., 2010; Li et al., 2016; Ling et al., 2010). These studies have provided insight into altered protein interactions arising from mutant TDP-43 expression and how these altered interactions influence pathways implicated in ALS pathophysiology. In one study, the TDP-43 interactome in TDP-43^{WT} and mutant TDP-43^{M337V} mESC-MNs was examined in standard conditions, and following exposure to oxidative stress. Using mass spectrometry and gene ontology enrichment analysis a number of pathways that were significantly dysregulated by the TDP-43^{M337V} mutation were identified. In standard conditions, TDP-43^{WT} was found to interact predominantly with proteins involved in transcription, translation and poly(A)-RNA binding. Expression of TDP-43^{M337V} significantly disrupted the TDP-43 interactome in standard conditions, as the number of TDP-43 interactors was significantly reduced compared to TDP-43^{WT}. Following oxidative stress, TDP-43^{WT} was found to interact with proteins of the endoplasmic reticulum and endosomal-extracellular trafficking pathways. Alternatively, expression of TDP-43^{M337V} was found to

impair interactions between TDP-43 and proteins relating to stress granule assembly, including Poly(A)-binding protein (PABP) and Eif4a1 (Feneberg et al., 2020). These findings suggest that expression of mutant TDP-43 significantly disrupts the TDP-43 interactome, both in standard conditions and in response to cellular stress.

1.5. Approaches for studying TDP-43 pathogenicity in ALS

1.5.1. Mouse models

1.5.1.1. TDP-43 depletion

To investigate loss of TDP-43 function associated with TDP-43 pathogenicity in ALS, various TDP-43 knockout and knockdown models have been developed. TDP-43 is a developmentally regulated protein that is essential for early embryonic development, as complete knockout of TDP-43 is embryonically lethal (Kraemer et al., 2010; Sephton et al., 2010; Wu et al., 2010). TDP-43 is also essential in the maintenance of adult viability, as ubiquitous knock-out of TDP-43 in adulthood using a Cre-driven promoter proves lethal after only several days (Chiang et al., 2010). Given this, subtler models of TDP-43 depletion have been established to probe disease-specific effects associated with loss of TDP-43. One approach is to perform tissue or cell specific conditional knockout of TDP-43. The selective knock-down or knock-out of TDP-43 in spinal motor neurons can be achieved using the HB9 or ChAT promoters (Misawa et al., 2003; Nakano et al., 2005). Such approaches have allowed the effects of targeted TDP-43 depletion in spinal motor neurons to be studied. For example, targeted TDP-43 depletion in spinal motor neurons using a HB9 promoter, has been shown to induce ALS-associated phenotypes including progressive motor dysfunction, muscle weakness and atrophy, motor neuron loss, astrocytosis and increased protein ubiquitination (Wu et al., 2012). Similar ALS-

associated phenotypes, including progressive weight loss, motor impairment at 60 weeks, denervation of the neuromuscular junction and degeneration of large motor axons, were observed in mice with TDP-43 conditional knock-out driven by a ChAT promoter and Cre/loxP recombination (Iguchi et al, 2013).

Taken together, these studies support a TDP-43 loss-of-function hypothesis as a contributing factor in ALS pathogenesis, as TDP-43 depletion is sufficient to induce motor neuron loss and a progressive motor phenotype reminiscent of ALS. However, these models alone are insufficient to study the full spectrum of TDP-43 pathogenicity as they do not allow assessment of toxic gain-of-function mechanisms associated with TDP-43 mislocalisation and aggregation.

1.5.1.2. Overexpression of wild-type and mutant TDP-43

Models overexpressing TDP-43 have typically been used to study gain-of-function mechanisms associated with pathological TDP-43. The most extensively characterised of these models is the transgenic TDP-43^{A315T} mouse developed by Wegorzewska and colleagues (Wegorzewska et al., 2009). These mice express the familial ALS associated mutation, A315T, in *Tardbp* under control of the mouse prion promoter (PrP), which drives expression of the transgene most extensively within the central nervous system (Borchelt et al., 1996; Wang et al., 2005). TDP-43^{A315T} mice were indistinguishable from their non-transgenic littermates until 3 months of age, when they developed a gait abnormality. This was followed by a reduction in weight and further deterioration of gait leading to a 'swimming' gait phenotype, where mice are unable to support their weight, moving instead by sliding on their stomachs. The average survival of TDP-43^{A315T} mice was 154 days, whereupon they died spontaneously or were euthanised when they were no longer able to feed. In addition to their motor abnormalities and

shortened lifespan, cytoplasmic accumulation of ubiquitinated proteins and reduced neuron numbers were observed in the brains of these mice, that was restricted to cortical layer V, which contains large pyramidal neurons that project to subcortical layers including the basal ganglia and spinal cord. Gliosis was also observed, which was similarly restricted to layer V. In addition to motor deficits, these mice also develop a non-motor phenotype of paralytic ileus arising from degeneration of the myenteric plexus (Wegorzewska et al., 2009). This study provided important insight into the effects of altered TDP-43 function, specifically on motor neurons within cortical layer V. However, a notable limitation of this model is the lack of a transgenic TDP-43^{WT} control to delineate the effects arising specifically from the A315T mutation as opposed to the transgene insertion or TDP-43 overexpression. Indeed, overexpression of full-length human wild-type TDP-43 (hTDP-43) has been associated with various functional and pathological abnormalities consistent with neurodegeneration. In a study by Xu and colleagues, overexpression of hTDP-43 under control of the PrP (TDP-43_{PrP}) in mice has been shown to induce a dose-dependent decrease in endogenous TDP-43 RNA and protein levels, together with evidence of TDP-43 cleavage, phosphorylation, aggregation, ubiquitination and mitochondrial abnormalities, the latter indicated by abnormal accumulations of mitochondria within the neurons. TDP-43_{PrP} mice also showed evidence of reactive gliosis, axonal and myelin degeneration, gait abnormalities and premature death (Xu et al., 2010). These phenotypes were remarkably similar to those observed in a subsequent study, examining the effects of homozygous TDP-43^{M337V} expression driven by the PrP in mice, suggesting they were the result of TDP-43 overexpression rather than from expression of the disease-associated mutation (Xu et al., 2011). Similar motor phenotypes resembling ALS have been observed in other models of wild-type TDP-43 overexpression, confirming that overexpression itself can induce neurodegeneration in mice and may mask disease-specific mechanisms (Igaz et al., 2011; Shan et al., 2010; Swarup et al., 2011; Wils et al., 2010; Yang et al., 2022). These effects

have been shown to be dose-dependent by Wils and colleagues, who found that homozygous mice expressing two copies of the human wild-type *TARDBP* transgene restricted to the CNS demonstrated earlier onset of motor dysfunction and significantly reduced survival compared to hemizygous mice expressing only one copy (Wils et al., 2010). However, in some models, expression of TDP-43 mutations has been associated with neurodegenerative phenotypes resembling ALS, which were not observed in comparative controls expressing wild-type TDP-43. For example, overexpression of A315T mutant TDP-43 driven by the PrP in mice led to delayed onset paralysis and mean survival of 60-75 days, whilst mice overexpressing wild-type TDP-43 remained asymptomatic at least up to 11 months of age. TDP-43 A315T mice develop pathological abnormalities including cytoplasmic ubiquitinated inclusions, TDP-43 fragmentation and gliosis, however wild-type mice also develop slight pathological abnormalities including diffuse ubiquitination and mild gliosis (Stallings et al., 2010). Similar findings were reported by Arnold and colleagues, who developed mouse models expressing either wild-type or ALS-linked mutant TDP-43 (Q331K and M337V) under control of the mouse PrP. Expression of exogenous human TDP-43 was only mildly overexpressed (1-1.5 X that of endogenous TDP-43) compared to other models. Analysis revealed adult-onset motor deficits including tremors, defective hindlimb clasping and impaired rotarod performance in mice expressing mutant TDP-43 compared to non-transgenic and wild-type mice. These impairments were observed at 10 months of age but did not appear to be progressive, as no further exacerbation of these phenotypes was observed after 17 months of age. Significant splicing abnormalities were observed in all mice expressing wild-type or mutant TDP-43 relative to non-transgenic mice, but neurodegeneration in mice expressing mutant TDP-43 was found to occur without loss of nuclear TDP-43, cytoplasmic TDP-43 aggregate formation or accumulation of insoluble TDP-43 (Arnold et al., 2013). However, re-examination of this model in a later study revealed higher expression of human TDP-43 in TDP-43^{Q331K} mutants

compared to TDP-43^{WT} mice in the cortex and spinal cord, calling into question whether the phenotypes observed were mutation specific, or the result of overexpression (Watkins et al., 2021).

Collectively, these studies demonstrate that overexpression of both wild-type and mutant forms of TDP-43 are capable of inducing motor system degeneration in a dose-dependent manner. It is worth noting however, that there is no evidence in patients with ALS that increased or decreased expression of TDP-43 is driving disease. For example, in Parkinson's disease, increasing *SCNA* gene dosage, which encodes the protein synuclein, has been associated with faster disease progression (Chartier-Harlin et al., 2004). Yet no such evidence linking *TARDBP* gene dosage and disease progression have been reported in ALS. This suggests that if models overexpressing TDP-43 are providing insight into ALS mechanisms, they are doing so by inducing specific cellular changes to TDP-43 function. However, given that overexpression of TDP-43 is itself toxic, these models make it difficult to dissect disease-specific mechanisms from those arising solely due to overexpression.

1.5.1.3. Physiologically relevant expression models

Given the pitfalls of TDP-43 overexpression, models that demonstrate more physiologically relevant expression of mutant forms of TDP-43 have been developed to study disease-specific mechanisms. One strategy is to generate transgenic models with low expression of exogenous human TDP-43. One such model has been previously developed by our group. This model carries the entire genomic locus of the human *TARDBP* gene, and expresses either human TDP-43^{WT} or TDP-43^{M337V} against a background of endogenous mouse TDP-43. Expression of human TDP-43 in this model is low and at a level less than endogenous mouse TDP-43 protein, thus overcoming issues of overexpression. TDP-43^{M337V} mice demonstrate reduced survival

relative to TDP-43^{WT} mice, with only around 50% of TDP-43^{M337V} mice surviving to 750 days compared to around 80% in TDP-43^{WT} mice. TDP-43^{M337V} mice also demonstrate evidence of age-dependent neurodegeneration. Whilst TDP-43^{M337V} mice are phenotypically normal at 3 months of age, they develop progressive motor dysfunction linked to a loss of neuromuscular junction integrity by 6 months of age (Gordon et al., 2019). Knock-in mouse models provide an additional means for generating models with physiological expression of TDP-43, where TDP-43 mutations are incorporated into the mouse endogenous TDP-43 gene. Knock-in models have benefits over transgenic approaches as they exclude the requirement for neuronal promoters to induce cell-type specific expression. A number of knock-in mouse models have been developed over the last few years. White and colleagues developed a knock-in mouse model expression the ALS-associated mutation, Q331K, in the mouse endogenous *Tardbp* gene using CRISPR/Cas9 technology. Characterisation of these mice revealed impairments to executive function and memory, deficits associated with FTD in human patients, in TDP-43^{Q331K} mutants, together with disrupted TDP-43 autoregulation and a reduction in the number of parvalbumin positive neurons. However, striking resilience of the motor system in the presence of the Q331K mutation was seen, as no significant motor or neuromuscular impairments were observed and motor neuron morphology was normal, with no evidence of TDP-43 mislocalisation or aggregation (White et al., 2018). In an additional knock-in mouse model, with incorporation of the Q331K mutation into the mouse endogenous *Tardbp* gene, mutants demonstrated altered splicing leading to enhanced exon skipping, although behavioural and motor phenotypes were not examined (Fratta et al., 2018). In the same study, expression of two *Tardbp* mutations in RRM2 and the LCD, which were identified through a large-scale chemical mutagenesis project, provided insight into both loss- and gain-of-function mechanisms associated with *Tardbp* mutations. Heterozygous RRM2 mutants did not exhibit a degenerative motor phenotype, but transcriptomic analysis of mutant and control PMEFs

revealed a splicing loss-of-function associated with the mutation. Splicing profiles in RRM2 mutants resembled those of models where TDP-43 expression was knocked down using shRNA. Conversely, the homozygous LCD mutant demonstrated a progressive motor phenotype, but not paralysis or premature death, and a splicing gain-of-function upon transcriptomic analysis where changes were opposite to those observed with TDP-43 knockdown (Fratta et al., 2018).

These models demonstrate that physiologically relevant expression of mutant forms of TDP-43 is possible using low expressing human TDP-43 transgenes and targeted knock-in of mutations into the endogenous mouse gene. Such approaches are generally accepted as the most relevant means for studying pathogenicity associated with TDP-43 mutations in mice, by overcoming non-specific toxicity associated with overexpression. These models also allow gain-of-function and loss-of-function mechanisms associated with mutations to be explored simultaneously.

1.5.2. Stem cell models of *TARDBP* mutations

1.5.2.1. mESC-MN models

In addition to mouse models, which provide valuable insight into clinical manifestations of TDP-43 pathogenicity, cellular models that allow further mechanistic probing *in vitro* are essential. Mouse embryonic stem cell-derived motor neurons (mESC-MNs) are an attractive model, that allows modelling of disease pathogenesis in a motor neuron specific model, high-throughput culturing and phenotypic analysis and overcomes ethical concerns surrounding the use of human ESCs. Initially used to generate mouse models, ESCs house the potential to differentiate into any cell type *in vitro*. The differentiation of ESCs to motor neurons was first described in 2002 (Wichterle et al., 2002), following advances in our understanding of the

extracellular signals and transcriptional mediators required to specify distinct neural cell fates within the CNS (Briscoe & Ericson, 2001; Echelard et al., 1993). Several protocols have been developed for the differentiation of mESCs to motor neurons (Bryson et al., 2014; Cortes et al., 2016; Machado et al., 2014), which include the addition of retinoic acid to induce a caudal identity and smoothened agonist to promote ventralisation (Davis-Dusenbery et al., 2014).

Early studies using mESC-MNs predominantly modelled SOD1 ALS in both neurons and astrocytes, to study disease mechanisms (Di Giorgio et al., 2008; Haidet-Phillips et al., 2011; Lopez-Gonzalez et al., 2009; Marchetto et al., 2008; Wada et al., 2012) and as a high-throughput model for drug screening (Yang et al., 2013). However more recently, mESC-MN models harbouring *TARDBP* mutations have also been developed. Gordon and colleagues, developed mESC-MNs as an *in vitro* model to complement their mouse and primary motor neuron models. These mESC-MNs express the same BAC construct found in the mouse model, which carries the entire genomic locus of the human *TARDBP* gene with either wild-type TDP-43 or mutant TDP-43, the latter expressing the TDP-43^{M337V} mutation. TDP-43^{M337V} mutant mESC-MNs demonstrated impaired survival and altered stress granule dynamics *in vitro* compared to human wild-type (TDP-43^{WT}) and non-transgenic controls (Gordon et al., 2019). Moreover, subsequent analysis of the TDP-43 interactome in unstressed and stressed conditions revealed significantly altered protein interactors in TDP-43^{M337V} mESC-MNs in both stressed and unstressed conditions compared to TDP-43^{WT} controls, alluding to both loss- and gain-of-function associated with the mutation (Feneberg et al., 2020).

mESC-MNs provide a valuable *in vitro* model to complement mouse models and allow further insight to be gained from more thorough mechanistic probing, to generate a more detailed understanding of the processes underlying pathogenicity induced by *TARDBP* mutations.

Given their high-throughput nature, they also provide a valuable *in vitro* system for screening of potential therapeutic compounds that may modify pathological phenotypes.

1.5.2.2. iPSC-MNs

The development of iPSCs in 2006 as a novel *in vitro* model for studying disease was a landmark discovery, which has since been harnessed to model a number of disorders including ALS. iPSCs are generated from somatic cells, typically skin fibroblasts, which are reprogrammed through the addition of Oct3/4, SOX2, c-Myc and Klf4. Following reprogramming they become pluripotent; possessing the potential to differentiate into any cell type (Takahashi & Yamanaka, 2006). Such was the significance of this finding that Shinya Yamanaka shared the 2012 Nobel Prize in Physiology and Medicine with Sir John B. Gurdon, who demonstrated in 1962 that the specialisation of cells is reversible. The first established protocol for differentiation of iPSCs to spinal motor neurons was developed in 2009 (Karumbayaram et al., 2009), which has since been refined and modified by other groups in later work (Bianchi et al., 2018; Bossolasco et al., 2018; Faye et al., 2020; Maury et al., 2015). iPSC-MN models allow molecular phenotypes and pathogenic mechanisms arising from both familial and sporadic ALS to be studied in human cells derived directly from ALS patients. Their use also overcomes the need for genetic engineering of cells or insertion of foreign transgenes.

Studies of iPSC-MNs from patients carrying the TDP-43^{M337V} mutation, have highlighted various pathophysiological changes not seen in iPSC-MNs from healthy controls, such as hyperexcitability and impaired calcium buffering (Dafinca et al., 2020; Devlin et al., 2015). Some studies report the formation of TDP-43 cytosolic aggregates under basal conditions in iPSC-MNs from patients with *TARDBP* mutations, Q343R, M337V and G298S (Egawa et al.,

2012; Fujimori et al., 2018). Conversely, others have not observed TDP-43 mislocalisation or aggregation under basal conditions, or following heat shock, in motor neurons from ALS patients carrying A382T and M337V *TARDBP* mutations (Bilican et al., 2012; Bossolasco et al., 2018; Seminary et al., 2018). iPSC-MNs have also proved valuable as an *in vitro* model for screening candidate drugs (Egawa et al., 2012), although their lengthy differentiation protocol relative to other *in vitro* models such as mESC-MNs, limits their feasibility as a high-throughput technique.

Protocols for iPSC differentiation *in vitro* are lengthy and complex. In addition, iPSC lines may acquire somatic mutations during the initial reprogramming stage. Such changes can result in clonal variation, whereby phenotypic differences among clones stemming from the same iPSC founder strain are observed (Gore et al., 2011). Therefore, simultaneous differentiation of multiple clones from the same iPSC strain is required to control for clonal variation. Yet, their utility and relevance as a model outweighs their limitations, as they are widely considered the gold standard for modelling ALS *in vitro*. The principal value of iPSC-MN models is that they are derived directly from ALS patients and are currently the only model available for studying pathogenicity associated with sporadic ALS, which amounts to ~90% of cases.

1.6. Aims

Since the discovery that TDP-43 is the predominant protein within pathological inclusions in 97% of ALS cases, TDP-43 has remained at the centre of ALS research. Yet despite almost 20 years of research, the mechanisms through which pathological TDP-43 may contribute to ALS are still unclear. Important questions remain about how TDP-43 loss-of-function and gain-of-function mechanisms may relate to the pathophysiology of the disease.

The aim of this thesis is to examine the effects of a familial ALS-associated mutation in the human *TARDBP* gene on cellular phenotypes in a mESC-MN model. This model has previously been shown to demonstrate impaired survival and altered stress granule characteristics, yet further characterisation has not yet been performed. The aims of the following chapters are:

1. To characterise the effects of increased culture duration on ALS-relevant phenotypes.
2. To test the hypothesis that alterations in cellular energy metabolism are potential drivers of neurodegeneration, and thus viable therapeutic targets.
3. To investigate whether expression of mutant TDP-43^{M337V} leads to impaired axonal transport in mESC-MNs.

CHAPTER 2 Methods

2.1. An *in vitro* model for studying the TDP-43^{M337V} mutation

2.1.1. Transgenic model for studying the effects of the TDP-43^{M337V} mutation

The effects of the TDP-43^{M337V} mutation were studied in a previously published mESC-MN model (Gordon et al., 2019; Mutihac et al., 2015). This model carries the entire genomic locus of the human *TARDBP* gene within a bacterial artificial chromosome (BAC) construct. The construct expresses either the human wild type (WT) *TARDBP* gene, or the *TARDBP* gene carrying the TDP-43^{M337V} mutation, which was inserted into exon 6 through site directed mutagenesis (Mutihac et al., 2015). mESCs were generated through targeted insertion of a single copy of the *TARDBP* WT or M337V BAC construct to the *Rosa26* locus.

2.1.2. Differentiation of mESCs to motor neurons

The differentiation protocol for mESC-MNs was based on previously published work (Bryson et al., 2014; Machado et al., 2014). In brief, mESCs were expanded on a feeder cell layer of mouse primary embryonic fibroblasts (PMEFs) (Thermo Fisher Scientific) in mESC media (Table 2.1). Following two days of expansion, embryoid bodies (EBs) were detached from PMEF's through treatment with 0.25% Trypsin-EDTA. The resultant cell suspension was plated onto 10 cm dishes (Corning) in ADFNK media (Table 2.2). Following two further days of incubation, EBs were split 1:4 across 10 cm dishes in ADFNK media supplemented with 1

μM retinoic acid (RA; Sigma) and 0.5 μM smoothened agonist (SAG; Merck). After three further days, EBs were collected and dissociated in Accumax (Sigma), then cells plated in ADFNK media containing RA and SAG along with growth factors (10 ng/mL GDNF, 10 ng/mL BDNF, 10 ng/mL CNTF and 10 ng/mL NT-3; Preprotech) onto poly-l-ornathine (1:10 in sterile water) and laminin-coated plates (2.5 μg/mL in HBSS). Motor neurons were formed after 3 days *in vitro* after plating down in ADFNK + RA + SAG + growth factors. To investigate the effects of increasing culture duration on cellular phenotypes, analysis of neurons was performed after 3, 5, 7 and 9 days *in vitro* (DIV 3 – DIV 9). Cellular phenotypes were assessed in unstressed conditions and following oxidative stress. To induce oxidative stress, mESC-MNs were treated with 0.5 mM sodium arsenite for 60 minutes.

Table 2.1 mESC media composition.

mESC media

Component	Working Concentration	Company
KO DMEM	100%	Invitrogen
ESC-screened fetal bovine serum (FBS)	15%	Thermo Fisher Scientific
Penicillin-Streptomycin-Glutamine	2 mM	Invitrogen
MEM non-essential amino acids	0.01%	Invitrogen
Leukemia inhibitory factor (LIF)	1 ng/ml	Millipore
EmbryoMax mESC qualified nucleosides	0.01%	Millipore
Beta-mercaptoethanol	0.1 mM	Sigma

Table 2.2 ADFNK media composition.

ADFNK media

Component	Working Concentration	Company
Advanced DMEM/F-12	50%	Invitrogen
Neurobasal Medium	50%	Invitrogen
Knockout Serum Replacement	10%	Invitrogen
Penicillin-Streptomycin-Glutamine	2 mM	Invitrogen
Beta-mercaptoethanol	0.1 mM	Sigma

2.2. Analysis of protein expression

2.2.1. Protein extraction

Cells were washed and scraped in phosphate-buffered saline (PBS), followed by centrifugation at 6000 *g* for 5 minutes. The supernatant was removed and the resultant pellet was lysed with RIPA buffer (0.5% sodium deoxycholate, 0.1% SDS 1% Nonidet P40 and 1% protease inhibitor cocktail (Sigma)), homogenised and incubated on ice for 30 minutes. Cells were centrifuged at 10,000 *g* for 10 minutes. The supernatant was collected and protein concentration quantified using a bicinchoninic acid (BCA) assay according to the manufacturer's instructions (Sigma).

2.2.2. Mitochondrial isolation

Mitochondrial isolation was performed using the Qproteome Mitochondria Isolation Kit (Qiagen) as described by the manufacturer. In brief, cells were scraped in PBS and centrifuged at 500 *g* for 10 minutes at 4°C. The supernatant was removed and discarded, while the pellet

was washed in 0.9% sodium chloride. Following washing, the pellet was resuspended in 800 μL ice-cold lysis buffer supplemented with protease inhibitor (1:100) and incubated for 10 minutes at 4°C in an end to end shaker. The lysate was centrifuged at 1,000 *g* for 10 minutes at 4°C and the supernatant containing the cytosolic fraction removed. The pellet was resuspended in 1.5 mL of ice-cold disruption buffer supplemented with protease inhibitor (1:100). Disruption was completed using a blunt-ended needle and syringe. The lysate was centrifuged at 1,000 *g* for 10 minutes at 4°C, then the supernatant carefully removed and transferred to a clean 1.5 mL tube and centrifuged at 6,000 *g* for 10 minutes at 4°C. The pellet containing the mitochondria was washed with 1 mL mitochondrial storage buffer and centrifuged at 6,000 *g* for 20 minutes at 4°C. The pellet was then resuspended in 50 μL of mitochondrial storage buffer and stored at -80°C prior to analysis with gel electrophoresis and Western blotting.

2.2.3. Western blotting

Protein lysates were heated with loading dye (NuPAGE® sample reducing agent (10X), NuPAGE® LDS sample buffer (4X) (Invitrogen) (100 μL: 250 μL)) for 5 minutes at 95°C. Proteins were separated by SDS-PAGE. Approximately 10 μg of each protein lysate was loaded onto NuPAGE™ 4-12% Bis-Tris gels (Life Technologies) and run with an X-Cell SureLock electrophoresis system (Life Technologies) in 1X MES SDS running buffer (Life Technologies) at a constant voltage (120 V) for 90 minutes. Gels were transferred to a methanol activated polyvinylidene difluoride (PVDF) membrane (Invitrogen) using the iBlot®2 dry transfer system (Thermo Fisher Scientific). Membranes were blocked in blocking buffer (Tris-buffered saline (TBS), 1% Tween, 5% skimmed milk (Sigma)) for 1 hour at room temperature and incubated overnight at 4°C with primary antibodies diluted in TBS + 1% Tween + 1%

skimmed milk (Table 2.3). After incubation with primary antibodies, membranes were incubated for 1 hour at room temperature with horseradish peroxidase (HRP)- conjugated anti-mouse IgG or anti-rabbit IgG (1:5000; BioRad) secondary antibodies. Membranes were visualised using the ChemiDoc™ MP Imaging system. The integrated optical density of each band was measured using ImageJ and expression normalised to beta actin levels detected from the same blot for comparative expression assessment. Optical densities were further normalised to the WT sample within each blot to compare relative expression of protein bands.

Table 2.3 Primary antibodies used for immunoblotting and immunocytochemistry.

Antigen	Host	Type	Manufacturer	Cat No	Dilution WB	Dilution ICC
ATPb	Mouse	Monoclonal	Abcam	ab14730	1:1000	1:500
Beta actin	Rabbit	Polyclonal	Abcam	ab227387	1:2000	-
Beta III tubulin	Chicken	Polyclonal	Millipore	ab9354	-	1:100
Choline Acetyltransferase (ChAT)	Goat	Polyclonal	Millipore	ab144P	-	1:100
COX5A	Mouse	Monoclonal	Abcam	ab110262	1:1000	-
COX IV	Mouse	Monoclonal	Abcam	ab14744	1:1000	-
Cytochrome C	Mouse	Monoclonal	Abcam	ab13575	1:1000	-
Dynactin 1	Rabbit	Polyclonal	Invitrogen	PA5-21289	1:1000	-
Dynein	Mouse	Monoclonal	Abcam	ab23905	1:1000	-
G3BP	Mouse	Monoclonal	Abcam	ab56574	1:1000	1:1000
GAPDH	Mouse	Monoclonal	Abcam	ab9484	1:1000	-
GFP	Rabbit	Polyclonal	Invitrogen	10474172	1:1000	1:1000

Islet 1	Mouse	Monoclonal	DSHB	40.2D6-A	-	1:100
KIF5A	Rabbit	Polyclonal	Abcam	ab5628	1:1000	-
KIF5B	Rabbit	Polyclonal	Abcam	ab25715	1:1000	-
MAP2	Rabbit	Polyclonal	Millipore	ab5622	-	1:1000
PGAM1	Rabbit	Polyclonal	Protein Tech	16126-1-AP	1:1000	-
PGK1	Mouse	Monoclonal	Abcam	ab113687	1:500	-
TAU	Mouse	Monoclonal	Millipore	MAB3420	1:500	-
*pan*TDP-43	Rabbit	Polyclonal	Protein Tech	10782-2-AP	1:1000	1:1000
TOMM20	Rabbit	Polyclonal	Abcam	ab186735	1:1000	1:1000

2.2.4. Immunofluorescence

To analyse protein expression by immunocytochemistry, motor neurons were seeded onto glass coverslips in a 24 well plate. Immunocytochemistry of motor neurons seeded into microfluidic chambers was also performed following live imaging, to examine the expression of axonal markers. In both cases, neurons were fixed in 500 μL 4% paraformaldehyde (PFA)-PBS for 20 minutes. Samples were washed three times in PBS, then blocked for 1 hour at room temperature in blocking buffer (0.1% Triton X-100, 1X PBS) supplemented with 5% normal donkey or goat serum. After blocking, coverslips were incubated overnight at 4°C with primary antibodies diluted in blocking buffer supplemented with 1% donkey or goat serum (Table 2.3). After 3 washes with 0.1% Triton-X/PBS, coverslips were incubated with fluorescently labelled secondary antibodies raised in donkey or goat; AlexaFluor®488; AlexaFluor®568, AlexaFluor®647 (1:500; Life Technologies). Secondary antibodies were diluted in blocking

buffer supplemented with 1% donkey or goat serum and incubated for 1 hour at room temperature, protected from light. Cells were then washed three times in PBS, with 4', 6-Diamidino-2-Phenylindole (DAPI) included in the second wash (1:10,000) to stain nuclei. Mounting media was not required for microscopy of microfluidic chambers, which were stored in PBS following immunocytochemistry until visualisation. Coverslips were mounted in ProLong™ Glass Antifade Mountant (Thermo Fisher Scientific) for visualisation.

To stain mitochondria in living cells, MitoTracker™ (Thermo Fisher Scientific; M7512) was prepared at 100 nM in growth medium. Cells were incubated in MitoTracker™ for 45 minutes at 37°C. Following incubation, cells were washed twice with PBS then fixed in 4% paraformaldehyde (PFA)-PBS for 20 minutes. Cells were then washed in PBS, blocked in blocking buffer and stained for TOMM20 as described above.

2.3. Analysis of mRNA expression

2.3.1. RNA extraction

Neurons were scraped in 1 mL of PBS then centrifuged at 500 *g* for 5 minutes at 4°C. RNA was extracted from the cell pellet using the RNeasy Mini Kit as per the manufacturer's instructions (Qiagen). In brief, the pellet was resuspended in 350 µL buffer RLT and the cells were homogenized through vortexing. Following homogenisation, 350 µL of 70% ethanol was then added to the lysate and the sample transferred to a RNeasy spin column inserted into a 2 mL collection tube. The sample was centrifuged for 15 seconds at 8000 *g*. The flow through was discarded and 700 µL of Buffer RW1 was added to the RNeasy spin column. Samples were centrifuged for 15 seconds at 8000 *g*. The flow through was discarded and 500 µL of

Buffer RPE was added to the spin column and again centrifuged for 15 seconds at 8000 *g*. The flow through was discarded and another 500 µL of Buffer RPE was added to the spin column and centrifuged for 15 seconds at 8000 *g* to further wash the membrane. To capture the RNA, the spin column was transferred to a new 1.5 mL collection tube and 30 µL of RNase free water was added directly into the spin column. The sample was centrifuged for 1 minute at full speed and RNA was eluted. The resultant RNA concentration was measured using a NanoDrop™ spectrophotometer, then samples stored at -80°C until further use.

2.3.2. cDNA preparation

cDNA was generated using the High-Capacity cDNA reverse transcription kit (Thermo Fisher Scientific) as described by the manufacturer. Briefly, in PCR tubes RNA was diluted with nuclease-free water to a concentration of 0.5 µg in 10 µL. A cDNA conversion master mix was then prepared as described in (Table 2.4). 10 µL of the cDNA master mix was added to the 10 µL of diluted RNA sample to generate a final reaction volume of 20 µL. Samples were then placed in a thermocycler and converted to cDNA (Table 2.5).

Table 2.4 Preparation of cDNA master mix. Volumes indicated are required per reaction.

Compound	Volume per reaction (µL)
10 X RT Buffer	2
25 X dNTPs	0.8
10 X RT Primers	2
Reverse transcriptase enzyme	1
Nuclease free H_2O	4.2

Table 2.5 cDNA conversion protocol.

Temperature (°C)	25	37	85	4
Time (minutes)	10	120	5	∞

2.3.3. Quantitative reverse transcription PCR

Quantitative reverse transcription (qRT)-PCR was performed using the Fast SYBR Green Master Mix (Thermo Fischer Scientific) with 0.5 µL cDNA and 250 µM primers (Table 2.6). Samples (10 µL) were run in triplicate on the LightCycler® 480 II (Roche). Relative change in gene expression was analysed using the $2^{-\Delta\Delta CT}$ method (Livak and Schmittgen, 2001). Expression levels were normalised to the WT and two reference genes were used for all reactions (RPL13A, 18S). The geometric mean of both genes was used as the reference for gene expression estimation.

Table 2.6 Primers for qRT-PCR.

Primer	Sequence
Human TDP-43 sense	5'-GTGTGGGCTTCGCTACAGG-3'
Human TDP-43 antisense	5'-CAACATACACCAGATTTCCCCAG-3'
Mouse TDP-43 sense	5'-ATGAGAACGATGAACCCATTGAA-3'
Mouse TDP-43 antisense	5'-TGAGACACGGGATTCCGGTAG-3'
Mouse 18S sense	5'-GAGGCCCTGTAATTGGAATGAG-3'
Mouse 18S antisense	5'-GCAGCAACTTTAATATACGCTATTGG-3'
Mouse GAPDH sense	5'-GGCTGCCCAGAACATCCCT-3'
Mouse GAPDH antisense	5'-ATGCCTGCTTCACCACCTTCTTG-3'

Mouse PGK1 sense	5'-GGTCGTGATGAGGGTGGAC-3'
Mouse PGK1 antisense	5'-CAGCAGAGATTTGAGTTCAGCA-3'

2.4. Network analysis

2.4.1. RNA sequencing

RNA sequencing of iPSC-derived motor neurons was performed by other members of the Talbot group as described elsewhere (Dafinca et al., 2020). In brief, iPSCs were differentiated to form motor neurons over several weeks. RNA was extracted from whole motor neuron cultures at day 28. The paired-end Illumina TruSeq sample preparation kit was utilised for library preparation and samples were run on the Illumina HiSeq 4000 sequencer for 75 cycles. Samples underwent quality control analysis, where samples demonstrating significant biases were removed prior to downstream analysis. In total, 4 samples from a healthy control line, 4 samples from a TDP-43^{A383T}ALS patient cell line, and 6 samples from a TDP-43^{M337V} ALS patient cell line were used in the analysis. A counts table and normalised abundances represented as transcripts per million (TPM) were obtained using *Salmon.* Differential expression analysis was performed using *DESeq2*, with Benjamini-Hochberg corrected *p* values reported for the differential expression analysis.

2.4.2. Analysis of TDP-43 interactome data

The TDP-43 interactome was analysed in work by Dr Emily Feneberg and is fully documented elsewhere (Feneberg et al., 2020). In brief, three differentiations of mESC-MNs carrying human TDP-43^{WT} or TDP-43^{M337V} were examined in basal or sodium arsenite treated conditions (0.5 mM sodium arsenite for 60 minutes). Protein was extracted and 500 μg of the

protein lysate used per immunoprecipitation reaction. YPet-tagged human TDP-43 was co-immunoprecipitated using GFP antibody-coated magnetic-agarose beads TDP-43 interactors were identified by high-performance liquid-chromatography tandem mass spectrometry (LC-MS/MS) using an Orbitrap Fusion Lumos mass spectrometer (ThermoScientific). Mass spectrometry data was analysed using Progenesis QI for Proteomics software v3.0 (Nonlinear Dynamics). Gene ontology (GO) enrichment analysis was performed using TopGo (R-studio Version 1.1.383), to investigate interactors of the TDP-43^{WT} or TDP-43^{M337V} +/- sodium arsenite interactome. The background list comprised all proteins identified over all twelve samples combined. Pathways were investigated using PANTHER and a visual network of the protein-protein interactions was generated using STRING.

2.5. Live Cell Assays

2.5.1. MTS Assay

Cellular survival was analysed using the CellTiter 96® AQ_{ueous} One Solution Cell Proliferation Assay in basal and sodium arsenite treated conditions (0.5 mM for 1 hour). mESCs were seeded into 96 well plates at a density of 100,000 cells/well. Cells were immersed in 100 µL of normal culture medium per well together with 20 µL of CellTiter 96® AQ_{ueous} One Solution Reagent and incubated at 37°C, 5% CO_2 for 3 hours. Absorbance was read at 490 nm using a 96 well plate reader.

2.5.2. Seahorse XF Extracellular Flux Assays

The Seahorse XF Cell Mito Stress Test (Agilent) was used to investigate mitochondrial function in mESC-MNs. This live-cell assay allows oxygen consumption rate to be analysed

in real-time, through the sequential addition of compounds (oligomycin, FCCP and Rotenone/Antimycin A), which inhibit components of the mitochondrial respiratory chain. This allows measurements of basal respiration, maximal respiration, ATP production and spare respiratory capacity to be calculated. The Seahorse XF Glycolytic Rate Assay (Agilent) was used to investigate glycolysis in mESC-MNs. As with the Mito Stress Test, the Glycolytic Rate Assay is a live cell assay, which allows measurement of proton efflux rate (PER) in real-time. Glycolytic rate can be measured in basal conditions, as well as compensatory glycolysis following mitochondrial inhibition with the addition of Rotenone/Antimycin A. To confirm pathway specificity, 2-deoxy-D-glucose (2-DG) is added, which inhibits glycolysis through competitive binding of glucose hexokinase. Reduction in PER following addition of 2-DG confirms PER produced prior to addition is primarily due to glycolysis.

For both assays, cells were plated in a 96 well Seahorse microplate at a density of 6.5 x 10^4 cells per well in normal growth medium and incubated at 37°C, 5% CO_2 for four days. To investigate the effects of oxidative stress on mitochondrial function, cells were incubated with growth medium supplemented with sodium arsenite at 0.5 mM for 1 hour prior to the assay. To assess mitochondrial respiration and glycolysis in basal conditions, a subset of cells was left untreated. To investigate the effects of a potential therapeutic compound, terazosin, cells were incubated with terazosin at 2.5 μM 24 hours prior to the assay. To allow uptake of the drug, media was further supplemented with 0.1% DMSO. Control cells were included that were incubated in untreated media supplemented with 0.1% DMSO. The effects of terazosin in stressed conditions were also investigated. Cells treated with 2.5 μM terazosin and 0.1% DMSO for 24 hours, followed by sodium arsenite applied at 0.5 mM for 1 hour prior to the assay. Controls were included that were not pre-treated with terazosin, but were incubated in

untreated media with 0.1% DMSO followed by sodium arsenite applied at 0.5 mM for 1 hour for one hour prior to the assay.

Following treatment, cells were washed once in Seahorse XF DMEM, supplemented with 1 mM pyruvate, 2 mM glutamine and 10 mM glucose. Motor neurons were then incubated in 180 µL Seahorse XF DMEM at 37 °C, no CO_2 for 45 minutes. For the Mito Stress Test, stock solutions were prepared for oligomycin, FCCP and Rotenone/Antimycin A. An initial dose-response experiment was performed to determine the optimal concentrations of oligomycin and FCCP to elicit the appropriate cellular response as detailed by the manufacturer (Agilent). In subsequent experiments, the sensor cartridge was then loaded with the appropriate volume and concentration of oligomycin, FCCP and Rotenone/Antimycin A (Table 2.7). For the Glycolytic Rate Assay, stock solutions were prepared for Rotenone/Antimycin A and 2-deoxy-D-glucose (2-DG). The sensor cartridge was then loaded with the appropriate volume and concentration of Rotenone/Antimycin A (50 µM) and 2-DG (500 mM) (Table 2.8). The calibration plate with the loaded sensor cartridge was then placed on the instrument tray and loaded into the Seahorse XF Analyzer to allow calibration. Following calibration, the calibration plate was removed and replaced with the cell culture microplate to run the assay. For the Glycolytic Rate Assay, 180 µL of fresh Seahorse XF media was added to each well prior to loading the cell microplate. Following completion of the assay, oxygen consumption and proton efflux rates were normalised by cell number per well using the CyQuant Cell Proliferation Assay as described below (Thermo Fisher Scientific, see section 2.4.3).

Table 2.7 Mito Stress Test compound preparation. Volumes are appropriate for loading to XFe/XF96 sensor cartridges at a starting assay medium volume of 180 µL per well.

Port	Compound	Final well conc (μM)	Stock solution (μL)	Media (μL)	Volume added to port (μL)
A	Oligomycin	1.5	450	2,550	20
B	FCCP	1	150	2,850	22
C	Rotenone/Antimycin A	0.5	300	2,700	25

Table 2.8 Glycolytic Rate Assay compound preparation. Volumes are appropriate for loading XFe/XF96 sensor cartridges a starting assay medium volume of 180 μL per well.

Port	Compound	Final well conc (μM)	Stock solution volume (μL)	Media volume (μL)	Volume added to port (μL)
A	Rotenone/Antimycin A	0.5	300	2,700	20
B	2-DG	50	3,000	0	22

2.5.3. CyQuant® Cell Proliferation Assay

Media was removed from wells of the 96 well plate and the microplate frozen at -80°C to lyse cell membranes. Following freezing, the microplate was thawed at room temperature and cell count determined using the CyQUANT® Cell Proliferation Assay (Thermo Fisher Scientific). The cell-lysis buffer stock solution (20X) was diluted in distilled water to generate a 1X cell-lysis buffer solution. Immediately prior to running the experiment, CyQUANT® GR stock solution was diluted 400-fold into the 1X cell-lysis buffer. 200 μL of the CyQUANT® GR

dye/cell-lysis buffer was added to each sample well and incubated at room temperature for 10 minutes protected from light. Sample fluorescence was then measured using a fluorescence microplate reader with filters appropriate for 480 nm excitation and 520 nm emission.

2.6. Microscopy

2.6.1. Confocal microscopy of fixed samples

Coverslips were imaged using a Zeiss Axio Observer confocal microscope and Zeiss imaging software. Images were acquired with a 63x objective and 10.24 resolution. Samples were blinded prior to imaging and analysis. Confocal images were analysed using ImageJ software (Fiji/ImageJ). To analyse TDP-43 mislocalisation, the nuclear region was identified through generating regions of interest (ROIs) in the DAPI channel, which were then applied to the TDP-43 channel. Similarly, the cytoplasmic boundary of neurons was determined using ROIs of ChAT staining. To quantify the fluorescence intensity of TDP-43 in the nuclear and cytoplasmic regions, mean grey area was multiplied by pixel count. The ratio of cytoplasmic TDP-43 to nuclear TDP-43 was then calculated. MitoTracker intensity values were normalised over TOMM20 to control for the number of mitochondria. The number of neurons with stress granules were counted and given as a percentage of the total cell number. The number and area of stress granules per neuron were analysed using a Fiji/ImageJ plugin, for the recognition of stress granules of between 100 nm^2 and 1.5 μm^2 (Figure 2.1A, Fiji version 2.1.0/1.53c of ImageJ). Co-localisation was performed using the JaCoP plugin in Fiji/Image J (Figure 2.1B).

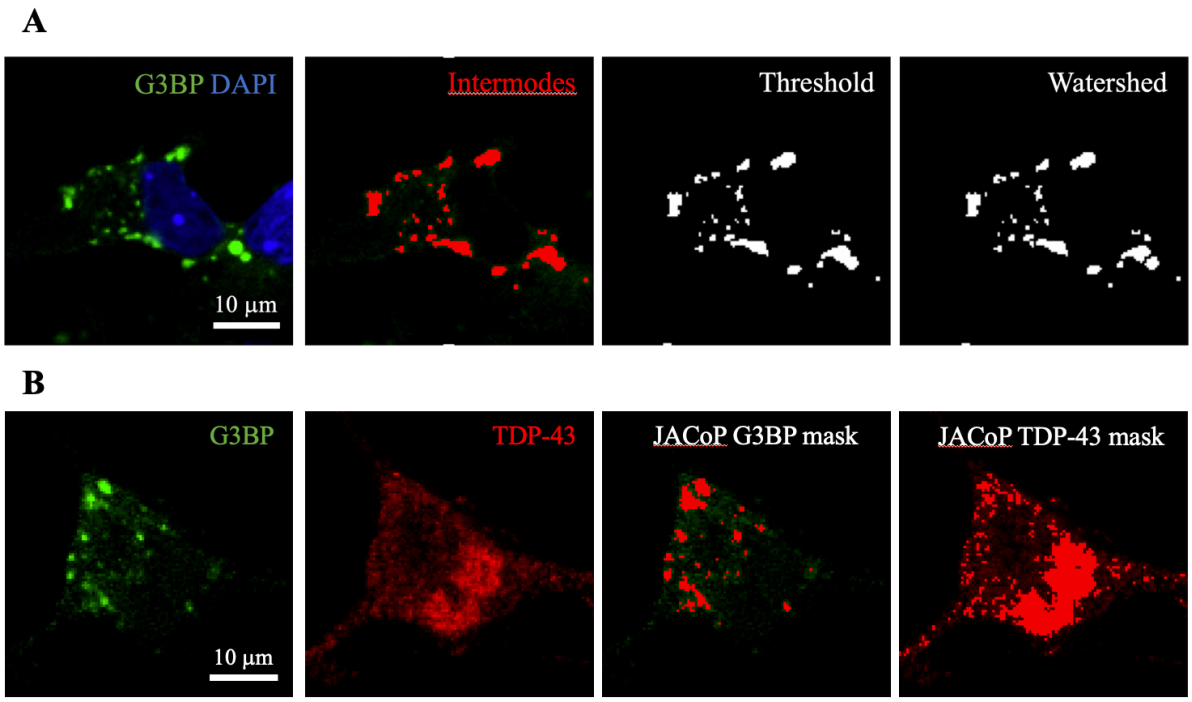


Figure 2.1 Stress granule quantification and co-localisation analysis in FIJI/ImageJ. **A** Stress granule size and number quantified through thresholding with the 'intermodes' algorithm and Watershed plugin in FIJI/ImageJ. **B** TDP-43 and G3BP co-localization analysis using the JACoP plugin in FIJI/ImageJ.

2.6.2. Live cell microscopy

Microfluidic chambers (Xona, RD450) were plasma bonded to glass-bottomed dishes (Wilco) by a 2-minute treatment at 300-500 millitorr. Devices were coated in poly-l-ornathine overnight at 4°C (1:10 in sterile water), then washed in sterile water and coated in laminin (2.5 µg/mL in HBSS) overnight at 4°C. Neuronal progenitors were plated into the top left-hand side of the microfluidic chambers at a density of approximately 100,000 cells per chamber in 5 µL growth media. Media on the right-hand side of the chamber was supplemented with growth factors (BDNF, GDNF, CNTF and NT-3) at 10X higher concentration (100 ng/mL), to encourage axons to extend through the channels. To allow sufficient time for the axons to extend across the channels, chambers were imaged 5-10 days after plating. Mitochondrial transport was assessed using MitoTracker™ Red CMXRos (M7512). Cells were treated with

MitoTracker at 20 nM in normal growth media for 20 minutes at 37 °C. Cells were then washed in PBS and imaging solution applied to the chambers. Cholera toxin subunit-B (CTB) is an extensively studied and highly efficient retrograde tracer, which is taken up into signalling endosomes in neurons. CTB AlexaFluor® 488 conjugate (Invitrogen, C34775) was added to the axonal side of the microfluidic chamber at 50 ng/mL in normal growth media for 30 minutes at 37 °C. Cells were then washed in PBS and imaging solution applied to the chambers. Live imaging was performed using the Zeiss Axio Observer 7 spinning disk microscope, with images taken every 2 seconds over 300 frames at 63X magnification in the confocal setting. To confirm axonal identity within microgrooves, chambers were stained for the axonal marker TAU and the dendritic marker MAP2. Analysis of bi-directional mitochondria and signalling endosome transport was performed using the difference tracker FIJI/Image J plugin developed by Andrews and colleagues (Andrews et al., 2010). Subsequent analysis was conducted in R using a script developed by Dr Jakub Scaber in Python to analyse various parameters of particle movement including average speed, maximum speed, direction of movement, pausing time and distance travelled.

2.7. Statistical analysis

Statistical analyses were performed using GraphPad Prism 9 (GraphPad Software Inc., CA USA). All data were examined for normality and statistical tests were chosen accordingly. A two-tailed unpaired Student's *t*-test was performed where indicated for comparison of two groups. In the case of not normally distrusted data, the Mann-Whitney U test was performed for comparison of two groups. When comparing relative protein expression in TDP-43^{M337V} mESC-MNs to a normalised TDP-43^{WT} control value, a one-sample *t*-test was performed with the hypothetical value set to 1. For normally distributed data where three or more groups were

compared, a one-way ANOVA was used followed by Dunnett's multiple comparison test. For normally distributed data where three or more groups were compared across two independent variables, a two-way ANOVA was performed with Bonferroni's multiple comparisons test. The null hypothesis was rejected at a significance level of $p = 0.05$. For all experiments involving mESC-MNs a minimum of 3*n* biological replicates were included unless otherwise stated.

CHAPTER 3 Investigating the effects of increased culture duration on cellular phenotypes in mESC-MNs

3.1. Introduction and aims

3.1.1. A physiologically relevant model for studying the effects of TDP-43 mutations

The majority of studies investigating the role of TDP-43 in ALS pathogenesis have relied on overexpression models of WT or mutant forms of TDP-43. However, the relevance of such models to investigating the mechanisms underlying neurodegeneration is unclear. Given that TDP-43 overexpression is itself toxic, more physiologically relevant models that express TDP-43 at lower levels may provide greater insight into how mutant forms of TDP-43 contribute to neurodegeneration. Our group has previously developed a BAC transgenic mouse model, which carries the entire genomic locus of the human *TARDBP* gene. In addition to mouse endogenous TDP-43, these mice express either human TDP-43^{WT} or TDP-43^{M337V} at low levels. By limiting TDP-43 overexpression, this model allows probing of disease-specific mechanisms linked to the expression of mutant forms of human TDP-43. TDP-43^{M337V} mice demonstrate reduced survival and progressive motor dysfunction compared to TDP-43^{WT} controls (Gordon et al., 2019). TDP-43^{M337V} mice also demonstrate impaired retrograde transport of signalling endosomes in the sciatic nerve, which precede the onset of a motor phenotype at 6 months (Sleigh et al., 2020). Moreover, primary motor neurons extracted from the spinal cords of TDP-43^{M337V} embryonic mice demonstrate striking TDP-43 mislocalisation and altered stress granule characteristics compared to TDP-43^{WT} controls (Gordon et al., 2019).

The TDP-43^{M337V} BAC transgenic mouse has provided valuable insight into the potential pathological processes that may underlie TDP-43-linked neurodegeneration. However *in vitro* model systems are crucial to allow further probing of neurodegenerative processes, by providing a high-throughput platform for phenotypic screening and therapeutic testing. In addition to the BAC transgenic mouse, our group also generated *in vitro* HEK cell and mESC-MN models, which stably express the TDP-43^{WT} and TDP-43^{M337V} BAC genetic constructs. TDP-43 mislocalisation, stress granule dynamics and survival have previously been characterised in these models, yielding a variety of phenotypes linked to the expression of TDP-43^{M337V}. In HEK cells, expression of TDP-43^{M337V} led to increased TDP-43 mislocalisation following oxidative stress, which was not detected in HEK cells expressing TDP-43^{WT} (Mutihac et al., 2015). Whilst no detectable TDP-43 mislocalisation was observed in mESC-MNs, expression of TDP-43^{M337V} resulted in altered stress granule characteristics, including fewer stress granules per neuron, smaller stress granules and fewer motor neurons positive for stress granules. TDP-43^{M337V} mESC-MNs have also been shown to exhibit reduced viability in response to oxidative stress compared to TDP-43^{WT} motor neurons (Feneberg et al., 2020; Gordon et al., 2019).

3.1.2. Unmasking of phenotypes in cellular models with ageing

Phenotypes in mESC-MNs are typically examined after 3 days *in vitro* (Bryson et al., 2014). Nonetheless, several studies investigating mutant phenotypes in iPSC-MN models of ALS, have unmasked phenotypes through "ageing" motor neurons *in vitro* which were not observed at earlier time points. Kreiter and colleagues investigated the effects of ageing motor neurons *in vitro* on neurodegenerative phenotypes in healthy control and mutant TDP-43 iPSC-MNs. Following ageing up to 32 days *in vitro* they observed a number of neurodegenerative

phenotypes specifically in mutant TDP-43 motor neurons, including neuronal loss, disrupted cytoskeletal morphology, disrupted lysosome and mitochondria morphology and transport. These phenotypes were not apparent after only 5 days *in vitro* (Kreiter et al., 2018). Similarly, Fujimori and colleagues identified a reduction in the neurite length of iPSC-MNs from sporadic ALS patients, that was not detected after 20 days *in vitro* but became apparent after 40 days *in* vitro (Fujimori et al., 2018). Given this, it was hypothesised that maintaining mESC-MNs *in vitro* for an extended period prior to analysis may exacerbate existing phenotypes and/or unmask novel phenotypes that are not observed at earlier time points.

3.1.3. Aims

The overall goal of the work described in this chapter was to investigate whether phenotypes could be unmasked or exacerbated by increasing the culture duration of mESC-MNs prior to analysis. The specific aims of this chapter were to:

1. Differentiate mESCs to motor neurons and confirm expression of the exogenous *TARDBP* BAC construct.
2. Investigate the effects of increasing culture duration on the expression of synaptic markers in mESC-MNs.
3. Investigate the effects of increasing culture duration of mESC-MNs on TDP-43 mislocalisation.
4. Investigate the effects of increasing culture duration of mESC-MNs on stress granule formation and on TDP-43 and stress granule co-localisation.
5. Investigate the effects of increasing culture duration of mESC-MNs on cell viability.

3.2. Results

3.2.1. mESCs differentiate to motor neurons and express the exogenous *TARDBP* BAC construct

mESCs were plated onto primary mouse embryonic fibroblasts (PMEFs) and differentiated in ADFNK media supplemented with RA, SAG and growth factors. RA induces a caudal (spinal cord) identity, while addition of SAG, a small molecule agonist of the Shh signalling pathway, promotes ventralisation (Davis-Dusenbery et al., 2014). mESCs began to extend processes after 13 days, and by day 15 (DIV 3) clusters of neurons could be observed *in vitro* (Figure 3.1). Successful differentiation of mESCs to motor neurons was confirmed by the expression of motor neuron markers including beta III tubulin, islet 1 and choline acetyltransferase (ChAT) (Figure 3.2A). Quantification of ChAT expression confirmed a differentiation efficiency of approximately 80% at each specified timepoints, for both TDP-43^{WT} and TDP-43^{M337V}expressing motor neurons (Figure 3.2B-C).

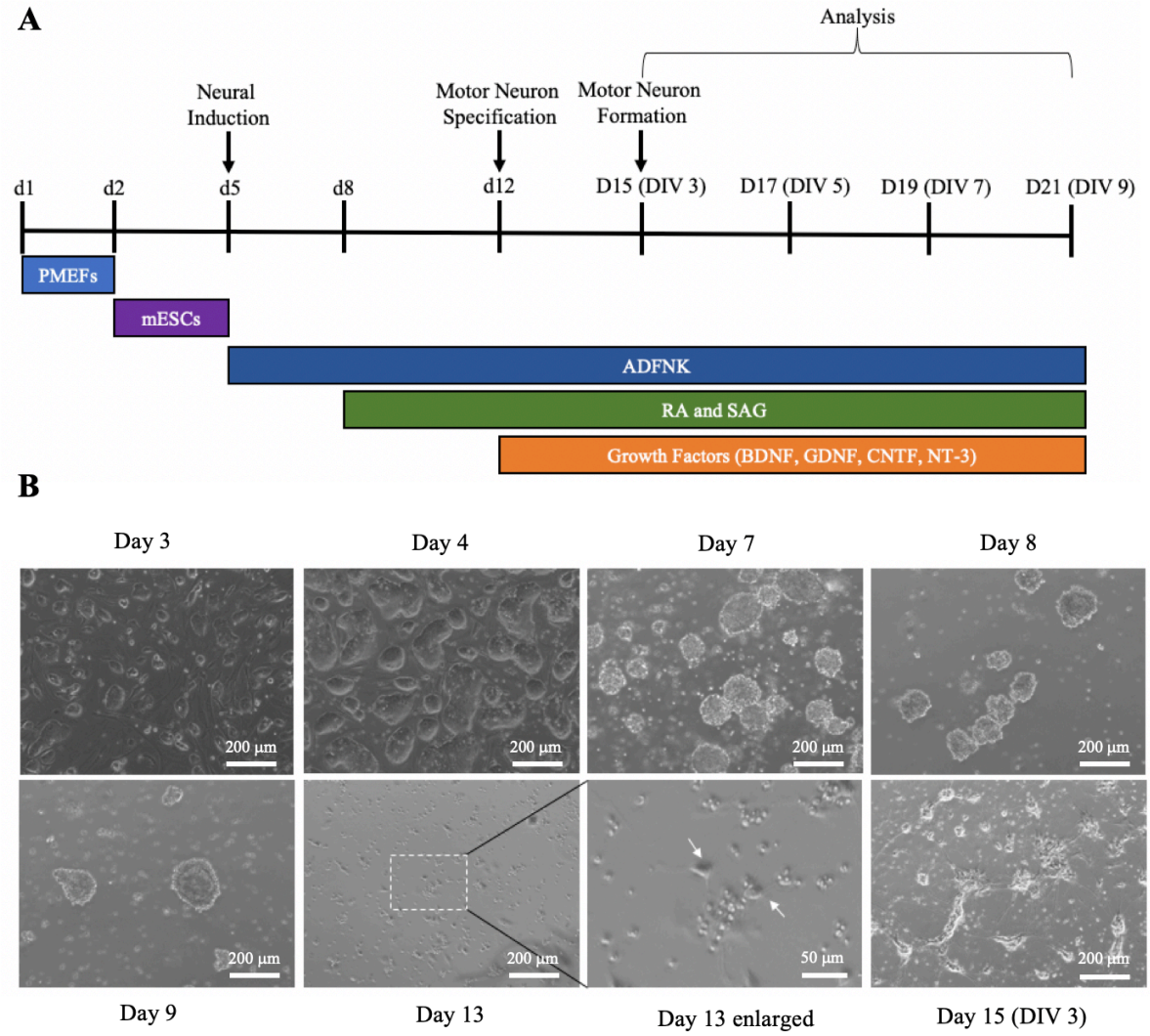


Figure 3.1 Differentiation of mESCs to form motor neurons. A mESC-MNs were plated onto primary mouse embryonic fibroblasts (PMEFs) and cultured in ADFNK media supplemented with retinoic acid (RA), smoothened agonist (SAG) and growth factors to induce motor neuron formation. Motor neurons were formed at day 15, 3 days after seeding *in vitro* (DIV 3). To assess the effects of increasing culture duration on cellular phenotypes, mESC-MNs were maintained *in vitro* and examined after 5, 7 and 9 days *in vitro* (DIV 5, DIV 7, DIV 9). **B** Images depicting the differentiation of mESCs to motor neurons. At day 13, one day after seeding, the motor neurons begin to form processes (white arrows), with networks of neurons formed by day 15 (DIV 3). Images taken at 10X magnification.

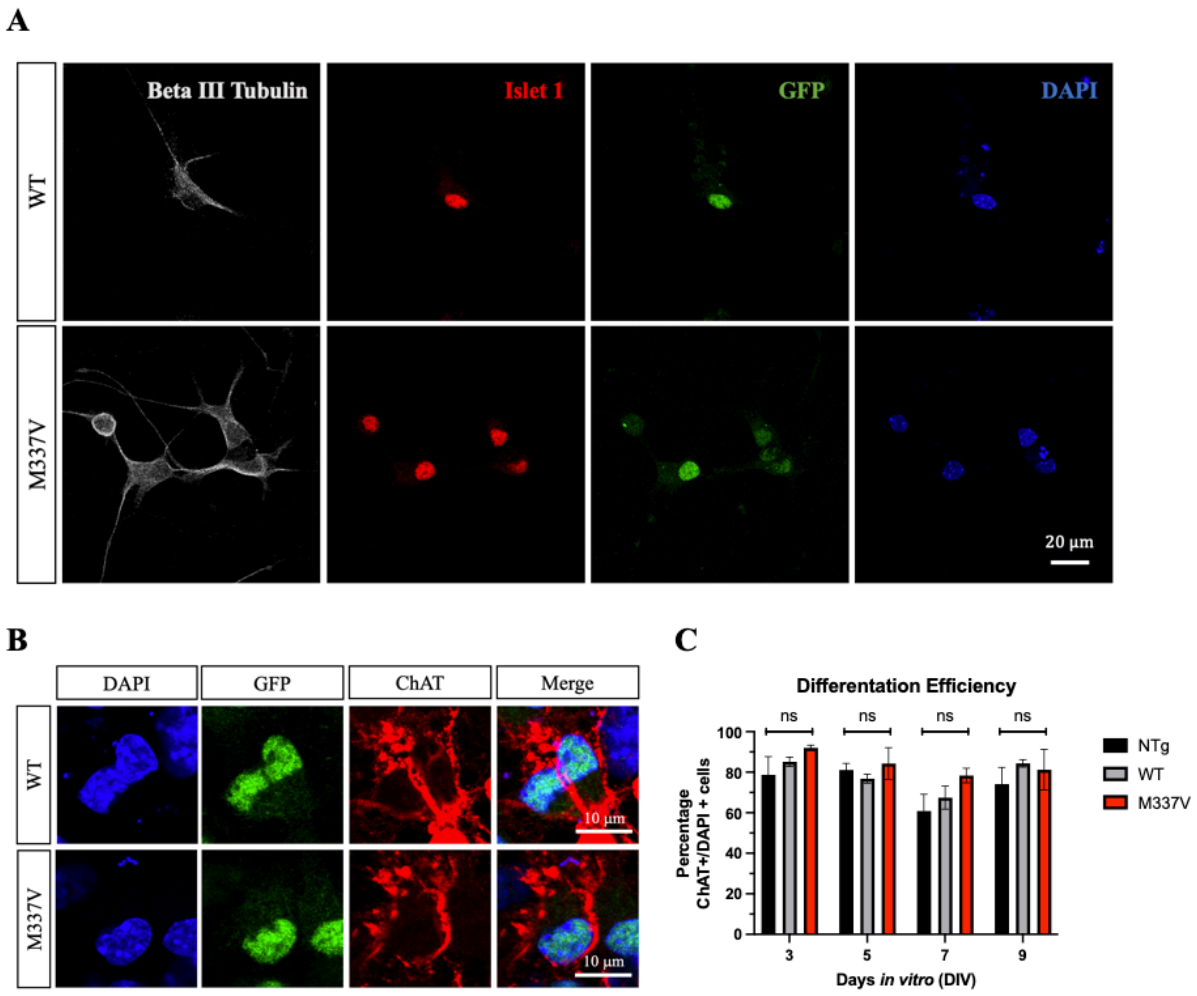


Figure 3.2 Expression of motor neuron markers in mESC-MNs. A After 3 days *in vitro* (DIV 3), mESC-MNs express the pan-neural marker beta III tubulin and the motor neuron progenitor marker islet 1. Expression of GFP confirms the presence of the Ypet-tagged exogenous human *TARDBP* construct. **B** mESC-MNs express the post-mitotic motor neuron marker choline acetyltransferase (ChAT). **C** Differentiation efficiency based on the percentage of ChAT positive cells in non-transgenic (NTg), TDP-43^{WT} (WT) and TDP-43^{M337V} (M337V) mESC-MNs at DIV 3-9. Two-way ANOVA with Dunnett's multiple comparisons, error bars SEM, $n = 3$.

mESC-MNs incorporated a *TARDBP* BAC genetic construct, which contains the entire genomic locus of the human *TARDBP* gene, integrated in a single copy into the mouse Rosa26 locus. The Rosa26 locus lies within exon 6 and is a popular locus used for the integration of transgene constructs in mice, which can result in either ubiquitous or conditional gene expression (Friedrich & Soriano, 1991; Zambrowicz et al., 1997). In mESC-MNs, integration of the *TARDBP* BAC construct into this region results in the expression of either TDP-43^{WT} or

the TDP-43^{M337V} mutant form of the protein, where the latter contains a single base pair change in exon 6 of the *TARDBP* gene (Figure 3.3A). To confirm expression of the construct in mESC-MNs, DNA isolated from cells was amplified through PCR, with primers pairs specific to amplify exon 6 of the human *TARDBP* and the mouse *Tardbp* gene. Sequencing of the resultant PCR product confirmed the presence of the wild-type (WT) and M337V mutant human *TARDBP* constructs, with the A to G mutation in M337V mESC-MNs (Figure 3.3B-C). Quantitative PCR (q-PCR) was performed to investigate mRNA expression of endogenous mouse *Tardbp* and exogenous human *TARDBP*, carried by the BAC construct, in mESC-MNs. RNA from TDP-43^{WT} and TDP-43^{M337V} mESC-MNs was extracted and converted to cDNA. RT-qPCR was then performed and relative change in gene expression analysed using the $2^{-\Delta\Delta CT}$ method. RT-qPCR confirmed the expression of similar levels of mouse endogenous *Tardbp* and human exogenous *TARDBP* mRNA in TDP-43^{WT} and TDP-43^{M337V} mESC-MNs (Figure 3.4A). Western blot analysis was performed to assess protein expression of endogenous and exogenous TDP-43, using a *pan*TDP-43 antibody. Results confirmed expression of endogenous mouse TDP-43 in TDP-43^{WT} and TDP-43^{M337V} mESC-MNs, with a band detected at 43 kDa. Expression of exogenous human TDP-43 was also observed in TDP-43^{WT} and TDP-43^{M337V} mESC-MNs, with a band detected at 72 kDa; the higher molecular weight resulting from inclusion of the Ypet tag (Figure 3.4B). Quantification confirmed comparable levels of endogenous mouse TDP-43 expression, in TDP-43^{NTg}, TDP-43^{WT} and TDP-43^{M337V} mESC-MNs (Figure 3.4C). Exogenous human TDP-43 was also expressed at similar levels in both TDP-43^{WT} and TDP-43^{M337V} mESC-MNs, and at approximately 0.4-fold and 0.6-fold respectively, relative to endogenous mouse TDP-43 expression (Figure 3.4D).

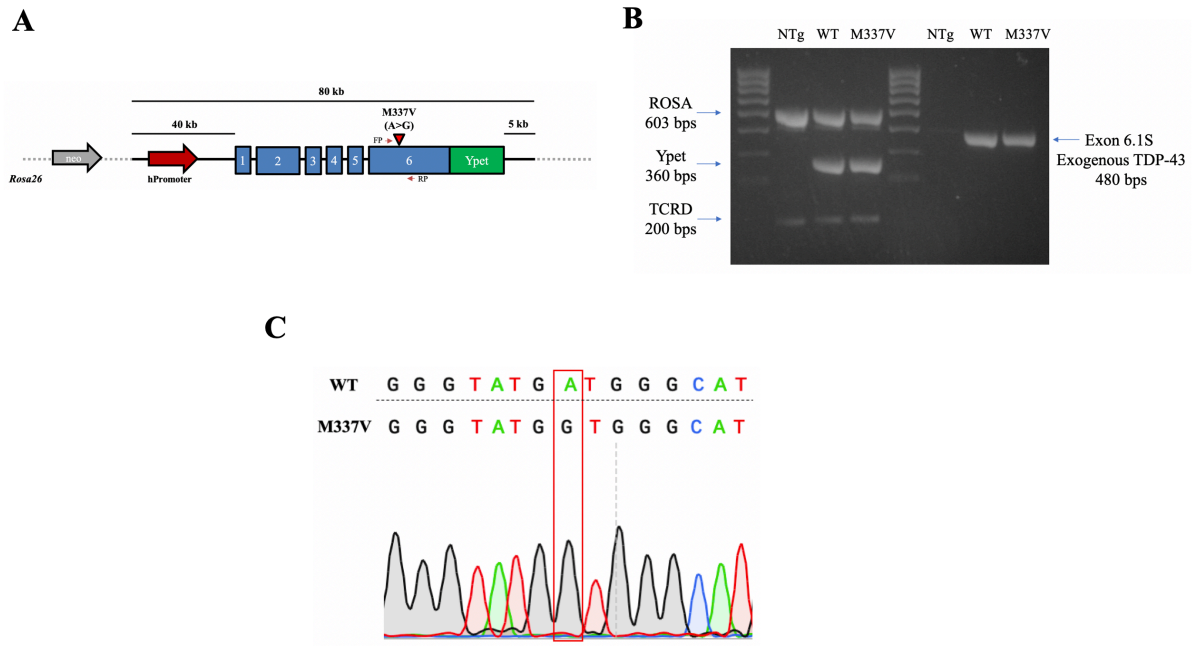


Figure 3.3 mESC-MNs express exogenous human TDP-43 and endogenous mouse Tdp43. A mESCs express full-length exogenous human *TARDBP* targeted to the ROSA26 locus, with either the wild-type (WT) form of the protein, or the M337V mutant form (single base pair change in exon 6 from A to G). The construct carries a Ypet tag. The approximate location of forward (FP) and reverse (RP) primers is indicated by red arrows. Adapted from Gordon *et al.,* 2019. **B** Expression of the Ypet tag and exogenous human TDP-43 in TDP-43^{WT} and TDP-43^{M337V} mESC-MNs is confirmed by PCR. **C** Expression of the single base pair change from A to G in exon 6 in TDP-43^{M337V} mESC-MNs is confirmed with Sanger sequencing.

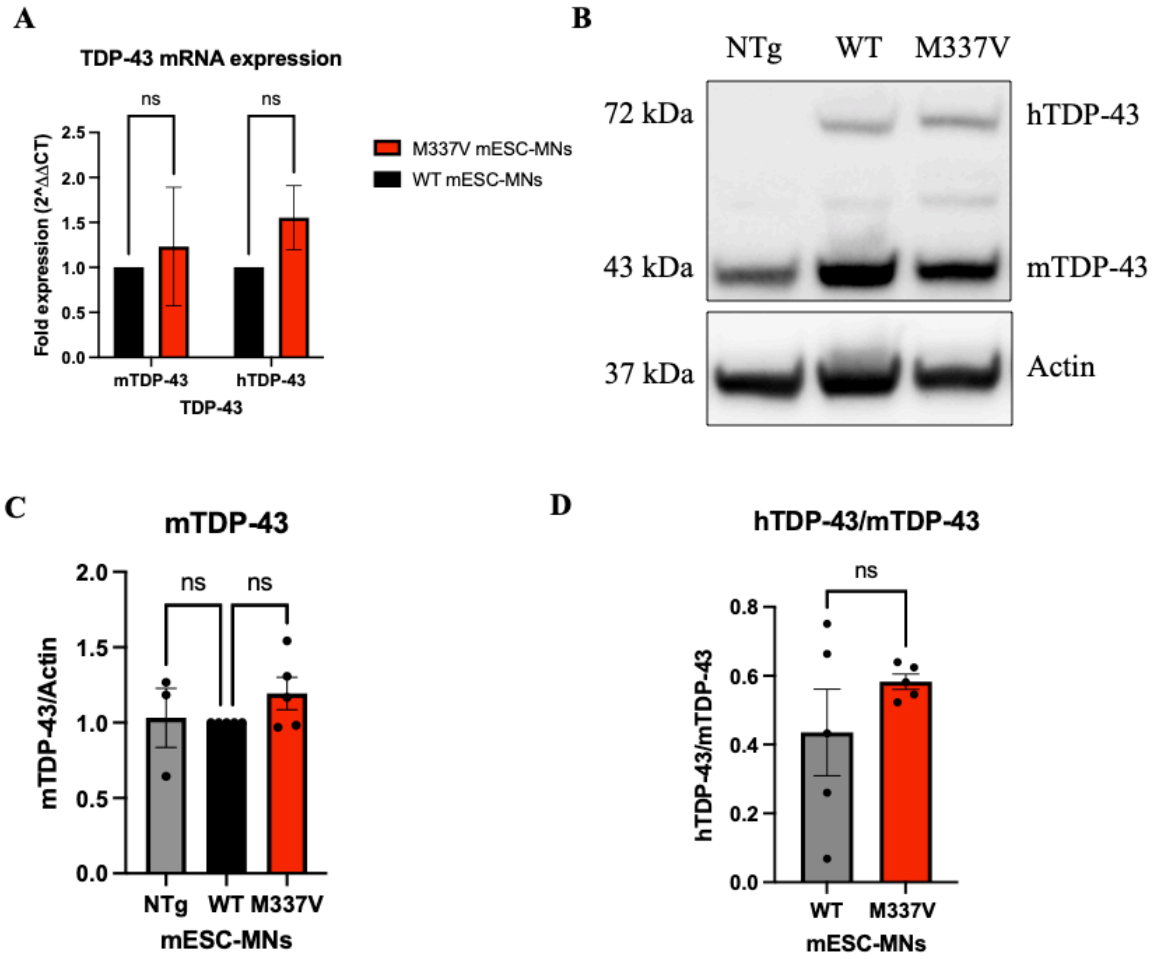


Figure 3.4 TDP-43 expression in mESC-MNs. A Quantitative RT-PCR confirms mRNA expression of mouse endogenous (mTDP-43) and human exogenous TDP-43 (hTDP-43), carried by the BAC construct, in TDP-43^{WT} and TDP-43^{M337V} mESC-MNs. Two-way ANOVA with Dunnett's multiple comparisons (n = 2), error bars SEM **B** Western blotting confirms expression of mouse endogenous TDP-43 protein (mTDP-43) in all mESC-MNs (NTg, WT and M337V) and human exogenous TDP-43 protein (hTDP-43), carrying the Ypet tag, at 72 kDa only in TDP-43^{WT} and TDP-43^{M337V} mESC-MNs expressing the BAC construct. **C** Quantification of Western blot results confirms comparable expression of mouse endogenous TDP-43 (mTDP-43) in TDP-43^{NTg}, TDP-43^{WT} and TDP-43^{M337V} mESC-MNs. One-way ANOVA with Dunnett's multiple comparisons (n = 5 for all except TDP-43^{NTg} where n = 3), error bars SEM. **D** Western blot quantification of human exogenous TDP-43 protein expression relative to that of mouse endogenous TDP-43. Unpaired t-test (n = 5), error bars SEM.

3.2.2. Increasing culture duration does not significantly increase the expression of synaptic markers in mESC-MNs

To assess the effects of increasing culture duration on neuronal maturity, I investigated the expression of synaptic markers at various time points. Time points were chosen based on previously published protocols investigating the effects of 'ageing' iPSC-MNs *in vitro*. Fujimori and colleagues investigated the effects of maturing iPSC-MNs *in vitro,* by first examining phenotypes at 20 days post seeding, then again at various time points until a final time point of 60 days; where neurons were cultured for three times as long as the initial time point examined (Fujimori et al., 2018). The time required for differentiation of mESC-MNs is much less, with motor neurons formed after as little as 3 days post seeding in motor neuron differentiation medium. Given this, phenotypes were examined at the initial time point of 3 days *in vitro* (DIV 3), then after 5 days *in vitro* (DIV 5) and 7 days *in vitro* (DIV 7), and at a final time point of 9 days *in vitro* (DIV 9).

To investigate the effects of increasing culture duration on neuronal maturation, the expression of synaptic markers was examined at each of the pre-specified time points (DIV 3-9). mESC-MNs were probed for synaptophysin and SV2A; two integral membrane glycoproteins localised to synaptic vesicles (Figure 3.5A). Synaptophysin integrated density was not significantly altered by increasing culture duration in either TDP-43^{WT} or TDP-43^{M337V} mESC-MNs (TDP-43^{WT}: DIV 3 vs. DIV 9, $p = 0.1034$ ($n = 3$); TDP-43^{M337V}: DIV 3 vs. DIV 9, $p = 0.9739$ ($n = 3$); Figure 3.5B). The integrated density of SV2A in TDP-43^{WT} mESC-MNs was not significantly altered by increasing culture duration (DIV 3 vs. DIV 9, $p = >0.999$ ($n = 3$); Figure 3.5C). SV2A integrated density was found to increase in TDP-43^{M337V} mESC-MNs with increasing culture duration, from approximately 300 pixels on DIV 3 to approximately 450

pixels on DIV 9, but this increase was not significant (DIV 3 vs. DIV 9, $p = 0.9264$ ($n = 3$); Figure 3.5C). The number of synaptophysin particles identified in TDP-43^{WT} and TDP-43^{M337V} mESC-MNs was not significantly affected by increasing culture duration (TDP-43^{WT}: DIV 3 vs. DIV 9 $p = 0.4115$ ($n = 3$); TDP-43^{M337V}: DIV 3 vs. DIV 9 $p = 0.6508$ ($n = 3$); Figure 3.5D). Similarly, the number of SV2A particles was not significantly altered by increasing culture duration (TDP-43^{WT}: DIV 3 vs. DIV 9, $p = 0.9032$ ($n = 3$); TDP-43^{M337V}: DIV 3 vs. DIV 9, $p = > 0.999$ ($n = 3$); Figure 3.5E). Together, these findings suggest that increasing culture duration from DIV 3 up to DIV 9 does not significantly alter neuronal maturity as measured by the expression of synaptic markers.

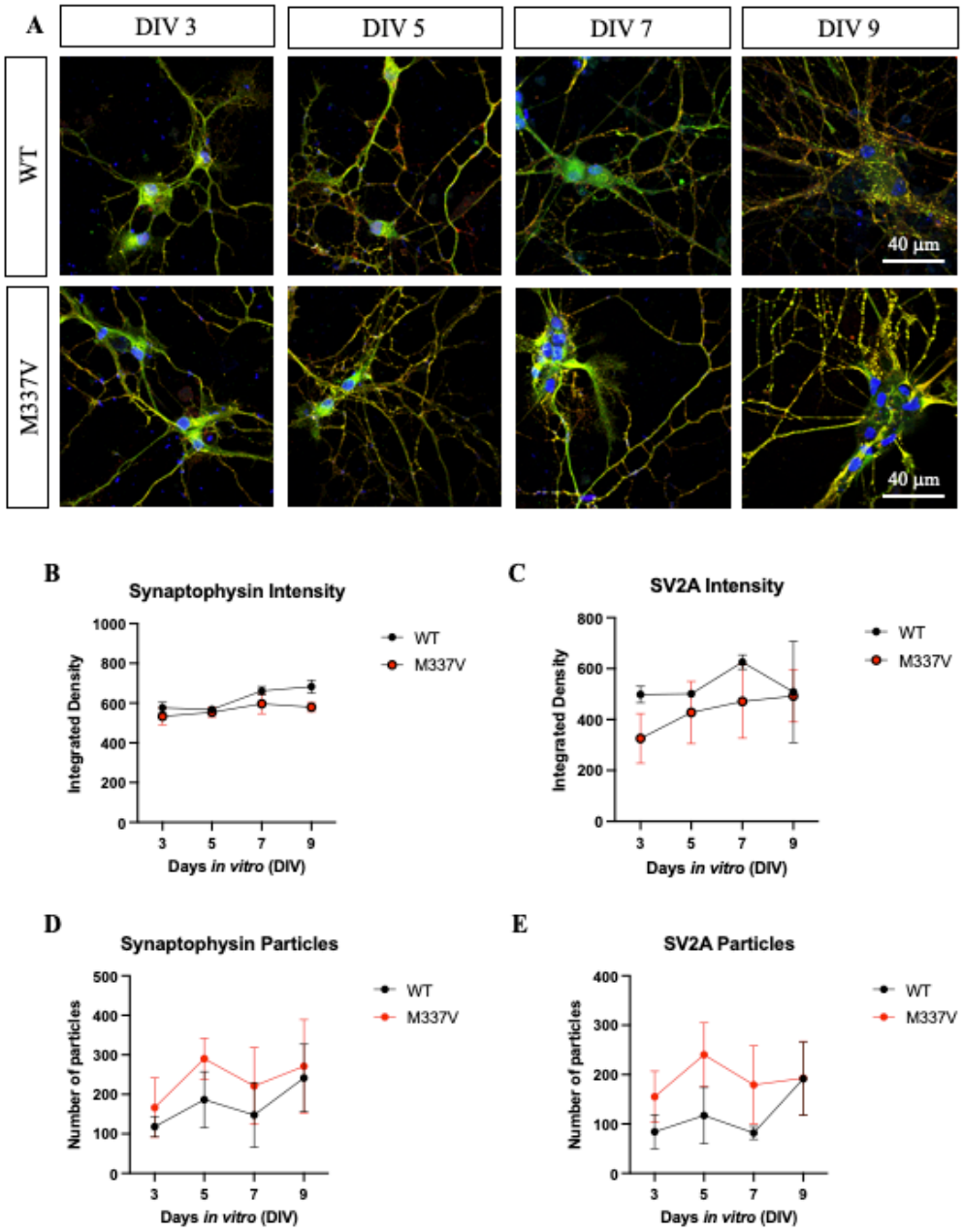


Figure 3.5 mESC-MNs express synaptic markers in vitro. A Expression of SV2A and synaptophysin in mESC-MNs at 3, 5, 7 and 9 days *in vitro* (DIV 3-9). **B** Synaptophysin integrated density in TDP-43^{WT} (WT) and TDP-43^{M337V} (M337V) mESC-MNs at DIV 3-9, n = 3. **C** SV2A integrated density in TDP-43^{WT} (WT) and TDP-43^{M337V} (M337V) mESC-MNs at DIV 3-9, n = 3. **D** Number of synaptophysin particles in TDP-43^{WT} (WT) and TDP-43^{M337V} (M337V) mESC-MNs at DIV 3-9, n = 3. **E** Number of SV2A particles in TDP-43^{WT} (WT) and TDP-43^{M337V} (M337V) mESC-MNs at DIV 3-9. Statistics for B-E: Two-way ANOVA with Dunnett's multiple comparisons (n = 3), error bars SEM.

3.2.3. Investigating the effects of increasing culture duration on TDP-43 mislocalisation in mESC-MNs

Mislocalisation of TDP-43, from a primarily nuclear to a primary cytoplasmic distribution, is the pathological hallmark of ALS. Previous work has identified significant TDP-43 mislocalisation in primary motor neurons derived from the spinal cords of embryonic TDP-43^{M337V} mice, which was not observed in primary motor neurons derived from TDP-43^{WT} mice. However, no TDP-43 mislocalisation was observed in TDP-43 mESC-MNs carrying the same BAC genetic construct, that were differentiated *in vitro* (Gordon et al., 2019). Based on previous studies whereby maturing motor neurons led to the development of pathological phenotypes, it was hypothesised that TDP-43 mislocalisation may be uncovered by culturing mESC-MNs for an extended period *in vitro*. I sought to investigate whether increasing culture duration leads to increased TDP-43 mislocalisation in TDP-43^{M337V} mESC-MNs. To investigate whether oxidative stress exacerbated mislocalisation relative to the unstressed conditions, motor neurons were treated with sodium arsenite at 0.5 mM for 60 minutes prior to fixation.

Immunocytochemistry was performed to detect total cellular TDP-43, including both endogenous mouse and exogenous human TDP-43 (Figure 3.6A). Motor neurons were counterstained for DAPI to determine the nuclear region and ChAT to identify the cytoplasmic boundary of individual neurons (data not shown). I first examined whether differences in the cytoplasmic localisation of TDP-43 could be detected between TDP-43^{WT} and TDP-43^{M337V} at DIV 3. In unstressed conditions, no significant differences were observed in the ratio of cytoplasmic to nuclear TDP-43 (endogenous + exogenous) between TDP-43^{WT} and TDP-43^{M337V} mESC-MNs at DIV 3 (Mann Whitney test, $p = 0.7616$, $n = 3$; Figure 3.6B). In both

cases, a ratio of approximately 0.20 was observed, suggesting TDP-43 is predominantly localised to the nucleus in both TDP-43^{WT} and TDP-43^{M337V} mESC-MNs in unstressed conditions. Increasing culture duration up to DIV 9 did not significantly increase the proportion of cytoplasmic TDP-43 in either TDP-43^{WT} or TDP-43^{M337V} mESC-MNs. Conversely, the proportion of cytoplasmic TDP-43 dropped by approximately 40% relative to that observed at DIV 3 in both TDP-43^{WT} and TDP-43^{M337V} mESC-MNs, although this reduction was not significant (TDP-43^{WT}: DIV 3 vs DIV 9, two-way ANOVA, $p = 0.3541$; TDP-43^{M337V}: DIV 3 vs DIV 9, two-way ANOVA, $p = 0.2341$; Figure 3.6C). Following oxidative stress, the proportion of cytoplasmic to nuclear TDP-43 was not significantly different in TDP-43^{WT} and TDP-43^{M337V} mESC-MNs, with a ratio of approximately 0.15 observed in both cases (Mann Whitney test, $p = 0.9815$, $n = 3$; Figure 3.6D). Increasing culture duration did not significantly alter the cellular distribution of TDP-43 following oxidative stress, although the proportion of TDP-43 dropped by approximately 30% relative to that observed at DIV 3 in both TDP-43^{WT} and TDP-43^{M337V} mESC-MNs (TDP-43^{WT}: DIV 3 vs DIV 9, two-way ANOVA, $p = 0.2748$; TDP-43^{M337V}: DIV 3 vs DIV 9, two-way ANOVA, $p = 0.3477$; Figure 3.6E). These observations suggest that the cellular distribution of TDP-43 is not significantly different between TDP-43^{WT} and TDP-43^{M337V} mESC-MNs. Additionally, comparisons of unstressed and stressed conditions suggest that oxidative stress induced by sodium arsenite does not alter the cellular distribution of TDP-43.

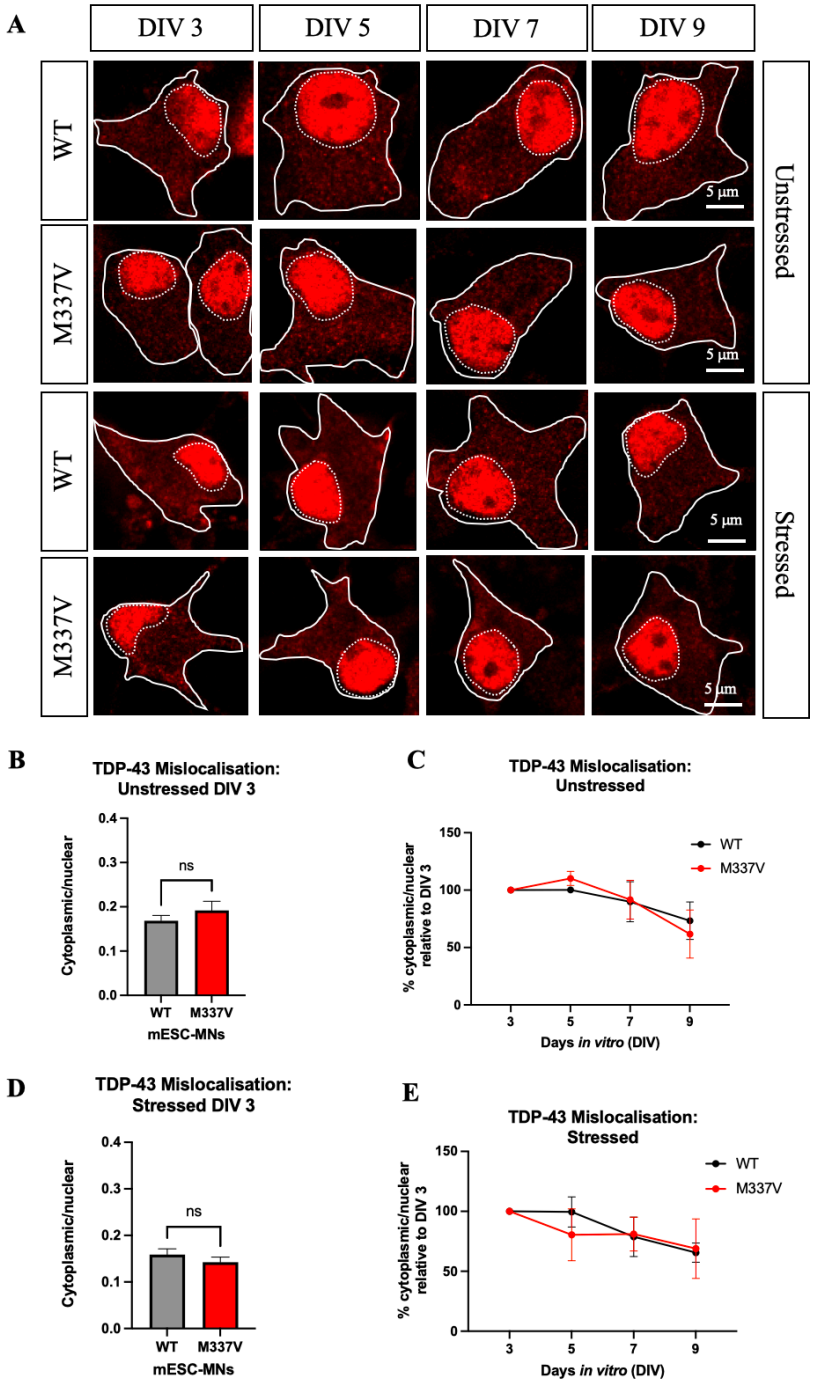


Figure 3.6 mESC-MNs do not demonstrate TDP-43 mislocalisation. **A** TDP-43 localisation in TDP-43^{WT} and TDP-43^{M337V} mESC-MNs at 3, 5, 7 and 9 days *in vitro* (DIV 3-9) in unstressed and oxidative stressed (sodium arsenite) conditions. White lines indicate the cytoplasmic boundary, with the nuclear boundary depicted by white dotted lines (DAPI not shown). **B** Ratio of cytoplasmic to nuclear TDP-43 at DIV 3 in unstressed conditions. Mann Whitney test ($n = 3$), error bars SEM. **C** Effects of increasing culture duration on the ratio of cytoplasmic to nuclear TDP-43 relative to DIV 3. Two-way ANOVA with Dunnett's multiple comparisons ($n = 3$), error bars SEM. **D** Ratio of cytoplasmic to nuclear TDP-43 at DIV 3 following oxidative stress induced by sodium arsenite. Mann Whitney test ($n = 3$), error bars SEM. **E** Effects of increasing culture duration on the ratio of cytoplasmic to nuclear TDP-43 relative to DIV 3 following oxidative stress. Two-way ANOVA with Dunnett's multiple comparisons ($n = 3$), error bars SEM.

I next sought to examine whether the cellular distribution of human TDP-43 was significantly different between TDP-43^{WT} and TDP-43^{M337V} mESC-MNs. Immunocytochemistry was performed for GFP, to detect the Ypet tag carried by the exogenous BAC construct (Figure 3.7A). In addition, mESC-MNs were stained for DAPI and ChAT as described previously (data not shown). I first investigated whether differences in the cellular distribution of GFP-TDP-43 between TDP-43^{WT} and TDP-43^{M337V} could be observed at DIV 3. In unstressed conditions, no significant differences were observed in the ratio of cytoplasmic to nuclear GFP-TDP-43 between TDP-43^{WT} and TDP-43^{M337V} mESC-MNs at DIV 3 (Mann Whitney test, $p = 0.2577$, $n = 3$; Figure 3.7B). A ratio of between 0.20 and 0.25 was observed in TDP-43^{WT} and TDP-43^{M337V} mESC-MNs respectively, suggesting GFP-TDP-43 is predominantly localised to the nucleus in both cases. Increasing culture duration up to DIV 9 reduced proportion of cytoplasmic TDP-43, with the ratio of cytoplasmic to nuclear TDP-43 reduced by approximately 20% relative to that observed at DIV 3 in both TDP-43^{WT} and TDP-43^{M337V} mESC-MNs, although this reduction was not significant (TDP-43^{WT}: DIV 3 vs DIV 9, two-way ANOVA, $p = 0.6081$; TDP-43^{M337V}: DIV 3 vs DIV 9, two-way ANOVA, $p = 0.7486$; Figure 3.7C). Following oxidative stress, the proportion of cytoplasmic to nuclear TDP-43 was not significantly different in TDP-43^{WT} and TDP-43^{M337V} mESC-MNs, with a ratio of approximately 0.15 observed in both cases (Mann Whitney test, $p = 0.4259$, $n = 3$; Figure 3.7D). Although not significant, increasing culture duration led to a reduction in the percentage of cytoplasmic GFP-TDP-43 (TDP-43^{WT}: DIV 3 vs DIV 9, two-way ANOVA, $p = 0.2520$; TDP-43^{M337V}: DIV 3 vs DIV 9, two-way ANOVA, $p = 0.3304$; Figure 3.7E). A 30-40% reduction in the ratio of cytoplasmic to nuclear TDP-43 was observed at DIV 9 in both TDP-43^{WT} and TDP-43^{M337V} relative to DIV 3. These findings mirror observations of the cellular distribution of total cellular TDP-43, and suggest that expression of TDP-43^{M337V} does not alter

the cellular localisation of either endogenous mouse or exogenous human TDP-43 relative to controls in mESC-MNs.

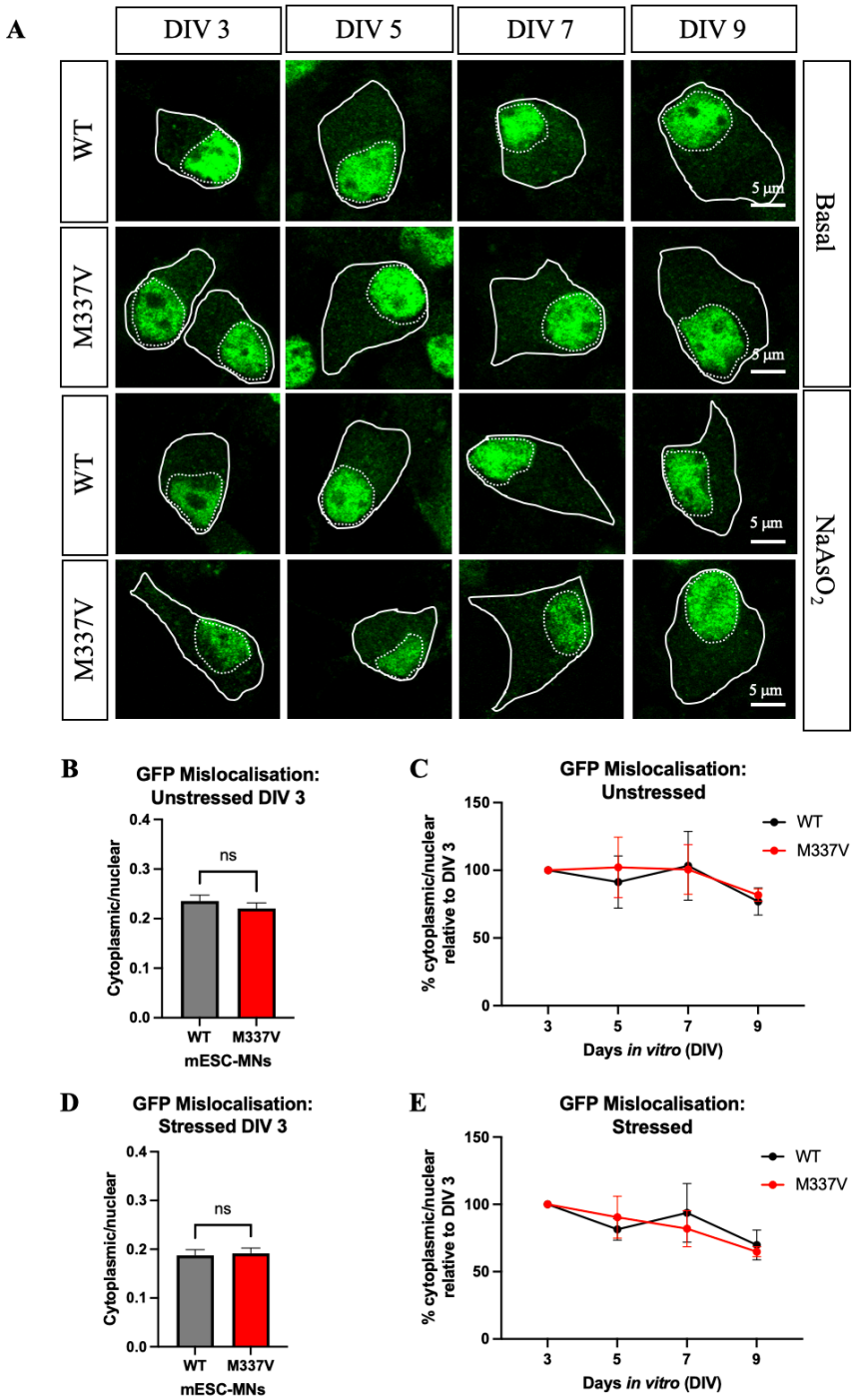


Figure 3.7 mESC-MNs do not demonstrate GFP-TDP-43 mislocalisation. A GFP-TDP-43 localisation in TDP-43^{WT} and TDP-43^{M337V} mESC-MNs at 3, 5, 7 and 9 days *in vitro* (DIV 3-9) in unstressed and stressed (sodium arsenite) conditions. White lines indicate the cytoplasmic boundary, with the nuclear boundary depicted by white dotted lines (DAPI not shown). **B** Ratio of cytoplasmic to nuclear GFP-TDP-43 at DIV 3 in unstressed conditions. Mann Whitney test (n = 3), error bars SEM. **C** Effects of increasing culture duration on the ratio of cytoplasmic to nuclear GFP-TDP-43 relative to DIV 3. Two-way ANOVA with Dunnett's multiple comparisons (n = 3), error bars SEM. **D** Ratio of cytoplasmic to nuclear GFP-TDP-43 at DIV 3 following oxidative stress induced by sodium arsenite. Mann Whitney test (n = 3), error bars SEM. **E** Effects of increasing culture duration on the ratio of cytoplasmic to nuclear GFP-TDP-43 relative to DIV 3 following oxidative stress. Two-way ANOVA with Dunnett's multiple comparisons (n = 3), error bars SEM.

3.2.4. Investigating the effects of increasing culture duration on stress granule formation in mESC-MNs

The reversible formation of stress granules in response to cellular stress is a key cellular protective mechanism, thought to conserve energy by stalling cellular translation. Impaired stress granule formation and the failure of stress granules to dissociate upon removal of the stressor, has been proposed as a potential pathological process in ALS. Previous work has identified fewer and smaller stress granules in TDP-43^{M337V} mESC-MNs (Feneberg et al., 2020; Gordon et al., 2019). It was hypothesised that increasing culture duration of mESC-MNs *in vitro* may exacerbate stress granule impairments observed. To induce stress granule formation mESC-MNs were treated with 0.5 mM of sodium arsenite for 60 minutes prior to fixation. Stress granules were examined at DIV 3-9 by staining with G3BP, a protein essential for the formation of stress granules (Figure 3.8A). Stress granule number and size was analysed in FIJI/Image J using the 'intermodes' threshold plugin. Stress granules in close proximity were segmented using the watershed plugin. In line with previous reports by Gordon and colleagues, I observed significantly fewer stress granules per neuron in TDP-43^{M337V} mESC-MNs relative to TDP-43^{WT} controls at DIV 3 (Mann Whitney test, $p = < 0.0001$; Figure 3.8B). On average, TDP-43^{WT} mESC-MNs demonstrated approximately 10 stress granules per neuron, compared with approximately 6 stress granules per neuron in TDP-43^{M337V} mESC-MNs. Increasing culture duration up to DIV 9 did not significantly alter the number of stress granules per neuron in either TDP-43^{WT} or TDP-43^{M337V} mESC-MNs (TDP-43^{WT}: DIV 3 vs DIV 9, two-way ANOVA, $p = 0.4439$; TDP-43^{M337V}: DIV 3 vs DIV 9, two-way ANOVA, $p = 0.9909$; Figure 3.8C). Analysis of stress granule size at DIV 3 revealed significantly smaller stress granules in TDP-43^{M337V} mESC-MNs compared to TDP-43^{WT} controls, in line with previous findings (Mann Whitney test, $p = 0.0053$; Figure 3.8D). Stress granules in TDP-43^{M337V} mESC-MNs

were approximately 0.8 μm in diameter, compared to 1 μm in TDP-43^{WT} mESC-MNs. Increasing culture duration led to significant reductions in stress granule size in both TDP-43^{WT} and TDP-43^{M337V} mESC-MNs (Two-way ANOVA: TDP-43^{WT}: DIV 3 vs DIV 7, p = 0.0018; TDP-43^{WT}: DIV 3 vs DIV 9, p = 0.0124; TDP-43^{M337V}: DIV 3 vs DIV 7, p = 0.0153; TDP-43^{M337V}: DIV 3 vs DIV 9, p = 0.0003; Figure 3.8E). These findings confirm that expression of TDP-43^{M337V} leads to altered stress granule characteristics in mESC-MNs, including fewer and smaller stress granules at DIV 3. Increasing culture duration up to DIV 9 does not significantly alter stress granule number, but leads to reduced stress granule size in both TDP-43^{WT} and TDP-43^{M337V} mESC-MNs.

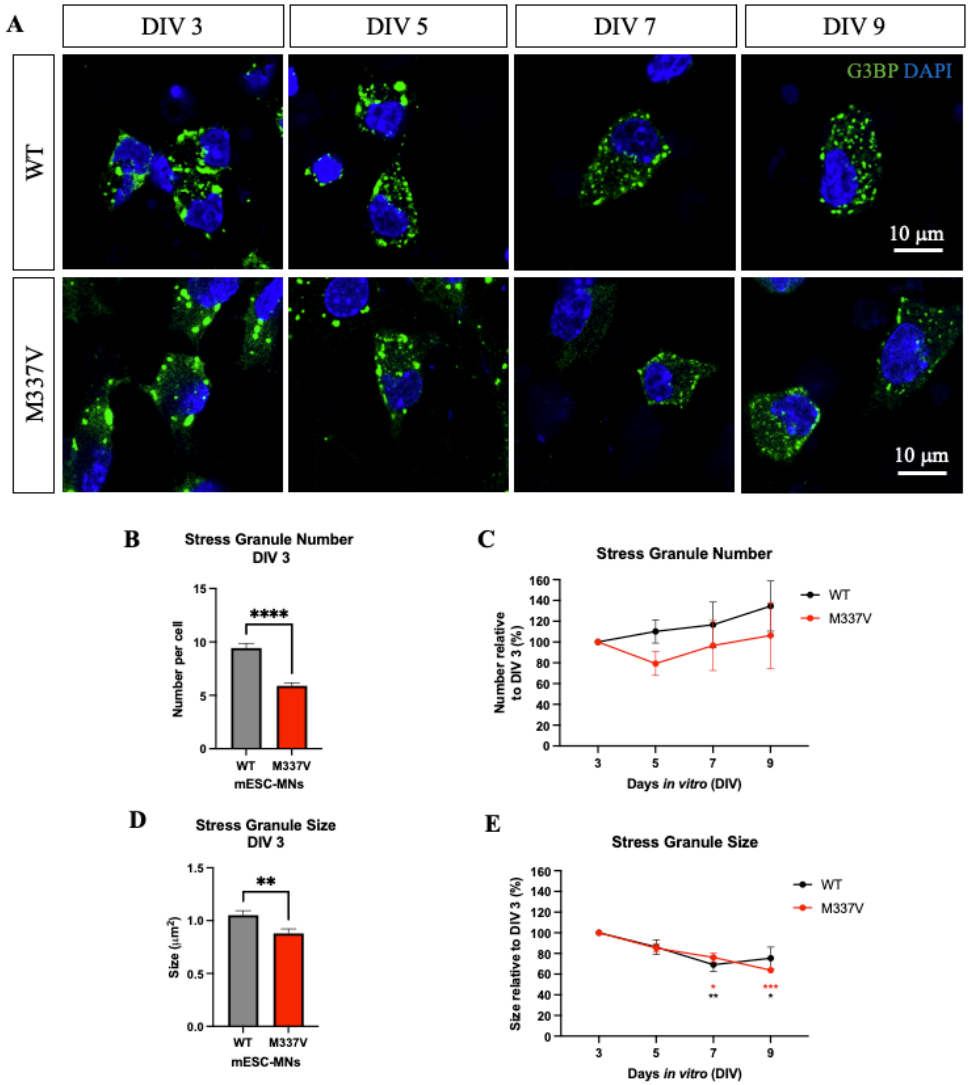


Figure 3.8 Increasing culture duration leads to reduced stress granule size in mESC-MNs. A Formation of G3BP+ stress granules identified by immunocytochemistry in TDP-43^{WT} and TDP-43^{M337V} mESC-MNs following oxidative stress at 3, 5, 7 and 9 days *in vitro* (DIV 3-9). **B** Stress granule number in TDP-43^{WT} and TDP-43^{M337V} mESC-MNs at DIV 3. Mann Whitney test ($n = 3$), error bars SEM. **C** Effects of increasing culture duration on stress granule number in TDP-43^{WT} and TDP-43^{M337V} mESC-MNs relative to DIV 3. Two-way ANOVA with Dunnett's multiple comparisons ($n = 3$), error bars SEM. **D** Stress granule size in TDP-43^{WT} and TDP-43^{M337V} mESC-MNs at DIV 3. Mann Whitney test ($n = 3$), error bars SEM. **E** Effects of increasing culture duration on stress granule size in TDP-43^{WT} and TDP-43^{M337V} mESC-MNs relative to DIV 3. Two-way ANOVA with Dunnett's multiple comparisons ($n = 3$), error bars SEM.

3.2.5. Investigating co-localisation of TDP-43 and stress granules in mESC-MNs

In the previous section I observed a significant reduction in stress granule number and significantly reduced stress granule size in TDP-43^{M337V} mESC-MNs compared to TDP-43^{WT} controls. In previous work by Feneberg and colleagues, analysis of the TDP-43^{M337V} interactome revealed loss of interaction with the stress granule assembly factor, poly-A binding protein (PABP) (Feneberg et al., 2020). Moreover, reduced co-localisation between TDP-43 and the stress granule marker, TIA-1, has previously been observed in TDP-43^{M337V} primary motor neurons compared to TDP-43^{WT} controls (Gordon et al., 2019). These findings led to the hypothesis that loss of TDP-43 interaction with stress granules may underlie impairments to stress granule number and size. Given this, I sought to investigate whether expression of TDP-43^{M337V} altered co-localisation between TDP-43 and the stress granule marker G3BP in our mESC-MN model. To induce stress granule formation, motor neurons were treated with sodium arsenite at 0.5 mM for 1 hour, then fixed in PFA and immunocytochemistry performed. Co-localisation was assessed at DIV 3 and at DIV 9 to investigate the effects of increasing culture duration on TDP-43 and G3BP co-localisation. Manders correlation coefficients, M1 and M2, were generated using the FIJI/ImageJ plugin, JaCoP. The M1 coefficient measures the fraction of red fluorescence (TDP-43) in areas of green fluorescence (G3BP). Conversely, the M2 coefficient measures the fraction of green fluorescence (G3BP) in areas of red fluorescence (TDP-43) (Manders et al., 1993).

Staining with G3BP and *pan*TDP-43 allowed assessment of co-localisation between stress granules and total cellular TDP-43, encompassing both mouse endogenous Tdp43 and human exogenous TDP-43 (Figure 3.9A and 3.10A). Analysis revealed no significant differences in

Manders M1 or M2 coefficients in TDP-43^{M337V} mESC-MNs compared to TDP-43^{WT} controls at DIV 3. Manders M1 coefficient was approximately 0.15 for both TDP-43^{WT} and TDP-43^{M337V}, indicating that only 15% of TDP-43 (red pixels) co-localises with G3BP (green pixels) in both cases (M1: Mann Whitney test, $p = 0.7645$, Figure 3.9B). Manders M2 coefficient was not significantly different between TDP-43^{WT} and TDP-43^{M337V} mESC-MNs (M2: Mann Whitney test, $p = 0.5577$, Figure 3.9C). A mean M2 coefficient of 0.14 was observed in TDP-43^{WT} mESC-MNs, suggesting that 14% of G3BP (green pixels) co-localised with TDP-43 (red pixels). In TDP-43^{M337V} mESC-MNs, the Manders M2 coefficient was 0.10, indicating that 10% G3BP (green pixels) co-localises with TDP-43 (red pixels) in these neurons. At DIV 9, TDP-43^{WT} mESC-MNs demonstrated a mean M1 coefficient of approximately 0.20, compared with 0.10 in TDP-43^{M337V} mESC-MNs, although this difference was not significant (M1: Mann Whitney test, $p = 0.411$, Figure 3.10B). The M2 coefficient in TDP-43^{WT} mESC-MNs was approximately 0.15, similar to the value observed at DIV 3. Although not significantly different from TDP-43^{WT}, the M2 coefficient of 0.05 in TDP-43^{M337V} mESC-MNs was lower than that observed at DIV 3, indicating only 5% of G3BP was co-localised with TDP-43 in these neurons (M2: Mann Whitney test, $p = 0.1358$, Figure 3.10C).

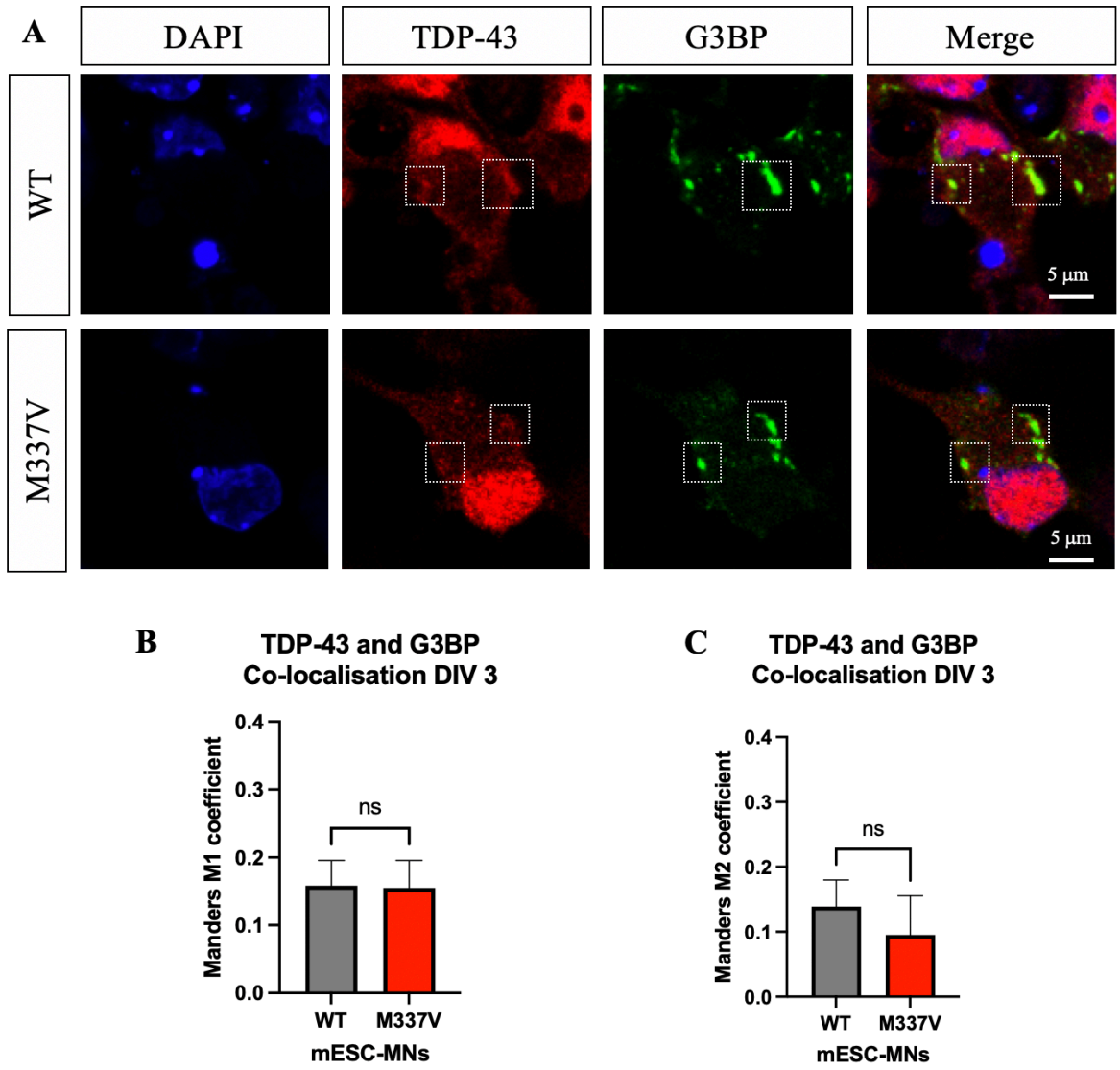


Figure 3.9 TDP-43 co-localisation with stress granules DIV 3. A Co-localisation of TDP-43 with G3BP+ stress granules investigated through immunocytochemistry at 3 days *in vitro* (DIV 3). **B** Manders M1 co-localisation coefficient, which quantifies the fraction of red fluorescence (TDP-43) in areas of green fluorescence (G3BP). **C** Manders M2 co-localisation coefficient, which quantifies the fraction of green fluorescence (G3BP) in areas of red fluorescence (TDP-43). Statistics for B and C: Mann Whitney unpaired t-test (n = 3), error bars SEM.

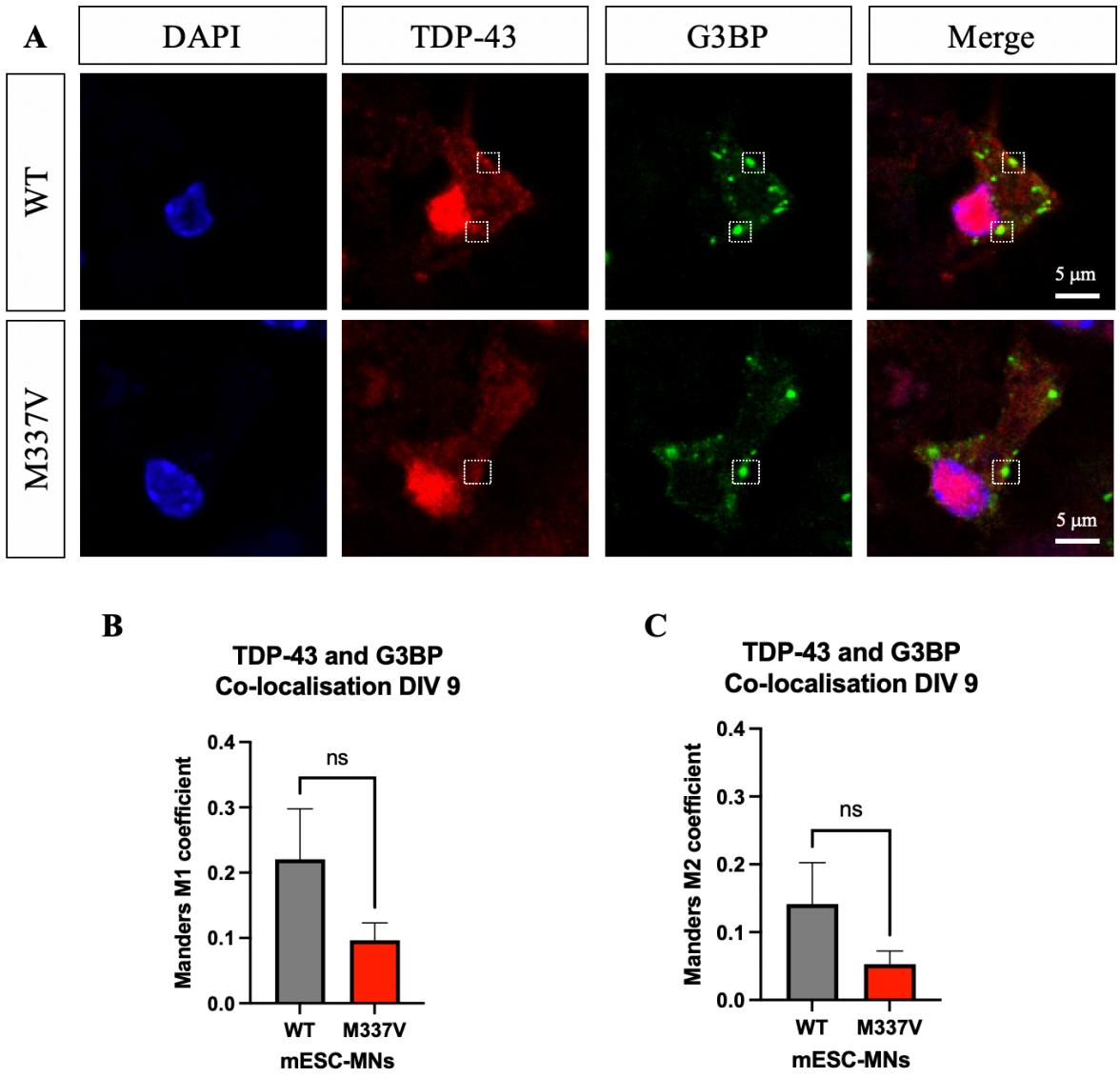


Figure 3.10 TDP-43 co-localisation with stress granules DIV 9. A Co-localisation of TDP-43 with G3BP+ stress granules investigated through immunocytochemistry at 9 days *in vitro* (DIV 9). **B** Manders M1 co-localisation coefficient, which quantifies the fraction of red fluorescence (TDP-43) in areas of green fluorescence (G3BP). **C** Manders M2 co-localisation coefficient, which quantifies the fraction of green fluorescence (G3BP) in areas of red fluorescence (TDP-43). Statistics for B and C: Mann Whitney test (n = 3), error bars SEM.

3.2.6. Investigating the effects of increasing culture duration on cellular viability in mESC-MNs

mESC-MNs expressing TDP-43^{M337V} have previously been shown to exhibit viability deficits compared to TDP-43^{WT} following exposure to oxidative stress after 2 days *in vitro* (Feneberg et al., 2020; Gordon et al., 2019). I first sought to replicate this viability phenotype in TDP-43^{WT} and TDP-43^{M337V} mESC-MNs at DIV 3 using the MTS viability assay. The MTS assay is a metabolic assay, based on the reduction of the MTS tetrazolium reagent to a coloured formazan dye by viable cells. The relative levels of formazan generated can be assessed on a well-to-well basis through absorbance measurements, which act as a surrogate measure of cellular viability. mESC-MNs were seeded into 96-well plates at a density of 100,000 cells per well and examined in unstressed or stressed conditions, with oxidative stress induced through treatment with 0.5 mM of sodium arsenite for 1 hour. TDP-43^{WT} mESC-MNs demonstrated the highest viability, which was not significantly reduced following oxidative stress ($p = 0.1553$; Figure 3.11A). Interestingly, TDP-43^{M337V} mESC-MNs demonstrated significantly reduced viability in both unstressed conditions and stressed conditions compared to TDP-43^{WT} unstressed controls (unstressed: $p = 0.0367$; stressed: $p = 0.0013$; Figure 3.11A). Next, I aimed to investigate whether increasing culture duration of mESC-MNs would exacerbate the observed impairments to cellular viability observed at DIV 3. Relative to survival at DIV 3, increasing culture duration up to DIV 9 did not significantly alter cellular viability in unstressed conditions, in either TDP-43^{WT} (DIV 3 vs. DIV 9: $p = 0.1501$) or TDP-43^{M337V} (DIV 3 vs. DIV 9: $p = > 0.999$) mESC-MNs (Figure 3.11B). Similarly, increasing culture duration did not significantly alter cellular viability following oxidative stress in either TDP-43^{WT} (DIV 3 vs. DIV 9: $p = 0.7641$) or TDP-43^{M337V} (DIV 3 vs. DIV 9: $p = 0.6726$) mESC-MNs (Figure 3.11C).

These findings confirm reduced cell viability in TDP-43^{M337V} mESC-MNs, which is not exacerbated by increasing culture duration.

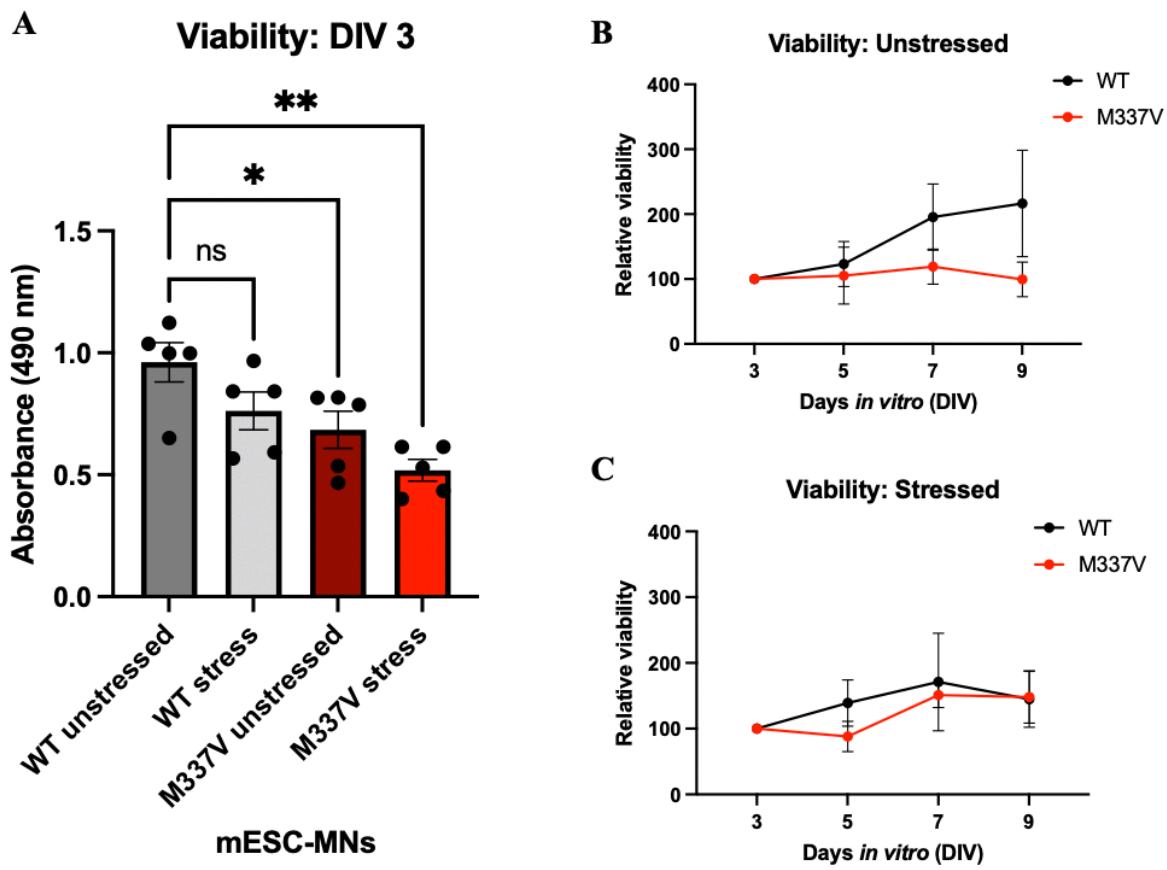


Figure 3.11 TDP-43^{M337V} mESC-MNs demonstrate impaired viability relative to TDP-43^{WT} motor neurons. A Cellular viability in TDP-43^{WT} and TDP-43^{M337V} mESC-MNs after 3 days *in vitro* (DIV 3) in unstressed conditions and following oxidative stress (0.5 mM sodium arsenite for 60 minutes). One-way ANOVA with Dunnett's multiple comparisons (n = 5), error bars SEM. * $p < 0.05$, ** $p < 0.01$. **B** Effects of increasing culture duration on cellular viability in TDP-43^{WT} and TDP-43^{M337V} mESC-MNs in unstressed conditions relative to DIV 3. Two-way ANOVA with Dunnett's multiple comparisons (n = 3), error bars SEM **C** Effects of increasing culture duration on cellular viability in TDP-43^{WT} and TDP-43^{M337V} mESC-MNs following oxidative stress relative to DIV 3. Two-way ANOVA with Dunnett's multiple comparisons (n = 3), error bars SEM.

3.3. Conclusions

The relevance of studying relatively immature *in vitro* models to gain mechanistic insight into neurodegenerative disorders has been widely discussed. Such *in vitro* models are valuable in providing a high-throughput platform for phenotypic screening, mechanistic probing and drug screening. However, the validity of such approaches relies on building robust models that are reflective of the disease process. In an attempt to improve the robustness of *in vitro* models, previous studies in iPSC-MNs have examined the effects of 'ageing' motor neurons *in vitro* (Fujimori et al., 2018; Kreiter et al., 2018). Here, I have employed a similar approach to investigate the effects of increasing culture duration in mESC-MNs on cellular maturation and disease-associated phenotypes induced by mutant TDP-43^{M337V}. This work demonstrates that increasing culture duration from DIV 3 to DIV 9 does not significantly alter the expression of synaptic markers in mESC-MNs, suggesting increasing culture duration up to DIV 9 does not increase neuronal maturity. Increasing culture duration does not significantly increase the percentage of cytoplasmic TDP-43 observed in either unstressed or oxidative stressed conditions. I have confirmed previous findings, that fewer and smaller stress granules are characteristic of TDP-43^{M337V} mESC-MNs at DIV 3. Whilst, increasing culture duration does not significantly alter stress granule numbers in mESC-MNs, reduced stress granule size was observed following longer culture periods in both TDP-43^{WT} or TDP-43^{M337V} mESC-MNs. Reduced cell viability in TDP-43^{M337V} mESC-MNs was observed at DIV 3 relative to TDP-43^{WT} controls both in unstressed conditions and in response to oxidative stress. Increasing culture duration did not significantly exacerbate survival deficits in TDP-43^{M337V} mESC-MNs.

TDP-43 mislocalisation has been a major focus of research in ALS. However, identifying TDP-43 mislocalisation in cellular models has proved challenging, often requiring the addition of cellular stressors to induce a cytoplasmic shift. Here, we show that there are no significant

differences in the levels of cytoplasmic TDP-43 observed between control and TDP-43^{M337V} mESC-MNs in either unstressed or oxidative stressed conditions. Furthermore, increasing culture duration does not unmask TDP-43 cytoplasmic mislocalisation in TDP-43^{M337V} mESC-MNs. Our observations are in line with previous findings in the TDP-43^{M337V} mESC-MN model, where no significant differences in mislocalisation were observed at DIV 3. Interestingly, we observed reduced cell viability in TDP-43^{M337V} mESC-MNs compared to TDP-43^{WT} controls in response to oxidative stress at DIV 3, in line with previous observations (Gordon et al., 2019), however increasing culture duration up to DIV 9 did not exacerbate these deficits. Given that we did not detect TDP-43 mislocalisation, these findings suggest that cell death can occur independent of TDP-43 mislocalisation and aggregation. These results support the hypothesis that TDP-43 mislocalisation is a feature of later stages in the disease process. Indeed, several studies have questioned the role of mislocalised and aggregated TDP-43 in ALS pathogenesis, instead arguing that these pathological hallmarks are signatures of end-stage disease rather than directly contributing to pathogenesis. Whilst previous studies have shown links between TDP-43 mislocalisation and cellular toxicity *in vitro,* this observation is not universally reported (Arnold et al., 2013; Barmada et al., 2010). In line with this, neurodegeneration has been shown to occur without the presence of TDP-43 aggregates (Arnold et al., 2013; Barmada et al., 2010; Igaz et al., 2011; Liu et al., 2013). More recently, in a novel gene associated with ALS, KANK1, TDP-43 mislocalisation was found to lie downstream of axonal dysfunction in iPSC-MNs (Zhang et al., 2022). Taken together, these findings suggest that whilst TDP-43 mislocalisation and aggregation can induce toxicity, alternative mechanisms such as axonal dysfunction are also capable of initiating neurodegeneration and cell death in ALS.

Stress granules have been proposed as a pathological mechanism linking cellular stress and protein aggregation in ALS. Dysregulation of stress granule formation, including altered stress granule size and number, have previously been reported in TDP-43 associated ALS models in response to various cellular stressors (Dewey et al., 2011; Gordon et al., 2019; Liu-Yesucevitz et al., 2010; McDonald et al., 2011). Previous work by our group has identified altered stress granule characteristics in primary motor neurons and mESC-MNs expressing TDP-43^{M337V} compared to TDP-43^{WT} controls, including fewer and smaller stress granules (Feneberg et al., 2020; Gordon et al., 2019). In line with these findings, here I observe reduced stress granule numbers and reduced stress granule size in TDP-43^{M337V} mESC-MNs compared to TDP-43^{WT} controls. Appropriate stress granule assembly and disassembly is an essential protective cellular response, required to conserve energy and maintain survival in response to stress. Reduced stress granule numbers and size in our TDP-43^{M337V} mESC-MNs relative to controls, suggests neurons are unable to respond appropriately to oxidative insults. Following analysis of the TDP-43 interactome of TDP-43^{WT} and TDP-43^{M337V} mESC-MNs, Feneberg and colleagues identified reduced interactions between TDP-43^{M337V} and the stress granule marker PABP in unstressed and stressed conditions (Feneberg et al., 2020). Given that TDP-43 has been shown to co-localise with stress granules (Colombrita et al., 2009; Dewey et al., 2011; Freibaum et al., 2010; Liu-Yesucevitz et al., 2010; McDonald et al., 2011; Meyerowitz et al., 2011) and is important in regulating efficient stress granule dynamics (Khalfallah et al., 2018) it was hypothesised that reduced interaction between TDP-43 and stress granule components could underlie dysregulation of stress granule characteristics. Here, I observed reduced co-localisation through immunocytochemical analysis between TDP-43 and G3BP in TDP-43^{M337V} mESC-MNs at DIV 9, although this difference was not statistically significant. Nevertheless, these observations taken together with previous work on the TDP-43 interactome in mESC-MNs, suggests that altered interactions between TDP-43^{M337V} and stress granule

components may be worth exploring further. It is not yet clear whether reduced interactions between TDP-43 and stress granule components could underlie altered stress granule dynamics. This could be examined in future work through investigating the effects of manipulating interactions between TDP-43 and stress granule components on stress granule dynamics.

Cell viability provides an attractive high-throughput phenotype for screening therapeutic compounds. Readouts of cell viability provide a quantitative measure that reflects overall cellular health, and whether potential therapeutics enhance or impair viability. Compounds that are found to enhance cell viability can then be studied further, to investigate the mechanisms through which they exert neuroprotective effects. Reduced viability in TDP-43^{M337V} mESC-MNs following oxidative stress has been previously characterised by our group (Gordon et al., 2019). Here, I have replicated these findings, and found reduced viability in TDP-43^{M337V} mESC-MNs following oxidative stress compared to TDP-43^{WT} controls. I have also identified significantly reduced viability in TDP-43^{M337V} mESC-MNs relative to TDP-43^{WT} mESC-MNs in unstressed conditions, suggesting that the TDP-43^{M337V} mutation alone is sufficient to impair viability in this model. Cell viability was assessed using the MTS assay, which determines survival based on the rate of cellular metabolism of a particular compound. Given this, it is possible that the reduced viability observed in TDP-43^{M337V} mESC-MNs may reflect underlying cellular metabolic deficits.

A major challenge of ALS research is consolidating findings across different model systems. There are a number of different *in vitro* ALS models currently available across a number of ALS-related genes and in multiple different cell types. These models include patient derived fibroblasts and iPSC-MNs, non-neuronal HEK cell models, mouse models expressing mutant

forms of mouse endogenous Tdp43, and transgenic mouse models expressing human TDP-43. Yet disparities in results across these different model systems make interpretation challenging. For example, within our own models, which carry the same BAC genetic construct, we observe distinct results. Whilst we do not observe TDP-43 mislocalisation in mESC-MNs, clear mislocalisation and nuclear clearing of TDP-43 have been reported in primary motor neurons carrying the TDP-43^{M337V} BAC construct. However, these models differ in several respects, which may explain their distinct phenotypic signatures. For example, primary motor neurons have developed in a multicellular environment with multiple physiological cues. Unlike the monoculture of mESC-MNs, the *in vivo* environment contains various signalling molecules alongside other non-neuronal cell types, including microglia and astrocytes, that may influence neuronal degeneration and associated phenotypes. Given this, primary motor neurons are likely to be intrinsically more vulnerable than mESC-MNs when removed from their *in vivo* milieu and cultured *in vitro*. To better mimic the *in vivo* environment *in vitro*, co-culture systems containing a mix of cell types will be crucial. Our lab is currently developing neuron and microglial co-culture models to investigate the contribution of glial cells to pathological phenotypes. mESC-MNs also represent a more immature state relative to primary motor neurons, and have likely undergone some form of clonal selection in culture, leading to preferential growth of more robust cells.

The limitations of this study ought to be considered when interpreting results. Due to time and resource constraints we were unable to robustly characterise the effects of increasing culture duration on neuronal maturity. Here, we have examined the expression of synaptic markers as a surrogate marker for maturation up to DIV 9. Yet further characterisation would be required, perhaps through transcriptomic analysis, to confirm the maturation status of neurons. Furthermore, functional maturation status could be assessed using whole-cell patch clamp

recordings or multi-electrode array recordings to investigate the electrophysiological properties of mESC-MNs and how these change over time. Whilst whole-cell patch clamping can be technically challenging, multi-electrode array recordings are comparatively more straightforward and would allow the same mESC-MNs can be examined repeatedly at multiple different time-points to assess changes in maturation. This would remove variability arising from the analysis of distinct wells at different time points, as has been performed in the current study. From our results it appears that increasing culture duration up to DIV 9 is not sufficient to significantly alter neuronal maturation or cellular phenotypes. However, it is possible that disease relevant phenotypes may be unmasked at later time points. It would be interesting to investigate neuronal maturation and phenotypes over a longer time frame, perhaps up to a month *in vitro*, similar to the culture duration of iPSC-MNs.

In this chapter I have investigated whether maintaining mESC-MNs in culture alters their maturation status or exaggerates cellular phenotypes associated with ALS. Whilst we did not observe any significant indication of altered maturity or increased TDP-43 mislocalisation, increasing culture duration significantly altered stress granule size in TDP-43^{WT} and TDP-43^{M337V} mESC-MNs. Furthermore, we observed reduced viability in TDP-43^{M337V} mESC-MNs compared to TDP-43^{WT} controls. The assay used to assess cell viability measures metabolic function as a surrogate marker for viability, suggesting possible underlying metabolic deficits in TDP-43^{M337V} mESC-MNs may underlie the observed impairments. Given this, we next sought to investigate changes to cellular metabolism in TDP-43^{M337V} mESC-MNs.

CHAPTER 4 Investigating the effects of the TDP-43^{M337V} mutation on cellular energy metabolism in mESC-MNs

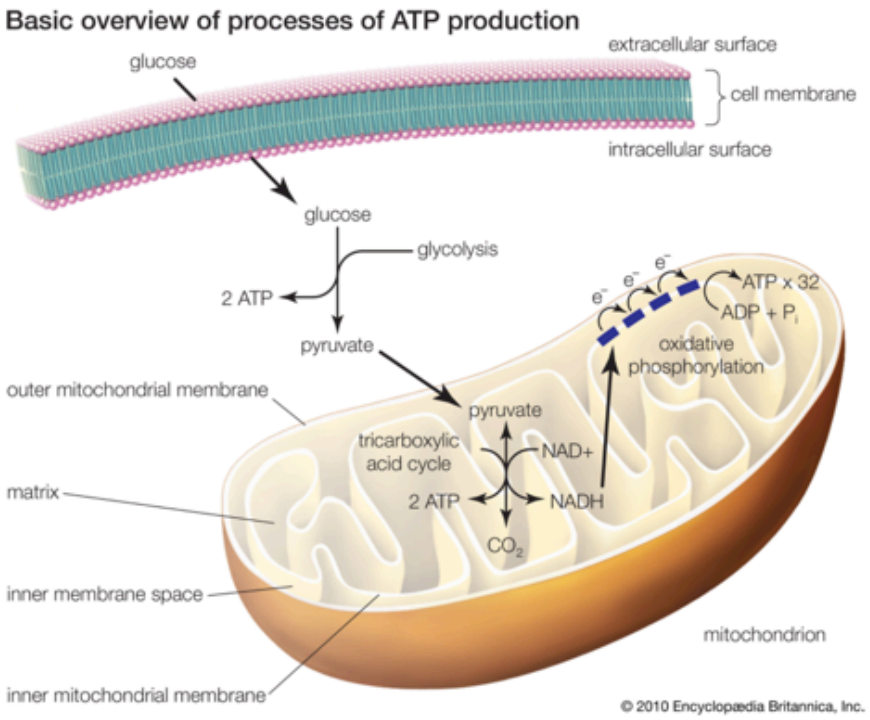
4.1. Introduction and aims

4.1.1. An overview of energy production within the CNS

The central nervous system (CNS) requires a substantial supply of energy to maintain healthy physiological function (Ames, 2000). Whilst the adult human brain accounts for only 2% of the total body weight, it consumes approximately 20% of the energy produced by the body (Rolfe & Brown, 1997). Motor neurons are large, polarised, excitable cells with long axons, which may render them uniquely vulnerable to metabolic dysregulation. Action potential propagation, synaptic transmission and axonal transport are all energetically expensive and require a constant supply of ATP to maintain homeostasis (Harris et al., 2012; Le Masson et al., 2014). To meet this high energy demand, neurons rely predominantly on glucose as an energy substrate, which is broken down through a series of enzymatic reactions to generate ATP. Glucose is taken up by cells through glucose transporters located in the cell membrane, and converted to pyruvate within the cell cytoplasm through the process of glycolysis, which results in a net production of two ATP molecules (Ames, 2000) (Figure 4.1A). Pyruvate then enters mitochondria, where it feeds into the tricarboxylic acid (TCA) cycle and is converted to carbon dioxide. This process leads to the production of two further molecules of ATP and the reduction of the co-enzyme nicotinamide adenine dinucleotide (NAD) to NADH. Mitochondrial NADH is then transported to the inner mitochondrial membrane, where it transfers electrons to complex I of the electron transport chain (ETC); a series of enzymatic complexes, collectively termed complexes I-IV. Electrons are transferred sequentially through

these complexes before combining with oxygen, the final electron acceptor, to form water. The energy generated during this process is captured and redirected to pump hydrogen ions (H^+) across the intermembrane space. Over time, this creates a proton gradient across the inner mitochondrial membrane, with a higher concentration of H^+ in the intermembrane space and a correspondingly lower concentration of H^+ in the mitochondrial matrix. This leads to the flow of H^+ ions down their electrochemical gradient through the terminal complex, ATP synthase. As H^+ ions pass through ATP synthase its position rotates, in a key process that allows ADP to bind to phosphate and results in the production of 32 molecules of ATP (Chaban et al., 2014) (Figure 4.1B).

A



B

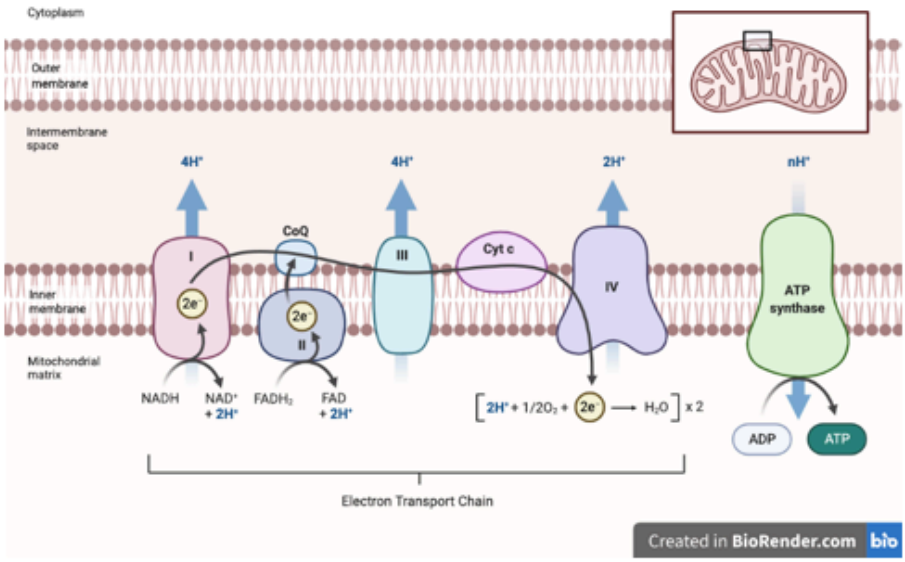


Figure 4.1 Pathways of ATP production. A ATP production through glycolysis, TCA cycle and oxidative phosphorylation (Encyclopaedia Britannica, Inc., 2010). **B** The process of oxidative phosphorylation involves the transfer of electrons through enzymatic complexes I-V in the mitochondrial respiratory chain (BioRender).

4.1.2. Systemic and cellular metabolic dysregulation is a feature of ALS

In ALS, clinical observations of weight loss, dyslipidaemia and hypermetabolism have been consistently reported in patients and are indicative of systemic metabolic dysregulation. Multiple studies have reported an association between body mass index (BMI) and survival, whereby mild obesity is associated with greater survival (Wills et al, 2014). Moreover, defective glucose metabolism has been previously reported in neuroimaging studies, where reductions in glucose metabolism have been observed in the frontal lobe and cortex of ALS patients (Ludolph et al., 1992). These observations suggest that metabolic function may influence disease severity and progression. Evidence of impaired energy homeostasis is also evident at the cellular level. Mitochondrial dysfunction is a prominent feature of many neurodegeneration diseases including ALS. Human iPSC-MN models, generated from familial and sporadic ALS patient fibroblasts, have been found to demonstrate various abnormalities indicative of impaired cellular energy metabolism, including impaired mitochondrial respiration, reduced ATP production and reduced mitochondrial membrane potential (Dafinca et al., 2016; Hor et al., 2021; Singh et al., 2021). A handful of studies have identified glycolytic impairments associated with ALS. Among other changes, impaired glycolysis was identified through analysis of whole-genome expression in the motor cortex of sporadic ALS patients (Lederer et al., 2007). In fibroblasts derived from sporadic ALS patients, reductions in the expression of PGK1 and another glycolytic enzyme, phosphoglucomutase 2 like 1, have been observed (Raman et al., 2015). Similarly, in a study examining proteomic changes in sporadic ALS patient-derived fibroblasts, reductions in the expression of proteins related to glycolysis were observed when compared to fibroblasts originating from age-matched healthy individuals (Szelechowski et al., 2018). Whilst reduced glycolysis appears to be a feature of ALS, other studies have reported significant upregulation of glycolysis, which is thought to be neuroprotective (Manzo et al., 2019; Valbuena et al., 2016). In support of this, terazosin, an

alpha 1-adrenoceptor antagonist which targets the glycolytic enzyme PGK1, has proven beneficial in a number of neurodegenerative diseases including Parkinson's disease and spinal muscular atrophy (Boyd et al., 2017; Cai et al., 2019). More recently, upregulation of PGK1 was found to restore deficits in axonal outgrowth in a mutant TDP-43 overexpression zebrafish model of ALS, and treatment with terazosin improved cell viability and stress granule formation in our TDP-43^{M337V} mESC-MN model (Figure 4.2) (Chaytow et al., 2022). Interestingly, upregulation of glycolysis through terazosin treatment has also been found to increase cell survival in response to oxidative stress in a model of gastrointestinal disorders (Liu et al., 2021). Taken together, these findings suggest that dysregulation of energy metabolism, both at the systemic and cellular level, is a feature of ALS and may represent a viable therapeutic target.

4.1.3. Aims

As described in the previous chapter, I observed significant reductions in cell viability in TDP-43^{M337V} mESC-MNs relative to TDP-43^{WT} controls, as measured through metabolic viability assays. Given this, it is possible that metabolic deficits in TDP-43^{M337V} mESC-MNs may underlie this reduced viability. In this chapter, I explore cellular energy metabolism in mESC-MNs, focussing on glycolysis and mitochondrial respiration. The aims of this chapter are:

1. To investigate the expression of glycolytic enzymes and mitochondrial proteins in mESC-MNs.
2. To investigate altered interactions between TDP-43^{M337V} and glycolytic or mitochondrial proteins.
3. To investigate glycolytic function in mESC-MNs under basal conditions and conditions of oxidative stress.
4. To investigate mitochondrial bioenergetics in mESC-MNs.

5. To examine how the pro-survival drug, terazosin, influences glycolysis and mitochondrial respiration in mESC-MNs.

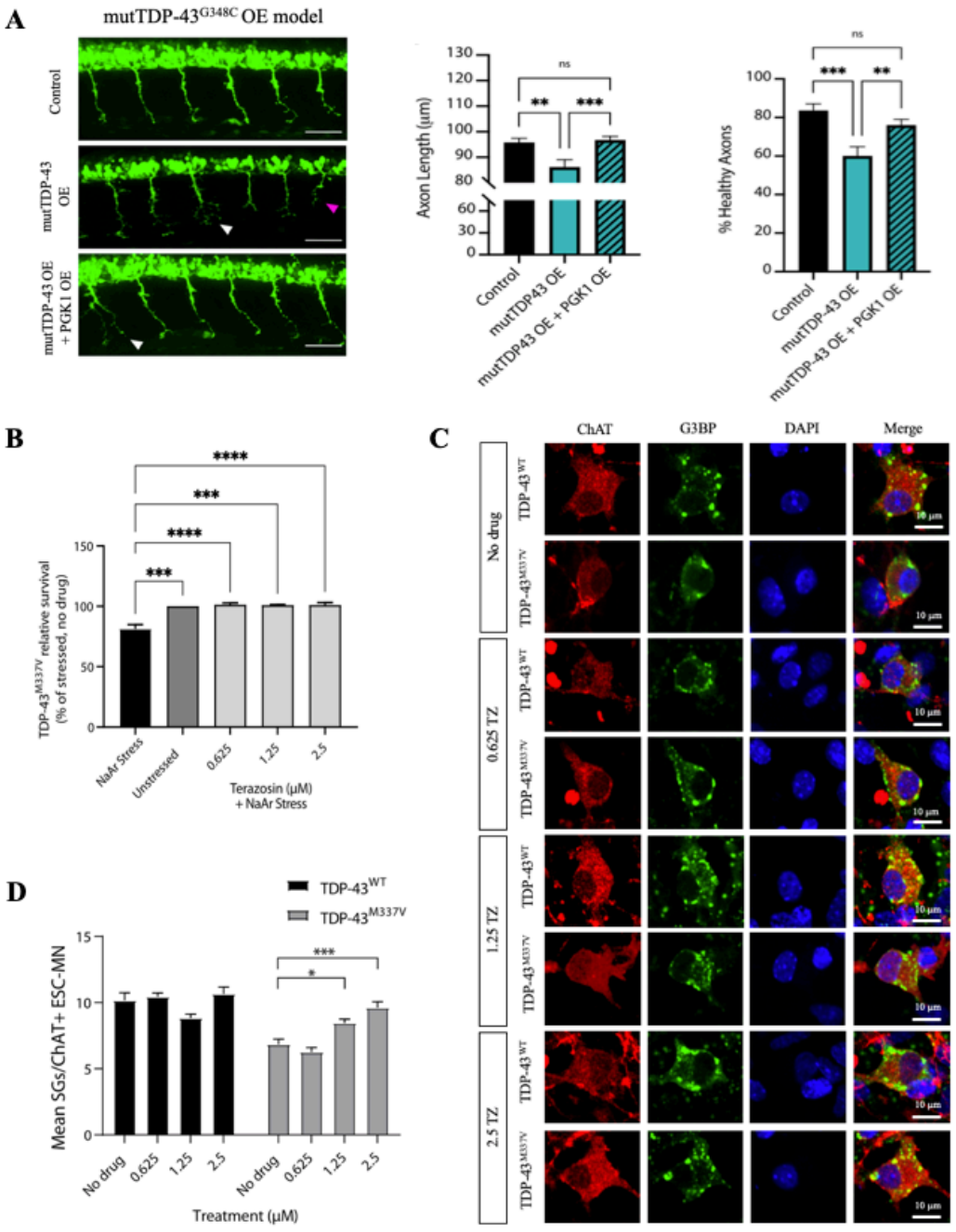


Figure 4.2 Upregulation of glycolysis may be neuroprotective in ALS (by Dr Helena Chaytow and Dr David Gordon). A Upregulating glycolysis in a mutant TDP-43^{G348C} overexpression (OE) zebrafish model, through overexpression of the glycolytic enzyme PGK1, leads to rescue of axon length and reduced branching. Magenta arrows indicate short branches and white arrows indicate branching. Scale bar = 50 µM. One-way ANOVA with Tukey's multiple comparisons test. ** $p < 0.01$, *** $p < 0.001$. Data and figure by Dr Helena Chaytow. **B** Treatment with the terazosin at 0.625, 1.25 and 2.5 µM rescues survival deficits in TDP-43^{M337V} mESC-MNs in response to oxidative stress. One-way ANOVA with Dunnett's multiple comparisons. *** $p < 0.001$, **** $p < 0.0001$. Data and figure by Dr David Gordon. **C** and **D** Terazosin (TZ) applied at 1.25 and 2.5 µM significantly increases stress granule number in TDP-43^{M337V} mESC-MNs compared to the untreated condition in response to oxidative stress. One-way ANOVA with Dunnett's multiple comparisons. * $p < 0.05$, *** $p < 0.001$. Data by Dr David Gordon (Chaytow et al., 2022).

4.2. Results

4.2.1. Altered expression of glycolytic enzymes and mitochondrial proteins in iPSC-MNs and mESC-MNs expressing TDP-43^{M337V}

Through its role as an RNA binding protein, TDP-43 influences the expression of many different genes through modulating transcription, splicing, nucleocytoplasmic transport, mRNA stability and translation (Lagier-Tourenne et al., 2010). First identified as a transcriptional repressor of the human immunodeficiency virus type 1 (HIV-1), TDP-43 has since been found to associate with over 6,000 RNAs in neurons (Ou et al., 1995; Polymenidou et al., 2011; Sephton et al., 2011). In TDP-43 models of ALS, significant dysregulation of transcripts relating to cellular bioenergetics has been observed. Upregulation of the rate-limiting glycolytic enzyme, PFK, has been observed in Drosophila, human ALS post-mortem tissue and iPSC-MNs with TDP-43 proteinopathy. This upregulation was thought to be neuroprotective, as overexpression of PFK in *Drosophila* was sufficient to reverse TDP-43 induced locomotor deficits (Manzo et al., 2019). Furthermore, altered expression of mitochondria-associated transcripts has been observed in both TDP-43 knockdown and TDP-43 aggregation cellular models, suggesting dysregulation can result from both TDP-43 loss and gain-of-function mechanisms (Briese et al., 2020; Zuo et al., 2021).

The Talbot laboratory has previously performed large-scale RNA sequencing of iPSC-MNs derived from healthy controls and patients carrying the carrying TDP-43^{M337V} and TDP-43^{I383T} mutations (Ababneh et al., 2020; Dafinca et al., 2020). Differential expression analysis was performed by Dr Jakub Scaber using DESeq2 (1.22.1(45)). Here, this dataset was utilised to examine the effects of TDP-43^{M337V} on the expression of glycolytic enzymes and mitochondrial

protein expression. Analysis revealed significant upregulation of multiple enzymes associated with the GO term 'canonical glycolysis' in iPSC-MNs expressing TDP-43^{M337V} compared to healthy controls (Figure 4.3). Upregulated transcripts in TDP-43^{M337V} iPSC-MNs included PGK1 (p = 0.00361), PFK (p = 0.00345), PGAM1 (p = 0.000215) and GAPDH (p = 0.0211). With regards to mitochondrial transcripts, TDP-43^{M337V} iPSC-MNs also demonstrated significant upregulation ($p < 0.01$) of 89 transcripts and significant downregulation ($p < 0.01$) of 28 transcripts associated with the GO term 'mitochondrion' (Figure 4.4). A number of the 89 upregulated transcripts encoded proteins associated with complex I, complex IV and complex V. These included COX5A (p = 0.002), COX6C (p = 0.008) and various subunits of complex V including ATP5B (p = 0.016). Significant downregulation of the complex II subunit, SDHD, was also observed. These findings suggest expression of TDP-43^{M337V} significantly dysregulates the expression of transcripts relating to glycolysis and the electron transport chain.

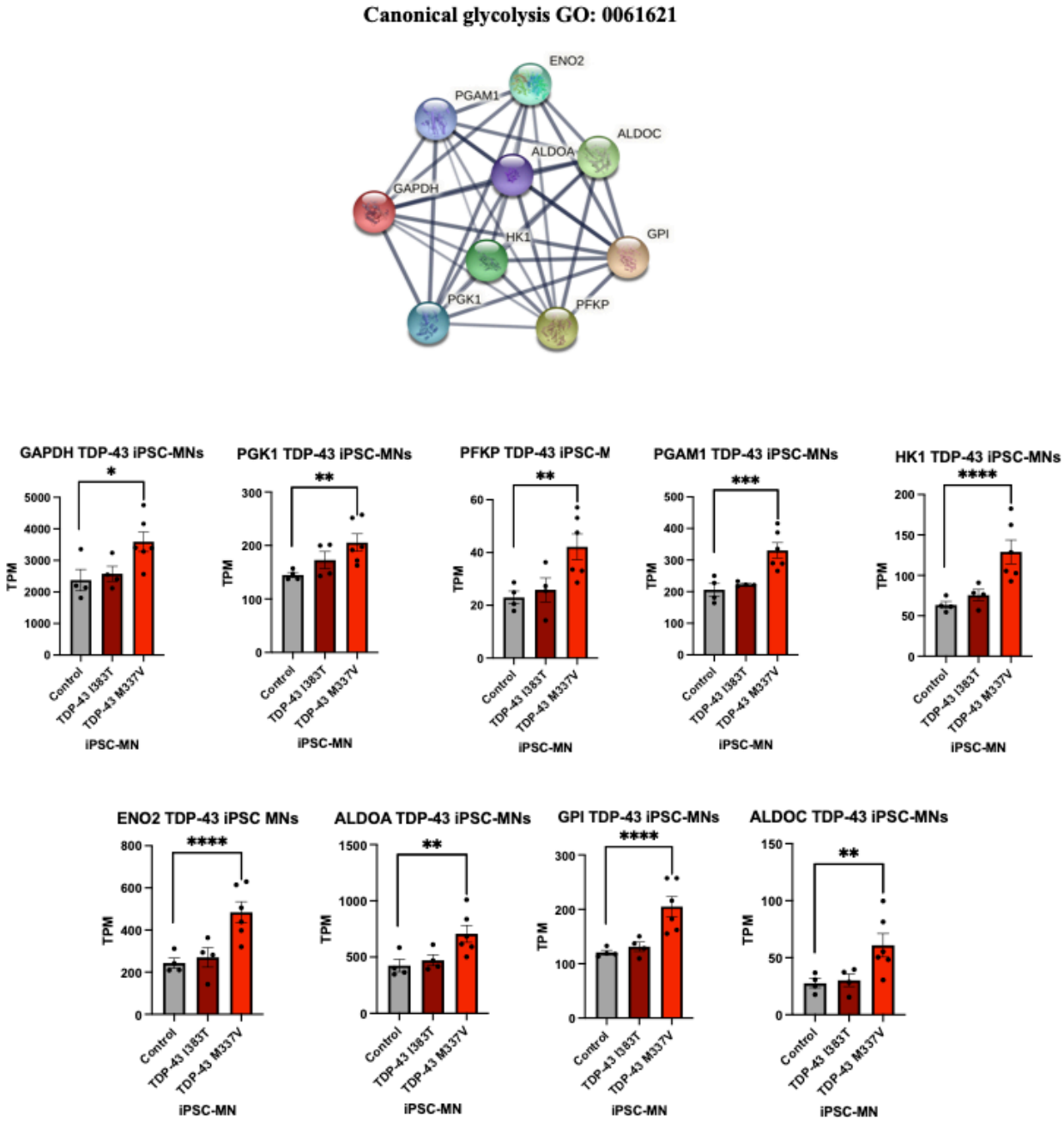


Figure 4.3 Increased expression of glycolytic enzymes in iPSC-MNs carrying the TDP-43^{M337V} pathogenic mutation. Transcriptomic data previously generated by members of the Talbot laboratory and reanalysed for expression of glycolytic proteins. Transcripts identified through *Panther* associated with the GO term 'canonical glycolysis'. Transcripts per million (TPM) are shown. * $p < 0.05$, ** $p < 0.01$, *** $p < 0.001$, **** $p < 0.0001$.

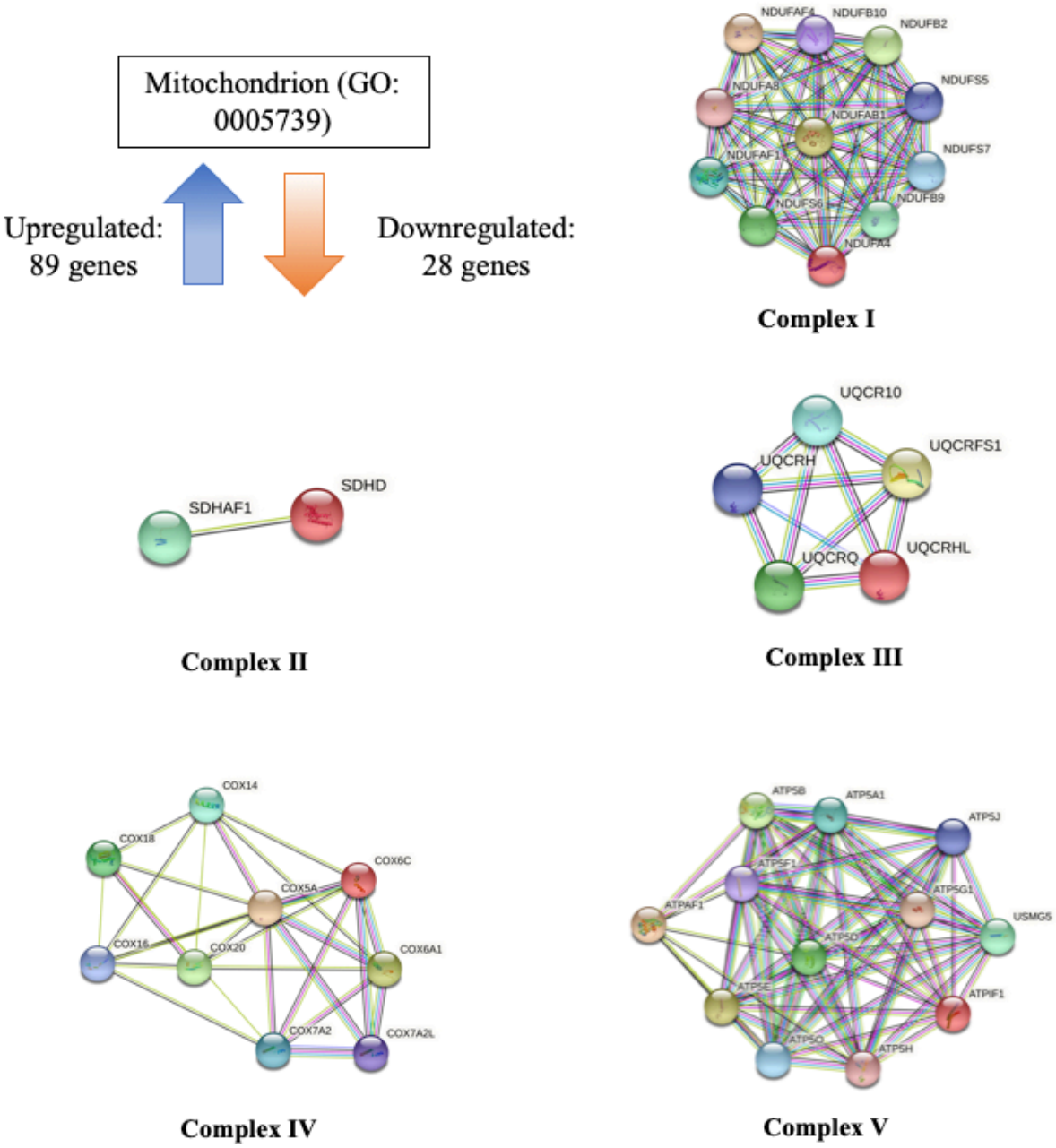


Figure 4.4 Dysregulated expression of mitochondrial proteins by the TDP-43^{M337V} mutation in iPSC-MNs. Transcriptomic data previously generated by members of the Talbot laboratory and reanalysed for expression of mitochondrial proteins. Transcripts shown demonstrated dysregulated expression in TDP-43^{M337V} iPSC-MNs compared to controls, as identified through *Panther* using the GO term 'mitochondrion'. Transcripts are grouped according their association with complexes I-V of the mitochondrial respiratory chain.

To investigate the expression of glycolytic enzymes and mitochondrial proteins in TDP-43^{M337V} mESC-MNs, quantitative reverse transcriptase PCR (qRT-PCR) and Western blotting were performed. Analysis revealed no significant differences in the expression of glycolytic enzymes, GAPDH (p = 0.3248) or PGK1 (p = 0.7859), at the mRNA level in TDP-43^{M337V} mESC-MNs relative to TDP-43^{WT} controls (Figure 4.5A-B). Analysis of protein expression revealed no significant differences in the expression of GAPDH (p = 0.0890), PGAM 1 (p = 0.0511) or PGK1 (p = 0.8637) in TDP-43^{M337V} mESC-MNs compared to TDP-43^{WT} controls (Figure 4.5C-H). Regarding to mitochondrial protein expression, no significant differences in outer mitochondrial membrane protein, TOMM20, were observed between TDP-43^{WT} and TDP-43^{M337V} mESC-MNs (p = 0.2027; Figure 4.6A-B), indicating no differences in mitochondrial mass. Similarly, no significant differences were observed in the expression of inner mitochondrial membrane proteins, cytochrome C (p = 0.2510), cytochrome C oxidase complex IV (COX IV) (p = 0.3362) and ATP synthase (ATPB) (p = 0.1976) between TDP-43^{M337V} and TDP-43^{WT} mESC-MNs (Figure 4.6C-E). However, TDP-43^{M337V} mESC-MNs demonstrated a significant increase in the expression of COX5A (p = 0.0254), relative to TDP-43^{WT} controls (Figure 4.6F). Taken together, these findings suggest selective dysregulation of the mitochondrial complex IV subunit COX5A in TDP-43^{M337V} mESC-MNs.

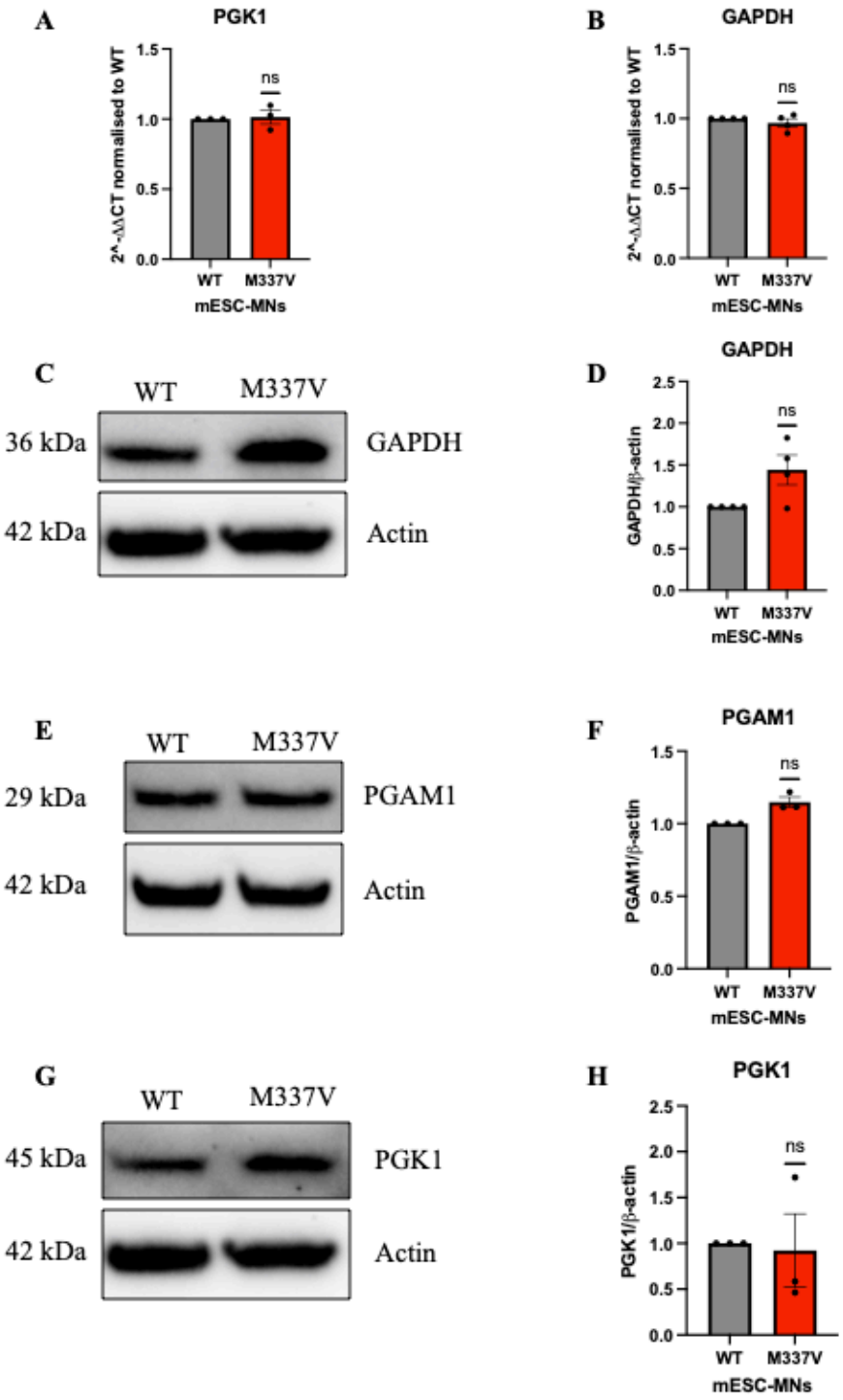


Figure 4.5 Expression of glycolytic enzymes in mESC-MNs. A-B Results of quantitative RT-PCR to assess expression of glycolytic enzymes, PGK1 and GAPDH, in TDP-43^{WT} and TDP-43^{M337V} mESC-MNs. **C** and **D** Western blot and quantification of GAPDH expression in TDP-43^{WT} and TDP-43^{M337V} mESC-MNs. **E** and **F** Western blot and quantification of PGAM1 expression in TDP-43^{WT} and TDP-43^{M337V} mESC-MNs. **G** and **H** Western blot and quantification of PGK1 expression in TDP-43^{WT} and TDP-43^{M337V} mESC-MNs. Statistics A-H: One sample *t*- test, ($n = \geq 3$).

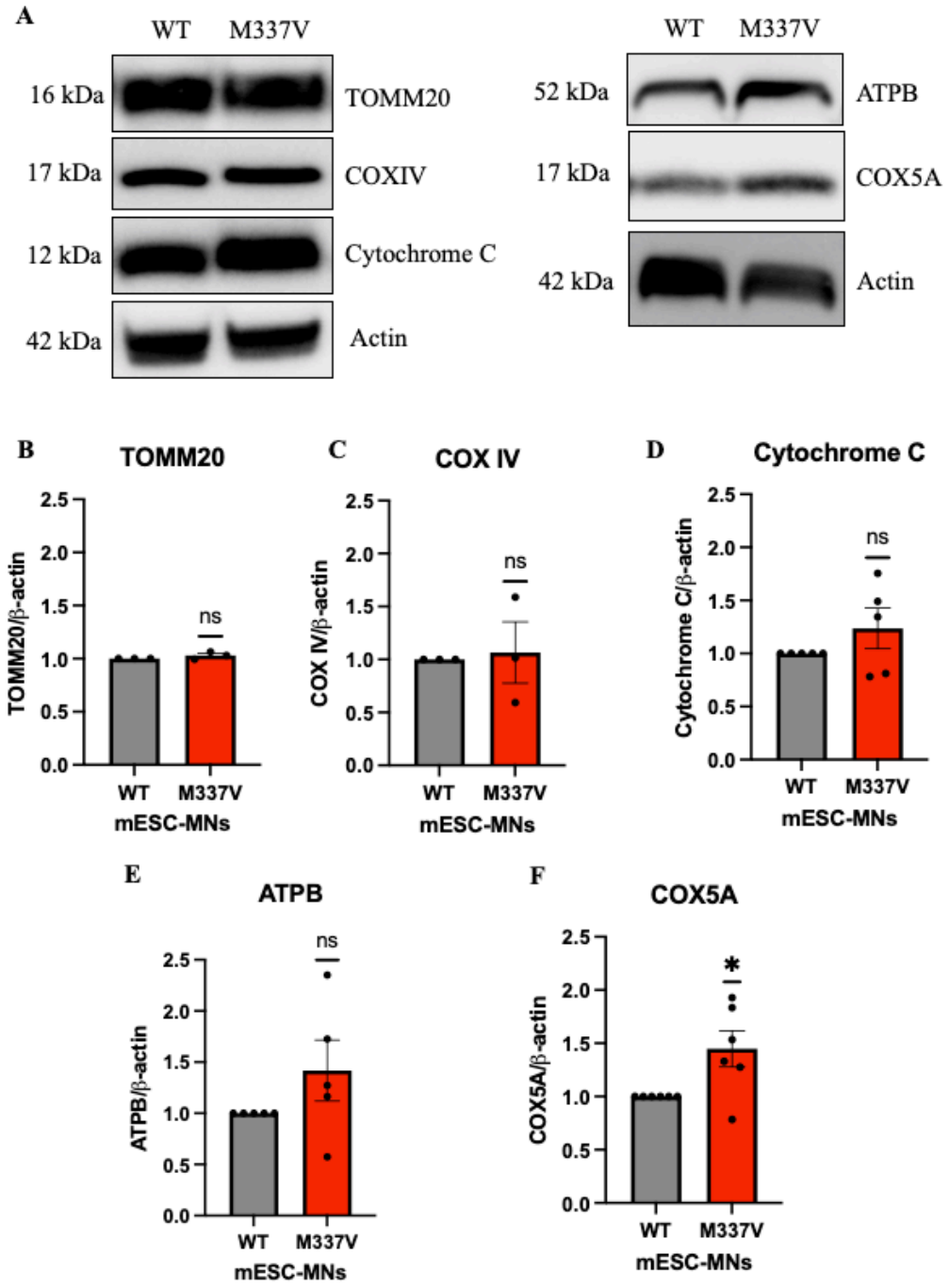


Figure 4.6 Increased expression of COX5A in TDP-43^{M337V} mESC-MNs. A Western blot of mitochondrial proteins in TDP-43^{WT} and TDP-43^{M337V} mESC-MNs. **B-F** Quantification of mitochondrial protein expression in TDP-43^{WT} and TDP-43^{M337V} mESC-MNs. Statistics A-F: One sample *t*-test, ($n = \geq 3$).

4.2.2. TDP-43^{M337V} and oxidative stress alter interactions with glycolytic and mitochondrial proteins in mESC-MNs

Interactions between TDP-43 and other proteins through its C-terminal region are critical in the regulation of cellular functions including the control of gene transcription, alternative splicing, maintenance of mRNA stability, translation and protein homeostasis (Y. M. Ayala et al., 2011; Buratti & Baralle, 2008; Ling et al., 2013). Previous work by Dr Emily Feneberg, a former member of the Talbot laboratory, investigated the TDP-43 interactome in mESC-MNs expressing either TDP-43^{WT} or TDP-43^{M337V}. Using mass spectrometry, interactors of TDP-43^{WT} and TDP-43^{M337V} in unstressed and oxidative stressed conditions were determined (Feneberg et al., 2020). In unstressed conditions, a significant reduction in TDP-43 interactors was observed in TDP-43^{M337V} mESC-MNs compared to TDP-43^{WT} controls (Figure 4.7A). Oxidative stress, induced through treatment with sodium arsenite, further reduced the number of TDP-43 interactors in both TDP-43^{WT} and TDP-43^{M337V} mESC-MNs (Figure 4.7B). I re-probed this dataset to examine whether TDP-43^{M337V} expression altered interactions with glycolytic and mitochondrial proteins. In the context of glycolysis, TDP-43^{WT} interacts with ALDOA, PGK1 and PGAM1 in unstressed conditions. Oxidative stress, leads to loss of interaction with PGK1 in TDP-43^{WT}, but interactions with ALDOA and PGAM1 remain intact. Expression of TDP-43^{M337V} leads to loss of interaction with all three proteins in unstressed conditions. TDP-43^{WT} was found to interact with a number of mitochondrial proteins, including subunits of Complex IV. Oxidative stress led to loss of interaction of TDP-43^{WT} with COX7C and COX6C, but a gain of interaction with COX2, COX41, COX5B and COX5A. Interestingly, TDP-43^{M337V} was found to interact with COX5A in unstressed conditions. Similarly, a gain of interaction with ATP synthase subunit B (ATPB) was observed following oxidative stress in TDP-43^{WT} mESC-MNs that was also observed in TDP-43^{M337V} mESC-MNs in unstressed

conditions (Figure 4.7C). These findings suggest that TDP-43^{M337V} expression and oxidative stress lead to dysregulated interactions between TDP-43 and proteins involved in cellular bioenergetics.

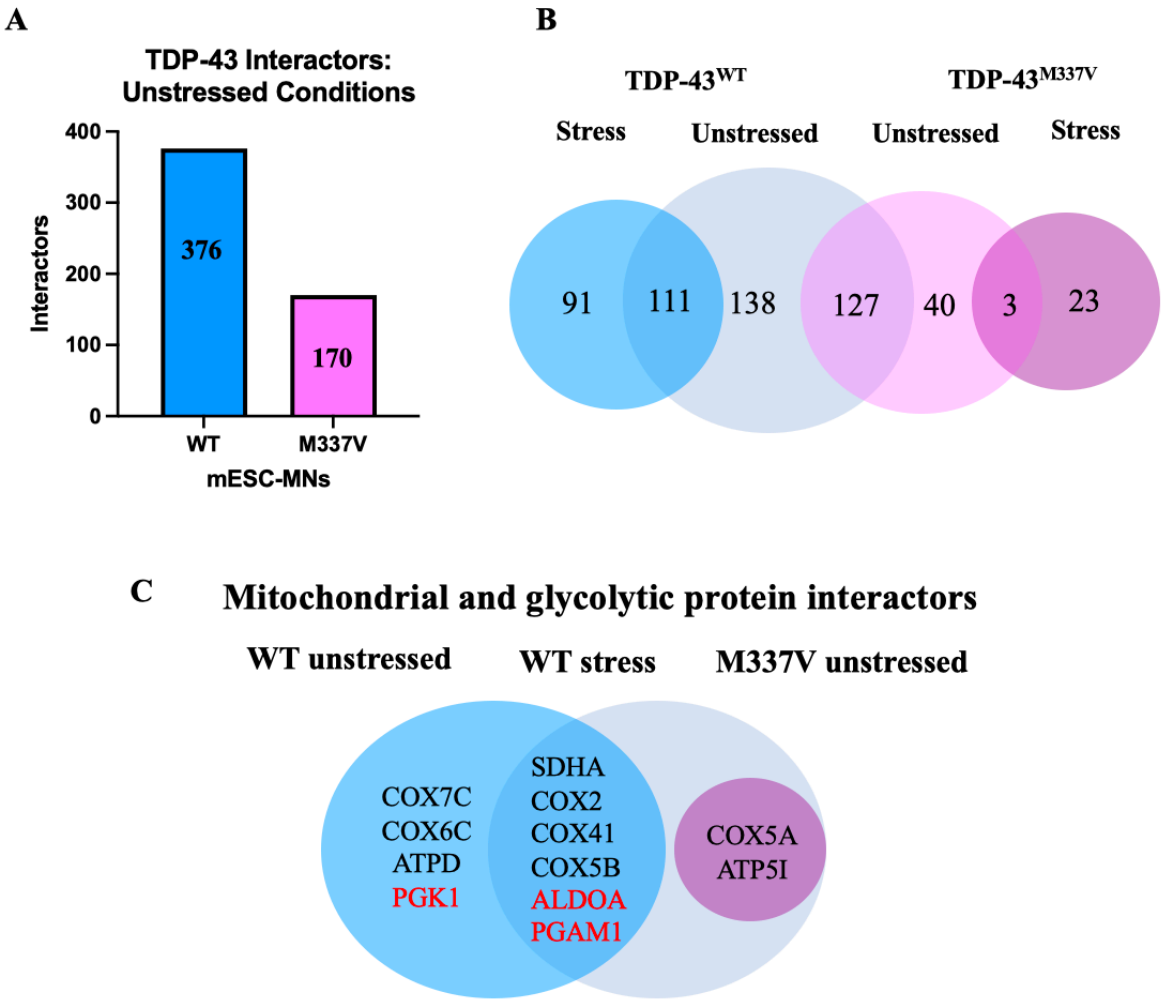


Figure 4.7 TDP-43^{M337V} interactome reveals dysregulated interaction with electron transport chain components. A Quantification of TDP-43 interactors in TDP-43^{WT} and TDP-43^{M337V} mESC-MNs. **B** Venn diagram depicting the number of TDP-43 interactors in TDP-43^{WT} and TDP-43^{M337V} mESC-MNs in unstressed and oxidative stressed conditions. **C** TDP-43 interactions with mitochondrial (black) and glycolytic (red) proteins in TDP-43^{WT} mESC-MNs in unstressed and stressed conditions and in TDP-43^{M337V} mESC-MNs in unstressed conditions.

In an attempt to validate dysregulated interactions identified in the TDP-43^{M337V} interactome, immunocytochemistry and co-localisation analysis were performed. ATPB interacted with TDP-43^{M337V} in unstressed conditions and with TDP-43^{WT} in stressed conditions, suggesting a possible toxic gain of interaction in TDP-43^{M337V} mESC-MNs. However, analysis revealed no significant differences in co-localisation in TDP-43^{M337V} mESC-MNs compared to TDP-43^{WT} controls (unpaired *t*-test: Manders M1, $p = 0.8538$; Manders M2, $p = 0.7831$) (Figure 4.8). To investigate whether the localisation of TDP-43 to mitochondria was altered in TDP-43^{M337V} mESC-MNs I performed mitochondrial fractionation of protein lysates extracted from TDP-43^{WT} and TDP-43^{M337V} mESC-MNs to compare levels of TDP-43 present within the mitochondrial fraction. Following mitochondrial fractionation, lysates underwent gel electrophoresis and Western blotting for TDP-43 and the mitochondrial marker, TOMM20. Staining against the nuclear marker, histone h3, was also performed to confirm isolation of the mitochondrial fraction. In a preliminary experiment I observed greater expression of TDP-43 within the mitochondrial fraction in TDP-43^{M337V} mESC-MNs compared with TDP-43^{WT} controls (Figure 4.9). However, these results are only preliminary ($n = 1$), and further experiments will be required to establish whether increased expression of TDP-43 within the mitochondrial fraction is observed in TDP-43^{M337V} mESC-MNs.

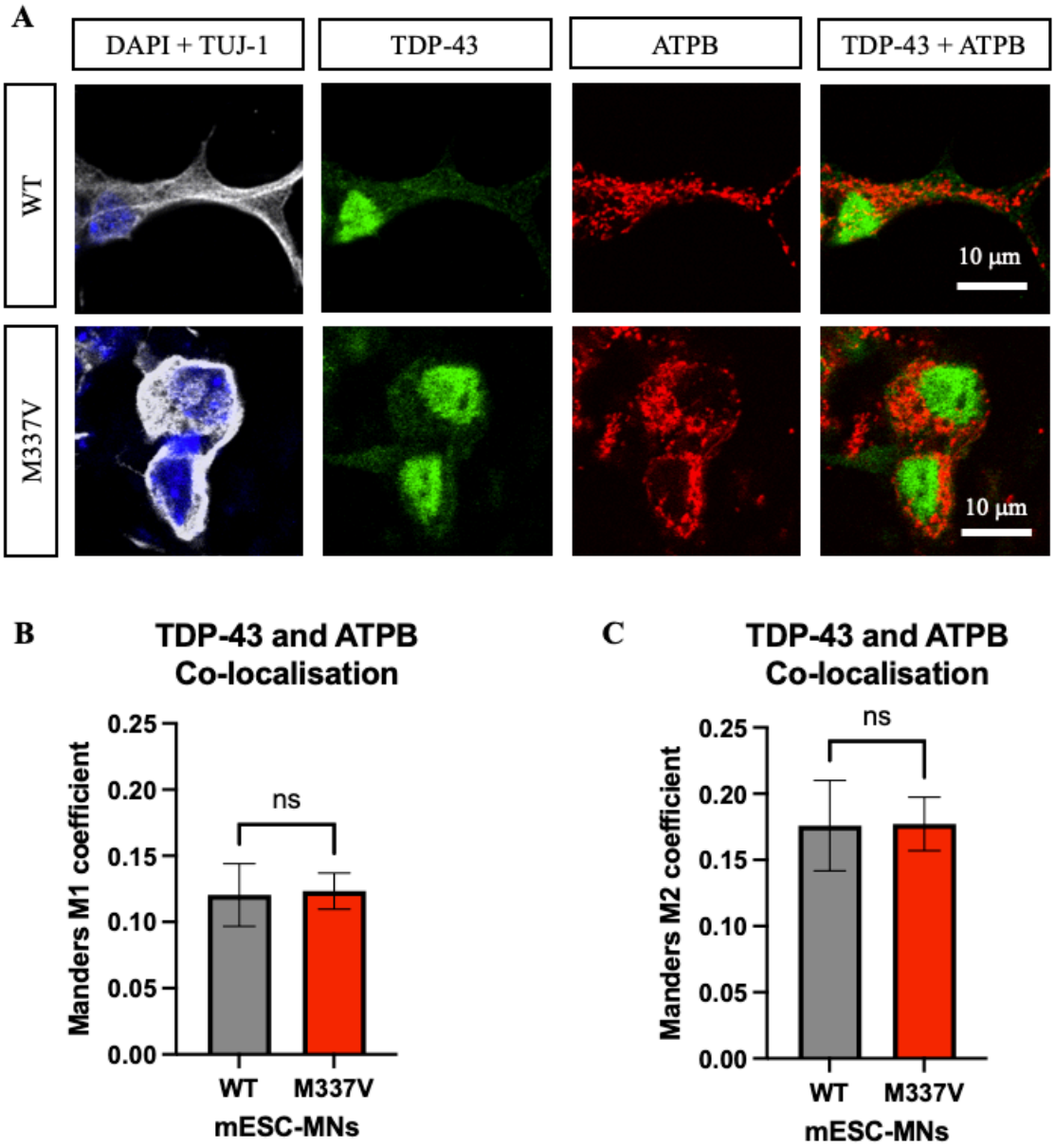


Figure 4.8 Co-localisation of ATPB and TDP-43 in TDP-43^{M337V} mESC-MNs. A Immunocytochemistry for TDP-43 and ATPB in TDP-43^{WT} and TDP-43^{M337V} mESC-MNs after 3 days *in vitro*. **B** Manders M1 co-localisation coefficient, which quantifies the fraction of red fluorescence (ATPB) in areas of green fluorescence (TDP-43). **C** Manders M2 co-localisation coefficient, which quantifies the fraction of green fluorescence (TDP-43) in areas of red fluorescence (ATPB). Statistics for B and C: Unpaired t-test (n = 3), error bars SEM.

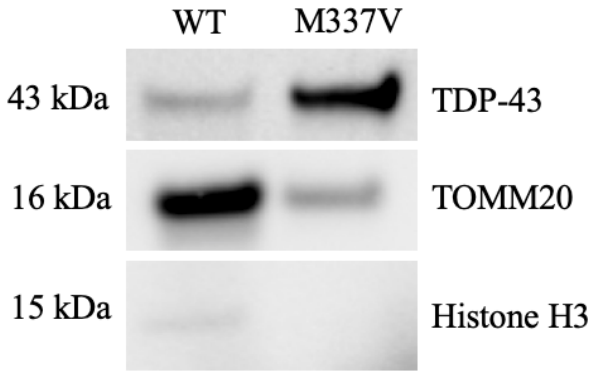


Figure 4.9 Mitochondrial fractionation in TDP-43^{WT} and TDP-43^{M337V} mESC-MNs. Western blot of protein lysates from the mitochondrial fraction probed for the mitochondrial marker TOMM20 and the nuclear marker Histone H3. Preliminary data, $n = 1$.

4.2.3. Basal glycolysis is significantly reduced in TDP-43^{M337V} mESC-MNs following oxidative stress

To investigate whether the TDP-43^{M337V} pathogenic mutation leads to functional impairments in glycolysis, I next analysed glycolytic flux in mESC-MNs using the Seahorse XF Analyzer. I also sought to examine whether the pro-survival drug, terazosin, which significantly improves cellular viability in TDP-43^{M337V} mESC-MNs, exerts its neuroprotective effects through increasing glycolysis. mESC-MNs precursors were plated into 96-well microplates at a density of 100,000 cells/well. The Glycolytic Rate Assay (Agilent) was performed at DIV 5, following differentiation of mESCs to motor neurons. This assay allows measurement of basal glycolysis and compensatory glycolysis, following addition of the mitochondrial complex I and complex III inhibitors, rotenone and antimycin A, to block mitochondrial respiration. Glycolysis is then terminated following addition of 2-deoxy-D-glucose (2-DG), which inhibits glycolysis through competitive binding of glucose hexokinase, the first enzyme in the glycolytic pathway (Figure 4.10). To investigate the effects of oxidative stress on glycolysis, motor neurons were treated with sodium arsenite at 0.5 mM for 1 hour prior to the assay. To examine the effects of terazosin

on glycolysis, TDP-43^{M337V} mESC-MNs were treated with 2.5 μM of terazosin in both unstressed and stressed conditions for 24 hours prior to extracellular flux analysis. TDP-43^{NTg} mESC-MNs, which do not carry the human *TARDBP* BAC construct, were examined alongside TDP-43^{WT} mESC-MNs as an additional control.

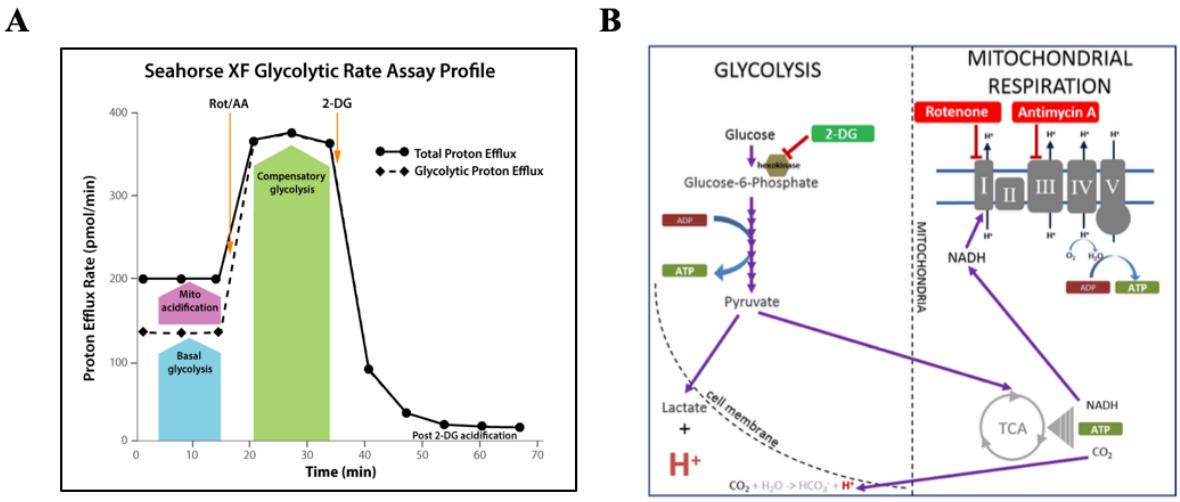


Figure 4.10 Seahorse Glycolytic Rate Assay (Adapted from Agilent). A Addition of rotenone/antimycin A (RotAA) inhibits complexes I and III of the mitochondrial respiratory chain, forcing neurons to utilise glycolysis and generate readouts for basal and compensatory glycolysis. Addition of the glucose analog, 2-deoxy-D-glucose (2-DG), inhibits glycolysis through competitive binding of glucose hexokinase, the first enzyme in the glycolytic pathway. **B** Glycolysis is measured by the Seahorse XF Analyzer as the extracellular acidification rate (ECAR), which results predominantly from the extrusion of protons following the breakdown of pyruvate with a small contribution from CO_2 produced from the TCA cycle. The contribution of ECAR resulting from mitochondrial TCA activity is calculated and removed by inhibiting complexes I and III with Rot/AA.

In unstressed conditions, comparable levels of basal glycolysis ($p = 0.9983$) and compensatory glycolysis ($p = >0.9999$) were observed in TDP-43^{NTg} mESC-MNs relative to TDP-43^{WT} controls. In unstressed conditions, the TDP-43^{M337V} mutant motor neurons demonstrated no significant differences in basal glycolysis ($p = 0.5692$) or compensatory glycolysis ($p = 0.9725$) relative to TDP-43^{WT} controls. Treatment with terazosin did not significantly alter basal glycolysis ($p = 0.1372$) or compensatory glycolysis ($p = 0.4652$) in TDP-43^{M337V} mESC-MNs relative to TDP-43^{WT} controls (Figure 4.11). Following oxidative stress induced by sodium arsenite, no significant differences in the levels of basal glycolysis ($p = 0.9170$) or compensatory glycolysis ($p = 0.9991$) were observed in TDP-43^{NTg} relative to TDP-43^{WT} controls. Whilst TDP-43^{M337V} mESC-MNs showed no significant differences in compensatory glycolysis compared to TDP-43^{WT} controls ($p = 0.0817$), a significant reduction in basal glycolysis was observed in TDP-43^{M337V} mESC-MNs compared to TDP-43^{WT} mESC-MNs following oxidative stress ($p = 0.0272$). In stressed conditions, treatment with terazosin increased levels of basal glycolysis in TDP-43^{M337V} mESC-MNs, to levels comparable with TDP-43^{WT} mESC-MNs (basal glycolysis: $p = 0.9810$) (Figure 4.12). These findings suggest reduced basal glycolysis is observed in TDP-43^{M337V} only in response to oxidative stress. Moreover, that in conditions of oxidative stress, treatment with terazosin significantly increases basal glycolysis in TDP-43^{M337V} to levels comparable with TDP-43^{WT} mESC-MNs.

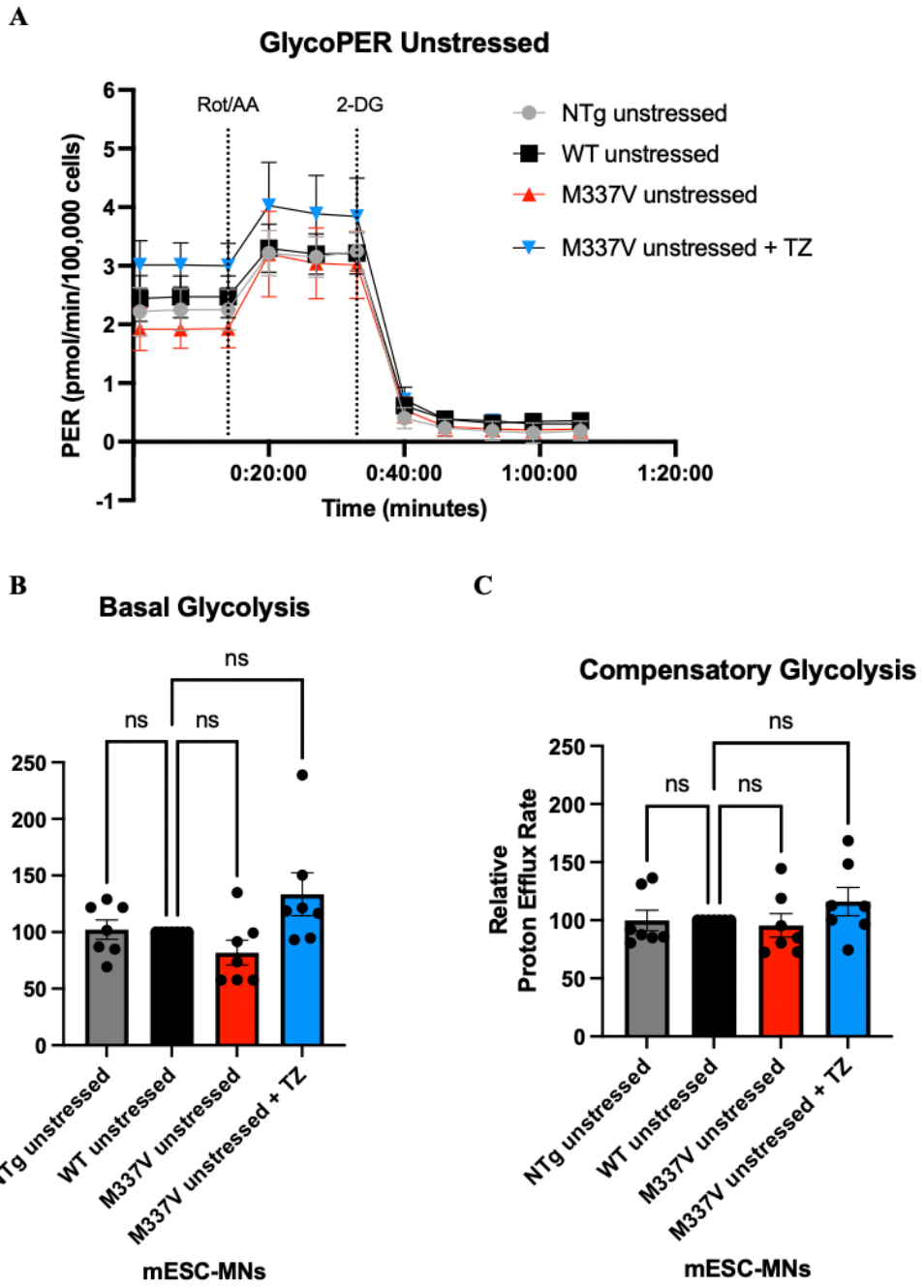


Figure 4.11 The TDP-43^{M337V} mutation does not significantly alter glycolysis in unstressed conditions. A Proton efflux rate (PER) in TDP-43^{NTg}, TDP-43^{WT} and TDP-43^{M337V} mESC-MNs in unstressed conditions. The effects of terazosin (TZ), applied at 2.5 µM or 24 hours prior to the assay, was examined in TDP-43^{M337V} mESC-MNs. **B** Basal glycolysis in TDP-43^{NTg}, TDP-43^{WT}, TDP-43^{M337V} and TDP-43^{M337V} + terazosin (TZ) mESC-MNs in unstressed conditions. **C** Compensatory glycolysis in TDP-43^{NTg}, TDP-43^{WT}, TDP-43^{M337V} and TDP-43^{M337V} + terazosin (TZ) mESC-MNs in unstressed conditions. For B-C: PER is shown relative to TDP-43^{WT} mESC-MNs. One-way ANOVA with Dunnett's multiple comparisons ($n = 6$), all conditions compared to TDP-43^{WT} controls. Error bars SEM.

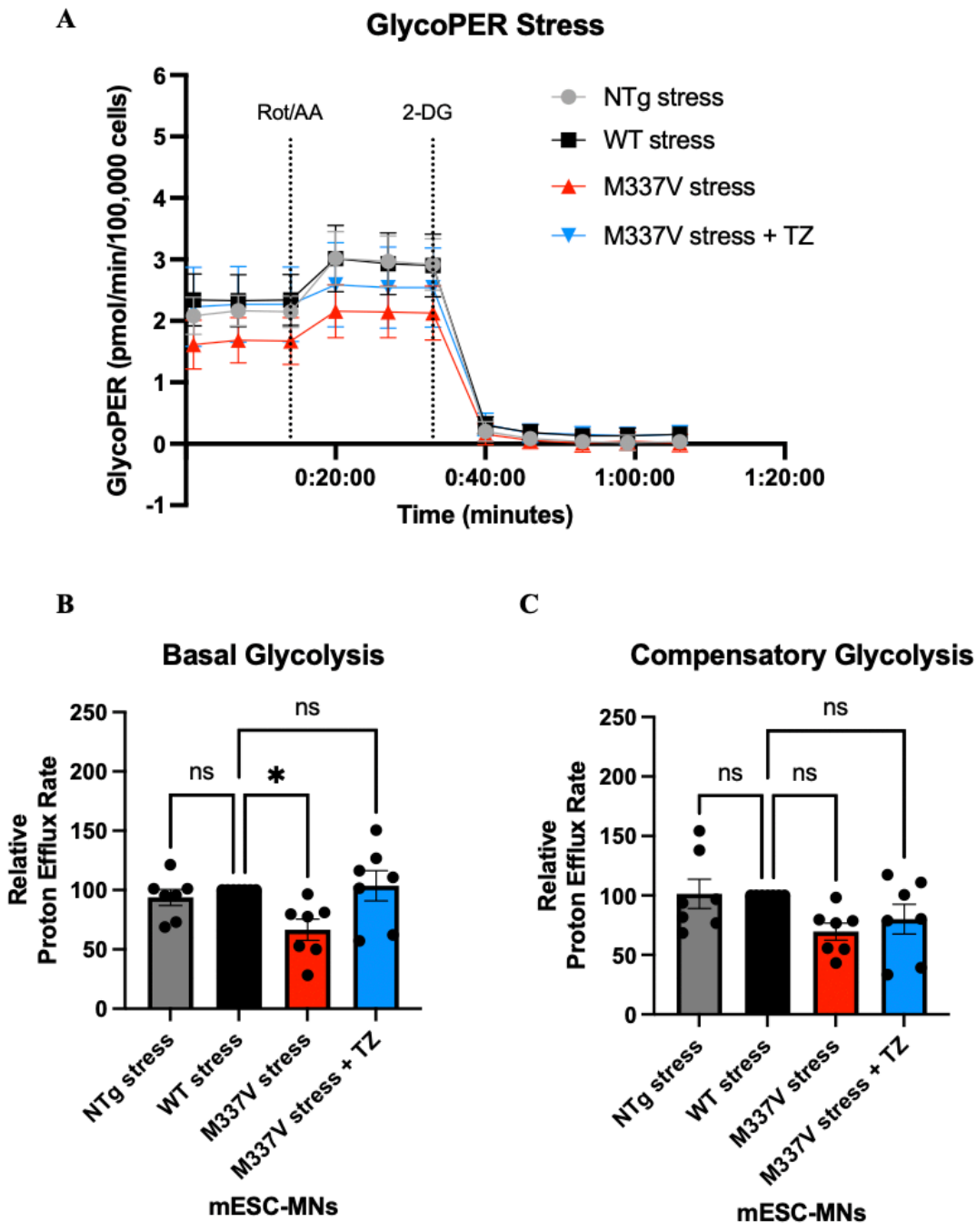


Figure 4.12 The TDP-43^{M337V} mutation significantly impairs glycolysis following oxidative stress, which is rescued by terazosin treatment. A Proton efflux rate (PER) in TDP-43^{NTg}, TDP-43^{WT} and TDP-43^{M337V} mESC-MNs following oxidative stress induced by sodium arsenite. The effects of terazosin (TZ), applied at 2.5 μM or 24 hours prior to the assay, was examined in TDP-43^{M337V} mESC-MNs. **B** Basal glycolysis in TDP-43^{NTg}, TDP-43^{WT}, TDP-43^{M337V} and TDP-43^{M337V} + terazosin (TZ) mESC-MNs following oxidative stress. **C** Compensatory glycolysis in TDP-43^{NTg}, TDP-43^{WT}, TDP-43^{M337V} and TDP-43^{M337V} + terazosin (TZ) mESC-MNs following oxidative stress. For B-C: PER is shown relative to TDP-43^{WT} mESC-MNs. One-way ANOVA with Dunnett's multiple comparisons (n = 6), all conditions compared to TDP-43^{WT} controls, * p <0.05. Error bars SEM.

4.2.4. Analysis of mitochondrial bioenergetics in mESC-MNs: mitochondrial membrane potential, oxidative phosphorylation and the effects of terazosin

Maintenance of the mitochondrial membrane potential is crucial for regulating ATP production through oxidative phosphorylation. To investigate whether TDP-43^{M337V} expression alters the mitochondrial membrane potential, I performed immunocytochemistry on unstressed cells for MitoTracker^{TM} Red CMXRed, as uptake of this dye is dependent on the mitochondrial membrane potential. Coverslips were counterstained for TOMM20, to allow MitoTracker intensity to be normalised to mitochondrial number. Whilst no significant differences were observed between TDP-43^{NTg} and TDP-43^{WT} mESC-MNs ($p = 0.2382$), significantly increased MitoTracker intensity was observed in TDP-43^{M337V} mESC-MNs relative to TDP-43^{WT} controls ($p = < 0.0001$) (Figure 4.13).

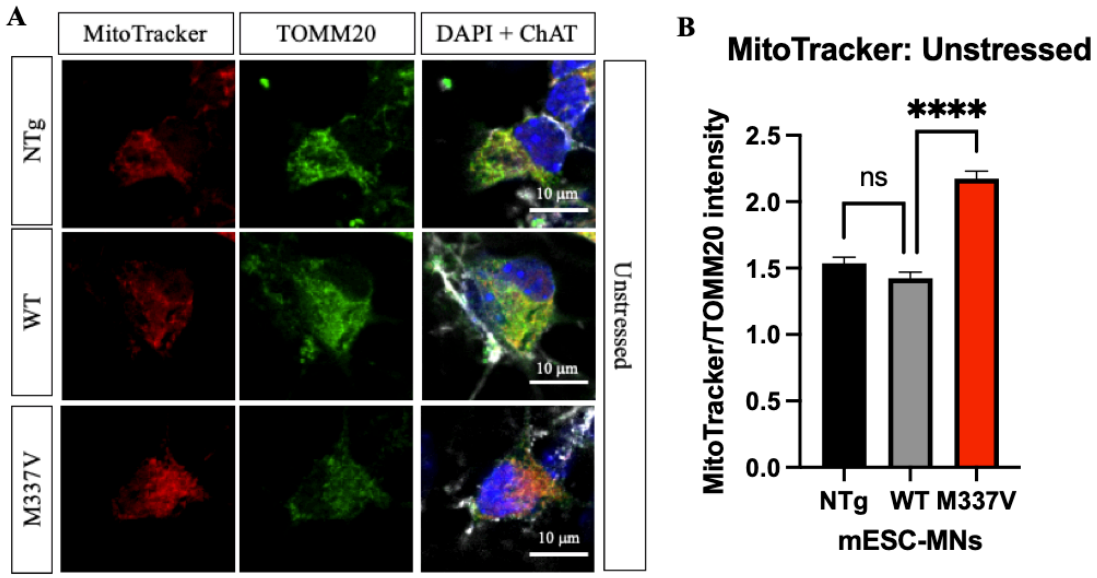


Figure 4.13 MitoTracker intensity is significantly increased in TDP-43^{M337V} mESC-MNs relative to controls in unstressed conditions. A MitoTracker and TOMM20 in TDP-43^{NTg}, TDP-43^{WT} and TDP-43^{M337V} mESC-MNs in unstressed conditions. B Quantification of MitoTracker intensity normalised to mitochondrial number (TOMM20) in TDP-43^{NTg}, TDP-43^{WT} and TDP-43^{M337V} mESC-MNs. One-way ANOVA with Tukey's multiple comparisons (n = ≥ 100 cells per group across 3n differentiations).

Next, to investigate whether expression of TDP-43^{M337V} significantly affected mitochondrial bioenergetics in mESC-MNs, mitochondrial respiration was analysed using the Seahorse XF Analyzer. As with the glycolytic rate assay, mESC-MNs precursors were plated into 96-well microplates at a density of 100,000 cells/well. At DIV 5, the Mito Stress Test (Agilent) was performed, which involves sequential addition of various compounds that target the enzymatic complexes present within the inner mitochondrial membrane. Addition of these drugs allows mitochondrial respiration to be manipulated to investigate levels of basal respiration, maximal respiration, ATP production and spare respiratory capacity (Figure 4.14). To investigate the effects of oxidative stress on mitochondrial respiration, motor neurons were treated with sodium arsenite at 0.5 mM for 1 hour prior to the assay. To examine the effects of terazosin on mitochondrial respiration, TDP-43^{M337V} mESC-MNs were treated with 2.5 μM of terazosin in both unstressed and stressed conditions for 24 hours prior to extracellular flux analysis. TDP-43^{NTg} mESC-MNs were included as an additional control alongside TDP-43^{WT} mESC-MNs.

In unstressed conditions, no significant differences were observed in levels of basal respiration, maximal respiration, ATP production or spare respiratory capacity between TDP-43^{NTg} and TDP-43^{WT} mESC-MNs (basal: p = 0.5466; maximal: p = 0.8210; ATP: p = 0.5323; spare respiratory capacity: p = 0.9062; n = 6). Similarly, comparable levels of mitochondrial respiration were observed between and TDP-43^{WT} and TDP-43^{M337V} mESC-MNs in unstressed conditions (basal: p = 0.9916; maximal: p = 0.8336; ATP: p = 0.9910; spare respiratory capacity: p = 0.7520). In unstressed conditions, treatment with terazosin did not significantly alter mitochondrial respiration in TDP-43^{M337V} mESC-MNs compared to TDP-43^{WT} controls (basal respiration: p = 0.4727, maximal respiration: p = >0.9999, ATP production: p = 0.6213, spare respiratory capacity: p = 0.6801) (Figure 4.15). Following oxidative stress, no significant differences in mitochondrial respiration were observed between TDP-43^{NTg} and TDP-43^{WT}

mESC-MNs (basal: $p = 0.9996$; maximal: $p = 0.4722$; ATP: $p = 0.9315$; spare respiratory capacity: $p = 0.6812$). Similarly, no significant differences in mitochondrial respiration were observed between TDP-43^{M337V} mESC-MNs and TDP-43^{WT} controls following oxidative stress (basal respiration: $p = 0.9978$; maximal respiration: $p = 0.6220$; ATP production: $p = 0.7464$, spare respiratory capacity: $p = 0.3933$). Treatment with terazosin in oxidative stress conditions significantly reduced basal respiration and ATP production in TDP-43^{M337V} mESC-MNs relative to TDP-43^{WT} controls (basal respiration: $p = 0.0051$, ATP: $p = 0.0148$), but did not significantly alter maximum respiration or spare respiratory capacity (maximum respiration: $p = 0.1317$, spare respiratory capacity: $p = 0.6172$) (Figure 4.16). These findings suggest that expression of the TDP-43^{M337V} mutation does not significantly alter mitochondrial respiration and that treatment with terazosin significantly reduces mitochondrial respiration.

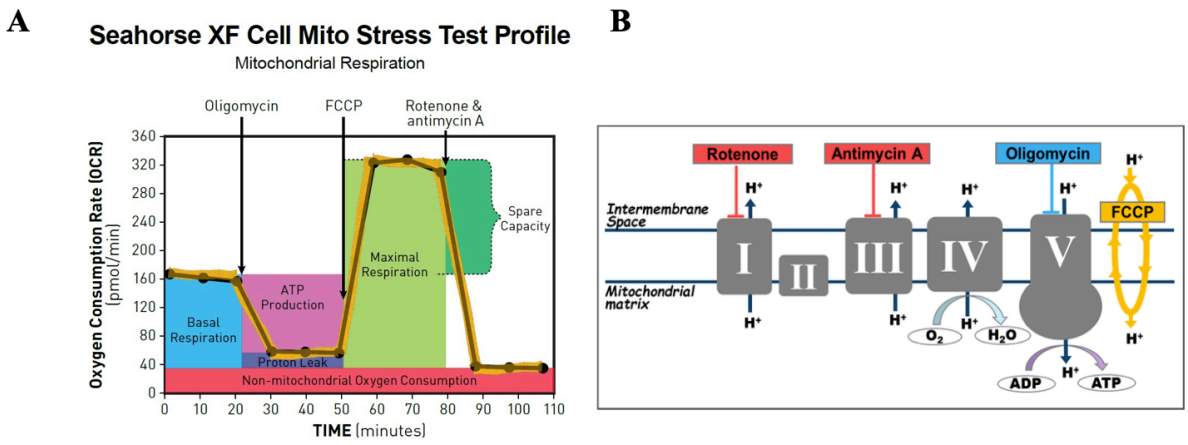


Figure 4.14 Seahorse Mito Stress Test (adapted from Agilent). A Mito Stress test profile allows the measurement of basal respiration, ATP production, maximal respiration and spare respiratory capacity through the sequential addition of compounds targeting complexes of the mitochondrial respiratory chain. **B** Schematic depicting the targets of compounds within the Mito Stress Test assay. Rotenone and antimycin A inhibit complexes I and III respectively, which inhibits mitochondrial respiration. Oligomycin inhibits ATP synthase (complex V), leading to a reduction in electron flow through the mitochondrial respiratory chain and results in a reduction in mitochondrial respiration and oxygen consumption rate (OCR). FCCP is an uncoupling agent that abolishes the proton gradient across the mitochondrial membrane and disrupts the mitochondrial membrane potential. This results in the uninhibited flow of electrons through the mitochondrial respiratory chain, leading to increased mitochondrial respiration and measurements of maximal respiration capacity.

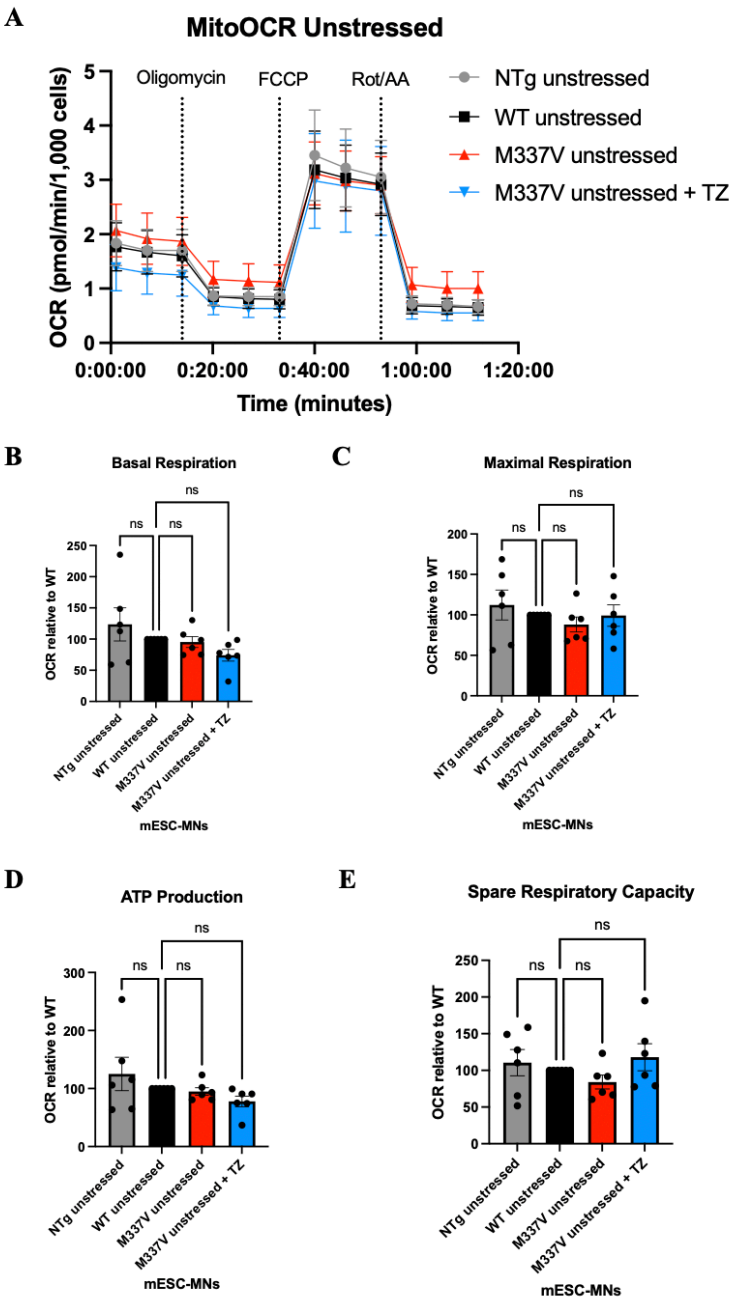


Figure 4.15 The TDP-43^{M337V} mutation does not significantly alter mitochondrial respiration in unstressed conditions. A Oxygen consumption rate (OCR) in TDP-43^{NTg}, TDP-43^{WT} and TDP-43^{M337V} mESC-MNs in unstressed conditions. The effects of terazosin (TZ), applied at 2.5 μM or 24 hours prior to the assay, was examined in TDP-43^{M337V} mESC-MNs. **B** Basal respiration in TDP-43^{NTg}, TDP-43^{WT}, TDP-43^{M337V} and TDP-43^{M337V} + terazosin (TZ) mESC-MNs in unstressed conditions. **C** Maximal respiration in TDP-43^{NTg}, TDP-43^{WT}, TDP-43^{M337V} and TDP-43^{M337V} + terazosin (TZ) mESC-MNs in unstressed conditions. **D** ATP production in TDP-43^{NTg}, TDP-43^{WT}, TDP-43^{M337V} and TDP-43^{M337V} + terazosin (TZ) mESC-MNs in unstressed conditions. **E** Spare respiratory capacity in TDP-43^{NTg}, TDP-43^{WT}, TDP-43^{M337V} and TDP-43^{M337V} + terazosin (TZ) mESC-MNs in unstressed conditions. For B-E: OCR is shown relative to TDP-43^{WT} mESC-MNs. One-way ANOVA with Dunnett's multiple comparisons (n = 6), all conditions compared to TDP-43^{WT} controls. Error bars SEM.

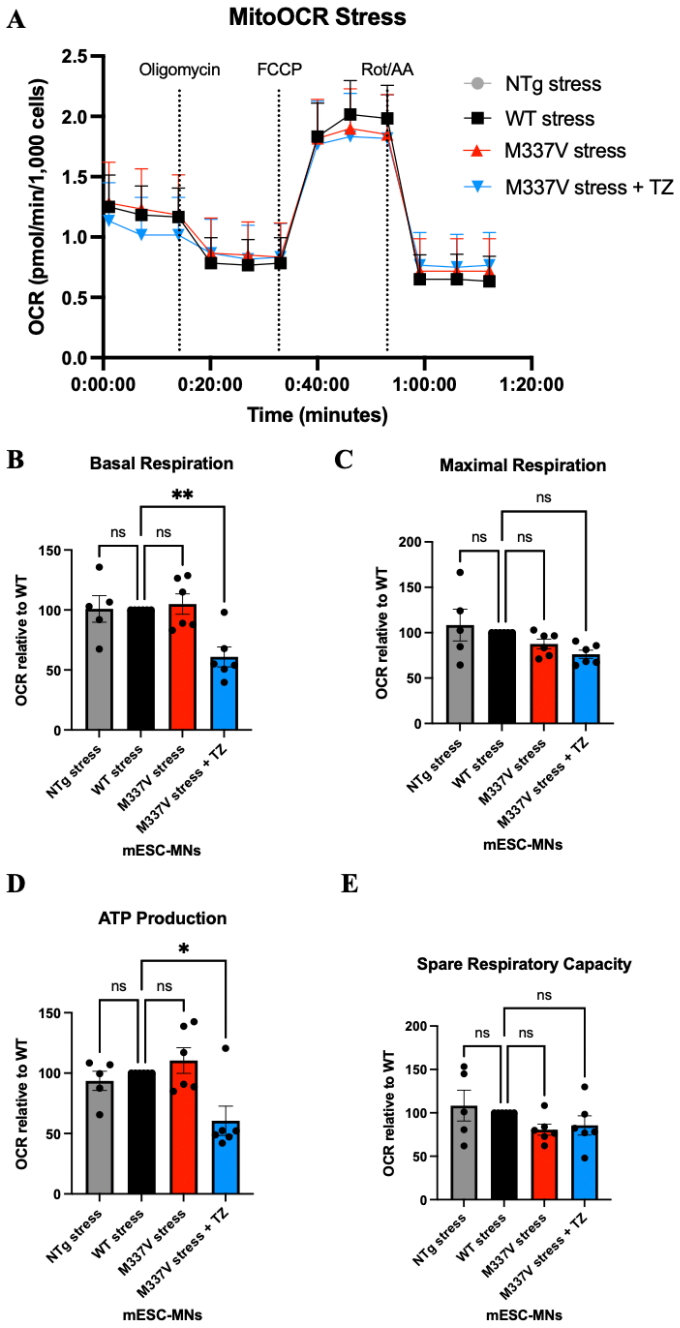


Figure 4.16 The TDP-43^{M337V} mutation significantly impairs spare respiratory capacity following oxidative stress and treatment with terazosin significantly reduces mitochondrial respiration. A Oxygen consumption rate (OCR) in TDP-43^{NTg}, TDP-43^{WT} and TDP-43^{M337V} mESC-MNs following oxidative stress induced by sodium arsenite. The effects of terazosin (TZ), applied at 2.5 µM or 24 hours prior to the assay, was examined in TDP-43^{M337V} mESC-MNs. **B** Basal respiration in TDP-43^{NTg}, TDP-43^{WT}, TDP-43^{M337V} and TDP-43^{M337V} + terazosin (TZ) mESC-MNs following oxidative stress. **C** Maximal respiration in TDP-43^{NTg}, TDP-43^{WT}, TDP-43^{M337V} and TDP-43^{M337V} + terazosin (TZ) mESC-MNs following oxidative stress. **D** ATP production in TDP-43^{NTg}, TDP-43^{WT}, TDP-43^{M337V} and TDP-43^{M337V} + terazosin (TZ) mESC-MNs following oxidative stress. **E** Spare respiratory capacity in TDP-43^{NTg}, TDP-43^{WT}, TDP-43^{M337V} and TDP-43^{M337V} + terazosin (TZ) mESC-MNs following oxidative stress. For B-E: OCR's are shown relative to TDP-43^{WT} mESC-MNs. One-way ANOVA with Dunnett's multiple comparisons ($n = 6$), samples compared to TDP-43^{WT} controls, *$p < 0.05$, ** $p < 0.01$. Error bars SEM.

4.3. Conclusions

In this chapter I have examined the bioenergetic profile associated with expression of the TDP-43^{M337V} mutation. Analysis of RNA sequencing data from TDP-43^{M337V} iPSC-MNs, identified significant dysregulation of glycolytic and mitochondrial proteins compared to control iPSC-MNs. Significantly increased expression of the mitochondrial complex IV subunit, COX5A, was identified in TDP-43^{M337V} mESC-MNs. Analysis of the TDP-43 interactome in mESC-MNs revealed dysregulated interactions induced by expression of the TDP-43^{M337V} mutation and exposure to oxidative stress. TDP-43^{M337V} mESC-MNs show impaired basal glycolysis relative to TDP-43^{WT} mESC-MNs in response to oxidative stress. Treatment with the pro-survival drug, terazosin, leads to increased basal glycolysis and reduced mitochondrial respiration under conditions of oxidative stress. This suggests that terazosin may exert its pro-survival effects, at least in part, through altering cellular bioenergetics.

Previous studies investigating glycolytic flux in iPSC-MNs, identified upregulation of basal acidification, glycolysis and glycolytic capacity in familial ALS and sporadic ALS patient lines compared to healthy controls (Hor et al., 2021). Conversely, reductions in both glycolysis-associated and mitochondria-associated ATP production, were observed in iPSC-MNs from sporadic ALS patients relative to healthy controls (Singh et al., 2021). Glycolytic function has not previously been investigated in our TDP-43^{M337V} mESC-MN model. Here, we report no significant differences in basal or compensatory glycolysis in TDP-43^{M337V} mESC-MNs in unstressed conditions compared to TDP-43^{WT} controls. However, interestingly, we observed significantly reduced basal glycolysis in TDP-43^{M337V} mESC-MNs relative to TDP-43^{WT} controls following oxidative stress (Figure 4.12). These findings are in line with analysis of cell survival, where reduced cell viability was observed in TDP-43^{M337V} mESC-MNs at DIV 3, only following exposure to oxidative stress (Gordon et al., 2019). It has been suggested that

neurodegeneration in ALS results from a multi-step pathogenic process, whereby predisposing genetic risk factors combine with molecular insults to trigger a pathological cascade, culminating in neurodegeneration and motor neuron loss (Chio et al., 2018). Oxidative stress is one such molecular insult that has long been implicated in ALS pathophysiology. Whether oxidative stress is itself the cause of pathogenesis or a downstream consequence of other pathological mechanisms remains unclear. Yet it has been suggested that exposure to oxidative stress may overwhelm cellular homeostatic control mechanisms, tipping the scales from a situation where the cell is able to cope with a toxic insult, to one where the cell succumbs to injury and neurodegeneration ensues (Barber & Shaw, 2010). It would be interesting investigate whether other cellular stressors associated with ALS pathogenesis, such as the ER stress, also induce glycolytic impairments in TDP-43^{M337V} mESC-MNs, or whether the observed impairments reported here are specific to oxidative stress.

Oxidative stress and mitochondrial dysfunction are tightly linked, and both have been heavily implicated in ALS pathogenesis. Under normal physiological conditions, mitochondria produce ROS as a by-product of respiration that are cleared by antioxidant molecules. The balance between ROS production and clearance is crucial in preventing oxidative stress (Barber & Shaw, 2010). Here, I observed no significant differences in mitochondrial respiration in TDP-43^{M337V} mESC-MNs compared to TDP-43^{WT} controls, either in unstressed or stressed conditions. However, I observed significantly increased mitochondrial membrane potential in TDP-43^{M337V} mESC-MNs compared to TDP-43^{WT} controls in unstressed conditions. This suggests that TDP-43^{M337V} mESC-MNs have increased movement of H+ ions across the mitochondrial membrane, which is associated with increased ATP production. Interestingly, this result starkly contrasts findings from the Seahorse Mito Stress Test, where no differences in mitochondrial respiration or ATP production were observed between TDP-43^{WT} and TDP-

43^{M337V} mESC-MNs. However, it is important to consider that the measurement of mitochondrial membrane potential may be confounded by the use of MitoTracker normalised to mitochondrial number using TOMM20; as uptake of the former is dependent on mitochondrial membrane potential, unlike the latter. Given this, MitoTracker and TOMM20 may identify two distinct populations of mitochondria. To rule out this possibility, normalising mitochondrial number through different approaches, ought to be considered carefully in future work. Nevertheless, if mitochondrial membrane potential is increased in TDP-43^{M337V} mESC-MNs, without accompanying increases in mitochondrial respiration parameters, this may suggest that increased mitochondrial membrane potential is a compensatory response required to maintain levels of mitochondrial respiration to those comparable with TDP-43^{WT} mESC-MNs.

Dysregulation of pathways lying upstream of mitochondrial respiration and glycolysis could also contribute to the observed deficits. Cellular energy metabolism is regulated by many upstream pathways, including the PBK/AKT pathway. The PBK/AKT pathway is a key regulator across multiple cellular pathways including metabolism, survival, proliferation and growth (Hemmings & Restuccia, 2012). Dysregulation of AKT signalling, therefore has the potential to impact multiple aspects of cellular health and survival. Given this, the PBK/AKT pathway provides an attractive candidate, that may provide a link between our observations of reduced cell viability and dysregulated cellular metabolism in TDP-43^{M337V} mESC-MNs in response to oxidative stress. Probing of RNA sequencing data from iPSC-MNs reveals significant downregulation of AKT1 and AKT2 in TDP-43^{M337V} iPSC-MNs compared to controls (data not shown). These observations suggest that further analysis of the AKT signalling pathway may yield greater insight into possible upstream mechanisms leading to the

observed impairments in glycolysis, mitochondrial respiration and cellular viability in response to oxidative stress.

In addition to examining the bioenergetic profile of TDP-43^{M337V} mESC-MNs, I have examined the effects of the pro-survival drug, terazosin, on cellular energy metabolism in this model. Here, I have shown that treatment with terazosin increases glycolysis, whilst reducing basal respiration and mitochondria-derived ATP production in TDP-43^{M337V} mESC-MNs following oxidative stress. These findings suggest terazosin may exert its pro-survival effects, at least in part, through inducing a metabolic shift away from mitochondrial respiration towards glycolysis. This is perhaps surprising given that neurons rely predominantly on ATP production from mitochondrial respiration to meet high energy demands. Yet these findings are consistent with previous reports on the physiological effects of alpha 1-adrenergic receptor antagonists (Binet & Claret, 1983; Cai et al., 2019; Lee et al., 2020) and that increasing glycolysis is neuroprotective in ALS (Manzo et al., 2019). The mechanisms through which increasing glycolysis and reducing mitochondrial respiration may be neuroprotective in our TDP-43^{M337V} mESC-MNs remains unclear. In a previous study, treatment with meclizine, an alpha 1-adrenergic receptor antagonist and glycolysis-enhancing agent was shown to protect against neuronal death in the 6-OHDA cell toxicity model of Parkinson's disease. In this case, upregulation of glycolysis through increased PFKFB3 expression was found to mitigate a reduction in mitochondrial membrane potential induced by 6-OHDA treatment and subsequent activation of the apoptotic pathways (Hong et al., 2016). Given this, it may be worthwhile investigating the effects of terazosin treatment on the mitochondrial membrane potential. Yet, here we observed a significantly increased mitochondrial membrane potential in TDP-43^{M337V} mESC-MNs compared to controls in unstressed conditions, suggesting alternative mechanisms may underlie terazosin's neuroprotective effects. It is interesting to note that the effects of

terazosin on cellular bioenergetics differ depending on whether mESC-MNs were unstressed or exposed to oxidative stress. Terazosin does not significantly alter glycolysis or mitochondrial respiration in unstressed conditions, however, following oxidative stress, terazosin treatment leads to a significant increase in basal glycolysis accompanied by reductions in basal respiration and ATP production. Given the tight links between oxidative stress and mitochondrial respiration, inducing a metabolic shift away from mitochondrial respiration and towards glycolysis following oxidative stress may exert neuroprotective effects through limiting ROS production, which would further exacerbate oxidative stress. To test this hypothesis, future work could investigate the effects of terazosin on ROS production using various commercially available products, such as MitoSOX^{TM}. Such approaches have been used in previous studies to quantify levels of oxidative stress (Meng et al., 2017).

There are certain limitations to this work that ought to be considered. Assessment of glycolysis and mitochondrial respiration was measured by proton efflux rate and oxygen consumption respectively, which allows accurate and real-time measurement of cellular bioenergetics with highly sensitive detection rates. Given this, differentiation efficiency is important to consider when interpreting results as additional cell types present within the cultures will contribute to the overall glycolytic output measured. As demonstrated in the previous chapter, our mESC-derived motor neuron cultures demonstrate a differentiation efficiency of between 70-80%. The remaining 20-30% of cells within the culture are unspecified cell types, that have not fully differentiated to motor neurons. If the percentage of undifferentiated cells within the culture is comparable between TDP-43^{WT} and TDP-43^{M337V} differentiations, this would not skew results, however it is difficult to verify this on an experiment-to-experiment basis. To overcome this issue, further optimisation of the differentiation protocol would need to be performed to increase differentiation efficiency and limit numbers of undifferentiated cells. Use of a

compound such as mitomycin C, which kills dividing cells, may prove beneficial. Secondly, to analyse the effects of cellular bioenergetics associated with mitochondrial function, we have focussed primarily on examining the effects of TDP-43^{M337V} expression on mitochondrial respiration. Yet mitochondria have additional important roles in calcium homeostasis and apoptosis that, due to time constraints, we were unable to explore in the present study. It would be interesting to examine whether any disturbances to calcium homeostasis or altered activation of apoptotic pathways are observed in TDP-43^{M337V} mESC-MNs relative to controls. Examination of calcium efflux rates through calcium imaging would provide insight into disturbances specific to TDP-43^{M337V} expression. We were also unable to validate interactions between TDP-43 and COX5A with immunocytochemistry co-localisation experiments, as the COX5A antibody was not amenable to immunocytochemical analysis. It will be important to verify this interaction in future work through co-immunoprecipitation; the gold-standard for assessing protein-protein interactions. Furthermore, given that impairments to mitochondrial respiration were observed in mESC-MNs only following oxidative stress, it would have been valuable to investigate the expression of mitochondrial respiratory chain components both in unstressed and the stressed condition, to examine whether changes in expression are induced by oxidative stress. Finally, we have only examined glycolysis and mitochondrial respiration in TDP-43 mESC-MNs. It would be interesting to investigate whether the deficits observed here could be replicated in iPSC-MNs carrying the same mutation, thus indicating whether the changes are specific to TDP-43^{M337V} expression.

In this chapter I have identified oxidative stress-induced impairments to basal glycolysis in TDP-43^{M337V} mESC-MNs compared to TDP-43^{WT} controls. The exact mechanisms underpinning this impairment remains to be elucidated in future work. Together with findings from the previous chapter, these results suggest that terazosin may exert its neuroprotective

effects following oxidative stress through inducing a metabolic shift away from mitochondrial respiration and towards glycolysis.

CHAPTER 5 Investigating the effects of the TDP-43^{M337V} mutation on axonal transport in mESC-motor neurons

5.1. Introduction and aims

5.1.1. TDP-43 and impaired axonal transport in ALS

Impaired axonal transport has been identified as a prominent feature in ALS pathophysiology for many years. Disruption of axonal transport provides an attractive theory as to why motor neurons, which boast uniquely long axons relative to other neuronal subtypes, may be selectively vulnerable in ALS. Moreover, dysregulation of axonal transport also represents a shared pathophysiological phenotype that has been observed across genetically distinct forms of the disease including *SOD1*, *C9ORF72*, *FUS* and *TARDBP* (Alami et al., 2014; Baldwin et al., 2016; Bilsland et al., 2010; De Vos et al., 2007; Fazal et al., 2021; Magrane et al., 2012). These observations, together with recent technological advances, have generated renewed interest in the study of axonal transport in ALS, which may hold potential as a therapeutic target.

Axonal transport is an essential process in the maintenance of neuronal function and survival. Human spinal motor neurons can have axons extending up to a metre in length and axonal transport is critical to allow effective communication between the cell soma and the synapse. Axonal transport supplies the distal synapse with newly synthesised proteins, lipids and mitochondria and clears debris such as damaged or misfolded proteins, to prevent the build-up of toxic aggregates. In addition, axonal transport is essential for long-range cellular communication via signalling endosomes, which allows the soma to receive, integrate and

respond to information from the cell periphery. Signalling endosomes can carry vital information that promotes survival, or alternatively alert the neuron to cellular stress and trigger apoptosis and cell death (Perlson et al., 2010).

Effective axonal transport requires three essential elements; a stable microtubule cytoskeleton, molecular motor proteins, and their respective adaptors. Microtubules, composed of dimers of alpha- and beta-tubulin, underlie neuronal polarity. Exposed beta-tubulin subunits at the 'plus' ends of microtubule filaments are orientated towards the axon terminal, whereas exposed alpha-tubulin subunits at the 'minus' end are orientated towards to cell soma. This polarity drives the directionality of axonal transport. Anterograde transport describes transport of cargo from the cell soma to the axon terminal, which ensures newly synthesised proteins, lipids and cellular organelles such as mitochondria, are delivered to the distal synapse. Alternatively, retrograde transport describes the transport of cargo towards the cell body. Retrograde transport has important roles in the removal of misfolded or aggregated proteins from the axon, as well as delivery of distal trophic signals to the cell soma. Anterograde and retrograde transport are regulated by different families of motor proteins. The kinesin family of motor proteins is mainly responsible for anterograde transport, whereas retrograde transport is reliant on a single multi-subunit motor complex, cytoplasmic dynein, and it's associated adaptor protein dynactin (Sleigh et al., 2019).

Initial evidence for disruption of axonal transport in ALS came from microscopy studies examining human post-mortem tissue. Researchers reported abnormal accumulations of cargo normally transported along axons, including cytoskeletal components, lysosomes and mitochondria, localised to the cell soma and proximal axon (Corbo & Hays, 1992; Hirano, Donnenfeld, et al., 1984; Hirano, Nakano, et al., 1984; Rouleau et al., 1996; Sasaki & Iwata,

1996a, 1996b). Since these early studies, significant advances have been made in the development of methods for high-resolution microscopy in living cells. Such developments mean it is now possible to observe axonal transport in real-time *in vitro* and *in vivo* at high-resolution, to provide novel insights into this dynamic process. This 'live imaging' technique has been utilised in a plethora of studies that have demonstrated impairments to axonal transport. In models of *TARDBP* mutations, significant impairments to retrograde signalling, mitochondrial transport and the transport of TDP-43 itself have previously been reported (Fazal et al., 2021; Kreiter et al., 2018; Sleigh et al., 2020). Of particular note, analysis of *in vivo* retrograde signalling in our TDP-43^{M337V} BAC transgenic mouse identified significant impairments in the speed and number of pausing endosomes when compared to controls (Sleigh et al., 2020).

5.1.2. Aims

Axonal transport deficits have not yet been examined in the TDP-43^{M337V} mESC-MN model. Given the observed impairments in retrograde signalling in the TDP-43^{M337V} BAC transgenic mouse, I sought to examine whether similar deficits existed *in vitro*, as this could provide a valuable high-throughput screening platform for novel therapeutics. The aims of this chapter are:

1. To examine bi-directional transport of mitochondria in mESC-MNs using live cell imaging of MitoTracker.
2. To examine bi-directional transport of signalling endosomes in mESC-MNs using live cell imaging of cholera toxin B (CTB).
3. To examine the expression of axonal transport related components in TDP-43^{M337V} iPSC-MNs and mESC-MNs.

5.2. Results

5.2.1. TDP-43^{M337V} mESC-MNs show significant impairments to bi-directional mitochondrial transport

In chapter 4, I identified significant reductions in basal glycolysis and mitochondrial spare respiratory capacity in mESC-MNs in response to oxidative stress. I hypothesised that these impairments may result from reduced mitochondrial transport to areas of increased energy demand. Therefore, I next sought to examine the bi-directional transport of mitochondria in mESC-MNs. Initial efforts were focussed on investigating mitochondrial transport in unstressed conditions. mESC-MNs were plated into pre-coated microfluidic chambers at a density of ~100,000 cells/chamber and after 5-7 days *in vitro* had begun to extend axons through the channels (Figure 5.1). The axonal identity of these processes was confirmed through staining for the axonal marker, TAU, and dendritic marker, MAP2 (Figure 5.2). Mitochondrial transport was examined through treatment with MitoTracker for 15 minutes at 20 nM, then images taken every 2 seconds for 300 frames (Figure 5.3A). Images were analysed using the difference tracker FIJI/ImageJ plugin developed by Andrews and colleagues (Andrews et al., 2010), with further downstream analysis conducted in R studio using a script developed by Dr Jakub Scaber in Python. This combined approach allowed the assessment of various parameters of mitochondrial movement including: the percentage of moving versus dynamic stationary mitochondria, direction of movement, speed of movement, pause time and distance travelled.

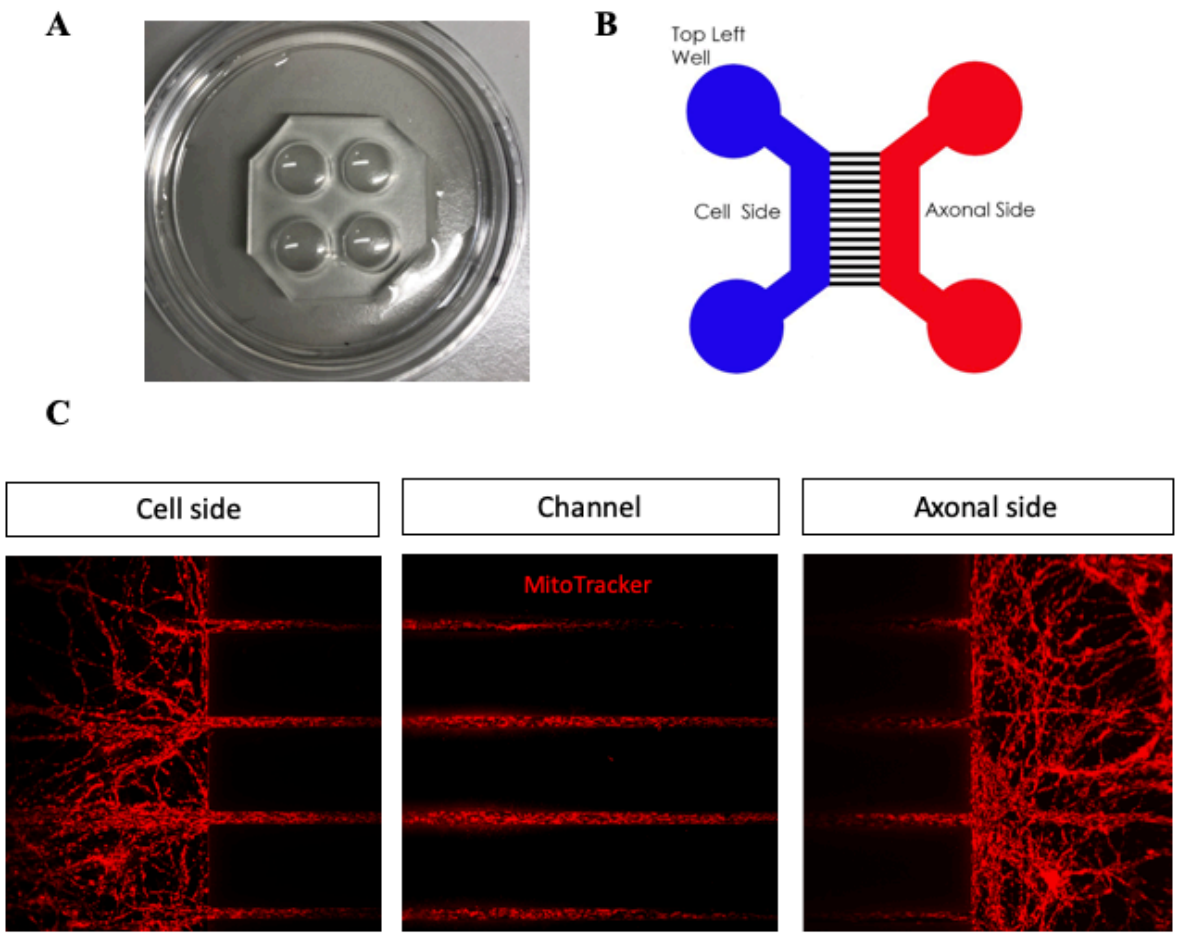


Figure 5.1 Analysis of axonal transport in mESC-MNs using microfluidic chambers. **A** Microfluidic chamber plasma bonded to glass-bottomed dishes. **B** Schematic depicting the structure of microfluidic chambers. mESC-MN precursors were plated into the top left well on the cell side. **C** Confocal microscopy image of MitoTracker showing processes extending through the channel from the cell side to the axonal side.

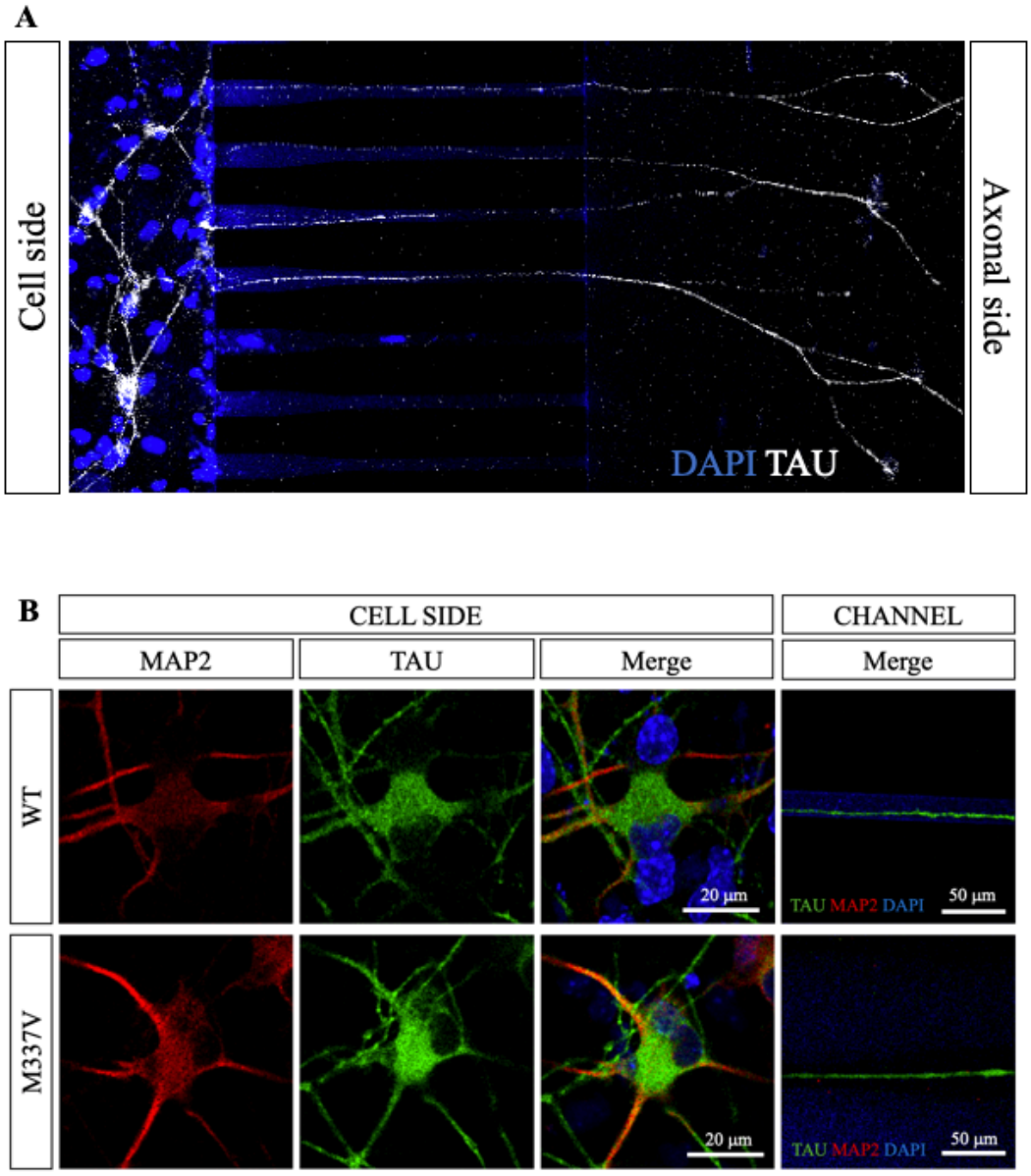


Figure 5.2 Processes extending through channels stain for axonal markers. A Microscopy image shows TAU positive axons extending through the channel from the cell side to the axonal side. **B** MAP2 and TAU staining further confirms axonal identity of processes within the channels.

Analysis revealed no notable differences in the percentage of moving mitochondria between TDP-43^{WT} and TDP-43^{M337V} mESC-MNs. In each case, ~60-70% of mitochondria were classified as 'moving' and ~30-40% of mitochondria in a 'dynamic stationary' state (Figure 5.3B-C). Assessment of the direction of moving mitochondria revealed that approximately 50% of mitochondria were moving in the anterograde direction, with the remaining 50% moving in the retrograde direction for both TDP-43^{M337V} mESC-MNs and TDP-43^{WT} controls (Figure 5.3D-E). Interestingly, the mean and maximum speed of anterograde transport of mitochondria was significantly reduced in TDP-43^{M337V} mESC-MNs compared to TDP-43^{WT} mESC-MNs (Figure 5.4A-B; p = < 0.0001 for both). The time that anterogradely travelling mitochondria were pausing was significantly increased in TDP-43^{M337V} mESC-MNs compared to controls (Figure 5.4C; p = 0.0015). However, the distance travelled by mitochondria in the anterograde direction was not significantly different in TDP-43^{M337V} mESC-MNs compared to controls (Figure 5.4D; p = 0.3623). Similarly, in the retrograde direction, I observed a significant reduction in the mean speed (Figure 5.5A; p = < 0.0001) and maximum speed (Figure 5.5B; p = < 0.0001) of mitochondrial transport in TDP-43^{M337V} mESC-MNs compared to TDP-43^{WT} controls. As with anterogradely moving mitochondria, a significantly increased pause time was observed for mitochondria moving retrogradely in TDP-43^{M337V} mESC-MNs compared to controls (Figure 5.5C; p = 0.0382). No significant differences in the distance travelled by retrogradely moving mitochondria was observed (Figure 5.5D; p = 0.0845). These findings suggest that the speed of mitochondrial movement and the length of time that mitochondria pause during transport is significantly dysregulated in TDP-43^{M337V} mESC-MNs compared to controls.

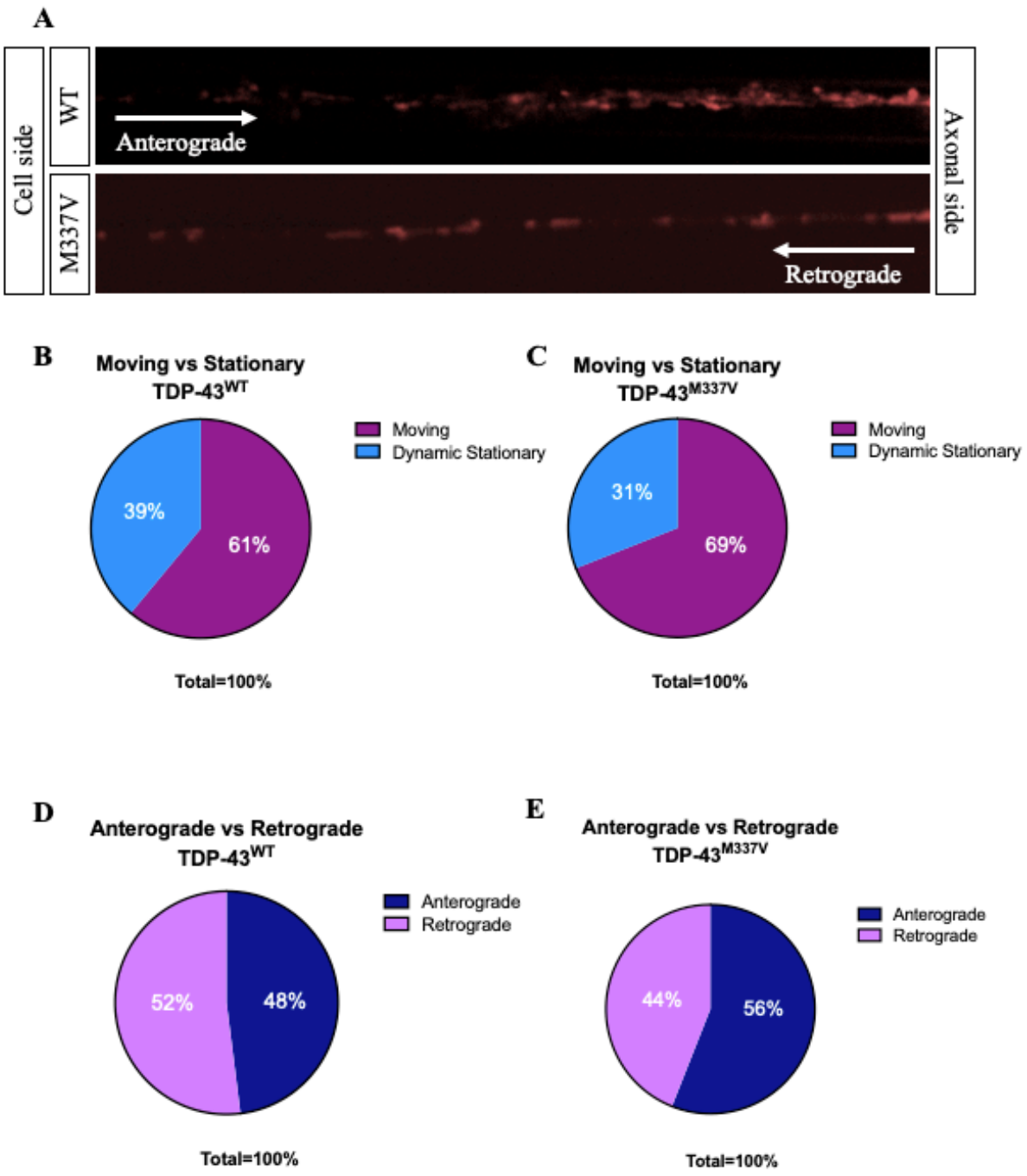


Figure 5.3 Mitochondria move bi-directionally in mESC-MNs. A Anterograde and retrograde transport of mitochondria assessed with MitoTracker in TDP-43^{WT} and TDP-43^{M337V} mESC-MNs. **B** Percentage of moving versus dynamic stationary mitochondria in TDP-43^{WT} mESC-MNs. **C** Percentage of moving versus dynamic stationary mitochondria in TDP-43^{M337V} mESC-MNs. **D** Percentage of mitochondria moving in the anterograde and retrograde directions in TDP-43^{WT} mESC-MNs. **E** Percentage of mitochondria moving in the anterograde and retrograde directions in TDP-43^{M337V} mESC-MNs. $n = 4$ differentiations.

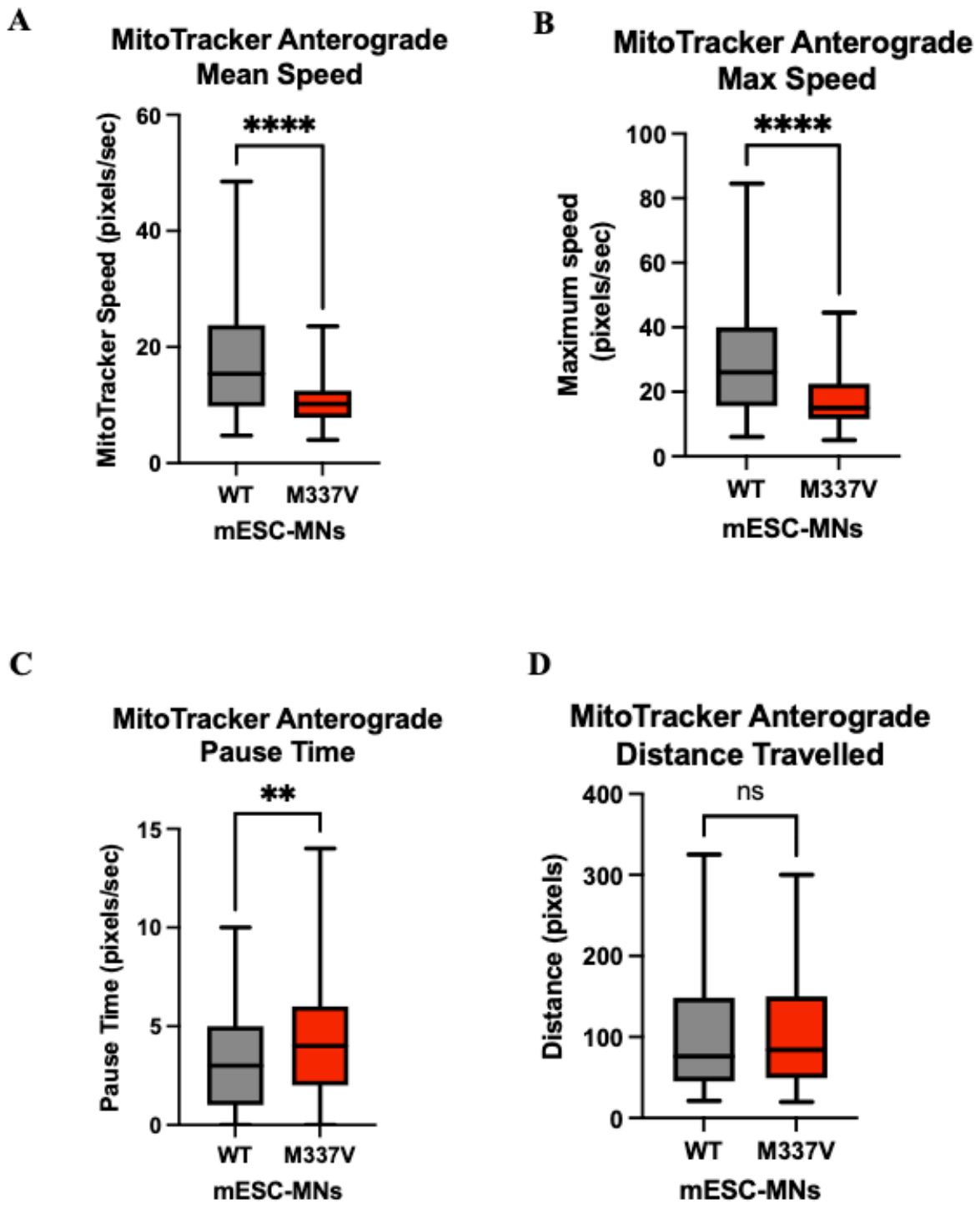


Figure 5.4 Anterograde mitochondrial transport in mESC-MNs. A mean speed, **B** maximum speed, **C** pause time and **D** distance travelled by mitochondria in TDP-43^{WT} versus TDP-43^{M337V} mESC-MNs in unstressed conditions. Unpaired t-test (n = ≥ 170 mitochondria analysed across 4n differentiations). Images were taken using a spinning disk confocal microscope every 2 seconds over 300 frames at 63X magnification.

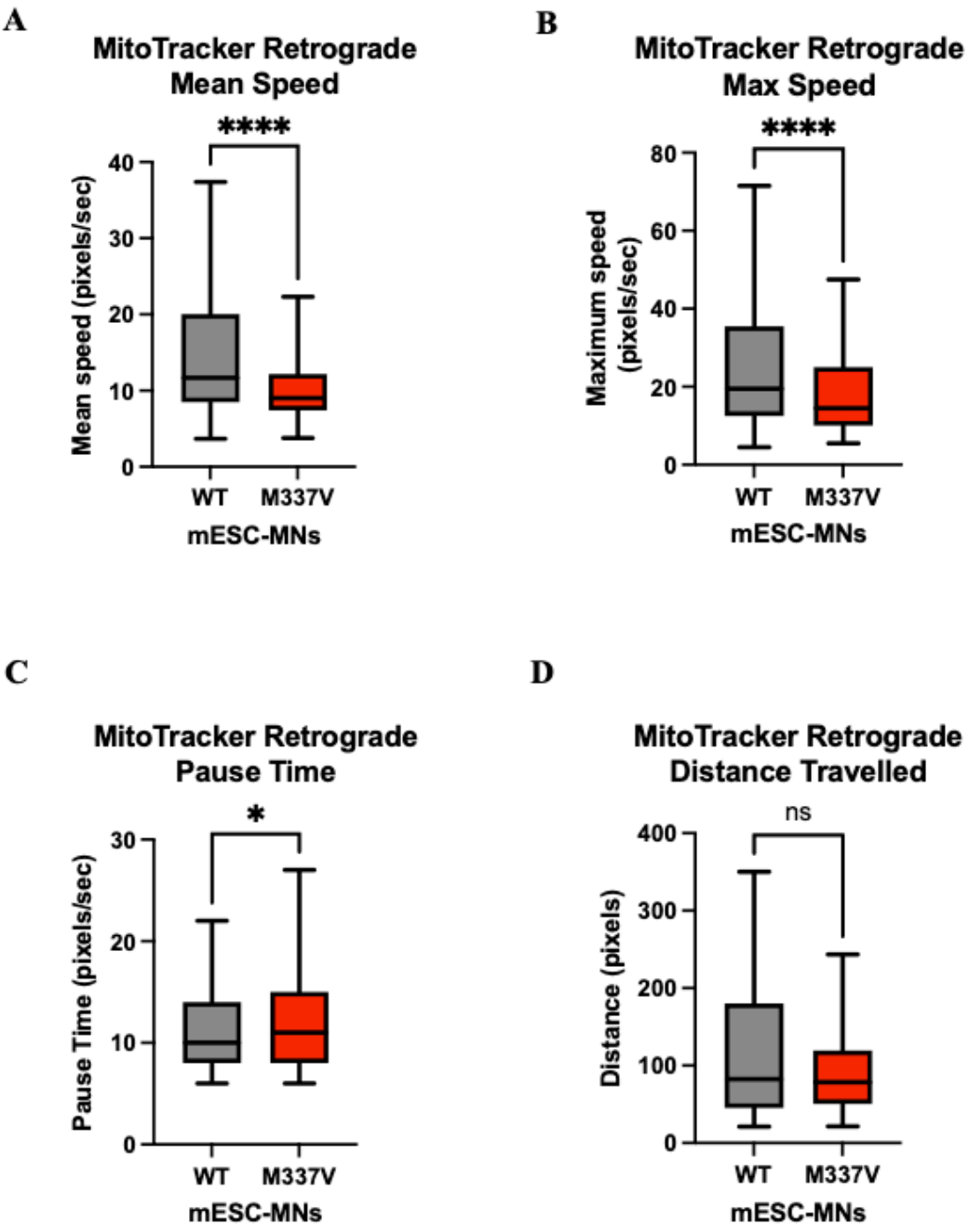


Figure 5.5 Retrograde mitochondrial transport in mESC-MNs. A mean speed, **B** maximum speed, **C** pause time and **D** distance travelled by mitochondria in TDP-43^{WT} versus TDP-43^{M337V} mESC-MNs in unstressed conditions. Unpaired t-test ($n = \geq 180$ mitochondria analysed across 4n differentiations). Images were taken using a spinning disk confocal microscope every 2 seconds over 300 frames at 63X magnification.

5.2.2. TDP-43^{M337V} mESC-MNs show a significant reduction in retrograde signalling

Deficits in the retrograde transport of signalling endosomes have previously been observed *in vivo* in the TDP-43^{M337V} mouse compared to controls. Impairments include a reduction in endosome speed, increased percentage of pausing endosomes and an increase in the percentage of time that endosomes were paused (Sleigh et al., 2020). Retrograde signalling relies upon the dynein/dynactin molecular motor complex and has important roles in the removal of misfolded or aggregated proteins from the axon, as well as delivery of distal trophic signals to the cell soma. I sought to investigate whether *in vitro* deficits in retrograde signalling could be observed in TDP-43^{M337V} mESC-MNs relative to TDP-43^{WT} controls. To investigate retrograde signalling, I analysed the transport of cholera toxin B (CTB); a highly efficient retrograde tracer that has previously been studied in neurons (T. Wang et al., 2016). mESC-MNs were plated into microfluidic chambers at a density of 100,000 cells/chamber and maintained *in vitro* for 5-7 days prior to imaging. Retrograde transport of CTB was examined through treatment with CTB at 50 ng/mL for 30 minutes prior to imaging (Figure 5.6A). Images were taken every 2 seconds for 150 frames and analysed using the difference tracker FIJI/Image J plugin (Andrews et al., 2010) and a script in R Studio developed by Dr Jakub Scaber in Python to quantify the percentage of moving versus stationary endosomes, direction of movement speed of movement, pause time and distance travelled.

Analysis revealed no notable differences in the percentage of moving endosomes in TDP-43^{M337V} mESC-MNs compared to TDP-43^{WT} controls, with approximately ~70% of endosomes moving in each case (Figure 5.6B-C). Of the moving endosomes, approximately 90% were moving retrogradely in TDP-43^{WT} mESC-MNs compared with only 8% moving retrogradely

in TDP-43^{M337V} mESC-MNs (Figure 5.6D-E). Analysis of the speed of moving endosomes identified a significant reduction in mean speed in TDP-43^{M337V} mESC-MNs compared to TDP-43^{WT} mESC-MNs (Figure 5.7A; p = < 0.0001). Conversely, TDP-43^{M337V} mESC-MNs showed a significantly increased maximum speed compared to controls (Figure 5.7B; p = 0.0015). No significant differences in the pause time of signalling endosomes were identified between TDP-43^{M337V} mESC-MNs and controls (Figure 5.7C; p = 0.202). The distance travelled by signalling endosomes was significantly reduced in TDP-43^{M337V} mESC-MNs compared to that observed in TDP-43^{WT} mESC-MNs (Figure 5.7D; p = 0.0066). Analysis of signalling endosomes moving in the anterograde direction revealed significantly reduced mean speed in TDP-43^{M337V} mESC-MNs compared to controls (Figure 5.8A; p = 0.0096). No significant differences in the maximum speed (Figure 5.8B; p = 0.2084) or pause time of signalling endosomes (Figure 5.8C; p = 0.7260) were observed between TDP-43^{M337V} mESC-MNs and controls. Signalling endosomes moving in the anterograde direction travelled significantly further in TDP-43^{M337V} mESC-MNs compared to controls (Figure 5.8D; p = 0.0002). These findings suggest bi-directional dysregulation of endosomal signalling in TDP-43^{M337V} mESC-MNs.

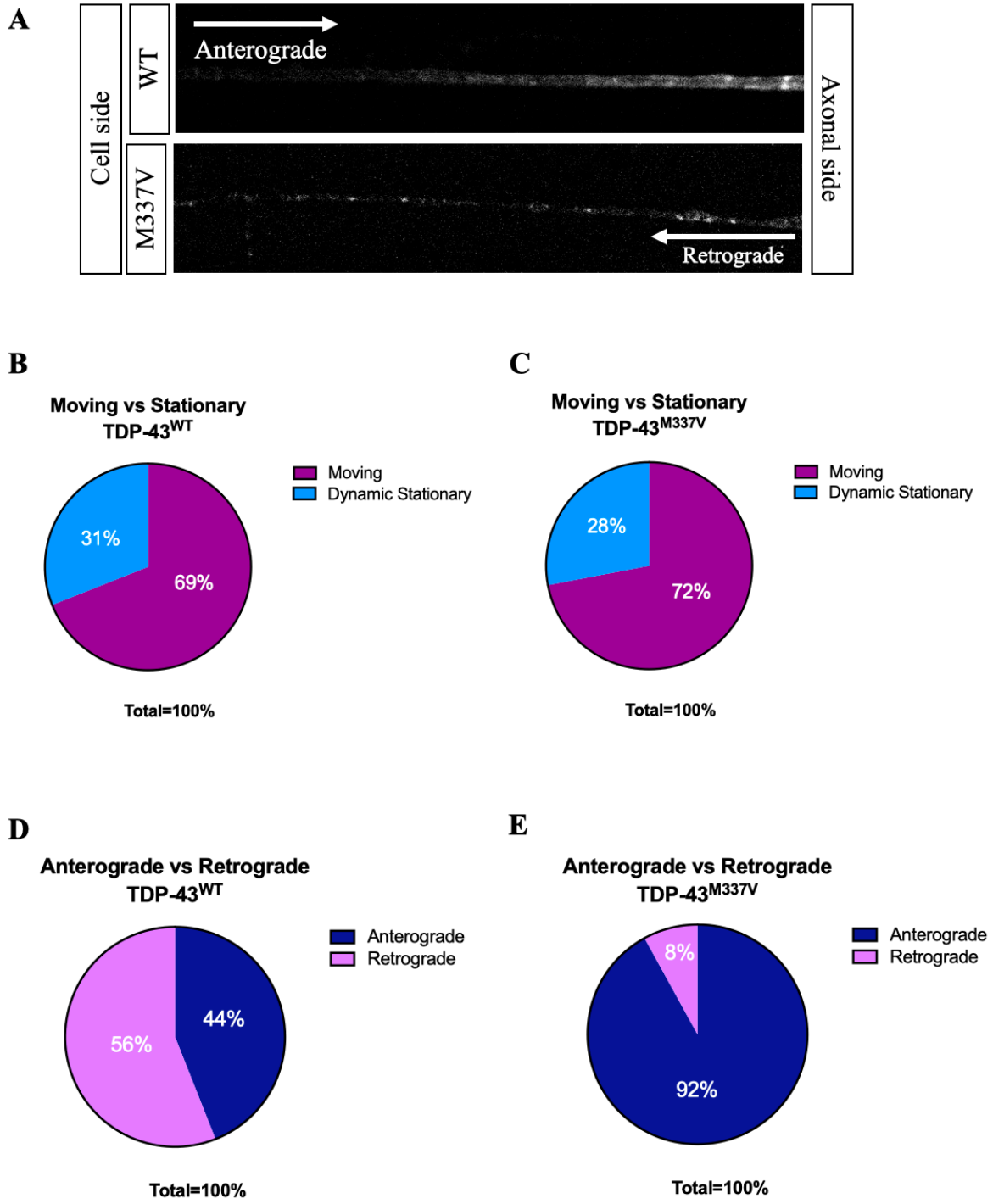


Figure 5.6 Bi-directional of CTB in mESC-MNs. A Anterograde and retrograde transport of signalling endosomes assessed with transport of cholera toxin B (CTB) in TDP-43^{WT} and TDP-43^{M337V} mESC-MNs. **B** Percentage of moving versus dynamic stationary endosomes in TDP-43^{WT} mESC-MNs. **C** Percentage of moving versus dynamic stationary endosomes in TDP-43^{M337V} mESC-MNs. **D** Percentage of endosomes moving in the anterograde and retrograde directions in TDP-43^{WT} mESC-MNs. **E** Percentage of endosomes moving in the anterograde and retrograde directions in TDP-43^{M337V} mESC-MNs. n = 3 differentiations.

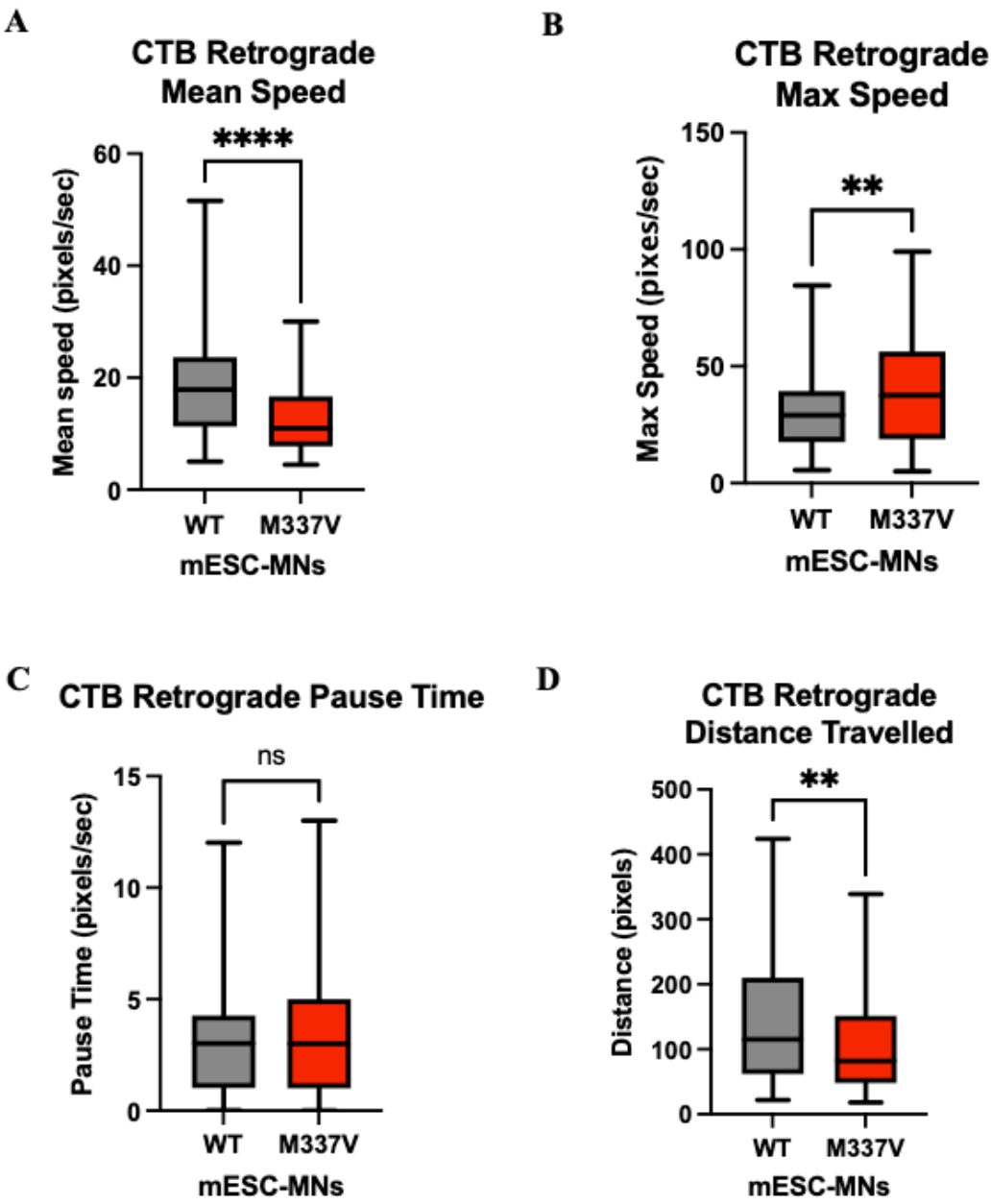


Figure 5.7 CTB retrograde transport is reduced in TDP-43^{M337V} mESC-MNs. A mean speed, **B** maximum speed, **C** pause time and **D** distance travelled by endosomes in TDP-43^{WT} versus TDP-43^{M337V} mESC-MNs in unstressed conditions. Unpaired t-test ($n = \geq 60$ endosomes analysed across 3n differentiations). Images were taken using a spinning disk confocal microscope every 2 seconds over 300 frames at 63X magnification.

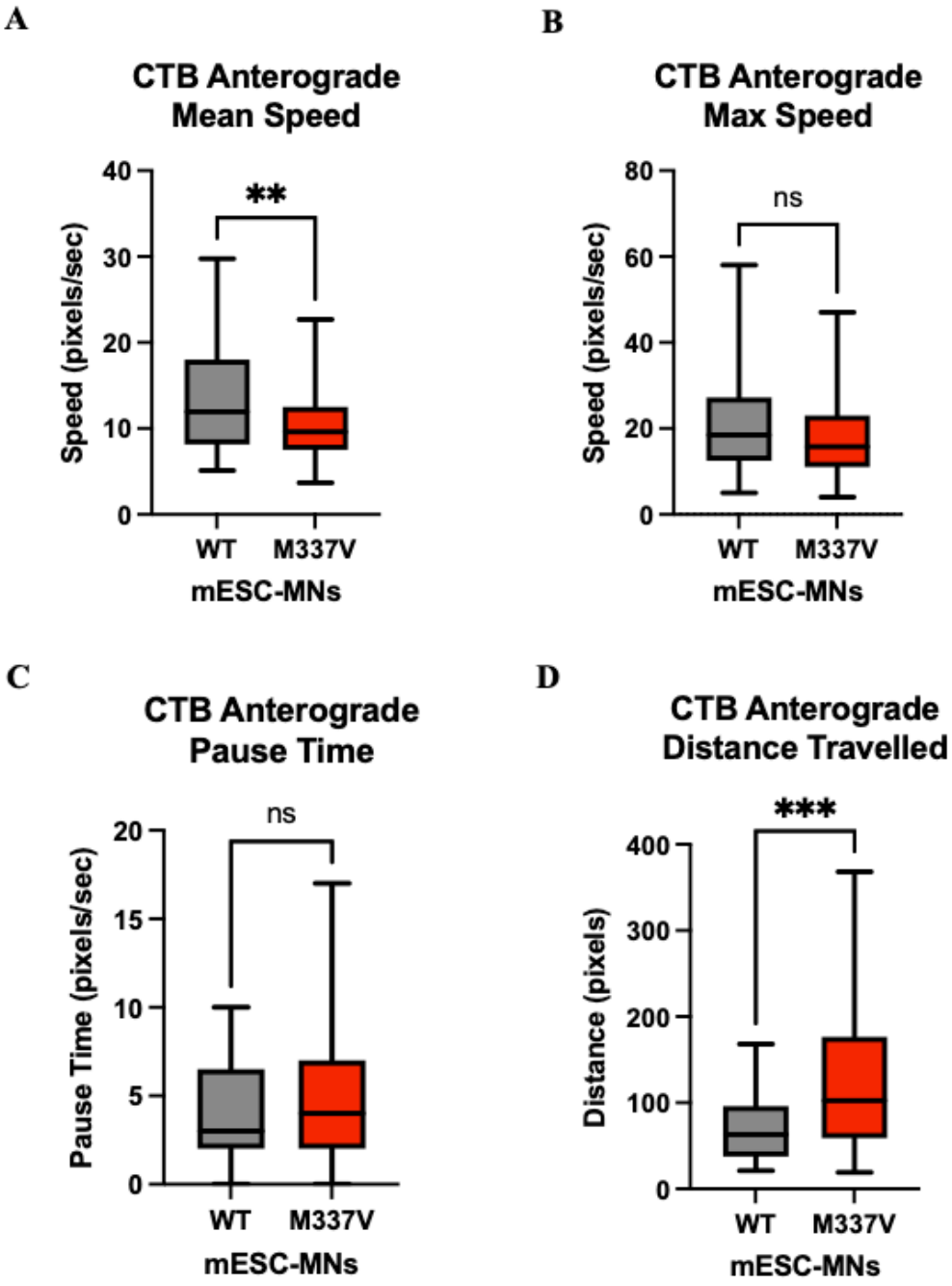


Figure 5.8 CTB anterograde transport is reduced in TDP-43^{M337V} mESC-MNs. A mean speed, **B** maximum speed, **C** pause time and **D** distance travelled by endosomes in TDP-43^{WT} versus TDP-43^{M337V} mESC-MNs in unstressed conditions. Unpaired t-test ($n = \geq 35$ endosomes analysed across 3n differentiations). Images were taken using a spinning disk confocal microscope every 2 seconds over 300 frames at 63X magnification.

5.2.3. TDP-43^{M337V} iPSC-MNs show dysregulated expression of transcripts relating to anterograde and retrograde transport

Axonal transport is regulated by molecular motor proteins that bind to and transport cargo from one end of the axon to the other. Transport in the anterograde direction is performed by members of the kinesin superfamily of motor proteins. The kinesin family is large, consisting of 15 subfamilies, but kinesin 1, kinesin 2 and kinesin 3 are thought to be the most functionally relevant for axonal transport. Kinesin 1 is formed of a dimer of kinesin heavy chains encoded by *KIF5A*, *KIF5B* and *KIF5C*, together with a dimer of kinesin light chains, encoded by *KLC1*, *KLC2*, *KLC3* and *KLC4*. Alternatively, retrograde transport is conducted by a single large multisubunit motor complex; cytoplasmic dynein. This complex is composed of two dynein heavy chains (*DYNC1H1*), two intermediate chains (*DYNC1IC1* and *DYNC1IC2*), two light intermediate chains (*DYNC1LI1* and *DYNC1LI2*) and three light chain families (Roadblock encoded by *DYNLRB1* and *DYNLRB2*, LC8 encoded by *DYNLL1* and *DYNLL2*, and Tctex encoded by *DYNLT1* and *DYNLT3*). However, dynein itself is not sufficient to conduct axonal transport and relies on the adaptor protein, dynactin (*DCTN1*), for efficient transport of cargo (Sleigh et al., 2019).

To investigate possible mechanisms through which the TDP-43^{M337V} mutation may lead to impaired axonal transport, I first sought to examine the expression of transcripts associated with axonal transport machinery in TDP-43^{M337V} iPSC-MNs. As mentioned in chapter 4, the Talbot laboratory has previously performed large-scale RNA sequencing of iPSC-MNs derived from healthy controls and patients carrying the TDP-43^{M337V} and TDP-43^{I383T} mutation (Ababneh et al., 2020; Dafinca et al., 2020). Similar analysis was also performed on spinal cord samples from TDP-43^{NTg}, TDP-43^{WT} and TDP-43^{M337V} mice. Here, these datasets were

analysed to examine the effects of TDP-43^{M337V} on the expression of transcripts associated with the molecular motors that drive axonal transport. In the TDP-43^{M337V} mouse, analysis revealed significant dysregulation of dynein (Dync1i2) and dynactin (Dctn1) motor proteins compared with TDP-43^{WT} and TDP-43^{NTg} controls, whilst no differences were observed in the expression of members of the kinesin superfamily of proteins (Figure 5.9). Analysis of iPSC-MN samples revealed significant dysregulation of kinesin transcripts, including kinesin 1 members (*KIF5A, KIF5B, KIF5C, KLC1* and *KLC2*) in TDP-43^{M337V} iPSC-MNs. Significant upregulation of *KIF5A, KIF5C, KLC1* and *KLC2* (p = 0.00081, p = 0.013, p = 0.00034, p = 0.000028 respectively) was accompanied by significant downregulation of *KIF5B* (p = 0.0093) in TDP-43^{M337V} iPSC-MNs compared to controls (Figure 5.10). Similarly, significant dysregulation of components of the dynein-dynactin complex was observed in TDP-43^{M337V} mESC-MNs (Figure 5.11). Significantly increased expression of dynactin 1 and dynactin 3 (*DCTN1*, p = 0.0014; *DCTN*3, p = 0.0018) were observed in TDP-43^{M337V} mESC-MNs compared with controls. Moreover, significantly increased expression of the dynein heavy chain, *DYNC1H1* (p = 0.0052), together with dynein intermediate chains (*DYNC1I1*, p = 4.87 x 10^{-8}; *DYNC1I2*, p = 0.021) were observed. There was also significant upregulation of the dynein light chain family member, Roadblock (*DYNLRB*, p = 0.00013), in TDP-43^{M337V} iPSC-MNs. Conversely, there was a significant reduction in the expression of dynein cytoplasmic 2 light intermediate chain 1 (*DYNC2LI1,* p = 0.0033) in TDP-43^{M337V} iPSC-MNs compared to controls. These observations suggest the TDP-43^{M337V} mutation leads to significant dysregulation in the expression of motor protein subunits.

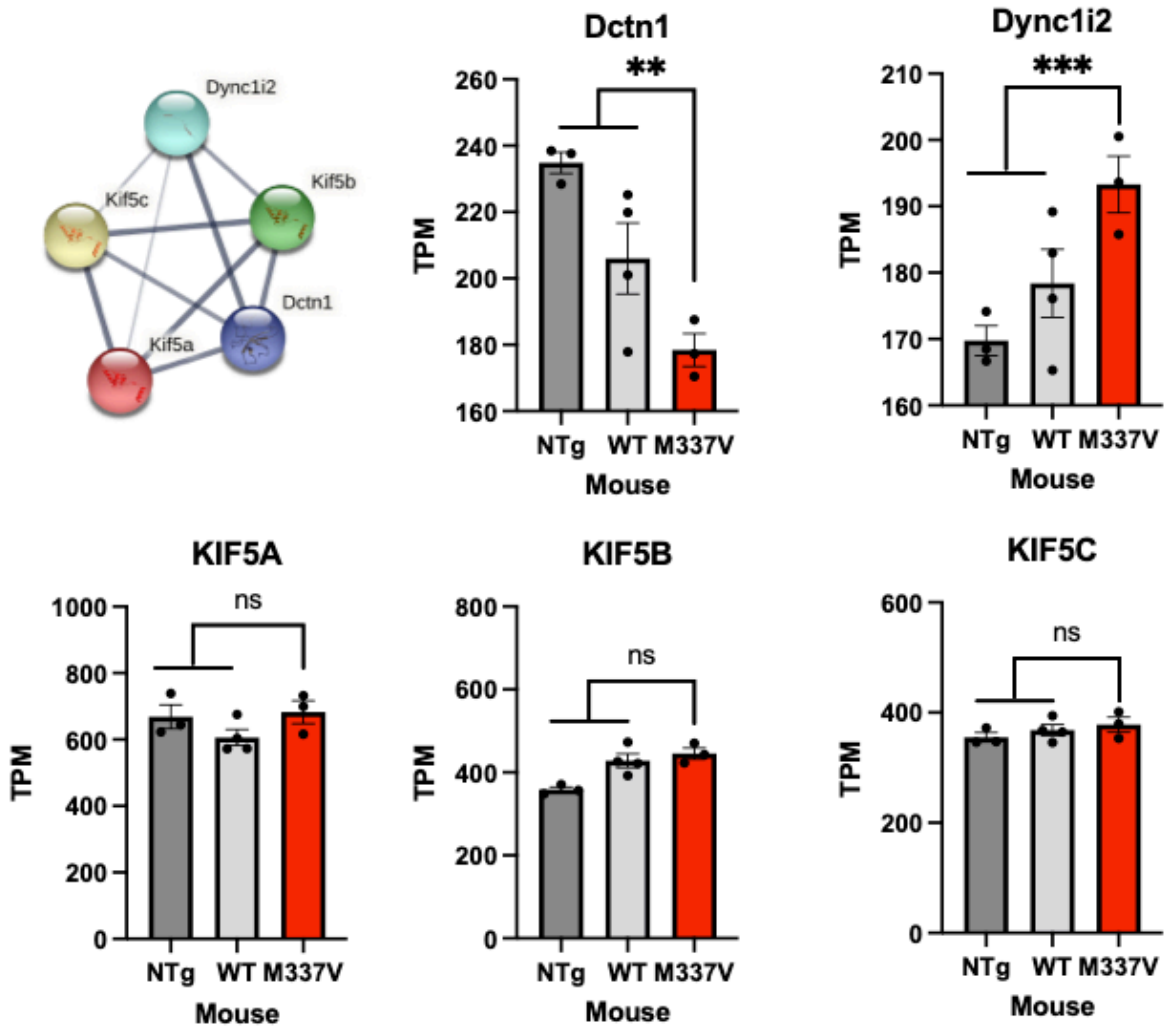


Figure 5.9 TDP-43^{M337V} mouse shows dysregulated expression of transcripts relating to retrograde transport but not anterograde transport compared to TDP-43^{WT} controls. Transcriptomic data generated by previous members of the Talbot group and re-analysed to identify components of the axonal transport machinery. Transcripts per million (TPM) are shown.

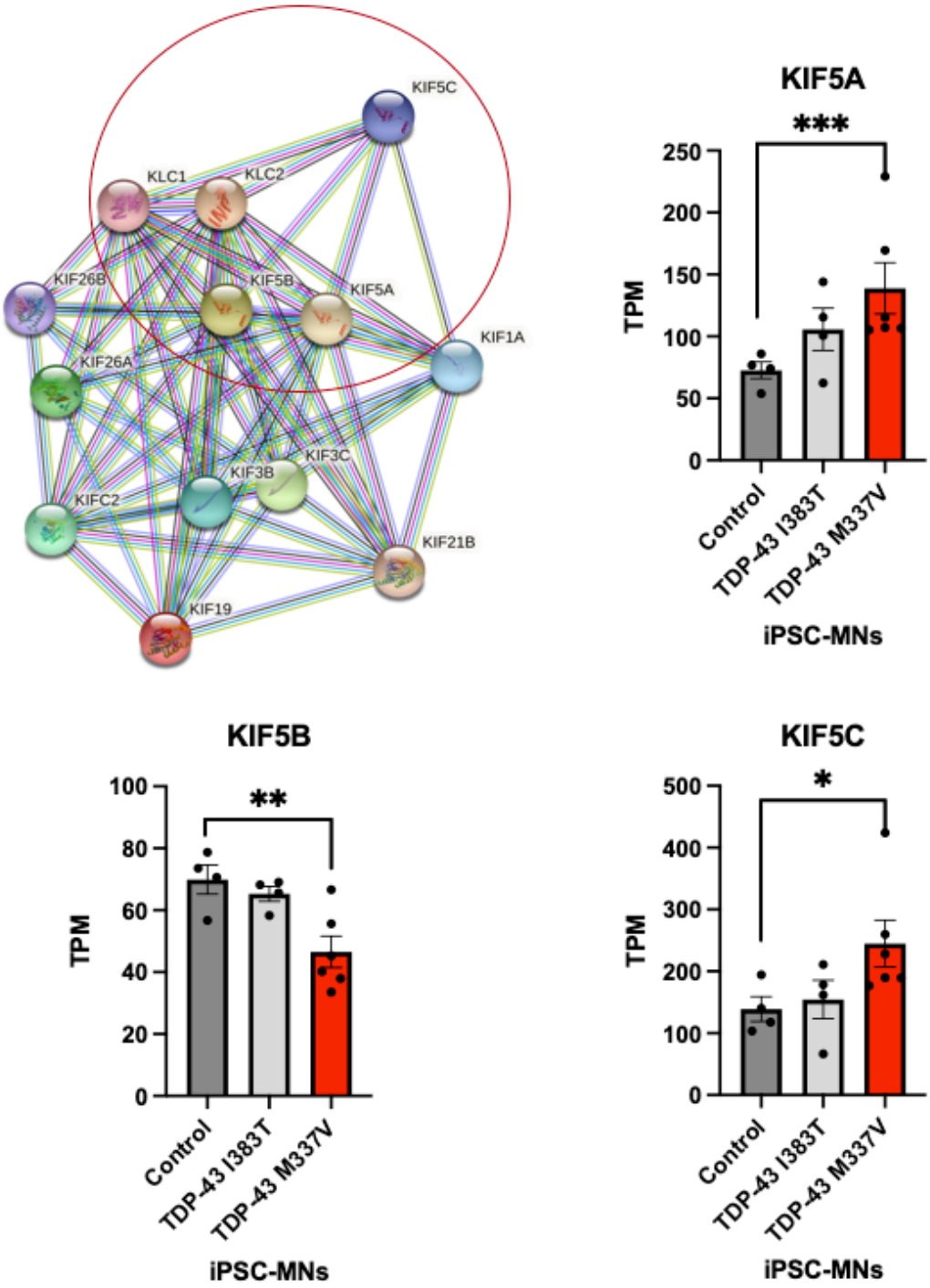


Figure 5.10 TDP-43^{M337V} iPSC-MNs show dysregulated expression of transcripts relating to anterograde transport. Transcriptomic data generated by previous members of the Talbot group and re-analysed to identify components of the axonal transport machinery. Transcripts per million (TPM) are shown.

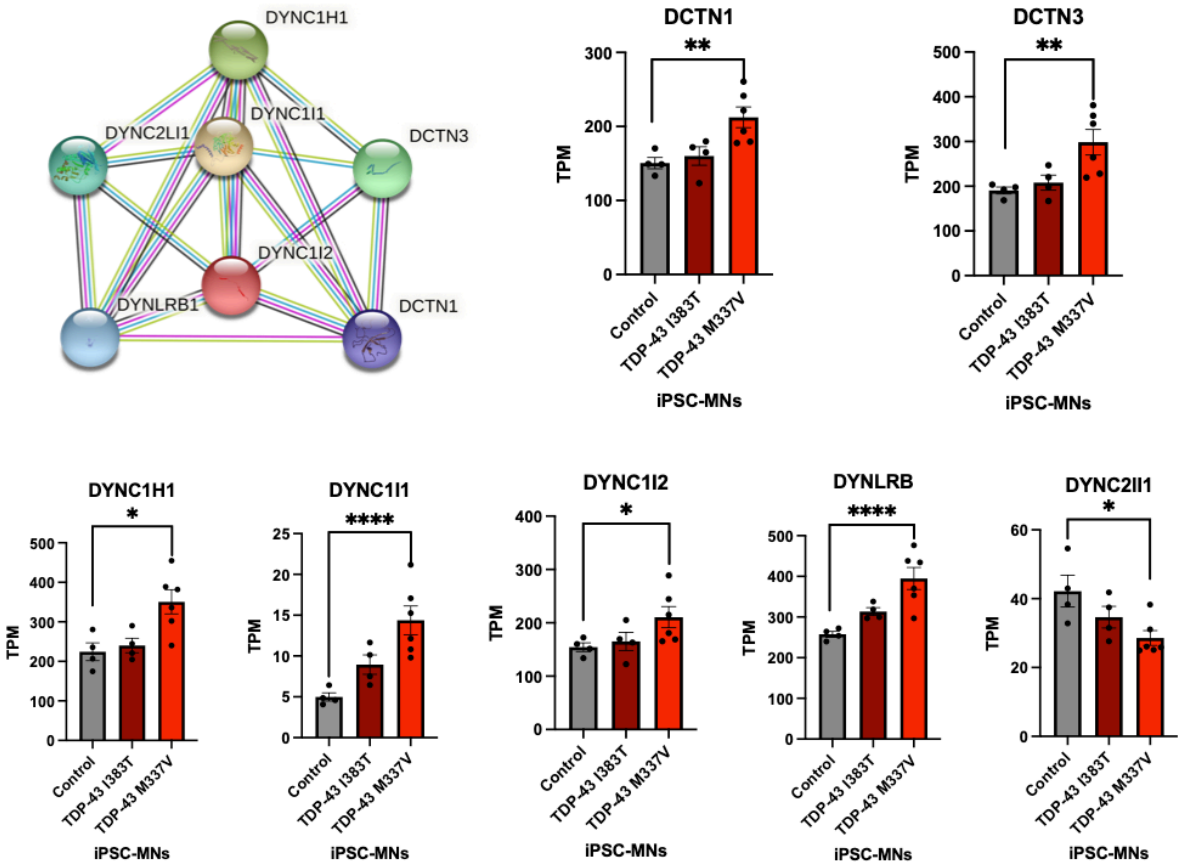


Figure 5.11 TDP-43^{M337V} iPSC-MNs show dysregulated expression of transcripts relating to retrograde transport. Transcriptomic data generated by previous members of the Talbot group and re-analysed to identify components of the axonal transport machinery. Transcripts per million (TPM) are shown.

5.2.4. Expression of motor protein subunits is not significantly altered in TDP-43^{M337V} mESC-MNs

Given changes in iPSC-MNs expressing the TDP-43^{M337V}, I next sought to investigate whether significant changes in the expression of molecular motor could be identified in TDP-43^{M337V} mESC-MNs. Protein lysates were extracted from TDP-43^{M337V} and TDP-43^{WT} mESC-MNs at DIV 3 and the expression of motor proteins examined using Western blotting (Figure 5.12A). The expression of retrograde motors, dynein and dynactin, was examined as well as the expression of anterograde motors, KIF5A and KIF5B. Analysis revealed no significant differences in the expression dynein or dynactin in TDP-43^{M337V} mESC-MNs compared with controls (p = 0.68 and p = 0.48 respectively; Figure 5.12B-C). Similarly, no significant differences in the expression of KIF5A or KIF5B were observed in TDP-43^{M337V} mESC-MNs compared with TDP-43^{WT} controls (p = 0.24 and p = 0.68 respectively; Figure 5.12D-E). These findings suggest that TDP-43^{M337V} does not significantly alter the expression of motor proteins in mESC-MNs.

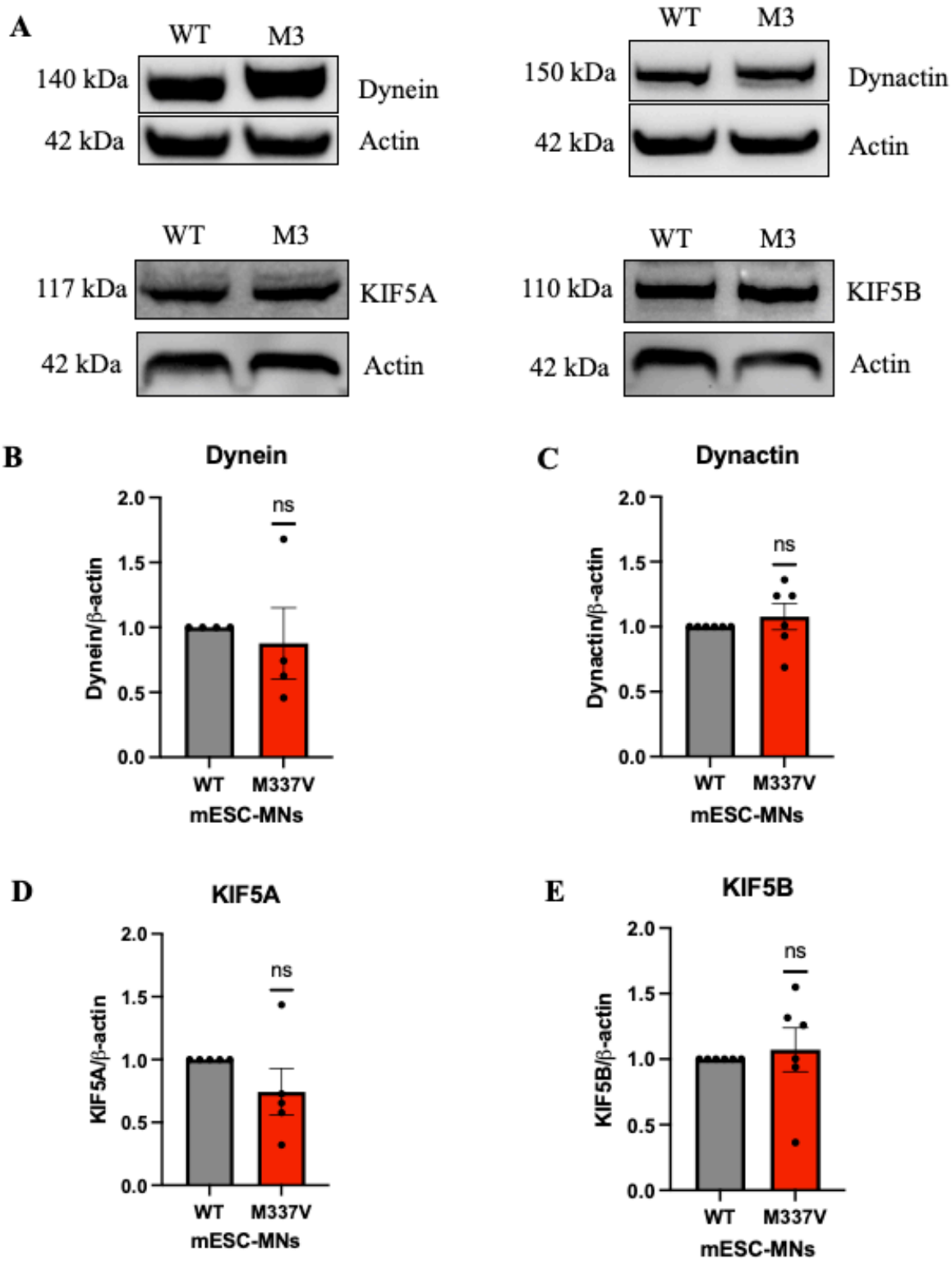


Figure 5.12 Expression of axonal transport components in mESC-MNs carrying the TDP-43^{M337V} mutation. A Western blotting of components of retrograde (dynein and dynactin) and anterograde (KIF5A and KIF5B) transport machinery. **B-E** Quantification of Western blot results for dynein, dynactin, KIF5A and KIF5B. One sample *t*-test ($n = \geq 4$).

5.3. Conclusions

In this chapter I have explored axonal transport in TDP-43^{M337V} motor neuron models. In TDP-43^{M337V} mESC-MNs, I observed significantly impaired axonal transport compared to TDP-43^{WT} controls. In TDP-43^{M337V} mESC-MNs, I observed a significant reduction in the speed of mitochondrial transport together with increased pausing of mitochondria during transport compared to controls, both in the anterograde and retrograde direction. Significant reductions in the retrograde transport of signalling endosomes were also observed, including reduced speed and distance travelled in TDP-43^{M337V} mESC-MNs compared to controls. The mechanisms underlying these impairments remain unclear. Analysis of transcriptomic data revealed significantly dysregulated expression of transcripts associated with anterograde and retrograde molecular motor proteins in TDP-43^{M337V} iPSC-MNs compared to controls. However, no notable changes in the expression of anterograde and retrograde motor proteins were observed in TDP-43^{M337V} mESC-MNs.

Dysregulation of axonal transport is an important pathophysiological phenomenon in ALS, that has been associated with various disease-associated mutations (Abo-Rady et al., 2020; Alami et al., 2014; Fazal et al., 2021; Fumagalli et al., 2021; Guo et al., 2020; Kiskinis et al., 2014; Wang et al., 2013). Previous work in our TDP-43^{M337V} BAC transgenic mouse, revealed significant reductions in the speed of endosomal trafficking and an increase in the percentage of pausing endosomes *in vivo* (Sleigh et al., 2020). Here, we have recapitulated these findings in TDP-43^{M337V} mESC-MNs expressing the same construct *in vitro*. However, the functional implications of such impairments remain unclear. Endosomal trafficking plays an important role in signalling communication throughout neurons, sending messages back to the cell body from distal portions of the neuron. Such messages are essential for neurotrophic signalling and

neuronal survival (Howe & Mobley, 2004; Ibanez, 2007). Given this, disrupted endosomal signalling has the potential to significantly impair neuronal health and survival.

In addition to impairments to retrograde endosomal signalling, we have also identified significant impairments to the bi-directional transport of mitochondria in TDP-43^{M337V} mESC-MNs compared to controls. These findings are in line with previous studies, that have identified impaired mitochondrial transport associated with *TARDBP* mutations (Kreiter et al., 2018; Wang et al., 2013). Mitochondria undergo constant bi-directional trafficking along axons. Anterograde transport is responsible for supplying fresh, healthy mitochondria from the cell body to axon terminals. In particular, the delivery of mitochondria to synapses is critical, where they have important roles in local ATP production that is essential for synaptic vesicle recycling, synaptic activity and synaptic remodelling (Smith et al., 2016; Verstreken et al., 2005). By contrast, retrograde transport of mitochondria is essential for the clearance of damaged or dysfunctional mitochondria from axon terminals (Cai et al., 2012). Impairment of retrograde transport has previously been shown to result in accumulation of aged organelles in axon terminals and a loss of cell body mitochondria (Mandal et al., 2021). Here, I observed reduced speed of mitochondrial movement and increased pausing of mitochondria, both in the anterograde and retrograde direction in TDP-43^{M337V} mESC-MNs compared to controls. This may suggest both a slower clearance of dysfunctional mitochondria within the axon and a reduction in the delivery of healthy mitochondria to axon terminals. Given the essential roles of synaptic mitochondria in providing ATP for the maintenance of neural network activity, disruption to anterograde mitochondrial transport could have implications for synaptic neurotransmission. This could be examined in future work by patch clamp electrophysiology, to assess whether neuronal activity is significantly perturbed by TDP-43^{M337V} expression in mESC-MNs.

The mechanisms underlying impairments in axonal transport that we observe here remain unclear. It is possible that deficits arise solely as the result of impaired viability in TDP-43^{M337V} mESC-MNs, which I observed in chapter 3. However, whether reduced viability leads to axonal transport deficits or vice versa is difficult to determine. This could only be concluded through a process of elimination, after alternative hypotheses have been ruled out. One such alternative hypothesis is that impaired axonal transport arises from disruption to axonal transport machinery; molecular motors, adaptor proteins and the microtubule cytoskeleton. Disruption to the expression of these components has been previously linked to ALS. For example, significant downregulation of transcripts relating to the anterograde molecular motor, kinesin, have been observed in the motor cortex of sporadic ALS patients (Pantelidou et al., 2007). More recently, large-scale genome wide association studies have established links between mutations in the anterograde motor protein, *KIF5A*, and ALS (Nicolas et al., 2018). Moreover, mutations in the retrograde adaptor protein, dynactin 1 (*DCTN1*), have been linked to the occurrence of lower motor neuron disease, ALS and frontotemporal dementia (Munch et al., 2005; Munch et al., 2004; Puls et al., 2003). Reduced expression of dynactin 1 in *C. elegans* has also been shown to disrupt the transport of autophagosomes and induce motor neuron degeneration (Ikenaka et al., 2013). Mutations in genes relating to the microtubule cytoskeleton, most notably in Tubulin Alpha A4 (*TUBA4A*), have also been linked with familial ALS and FTD (Pensato et al., 2015; Smith et al., 2014). Whilst I observed no differences in the expression of a small number of anterograde and retrograde motor proteins in TDP-43^{M337V} mESC-MN, I have not yet performed a broader analysis of motor protein expression of the integrity of the microtubule cytoskeleton. Future work examining the transcriptome of the isolated axonal compartment in TDP-43^{M337V} mESC-MNs, could indicate

whether specific disturbances to axonal transport machinery underlie the deficits observed here.

Previous studies have suggested that mutant forms of TDP-43 drive impairments in axonal transport. For example, Fazal and colleagues identified a significant reduction in the percentage of moving mitochondria in iPSC-MNs with *TARDBP* mutations. These impairments were associated with increased levels of insoluble TDP-43 together with increased TDP-43 cytoplasmic mislocalisation and phosphorylation. Treatment with a HDAC6 inhibitor led to a reduction in insoluble and phosphorylated TDP-43, prevented TDP-43 mislocalisation and reversed deficits in mitochondrial transport. Given this, the authors concluded that mutant forms of TDP-43 are sufficient to drive axonal transport deficits (Fazal et al., 2021). The mechanism through which mutant forms of TDP-43 may impair axonal transport is currently unclear, although downregulation of several transcripts encoding components of the cytoskeleton (including Nefl, Tubb2a and Tuba1b) has been observed in motor neurons from a TDP-43 knockdown mouse (Briese et al., 2020). However, axonal transport deficits have been shown to occur independent of TDP-43 mislocalisation and aggregation. Kreiter and colleagues identified significant impairments to mitochondrial transport in iPSC-MNs with *TARDBP* mutations that occurred independent of TDP-43 mislocalisation (Kreiter et al., 2018). Our results are in line with these findings, as we observe impairments to axonal transport without accompanying TDP-43 cytoplasmic mislocalisation. Taken together, these studies suggest that while TDP-43 cytoplasmic mislocalisation and aggregation may be sufficient to induce axonal transport deficits, they are not prerequisites for impairments.

Impairments to the bi-directional transport of signalling endosomes could also result from impairments to glycolysis. Local ATP production via glycolysis has previously been shown to

power fast axonal transport of vesicles in *Drosophila* larvae and cortical neurons, specifically through the activity of the glycolytic enzyme GAPDH. Localisation of GAPDH to vesicles provided 'on-board' energy to power transport and reducing glycolysis led to impaired vesicular transport (Zala et al., 2013). In chapter 4, I observed a trend towards reduced basal glycolysis in TDP-43^{M337V} mESC-MNs compared to controls, which became significant following exposure to oxidative stress. Given this, it is possible that impairments to the axonal transport of signalling endosomes in TDP-43^{M337V} mESC-MNs could be linked to reduced glycolysis. To investigate this further it would be interesting to determine whether oxidative stress, which significantly impairs basal glycolysis in TDP-43^{M337V} mESC-MNs, exacerbates axonal transport deficits. Moreover, future work could examine whether treatment with terazosin, the alpha 1-adrenoceptor antagonist that significantly increases basal glycolysis (Chapter 4), ameliorates axonal transport deficits in TDP-43^{M337V} mESC-MNs.

There are several limitations of the work presented here. Of particular note, the disparities in the percentage of retrogradely moving endosomes in TDP-43^{M337V} mESC-MNs compared to TDP-43^{WT} controls makes interpretation challenging. Whilst over half of moving endosomes were travelling retrogradely in TDP-43^{WT} mESC-MNs (56%), only a fraction (8%) were travelling retrogradely in TDP-43^{M337V} mESC-MNs. These observations suggest that further optimisation of the protocol is required, perhaps with analysis of endosomal trafficking after a shorter period of incubation with CTB, in order to capture retrogradely moving endosomes before they are recycled and carried anterogradely. Secondly, here we have examined axonal transport solely in the unstressed condition. In the previous chapters I observed significant impairments to cellular viability and energy metabolism only following exposure to oxidative stress. Given this, it would be interesting to investigate whether exposure to oxidative stress further exacerbates these phenotypes. Thirdly, in this study I have examined the expression of

only a few axonal transport proteins in mESC-MNs through Western blotting. RNA sequencing of the axonal compartment of mESC-MNs would provide a more detailed overview of any changes in the expression of axonal transport components between TDP-43^{WT} and TDP-43^{M337V} mESC-MNs.

In this chapter I have identified significantly impaired axonal transport of signalling endosomes and mitochondria in TDP-43^{M337V} mESC-MNs compared to TDP-43^{WT} controls. These deficits may provide a valuable high-throughput phenotypic readout to assess the effectiveness of potential therapeutic compounds. In future work it will be important to substantiate the results reported here by investigating possible mechanisms underlying these observed impairments.

CHAPTER 6 Conclusions

6.1. Summary of thesis findings

The aim of this thesis was to characterise the phenotypic signature of an *in vitro* mESC-MN model, which expresses pathogenic human TDP-43^{M337V} at low levels. In chapter 3, I confirmed that TDP-43 mislocalisation is absent from TDP-43^{M337V} mESC-MNs relative to controls. However, reduced stress granule number and size, as well as reduced cellular viability, are characteristic of TDP-43^{M337V} mESC-MNs. In chapter 4, I identified dysregulated cellular bioenergetics in TDP-43^{M337V} mESC-MNs in response to oxidative stress, evidenced by reduced basal glycolysis. In oxidative stress conditions, treatment with the pro-survival drug, terazosin, significantly increased glycolysis and reduced mitochondrial respiration, suggesting this drug may exert its neuroprotective effects through altering cellular energy metabolism. In chapter 5, I observed impairments to the bi-directional axonal transport of mitochondria and signalling endosomes in TDP-43^{M337V} mESC-MNs relative to TDP-43^{WT} controls. Taken together, these findings highlight ALS-associated pathways relating to the expression of TDP-43^{M337V} in mESC-MNs.

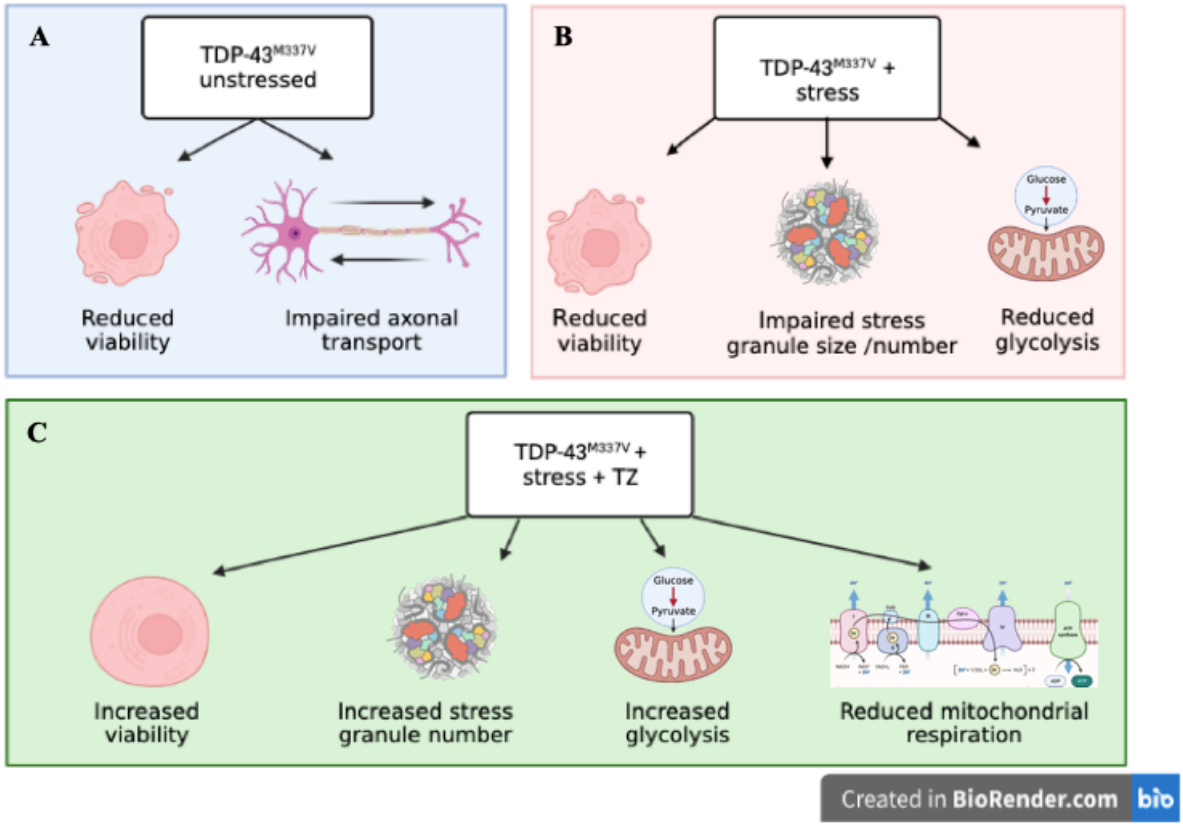


Figure 6.1 Summary of thesis findings. A TDP-43^{M337V} mESC-MNs demonstrate reduced viability and impaired axonal transport in unstressed conditions compared to TDP-43^{WT} controls. **B** In response to oxidative stress, TDP-43^{M337V} mESC-MNs demonstrate reduced viability, impaired stress granule formation and reduced glycolysis compared to TDP-43^{WT} mESC-MNs. **C** In response to oxidative stress, treatment with terazosin significantly improves survival and increases stress granule number, which was associated with increased glycolysis and reduced mitochondrial respiration. Generated in *BioRender.com*. Stress granule image: (Marcelo et al., 2021).

6.2. Relevant models provide insight into TDP-43 pathogenicity in ALS

The aetiology of ALS is immensely complex, with multiple pathophysiological mechanisms thought to contribute to disease onset and progression. A major challenge is to dissect the relative contribution of these mechanisms to ALS pathogenesis, and understand how they interact with genetic risk factors to initiate neurodegeneration. The temporal sequence of events also remains unclear, a greater understanding of which will prove crucial in the identification of tangible therapeutic targets. To gain insight into these questions, much of research has focussed on the development of mouse and cellular models, which express pathogenic mutations in genes linked to ALS. The SOD1-G93A mouse was the first mouse model of ALS, developed following the identification of links between SOD1 mutations and ALS in 1993 (Gurney et al., 1994). A vast amount of research has been conducted in this model, from which stems much of our current understanding of the aetiology and pathogenesis of ALS. The majority of preclinical drug screening has also been performed predominantly in the SOD1 mouse model, however promising candidates that showed efficacy in this model did not translate to a substantial benefit for patients in clinical trials (Petrov et al., 2017). In addition, SOD1 mutations affect only a small proportion of ALS patients and do not model TDP-43 proteinopathy, which is observed in the vast majority of ALS cases. Given this, the development of mutant TDP-43 models are crucial, in order to gain further mechanistic insight into the disease process.

To date, a number of models of TDP-43-associated ALS have been developed including wild-type and mutant TDP-43 overexpression, TDP-43 knock-down and knock-out, as well as transgenic and knock-in models of ALS-associated TDP-43 mutations (see *'Introduction'*).

Given that overexpression of TDP-43 is inherently toxic (Igaz et al., 2011; Shan et al., 2010; Swarup et al., 2011; Wils et al., 2010; Xu et al., 2011; Yang et al., 2022), models which express mutant TDP-43 at physiologically relevant levels are key in the identification of disease-specific mechanisms. Our group has previously developed several models, including HEK cells, mESC-MNs and a transgenic mouse model, expressing pathogenic human TDP-43^{M337V} at low levels (Gordon et al., 2019; Mutihac et al., 2015). In mESC-MNs, expression of TDP-43^{M337V} leads to impaired stress granule formation, reduced viability in response to oxidative stress and altered TDP-43 interactions (Feneberg et al., 2020; Gordon et al., 2019). Here, I have identified further phenotypes associated with expression of the TDP-43^{M337V} in mESC-MNs, including dysregulation of cellular bioenergetics and impaired axonal transport. Whilst the underlying causes of these phenotypes are currently unclear, this work has supported the validity of our mESC-MN model as a relevant model for probing mechanistic pathways associated with the disease. I have also shown, through examining the effects of terazosin on these phenotypes, that our mESC-MN model provides a valuable system for high-throughput phenotypic screening of potential therapeutic compounds.

Advances in our understanding of the pathophysiology of ALS relies upon the development of model systems that accurately reflect the human disease. However, the inherent clinical and genetic heterogeneity of ALS creates challenges for designing a unifying model of the disease. This has led to the development of various models that reflect different aspects of the disease, including specific disease-associated mutations or cellular pathological hallmarks. Each model has an inherent set of strengths and limitations, which is important to consider, as certain models may be better tailored to address specific questions. Nevertheless, consistent observations across different *in vitro* and *in vivo* models will be key to both our understanding of ALS pathophysiology and the identification of tangible therapeutic targets.

6.3. The role of TDP-43 mislocalisation and aggregation in ALS pathogenesis

A long-standing debate within the ALS field centres around the significance of TDP-43 mislocalisation and aggregation in ALS pathogenicity. Initiated by observations of cytoplasmic localisation and aggregation of TDP-43 in patient post-mortem tissue, it was hypothesised that that aggregation of TDP-43 within the cytoplasm conferred toxicity in ALS (Arai et al., 2006; Barmada et al., 2010; Igaz et al., 2011; Neumann et al., 2006). Yet this view was complicated by observations that neurotoxicity and cell death could occur without evidence of aggregation, instead suggesting this phenomenon is associated with later stages of the disease process, rather than a primary pathogenic mechanism initiating neurodegeneration (Barmada et al., 2010; Igaz et al., 2011; Urushitani et al., 2010; Walker et al., 2015). Instead, it was suggested that aberrant TDP-43 mislocalisation to the cytoplasm conferred toxicity, through both loss- and gain-of-function mechanisms (Barmada et al., 2010; Igaz et al., 2011; Sasaguri et al., 2016; Walker et al., 2015). Yet more recently, TDP-43 mislocalisation was found to lie downstream of axonal dysfunction in a novel ALS-associated KANK1 mutant model, suggesting mechanisms aside from TDP-43 mislocalisation may be sufficient to initiate pathogenesis (Zhang et al., 2022).

Findings from this thesis further support the view that TDP-43 mislocalisation and aggregation are not prerequisites for downstream toxicity associated with the expression of TDP-43 mutations. Whilst TDP-43^{M337V} mESC-MNs demonstrated no evidence of altered TDP-43 localisation or aggregation relative to controls, expression of TDP-43^{M337V} was associated with reduced viability and several pathophysiological changes associated with ALS including altered stress granule characteristics and dysregulated cellular bioenergetics in response to oxidative stress, as well as impaired bi-directional axonal transport in unstressed conditions.

Rather than pathophysiological mechanisms resulting from TDP-43 mislocalisation and aggregation, expression of the TDP-43^{M337V} pathogenic mutation may confer toxicity through altering TDP-43's function as an RNA-binding protein. This view is supported by the clustering of mutations in exon 6 of the *TARDBP* gene, which encodes the C-terminal binding domain (Prasad et al., 2019). Indeed, expression of TDP-43^{M337V} in mESC-MNs leads to significant dysregulation of the TDP-43 interactome. Specifically, TDP-43^{M337V} mESC-MNs demonstrated impaired interactions between TDP-43 and proteins of the endoplasmic reticulum, endosomal-extracellular transport systems and stress granule formation compared to TDP-43^{WT} mESC-MNs (Feneberg et al., 2020). TDP-43 also has important roles in regulating transcription, splicing and mRNA stability, which if disrupted has the potential to induce wide-spread dysregulation of gene expression (Lagier-Tourenne et al., 2010). In iPSC-MNs, expression of TDP-43^{M337V} leads to significant dysregulation of gene expression. In previous work, iPSC-MNs derived from patients expressing the TDP-43^{M337V} leads to altered expression of transcripts related to calcium homeostasis including, calcium permeable subunits of glutamatergic receptors and the mitochondrial calcium channel MICU1 (Dafinca et al., 2020). Here, I have also identified significant dysregulation of transcripts associated with cellular bioenergetics and axonal transport in TDP-43^{M337V} mESC-MNs relative to healthy controls. Taken together, these findings suggest that dysregulation of TDP-43 interactions and altered gene expression are additional avenues by which TDP-43^{M337V} expression may be sufficient to induce toxicity.

6.4. Selective vulnerability of motor neurons in ALS

Multiple mechanisms have been implicated in ALS pathophysiology including dysregulated RNA homeostasis, oxidative stress, mitochondrial dysfunction, axonal transport deficits, protein aggregation, excitotoxicity and neuroinflammation. Many of these mechanisms overlap

with other neurodegenerative disorders including Alzheimer's disease and Parkinson's disease. Yet, these disorders are fundamentally distinguished from one another by clinical presentation, unique neuropathological hallmarks and differences in the neuronal populations affected. Regarding the latter, with the exception of cortical neuron involvement in patients with ALS/FTD, neurodegeneration in ALS appears to predominantly target motor neuron populations leaving other neuron populations (visual, sensory, autonomic and auditory) relatively intact. This targeting is strikingly specific, as even within motor neuron populations certain sub-groups appear to be protected. UMNs in the primary motor cortex and hypoglossal MNs in the brainstem are consistently vulnerable, in contrast to sparing of neurons of the oculomotor nucleus, which control eye movement; a function that is largely preserved in ALS patients even to the end stages of disease in the majority (Mannen et al., 1977; Nimchinsky et al., 2000; Reiner et al., 1995). The cause of this selective vulnerability remains unclear, although certain neuroanatomical features may render motor neurons particularly susceptible to certain pathophysiological mechanisms.

Motor neurons are distinguishable from other neuronal subtypes due to their size, long axonal processes and subsequently high metabolic demands. Energy in the form of ATP is generated predominantly through mitochondrial oxidative phosphorylation. However, this high energy demand makes motor neurons particularly vulnerable to oxidative stress, due to a higher production of ROS resulting from the incomplete reduction of oxygen during oxidative phosphorylation (Barber & Shaw, 2010; Lenaz, 1998). In addition, molecular features of motor neurons may underlie their increased vulnerability to neurodegeneration. Altered expression of calcium binding proteins, which are essential in the maintenance of calcium homeostasis and regulation of neuronal activity, also distinguish motor neurons from neighbouring neuronal populations (Augustine et al., 2003). In human post-mortem samples, vulnerable motor neuron

populations, including cortical and spinal motor neurons, demonstrated notably reduced expression of calcium binding proteins compared with resistant neuron populations (oculomotor and trochlear neurons) (Alexianu et al., 1994).

It is clear that certain neuroanatomical and molecular features of motor neurons including their size, high metabolic demand, susceptibility to oxidative stress and reduced calcium binding protein expression may underlie their increased vulnerability to neurodegeneration in ALS. Further research into the physiological features distinguishing resistant neuronal subtypes, such as sensory neurons, from vulnerable motor neurons will provide further insight into the causes of selective vulnerability and may identify points of therapeutic intervention.

6.5. The heterogeneity of ALS creates challenges in diagnosis and treatment

ALS is a highly heterogeneous disease with significant genetic, pathological and clinical variability. To date, a number of disease-associated mutations have been identified, which are thought to dysregulate multiple downstream cellular pathways. However, the vast majority of ALS cases arise from apparently sporadic causes, making it challenging to identify the converging mechanisms underpinning motor neuron degeneration (Renton et al., 2014). Neuropathological variability is also observed in ALS post-mortem tissue. TDP-43 is the predominant protein species found within neuronal cytoplasmic inclusions in the majority of ALS cases, yet it is strikingly absent in cases arising as the result of SOD1 and FUS pathogenic mutations (Mackenzie et al., 2007; Vance et al., 2009). Phenotypic heterogeneity is also evident across ALS patients, marked by varying involvement of spinal and bulbar upper and lower motor neurons and differing sites of onset (Chio et al., 2011). Whilst the median survival

associated with ALS is 3 years from symptom onset, some patients can live with the disease for over 20 years (Turner et al., 2003). This heterogeneity creates challenges both for the diagnosis and treatment of ALS and has raised the questions as to whether ALS is in fact one disease, or should be classed as a spectrum of associated, but fundamentally different diseases (Turner, Hardiman, et al., 2013). Given this, there is an unmet need for reliable ALS biomarkers that aid diagnosis and allow patient stratification based on disease progression and prognosis. Biomarker development is also crucial in the context of ALS treatment. In clinical trials, robust biomarkers would provide a valuable quantitative measure for monitoring the effectiveness of therapeutics over time. Additionally, biomarkers that allow early disease detection in pre-symptomatic patients will be crucial in the delivery of therapeutics early enough to alter the disease course (Turner, Bowser, et al., 2013).

6.6. Drug repurposing in ALS

ALS, like all neurodegenerative diseases, remains incurable. The vast majority of candidate drugs identified since riluzole have failed to demonstrate efficacy in clinical trials (Petrov et al., 2017). This high failure rate, coupled with the high cost and time required to develop new drugs (Brown et al., 2021; Wouters et al., 2020), has led to a reluctance of pharmaceutical companies to fund research into novel therapeutics for ALS. In light of this, there has been renewed interest in drug repurposing; taking clinically approved or unapproved but previously evaluated pharmaceutical compounds and examining their therapeutic benefits for use in different disorders (Ashburn & Thor, 2004; Fetro & Scherman, 2020; Pushpakom et al., 2019). Drug repurposing has significant advantages over developing novel therapeutics from scratch including reduced risk of failure due to previously approved safety profiles, reduced time frames for drug development and reduced investment in preclinical and phase I and II stages of development (Pushpakom et al., 2019).

Edaravone, the free radical scavenger now clinically approved for the treatment of ALS in Japan and the United States, is one such repurposed drug that was originally indicated for treatment of acute cerebral infarction (Edaravone Acute Infarction Study, 2003). A number of other compounds have been examined for repurposing in ALS. For example, arimoclomol, originally indicated for the treatment of diabetic neuropathy and insulin resistance, has shown promising effects in SOD1 associated ALS (Benatar et al., 2018; Kalmar et al., 2008; Kieran et al., 2004). Similarly, ambroxol, a beta-glucocerebrosidase 2 (GBA2) inhibitor originally developed for the treatment of respiratory tract infectious disorders, has been found to delay disease onset, improve motor function and reduced neuronal death in SOD1 mice (Bouscary et al., 2019; Bouscary et al., 2020). In ALS patients, treatment with the anti-seizure compound ezogabine was found to reduce cortical and spinal motor neuron hyperexcitability in a recent double-blind placebo-controlled clinical trial (Wainger et al., 2021). Terazosin is a further drug that has shown potential for repurposing in the treatment of neurodegenerative and neuromuscular disorders including ALS. Clinically approved for the treatment of hypertension and enlarged prostate, terazosin has also been shown to exert neuroprotective effects in Parkinson's disease and spinal muscular atrophy (SMA) (Boyd et al., 2017; Cai et al., 2019). In our work, we have found that terazosin mitigates cell viability deficits observed in TDP-43^{M337V} mESC-MNs in response to oxidative stress and increases axon length in zebrafish models of TDP-43^{M337V} proteinopathy (Chaytow et al., 2022). Given it's known safety profile, terazosin represents a promising therapeutic agent for repurposing in ALS. Furthermore, measurements of terazosin levels in the brain indicate that it is capable of crossing the blood-brain barrier, which has proven to be a major challenge in the delivery of therapeutics for neurological disorders (Cai et al., 2019).

It is clear that ALS poses unique challenges in the development of pharmacological compounds that alter the disease course. The complexity of ALS coupled with the high costs and long lead times associated with drug discovery and development has resulted in slow progress. Regarding the latter, drug repurposing provides the opportunity to reduce delays and minimise costs, by screening the efficacy of existing compounds in the treatment of ALS. As these candidate drugs have previously been deemed safe in the treatment of human disease, they can bypass the lengthy early stages of clinical development, thus fast-tracking the drug discovery process.

6.7. Closing remarks

The multifaceted and complex nature of ALS presents a unique challenge to scientific research and drug discovery. The development of appropriate models that reflect the physiological environment in human disease will be crucial in advancing our understanding of disease mechanisms and the identification of new, more effective treatments. Recognising the limitations of currently available models is important, to ensure the appropriate interpretation of results and the identification of disease-specific mechanisms. Advances will likely result from research in both *in vitro* and *in vivo* model systems, with the aim of identifying robust, consistent and overlapping phenotypes. While ALS is still characterised as a single disorder, the clinical, pathological and genetic heterogeneity of the disease suggests a 'one-size fits all' approach to treatment will be insufficient. Instead, the future of ALS treatment is likely to involve a 'personalised medicine' approach, with treatments tailored to address the pathological basis of disease as appropriate to the individual.

REFERENCES

Ababneh, N. A., Scaber, J., Flynn, R., Douglas, A., Barbagallo, P., Candalija, A., Turner, M. R., Sims, D., Dafinca, R., Cowley, S. A., & Talbot, K. (2020, Aug 3). Correction of amyotrophic lateral sclerosis related phenotypes in induced pluripotent stem cell-derived motor neurons carrying a hexanucleotide expansion mutation in C9orf72 by CRISPR/Cas9 genome editing using homology-directed repair. *Hum Mol Genet, 29*(13), 2200-2217. https://doi.org/10.1093/hmg/ddaa106

Abe, K., Itoyama, Y., Sobue, G., Tsuji, S., Aoki, M., Doyu, M., Hamada, C., Kondo, K., Yoneoka, T., Akimoto, M., Yoshino, H., & Edaravone, A. L. S. S. G. (2014, Dec). Confirmatory double-blind, parallel-group, placebo-controlled study of efficacy and safety of edaravone (MCI-186) in amyotrophic lateral sclerosis patients. *Amyotroph Lateral Scler Frontotemporal Degener, 15*(7-8), 610-617. https://doi.org/10.3109/21678421.2014.959024

Abe, K., Pan, L. H., Watanabe, M., Kato, T., & Itoyama, Y. (1995, Oct 20). Induction of nitrotyrosine-like immunoreactivity in the lower motor neuron of amyotrophic lateral sclerosis. *Neurosci Lett, 199*(2), 152-154. https://doi.org/10.1016/0304-3940(95)12039-7

Abo-Rady, M., Kalmbach, N., Pal, A., Schludi, C., Janosch, A., Richter, T., Freitag, P., Bickle, M., Kahlert, A. K., Petri, S., Stefanov, S., Glass, H., Staege, S., Just, W., Bhatnagar, R., Edbauer, D., Hermann, A., Wegner, F., & Sterneckert, J. L. (2020, Mar 10). Knocking out C9ORF72 Exacerbates Axonal Trafficking Defects Associated with Hexanucleotide Repeat Expansion and Reduces Levels of Heat Shock Proteins. *Stem Cell Reports, 14*(3), 390-405. https://doi.org/10.1016/j.stemcr.2020.01.010

Abrahams, S., Goldstein, L. H., Suckling, J., Ng, V., Simmons, A., Chitnis, X., Atkins, L., Williams, S. C., & Leigh, P. N. (2005, Mar). Frontotemporal white matter changes in amyotrophic lateral sclerosis. *J Neurol, 252*(3), 321-331. https://doi.org/10.1007/s00415-005-0646-x

Abrahams, S., Leigh, P. N., Harvey, A., Vythelingum, G. N., Grise, D., & Goldstein, L. H. (2000). Verbal fluency and executive dysfunction in amyotrophic lateral sclerosis (ALS). *Neuropsychologia, 38*(6), 734-747. https://doi.org/10.1016/s0028-3932(99)00146-3

Afroz, T., Hock, E. M., Ernst, P., Foglieni, C., Jambeau, M., Gilhespy, L. A. B., Laferriere, F., Maniecka, Z., Pluckthun, A., Mittl, P., Paganetti, P., Allain, F. H. T., & Polymenidou, M. (2017, Jun 29). Functional and dynamic polymerization of the ALS-linked protein TDP-43 antagonizes its pathologic aggregation. *Nat Commun, 8*(1), 45. https://doi.org/10.1038/s41467-017-00062-0

Al-Chalabi, A., Calvo, A., Chio, A., Colville, S., Ellis, C. M., Hardiman, O., Heverin, M., Howard, R. S., Huisman, M. H. B., Keren, N., Leigh, P. N., Mazzini, L., Mora, G., Orrell, R. W., Rooney, J., Scott, K. M., Scotton, W. J., Seelen, M., Shaw, C. E., Sidle, K. S., Swingler, R., Tsuda, M., Veldink, J. H., Visser, A. E., van den Berg, L. H., & Pearce, N. (2014, Nov). Analysis of amyotrophic lateral sclerosis as a multistep

process: a population-based modelling study. *Lancet Neurol, 13*(11), 1108-1113. https://doi.org/10.1016/S1474-4422(14)70219-4

Alami, N. H., Smith, R. B., Carrasco, M. A., Williams, L. A., Winborn, C. S., Han, S. S. W., Kiskinis, E., Winborn, B., Freibaum, B. D., Kanagaraj, A., Clare, A. J., Badders, N. M., Bilican, B., Chaum, E., Chandran, S., Shaw, C. E., Eggan, K. C., Maniatis, T., & Taylor, J. P. (2014, Feb 5). Axonal transport of TDP-43 mRNA granules is impaired by ALS-causing mutations. *Neuron, 81*(3), 536-543. https://doi.org/10.1016/j.neuron.2013.12.018

Alexianu, M. E., Ho, B. K., Mohamed, A. H., La Bella, V., Smith, R. G., & Appel, S. H. (1994, Dec). The role of calcium-binding proteins in selective motoneuron vulnerability in amyotrophic lateral sclerosis. *Ann Neurol, 36*(6), 846-858. https://doi.org/10.1002/ana.410360608

Ames, A., 3rd. (2000, Nov). CNS energy metabolism as related to function. *Brain Res Brain Res Rev, 34*(1-2), 42-68. https://doi.org/10.1016/s0165-0173(00)00038-2

Anderson, P., & Kedersha, N. (2009, Jun). RNA granules: post-transcriptional and epigenetic modulators of gene expression. *Nat Rev Mol Cell Biol, 10*(6), 430-436. https://doi.org/10.1038/nrm2694

Andrews, S., Gilley, J., & Coleman, M. P. (2010, Nov 30). Difference Tracker: ImageJ plugins for fully automated analysis of multiple axonal transport parameters. *J Neurosci Methods, 193*(2), 281-287. https://doi.org/10.1016/j.jneumeth.2010.09.007

Arai, T., Hasegawa, M., Akiyama, H., Ikeda, K., Nonaka, T., Mori, H., Mann, D., Tsuchiya, K., Yoshida, M., Hashizume, Y., & Oda, T. (2006, Dec 22). TDP-43 is a component of ubiquitin-positive tau-negative inclusions in frontotemporal lobar degeneration and amyotrophic lateral sclerosis. *Biochem Biophys Res Commun, 351*(3), 602-611. https://doi.org/10.1016/j.bbrc.2006.10.093

Archbold, H. C., Jackson, K. L., Arora, A., Weskamp, K., Tank, E. M., Li, X., Miguez, R., Dayton, R. D., Tamir, S., Klein, R. L., & Barmada, S. J. (2018, Mar 15). TDP43 nuclear export and neurodegeneration in models of amyotrophic lateral sclerosis and frontotemporal dementia. *Sci Rep, 8*(1), 4606. https://doi.org/10.1038/s41598-018-22858-w

Armitage, P., & Doll, R. (1954, Mar). The age distribution of cancer and a multi-stage theory of carcinogenesis. *Br J Cancer, 8*(1), 1-12. https://doi.org/10.1038/bjc.1954.1

Armon, C. (2009, Nov 17). Smoking may be considered an established risk factor for sporadic ALS. *Neurology, 73*(20), 1693-1698. https://doi.org/10.1212/WNL.0b013e3181c1df48

Arnold, E. S., Ling, S. C., Huelga, S. C., Lagier-Tourenne, C., Polymenidou, M., Ditsworth, D., Kordasiewicz, H. B., McAlonis-Downes, M., Platoshyn, O., Parone, P. A., Da Cruz, S., Clutario, K. M., Swing, D., Tessarollo, L., Marsala, M., Shaw, C. E., Yeo, G. W., & Cleveland, D. W. (2013, Feb 19). ALS-linked TDP-43 mutations produce aberrant RNA splicing and adult-onset motor neuron disease without aggregation or

loss of nuclear TDP-43. *Proc Natl Acad Sci U S A, 110*(8), E736-745. https://doi.org/10.1073/pnas.1222809110

Ash, P. E., Bieniek, K. F., Gendron, T. F., Caulfield, T., Lin, W. L., Dejesus-Hernandez, M., van Blitterswijk, M. M., Jansen-West, K., Paul, J. W., 3rd, Rademakers, R., Boylan, K. B., Dickson, D. W., & Petrucelli, L. (2013, Feb 20). Unconventional translation of C9ORF72 GGGGCC expansion generates insoluble polypeptides specific to c9FTD/ALS. *Neuron, 77*(4), 639-646. https://doi.org/10.1016/j.neuron.2013.02.004

Ashburn, T. T., & Thor, K. B. (2004, Aug). Drug repositioning: identifying and developing new uses for existing drugs. *Nat Rev Drug Discov, 3*(8), 673-683. https://doi.org/10.1038/nrd1468

Augustine, G. J., Santamaria, F., & Tanaka, K. (2003, Oct 9). Local calcium signaling in neurons. *Neuron, 40*(2), 331-346. https://doi.org/10.1016/s0896-6273(03)00639-1

Aulas, A., & Vande Velde, C. (2015). Alterations in stress granule dynamics driven by TDP-43 and FUS: a link to pathological inclusions in ALS? *Front Cell Neurosci, 9*, 423. https://doi.org/10.3389/fncel.2015.00423

Ayala, V., Granado-Serrano, A. B., Cacabelos, D., Naudi, A., Ilieva, E. V., Boada, J., Caraballo-Miralles, V., Llado, J., Ferrer, I., Pamplona, R., & Portero-Otin, M. (2011, Sep). Cell stress induces TDP-43 pathological changes associated with ERK1/2 dysfunction: implications in ALS. *Acta Neuropathol, 122*(3), 259-270. https://doi.org/10.1007/s00401-011-0850-y

Ayala, Y. M., De Conti, L., Avendano-Vazquez, S. E., Dhir, A., Romano, M., D'Ambrogio, A., Tollervey, J., Ule, J., Baralle, M., Buratti, E., & Baralle, F. E. (2011, Jan 19). TDP-43 regulates its mRNA levels through a negative feedback loop. *EMBO J, 30*(2), 277-288. https://doi.org/10.1038/emboj.2010.310

Ayala, Y. M., Pantano, S., D'Ambrogio, A., Buratti, E., Brindisi, A., Marchetti, C., Romano, M., & Baralle, F. E. (2005, May 6). Human, Drosophila, and C.elegans TDP43: nucleic acid binding properties and splicing regulatory function. *J Mol Biol, 348*(3), 575-588. https://doi.org/10.1016/j.jmb.2005.02.038

Ayala, Y. M., Zago, P., D'Ambrogio, A., Xu, Y. F., Petrucelli, L., Buratti, E., & Baralle, F. E. (2008, Nov 15). Structural determinants of the cellular localization and shuttling of TDP-43. *J Cell Sci, 121*(Pt 22), 3778-3785. https://doi.org/10.1242/jcs.038950

Baldwin, K. R., Godena, V. K., Hewitt, V. L., & Whitworth, A. J. (2016, Jun 15). Axonal transport defects are a common phenotype in Drosophila models of ALS. *Hum Mol Genet, 25*(12), 2378-2392. https://doi.org/10.1093/hmg/ddw105

Barber, S. C., & Shaw, P. J. (2010, Mar 1). Oxidative stress in ALS: key role in motor neuron injury and therapeutic target. *Free Radic Biol Med, 48*(5), 629-641. https://doi.org/10.1016/j.freeradbiomed.2009.11.018

Barmada, S. J., Skibinski, G., Korb, E., Rao, E. J., Wu, J. Y., & Finkbeiner, S. (2010, Jan 13). Cytoplasmic mislocalization of TDP-43 is toxic to neurons and enhanced by a

mutation associated with familial amyotrophic lateral sclerosis. *J Neurosci, 30*(2), 639-649. https://doi.org/10.1523/JNEUROSCI.4988-09.2010

Beal, M. F., Ferrante, R. J., Browne, S. E., Matthews, R. T., Kowall, N. W., & Brown, R. H., Jr. (1997, Oct). Increased 3-nitrotyrosine in both sporadic and familial amyotrophic lateral sclerosis. *Ann Neurol, 42*(4), 644-654. https://doi.org/10.1002/ana.410420416

Beckman, J. S., Carson, M., Smith, C. D., & Koppenol, W. H. (1993, Aug 12). ALS, SOD and peroxynitrite. *Nature, 364*(6438), 584. https://doi.org/10.1038/364584a0

Benatar, M., Wuu, J., Andersen, P. M., Atassi, N., David, W., Cudkowicz, M., & Schoenfeld, D. (2018, Feb 13). Randomized, double-blind, placebo-controlled trial of arimoclomol in rapidly progressive SOD1 ALS. *Neurology, 90*(7), e565-e574. https://doi.org/10.1212/WNL.0000000000004960

Benjaminsen, E., Alstadhaug, K. B., Gulsvik, M., Baloch, F. K., & Odeh, F. (2018, Nov). Amyotrophic lateral sclerosis in Nordland county, Norway, 2000-2015: prevalence, incidence, and clinical features. *Amyotroph Lateral Scler Frontotemporal Degener, 19*(7-8), 522-527. https://doi.org/10.1080/21678421.2018.1513534

Bensimon, G., Lacomblez, L., & Meininger, V. (1994, Mar 3). A controlled trial of riluzole in amyotrophic lateral sclerosis. ALS/Riluzole Study Group. *N Engl J Med, 330*(9), 585-591. https://doi.org/10.1056/NEJM199403033300901

Bianchi, F., Malboubi, M., Li, Y., George, J. H., Jerusalem, A., Szele, F., Thompson, M. S., & Ye, H. (2018, Oct). Rapid and efficient differentiation of functional motor neurons from human iPSC for neural injury modelling. *Stem Cell Res, 32*, 126-134. https://doi.org/10.1016/j.scr.2018.09.006

Bilican, B., Serio, A., Barmada, S. J., Nishimura, A. L., Sullivan, G. J., Carrasco, M., Phatnani, H. P., Puddifoot, C. A., Story, D., Fletcher, J., Park, I. H., Friedman, B. A., Daley, G. Q., Wyllie, D. J., Hardingham, G. E., Wilmut, I., Finkbeiner, S., Maniatis, T., Shaw, C. E., & Chandran, S. (2012, Apr 10). Mutant induced pluripotent stem cell lines recapitulate aspects of TDP-43 proteinopathies and reveal cell-specific vulnerability. *Proc Natl Acad Sci U S A, 109*(15), 5803-5808. https://doi.org/10.1073/pnas.1202922109

Bilsland, L. G., Sahai, E., Kelly, G., Golding, M., Greensmith, L., & Schiavo, G. (2010, Nov 23). Deficits in axonal transport precede ALS symptoms in vivo. *Proc Natl Acad Sci U S A, 107*(47), 20523-20528. https://doi.org/10.1073/pnas.1006869107

Binet, A., & Claret, M. (1983, Mar 15). alpha-adrenergic stimulation of respiration in isolated rat hepatocytes. *Biochem J, 210*(3), 867-873. https://doi.org/10.1042/bj2100867

Blokhuis, A. M., Koppers, M., Groen, E. J. N., van den Heuvel, D. M. A., Dini Modigliani, S., Anink, J. J., Fumoto, K., van Diggelen, F., Snelting, A., Sodaar, P., Verheijen, B. M., Demmers, J. A. A., Veldink, J. H., Aronica, E., Bozzoni, I., den Hertog, J., van den Berg, L. H., & Pasterkamp, R. J. (2016, Aug). Comparative interactomics analysis of different ALS-associated proteins identifies converging molecular

pathways. *Acta Neuropathol, 132*(2), 175-196. https://doi.org/10.1007/s00401-016-1575-8

Bogdanov, M., Brown, R. H., Matson, W., Smart, R., Hayden, D., O'Donnell, H., Flint Beal, M., & Cudkowicz, M. (2000, Oct 1). Increased oxidative damage to DNA in ALS patients. *Free Radic Biol Med, 29*(7), 652-658. https://doi.org/10.1016/s0891-5849(00)00349-x

Borchelt, D. R., Davis, J., Fischer, M., Lee, M. K., Slunt, H. H., Ratovitsky, T., Regard, J., Copeland, N. G., Jenkins, N. A., Sisodia, S. S., & Price, D. L. (1996, Dec). A vector for expressing foreign genes in the brains and hearts of transgenic mice. *Genet Anal, 13*(6), 159-163. https://doi.org/10.1016/s1050-3862(96)00167-2

Bossolasco, P., Sassone, F., Gumina, V., Peverelli, S., Garzo, M., & Silani, V. (2018, Jul). Motor neuron differentiation of iPSCs obtained from peripheral blood of a mutant TARDBP ALS patient. *Stem Cell Res, 30*, 61-68. https://doi.org/10.1016/j.scr.2018.05.009

Bouscary, A., Quessada, C., Mosbach, A., Callizot, N., Spedding, M., Loeffler, J. P., & Henriques, A. (2019). Ambroxol Hydrochloride Improves Motor Functions and Extends Survival in a Mouse Model of Familial Amyotrophic Lateral Sclerosis. *Front Pharmacol, 10*, 883. https://doi.org/10.3389/fphar.2019.00883

Bouscary, A., Quessada, C., Rene, F., Spedding, M., Henriques, A., Ngo, S., & Loeffler, J. P. (2020, Oct 5). Drug repositioning in neurodegeneration: An overview of the use of ambroxol in neurodegenerative diseases. *Eur J Pharmacol, 884*, 173446. https://doi.org/10.1016/j.ejphar.2020.173446

Boyd, P. J., Tu, W. Y., Shorrock, H. K., Groen, E. J. N., Carter, R. N., Powis, R. A., Thomson, S. R., Thomson, D., Graham, L. C., Motyl, A. A. L., Wishart, T. M., Highley, J. R., Morton, N. M., Becker, T., Becker, C. G., Heath, P. R., & Gillingwater, T. H. (2017, Apr). Bioenergetic status modulates motor neuron vulnerability and pathogenesis in a zebrafish model of spinal muscular atrophy. *PLoS Genet, 13*(4), e1006744. https://doi.org/10.1371/journal.pgen.1006744

Briese, M., Saal-Bauernschubert, L., Luningschror, P., Moradi, M., Dombert, B., Surrey, V., Appenzeller, S., Deng, C., Jablonka, S., & Sendtner, M. (2020, Jul 24). Loss of Tdp-43 disrupts the axonal transcriptome of motoneurons accompanied by impaired axonal translation and mitochondria function. *Acta Neuropathol Commun, 8*(1), 116. https://doi.org/10.1186/s40478-020-00987-6

Briscoe, J., & Ericson, J. (2001, Feb). Specification of neuronal fates in the ventral neural tube. *Curr Opin Neurobiol, 11*(1), 43-49. https://doi.org/10.1016/s0959-4388(00)00172-0

Brown, A. L., Wilkins, O. G., Keuss, M. J., Hill, S. E., Zanovello, M., Lee, W. C., Bampton, A., Lee, F. C. Y., Masino, L., Qi, Y. A., Bryce-Smith, S., Gatt, A., Hallegger, M., Fagegaltier, D., Phatnani, H., Consortium, N. A., Newcombe, J., Gustavsson, E. K., Seddighi, S., Reyes, J. F., Coon, S. L., Ramos, D., Schiavo, G., Fisher, E. M. C., Raj, T., Secrier, M., Lashley, T., Ule, J., Buratti, E., Humphrey, J., Ward, M. E., & Fratta,

P. (2022, Mar). TDP-43 loss and ALS-risk SNPs drive mis-splicing and depletion of UNC13A. *Nature, 603*(7899), 131-137. https://doi.org/10.1038/s41586-022-04436-3

Brown, D. G., Wobst, H. J., Kapoor, A., Kenna, L. A., & Southall, N. (2021, Nov 10). Clinical development times for innovative drugs. *Nat Rev Drug Discov*. https://doi.org/10.1038/d41573-021-00190-9

Bryson, J. B., Machado, C. B., Crossley, M., Stevenson, D., Bros-Facer, V., Burrone, J., Greensmith, L., & Lieberam, I. (2014, Apr 4). Optical control of muscle function by transplantation of stem cell-derived motor neurons in mice. *Science, 344*(6179), 94-97. https://doi.org/10.1126/science.1248523

Bunina, T. L. (1962). [On intracellular inclusions in familial amyotrophic lateral sclerosis]. *Zh Nevropatol Psikhiatr Im S S Korsakova, 62*, 1293-1299. https://www.ncbi.nlm.nih.gov/pubmed/14016841

Buratti, E. (2015). Functional Significance of TDP-43 Mutations in Disease. *Adv Genet, 91*, 1-53. https://doi.org/10.1016/bs.adgen.2015.07.001

Buratti, E., & Baralle, F. E. (2001, Sep 28). Characterization and functional implications of the RNA binding properties of nuclear factor TDP-43, a novel splicing regulator of CFTR exon 9. *J Biol Chem, 276*(39), 36337-36343. https://doi.org/10.1074/jbc.M104236200

Buratti, E., & Baralle, F. E. (2008, Jan 1). Multiple roles of TDP-43 in gene expression, splicing regulation, and human disease. *Front Biosci, 13*, 867-878. https://doi.org/10.2741/2727

Buratti, E., & Baralle, F. E. (2010, Jul-Aug). The multiple roles of TDP-43 in pre-mRNA processing and gene expression regulation. *RNA Biol, 7*(4), 420-429. https://doi.org/10.4161/rna.7.4.12205

Byrne, S., Heverin, M., Elamin, M., Bede, P., Lynch, C., Kenna, K., MacLaughlin, R., Walsh, C., Al Chalabi, A., & Hardiman, O. (2013, Nov). Aggregation of neurologic and neuropsychiatric disease in amyotrophic lateral sclerosis kindreds: a population-based case-control cohort study of familial and sporadic amyotrophic lateral sclerosis. *Ann Neurol, 74*(5), 699-708. https://doi.org/10.1002/ana.23969

Cai, Q., Zakaria, H. M., Simone, A., & Sheng, Z. H. (2012, Mar 20). Spatial parkin translocation and degradation of damaged mitochondria via mitophagy in live cortical neurons. *Curr Biol, 22*(6), 545-552. https://doi.org/10.1016/j.cub.2012.02.005

Cai, R., Zhang, Y., Simmering, J. E., Schultz, J. L., Li, Y., Fernandez-Carasa, I., Consiglio, A., Raya, A., Polgreen, P. M., Narayanan, N. S., Yuan, Y., Chen, Z., Su, W., Han, Y., Zhao, C., Gao, L., Ji, X., Welsh, M. J., & Liu, L. (2019, Oct 1). Enhancing glycolysis attenuates Parkinson's disease progression in models and clinical databases. *J Clin Invest, 129*(10), 4539-4549. https://doi.org/10.1172/JCI129987

Camu, W., Khoris, J., Moulard, B., Salachas, F., Briolotti, V., Rouleau, G. A., & Meininger, V. (1999, Jun). Genetics of familial ALS and consequences for diagnosis. French

ALS Research Group. *J Neurol Sci, 165 Suppl 1*, S21-26. https://doi.org/10.1016/s0022-510x(99)00022-2

Caroscio, J. T., Mulvihill, M. N., Sterling, R., & Abrams, B. (1987, Feb). Amyotrophic lateral sclerosis. Its natural history. *Neurol Clin, 5*(1), 1-8. https://www.ncbi.nlm.nih.gov/pubmed/3561382

Cascella, R., Capitini, C., Fani, G., Dobson, C. M., Cecchi, C., & Chiti, F. (2016, Sep 9). Quantification of the Relative Contributions of Loss-of-function and Gain-of-function Mechanisms in TAR DNA-binding Protein 43 (TDP-43) Proteinopathies. *J Biol Chem, 291*(37), 19437-19448. https://doi.org/10.1074/jbc.M116.737726

Chaban, Y., Boekema, E. J., & Dudkina, N. V. (2014, Apr). Structures of mitochondrial oxidative phosphorylation supercomplexes and mechanisms for their stabilisation. *Biochim Biophys Acta, 1837*(4), 418-426. https://doi.org/10.1016/j.bbabio.2013.10.004

Chang, J. L., Lomen-Hoerth, C., Murphy, J., Henry, R. G., Kramer, J. H., Miller, B. L., & Gorno-Tempini, M. L. (2005, Jul 12). A voxel-based morphometry study of patterns of brain atrophy in ALS and ALS/FTLD. *Neurology, 65*(1), 75-80. https://doi.org/10.1212/01.wnl.0000167602.38643.29

Chartier-Harlin, M. C., Kachergus, J., Roumier, C., Mouroux, V., Douay, X., Lincoln, S., Levecque, C., Larvor, L., Andrieux, J., Hulihan, M., Waucquier, N., Defebvre, L., Amouyel, P., Farrer, M., & Destee, A. (2004, Sep 25-Oct 1). Alpha-synuclein locus duplication as a cause of familial Parkinson's disease. *Lancet, 364*(9440), 1167-1169. https://doi.org/10.1016/S0140-6736(04)17103-1

Chaytow, H., Carroll, E., Gordon, D., Huang, Y. T., van der Hoorn, D., Smith, H. L., Becker, T., Becker, C. G., Faller, K. M. E., Talbot, K., & Gillingwater, T. H. (2022, Aug 2). Targeting phosphoglycerate kinase 1 with terazosin improves motor neuron phenotypes in multiple models of amyotrophic lateral sclerosis. *EBioMedicine*, 104202. https://doi.org/10.1016/j.ebiom.2022.104202

Chen, Y., & Cohen, T. J. (2019, Mar 8). Aggregation of the nucleic acid-binding protein TDP-43 occurs via distinct routes that are coordinated with stress granule formation. *J Biol Chem, 294*(10), 3696-3706. https://doi.org/10.1074/jbc.RA118.006351

Chiang, P. M., Ling, J., Jeong, Y. H., Price, D. L., Aja, S. M., & Wong, P. C. (2010, Sep 14). Deletion of TDP-43 down-regulates Tbc1d1, a gene linked to obesity, and alters body fat metabolism. *Proc Natl Acad Sci U S A, 107*(37), 16320-16324. https://doi.org/10.1073/pnas.1002176107

Chio, A., Calvo, A., Mazzini, L., Cantello, R., Mora, G., Moglia, C., Corrado, L., D'Alfonso, S., Majounie, E., Renton, A., Pisano, F., Ossola, I., Brunetti, M., Traynor, B. J., Restagno, G., & Parals. (2012, Nov 6). Extensive genetics of ALS: a population-based study in Italy. *Neurology, 79*(19), 1983-1989. https://doi.org/10.1212/WNL.0b013e3182735d36

Chio, A., Calvo, A., Moglia, C., Mazzini, L., Mora, G., & group, P. s. (2011, Jul). Phenotypic heterogeneity of amyotrophic lateral sclerosis: a population based study. *J Neurol Neurosurg Psychiatry, 82*(7), 740-746. https://doi.org/10.1136/jnnp.2010.235952

Chio, A., Mazzini, L., D'Alfonso, S., Corrado, L., Canosa, A., Moglia, C., Manera, U., Bersano, E., Brunetti, M., Barberis, M., Veldink, J. H., van den Berg, L. H., Pearce, N., Sproviero, W., McLaughlin, R., Vajda, A., Hardiman, O., Rooney, J., Mora, G., Calvo, A., & Al-Chalabi, A. (2018, Aug 14). The multistep hypothesis of ALS revisited: The role of genetic mutations. *Neurology, 91*(7), e635-e642. https://doi.org/10.1212/WNL.0000000000005996

Chio, A., Traynor, B. J., Lombardo, F., Fimognari, M., Calvo, A., Ghiglione, P., Mutani, R., & Restagno, G. (2008, Feb 12). Prevalence of SOD1 mutations in the Italian ALS population. *Neurology, 70*(7), 533-537. https://doi.org/10.1212/01.wnl.0000299187.90432.3f

Coffman, C. J., Horner, R. D., Grambow, S. C., Lindquist, J., & Project, V. A. C. S. P. (2005). Estimating the occurrence of amyotrophic lateral sclerosis among Gulf War (1990-1991) veterans using capture-recapture methods. *Neuroepidemiology, 24*(3), 141-150. https://doi.org/10.1159/000083297

Colombrita, C., Zennaro, E., Fallini, C., Weber, M., Sommacal, A., Buratti, E., Silani, V., & Ratti, A. (2009, Nov). TDP-43 is recruited to stress granules in conditions of oxidative insult. *J Neurochem, 111*(4), 1051-1061. https://doi.org/10.1111/j.1471-4159.2009.06383.x

Corbo, M., & Hays, A. P. (1992, Sep). Peripherin and neurofilament protein coexist in spinal spheroids of motor neuron disease. *J Neuropathol Exp Neurol, 51*(5), 531-537. https://doi.org/10.1097/00005072-199209000-00008

Cortes, D., Robledo-Arratia, Y., Hernandez-Martinez, R., Escobedo-Avila, I., Bargas, J., & Velasco, I. (2016). Transgenic GDNF Positively Influences Proliferation, Differentiation, Maturation and Survival of Motor Neurons Produced from Mouse Embryonic Stem Cells. *Front Cell Neurosci, 10*, 217. https://doi.org/10.3389/fncel.2016.00217

Coyle, J. T., & Puttfarcken, P. (1993, Oct 29). Oxidative stress, glutamate, and neurodegenerative disorders. *Science, 262*(5134), 689-695. https://doi.org/10.1126/science.7901908

Coyne, A. N., Zaepfel, B. L., & Zarnescu, D. C. (2017). Failure to Deliver and Translate-New Insights into RNA Dysregulation in ALS. *Front Cell Neurosci, 11*, 243. https://doi.org/10.3389/fncel.2017.00243

Cruz, M. P. (2018, Jan). Edaravone (Radicava): A Novel Neuroprotective Agent for the Treatment of Amyotrophic Lateral Sclerosis. *P T, 43*(1), 25-28. https://www.ncbi.nlm.nih.gov/pubmed/29290672

Dafinca, R., Barbagallo, P., Farrimond, L., Candalija, A., Scaber, J., Ababneh, N. A., Sathyaprakash, C., Vowles, J., Cowley, S. A., & Talbot, K. (2020, May 12).

Impairment of Mitochondrial Calcium Buffering Links Mutations in C9ORF72 and TARDBP in iPS-Derived Motor Neurons from Patients with ALS/FTD. *Stem Cell Reports, 14*(5), 892-908. https://doi.org/10.1016/j.stemcr.2020.03.023

Dafinca, R., Scaber, J., Ababneh, N., Lalic, T., Weir, G., Christian, H., Vowles, J., Douglas, A. G., Fletcher-Jones, A., Browne, C., Nakanishi, M., Turner, M. R., Wade-Martins, R., Cowley, S. A., & Talbot, K. (2016, Aug). C9orf72 Hexanucleotide Expansions Are Associated with Altered Endoplasmic Reticulum Calcium Homeostasis and Stress Granule Formation in Induced Pluripotent Stem Cell-Derived Neurons from Patients with Amyotrophic Lateral Sclerosis and Frontotemporal Dementia. *Stem Cells, 34*(8), 2063-2078. https://doi.org/10.1002/stem.2388

Davis-Dusenbery, B. N., Williams, L. A., Klim, J. R., & Eggan, K. (2014, Feb). How to make spinal motor neurons. *Development, 141*(3), 491-501. https://doi.org/10.1242/dev.097410

De Vos, K. J., Chapman, A. L., Tennant, M. E., Manser, C., Tudor, E. L., Lau, K. F., Brownlees, J., Ackerley, S., Shaw, P. J., McLoughlin, D. M., Shaw, C. E., Leigh, P. N., Miller, C. C. J., & Grierson, A. J. (2007, Nov 15). Familial amyotrophic lateral sclerosis-linked SOD1 mutants perturb fast axonal transport to reduce axonal mitochondria content. *Hum Mol Genet, 16*(22), 2720-2728. https://doi.org/10.1093/hmg/ddm226

DeJesus-Hernandez, M., Mackenzie, I. R., Boeve, B. F., Boxer, A. L., Baker, M., Rutherford, N. J., Nicholson, A. M., Finch, N. A., Flynn, H., Adamson, J., Kouri, N., Wojtas, A., Sengdy, P., Hsiung, G. Y., Karydas, A., Seeley, W. W., Josephs, K. A., Coppola, G., Geschwind, D. H., Wszolek, Z. K., Feldman, H., Knopman, D. S., Petersen, R. C., Miller, B. L., Dickson, D. W., Boylan, K. B., Graff-Radford, N. R., & Rademakers, R. (2011, Oct 20). Expanded GGGGCC hexanucleotide repeat in noncoding region of C9ORF72 causes chromosome 9p-linked FTD and ALS. *Neuron, 72*(2), 245-256. https://doi.org/10.1016/j.neuron.2011.09.011

Deng, H. X., Chen, W., Hong, S. T., Boycott, K. M., Gorrie, G. H., Siddique, N., Yang, Y., Fecto, F., Shi, Y., Zhai, H., Jiang, H., Hirano, M., Rampersaud, E., Jansen, G. H., Donkervoort, S., Bigio, E. H., Brooks, B. R., Ajroud, K., Sufit, R. L., Haines, J. L., Mugnaini, E., Pericak-Vance, M. A., & Siddique, T. (2011, Aug 21). Mutations in UBQLN2 cause dominant X-linked juvenile and adult-onset ALS and ALS/dementia. *Nature, 477*(7363), 211-215. https://doi.org/10.1038/nature10353

Deshaies, J. E., Shkreta, L., Moszczynski, A. J., Sidibe, H., Semmler, S., Fouillen, A., Bennett, E. R., Bekenstein, U., Destroismaisons, L., Toutant, J., Delmotte, Q., Volkening, K., Stabile, S., Aulas, A., Khalfallah, Y., Soreq, H., Nanci, A., Strong, M. J., Chabot, B., & Vande Velde, C. (2018, May 1). TDP-43 regulates the alternative splicing of hnRNP A1 to yield an aggregation-prone variant in amyotrophic lateral sclerosis. *Brain, 141*(5), 1320-1333. https://doi.org/10.1093/brain/awy062

Devlin, A. C., Burr, K., Borooah, S., Foster, J. D., Cleary, E. M., Geti, I., Vallier, L., Shaw, C. E., Chandran, S., & Miles, G. B. (2015, Jan 12). Human iPSC-derived motoneurons harbouring TARDBP or C9ORF72 ALS mutations are dysfunctional

despite maintaining viability. *Nat Commun, 6*, 5999. https://doi.org/10.1038/ncomms6999

Dewey, C. M., Cenik, B., Sephton, C. F., Dries, D. R., Mayer, P., 3rd, Good, S. K., Johnson, B. A., Herz, J., & Yu, G. (2011, Mar). TDP-43 is directed to stress granules by sorbitol, a novel physiological osmotic and oxidative stressor. *Mol Cell Biol, 31*(5), 1098-1108. https://doi.org/10.1128/MCB.01279-10

Dewey, C. M., Cenik, B., Sephton, C. F., Johnson, B. A., Herz, J., & Yu, G. (2012, Jun 26). TDP-43 aggregation in neurodegeneration: are stress granules the key? *Brain Res, 1462*, 16-25. https://doi.org/10.1016/j.brainres.2012.02.032

Di Giorgio, F. P., Boulting, G. L., Bobrowicz, S., & Eggan, K. C. (2008, Dec 4). Human embryonic stem cell-derived motor neurons are sensitive to the toxic effect of glial cells carrying an ALS-causing mutation. *Cell Stem Cell, 3*(6), 637-648. https://doi.org/10.1016/j.stem.2008.09.017

Echelard, Y., Epstein, D. J., St-Jacques, B., Shen, L., Mohler, J., McMahon, J. A., & McMahon, A. P. (1993, Dec 31). Sonic hedgehog, a member of a family of putative signaling molecules, is implicated in the regulation of CNS polarity. *Cell, 75*(7), 1417-1430. https://doi.org/10.1016/0092-8674(93)90627-3

Edaravone Acute Infarction Study, G. (2003). Effect of a novel free radical scavenger, edaravone (MCI-186), on acute brain infarction. Randomized, placebo-controlled, double-blind study at multicenters. *Cerebrovasc Dis, 15*(3), 222-229. https://doi.org/10.1159/000069318

Ederle, H., Funk, C., Abou-Ajram, C., Hutten, S., Funk, E. B. E., Kehlenbach, R. H., Bailer, S. M., & Dormann, D. (2018, May 4). Nuclear egress of TDP-43 and FUS occurs independently of Exportin-1/CRM1. *Sci Rep, 8*(1), 7084. https://doi.org/10.1038/s41598-018-25007-5

Egawa, N., Kitaoka, S., Tsukita, K., Naitoh, M., Takahashi, K., Yamamoto, T., Adachi, F., Kondo, T., Okita, K., Asaka, I., Aoi, T., Watanabe, A., Yamada, Y., Morizane, A., Takahashi, J., Ayaki, T., Ito, H., Yoshikawa, K., Yamawaki, S., Suzuki, S., Watanabe, D., Hioki, H., Kaneko, T., Makioka, K., Okamoto, K., Takuma, H., Tamaoka, A., Hasegawa, K., Nonaka, T., Hasegawa, M., Kawata, A., Yoshida, M., Nakahata, T., Takahashi, R., Marchetto, M. C., Gage, F. H., Yamanaka, S., & Inoue, H. (2012, Aug 1). Drug screening for ALS using patient-specific induced pluripotent stem cells. *Sci Transl Med, 4*(145), 145ra104. https://doi.org/10.1126/scitranslmed.3004052

Ellison, D. (2012). *Neuropathology : a reference text of CNS pathology* (3rd ed.) https://yale.idm.oclc.org/login?URL=https://www.clinicalkey.com/dura/browse/bookChapter/3-s2.0-C20090442065

Fallini, C., Bassell, G. J., & Rossoll, W. (2012, Aug 15). The ALS disease protein TDP-43 is actively transported in motor neuron axons and regulates axon outgrowth. *Hum Mol Genet, 21*(16), 3703-3718. https://doi.org/10.1093/hmg/dds205

Fang, T., Al Khleifat, A., Meurgey, J. H., Jones, A., Leigh, P. N., Bensimon, G., & Al-Chalabi, A. (2018, May). Stage at which riluzole treatment prolongs survival in patients with amyotrophic lateral sclerosis: a retrospective analysis of data from a dose-ranging study. *Lancet Neurol, 17*(5), 416-422. https://doi.org/10.1016/S1474-4422(18)30054-1

Faye, P. A., Vedrenne, N., Miressi, F., Rassat, M., Romanenko, S., Richard, L., Bourthoumieu, S., Funalot, B., Sturtz, F., Favreau, F., & Lia, A. S. (2020, Jun 27). Optimized Protocol to Generate Spinal Motor Neuron Cells from Induced Pluripotent Stem Cells from Charcot Marie Tooth Patients. *Brain Sci, 10*(7). https://doi.org/10.3390/brainsci10070407

Fazal, R., Boeynaems, S., Swijsen, A., De Decker, M., Fumagalli, L., Moisse, M., Vanneste, J., Guo, W., Boon, R., Vercruysse, T., Eggermont, K., Swinnen, B., Beckers, J., Pakravan, D., Vandoorne, T., Vanden Berghe, P., Verfaillie, C., Van Den Bosch, L., & Van Damme, P. (2021, Apr 1). HDAC6 inhibition restores TDP-43 pathology and axonal transport defects in human motor neurons with TARDBP mutations. *EMBO J, 40*(7), e106177. https://doi.org/10.15252/embj.2020106177

Feneberg, E., Gordon, D., Thompson, A. G., Finelli, M. J., Dafinca, R., Candalija, A., Charles, P. D., Mager, I., Wood, M. J., Fischer, R., Kessler, B. M., Gray, E., Turner, M. R., & Talbot, K. (2020, Oct). An ALS-linked mutation in TDP-43 disrupts normal protein interactions in the motor neuron response to oxidative stress. *Neurobiol Dis, 144*, 105050. https://doi.org/10.1016/j.nbd.2020.105050

Ferguson, T. A., & Elman, L. B. (2007). Clinical presentation and diagnosis of amyotrophic lateral sclerosis. *NeuroRehabilitation, 22*(6), 409-416. https://www.ncbi.nlm.nih.gov/pubmed/18198425

Ferrante, R. J., Browne, S. E., Shinobu, L. A., Bowling, A. C., Baik, M. J., MacGarvey, U., Kowall, N. W., Brown, R. H., Jr., & Beal, M. F. (1997, Nov). Evidence of increased oxidative damage in both sporadic and familial amyotrophic lateral sclerosis. *J Neurochem, 69*(5), 2064-2074. https://doi.org/10.1046/j.1471-4159.1997.69052064.x

Fetro, C., & Scherman, D. (2020, Apr). Drug repurposing in rare diseases: Myths and reality. *Therapie, 75*(2), 157-160. https://doi.org/10.1016/j.therap.2020.02.006

Fratta, P., Sivakumar, P., Humphrey, J., Lo, K., Ricketts, T., Oliveira, H., Brito-Armas, J. M., Kalmar, B., Ule, A., Yu, Y., Birsa, N., Bodo, C., Collins, T., Conicella, A. E., Mejia Maza, A., Marrero-Gagliardi, A., Stewart, M., Mianne, J., Corrochano, S., Emmett, W., Codner, G., Groves, M., Fukumura, R., Gondo, Y., Lythgoe, M., Pauws, E., Peskett, E., Stanier, P., Teboul, L., Hallegger, M., Calvo, A., Chio, A., Isaacs, A. M., Fawzi, N. L., Wang, E., Housman, D. E., Baralle, F., Greensmith, L., Buratti, E., Plagnol, V., Fisher, E. M., & Acevedo-Arozena, A. (2018, Jun 1). Mice with endogenous TDP-43 mutations exhibit gain of splicing function and characteristics of amyotrophic lateral sclerosis. *EMBO J, 37*(11). https://doi.org/10.15252/embj.201798684

Freibaum, B. D., Chitta, R. K., High, A. A., & Taylor, J. P. (2010, Feb 5). Global analysis of TDP-43 interacting proteins reveals strong association with RNA splicing and

translation machinery. *J Proteome Res, 9*(2), 1104-1120. https://doi.org/10.1021/pr901076y

Friedrich, G., & Soriano, P. (1991, Sep). Promoter traps in embryonic stem cells: a genetic screen to identify and mutate developmental genes in mice. *Genes Dev, 5*(9), 1513-1523. https://doi.org/10.1101/gad.5.9.1513

Fujimori, K., Ishikawa, M., Otomo, A., Atsuta, N., Nakamura, R., Akiyama, T., Hadano, S., Aoki, M., Saya, H., Sobue, G., & Okano, H. (2018, Oct). Modeling sporadic ALS in iPSC-derived motor neurons identifies a potential therapeutic agent. *Nat Med, 24*(10), 1579-1589. https://doi.org/10.1038/s41591-018-0140-5

Fumagalli, L., Young, F. L., Boeynaems, S., De Decker, M., Mehta, A. R., Swijsen, A., Fazal, R., Guo, W., Moisse, M., Beckers, J., Dedeene, L., Selvaraj, B. T., Vandoorne, T., Madan, V., van Blitterswijk, M., Raitcheva, D., McCampbell, A., Poesen, K., Gitler, A. D., Koch, P., Berghe, P. V., Thal, D. R., Verfaillie, C., Chandran, S., Van Den Bosch, L., Bullock, S. L., & Van Damme, P. (2021, Apr). C9orf72-derived arginine-containing dipeptide repeats associate with axonal transport machinery and impede microtubule-based motility. *Sci Adv, 7*(15). https://doi.org/10.1126/sciadv.abg3013

Gautier, G., Verschueren, A., Monnier, A., Attarian, S., Salort-Campana, E., & Pouget, J. (2010, Aug). ALS with respiratory onset: clinical features and effects of non-invasive ventilation on the prognosis. *Amyotroph Lateral Scler, 11*(4), 379-382. https://doi.org/10.3109/17482960903426543

Goldstein, L. H., & Abrahams, S. (2013, Apr). Changes in cognition and behaviour in amyotrophic lateral sclerosis: nature of impairment and implications for assessment. *Lancet Neurol, 12*(4), 368-380. https://doi.org/10.1016/S1474-4422(13)70026-7

Gordon, D., Dafinca, R., Scaber, J., Alegre-Abarrategui, J., Farrimond, L., Scott, C., Biggs, D., Kent, L., Oliver, P. L., Davies, B., Ansorge, O., Wade-Martins, R., & Talbot, K. (2019, Jan). Single-copy expression of an amyotrophic lateral sclerosis-linked TDP-43 mutation (M337V) in BAC transgenic mice leads to altered stress granule dynamics and progressive motor dysfunction. *Neurobiol Dis, 121*, 148-162. https://doi.org/10.1016/j.nbd.2018.09.024

Gordon, P. H., Salachas, F., Lacomblez, L., Le Forestier, N., Pradat, P. F., Bruneteau, G., Elbaz, A., & Meininger, V. (2013). Predicting survival of patients with amyotrophic lateral sclerosis at presentation: a 15-year experience. *Neurodegener Dis, 12*(2), 81-90. https://doi.org/10.1159/000341316

Gore, A., Li, Z., Fung, H. L., Young, J. E., Agarwal, S., Antosiewicz-Bourget, J., Canto, I., Giorgetti, A., Israel, M. A., Kiskinis, E., Lee, J. H., Loh, Y. H., Manos, P. D., Montserrat, N., Panopoulos, A. D., Ruiz, S., Wilbert, M. L., Yu, J., Kirkness, E. F., Izpisua Belmonte, J. C., Rossi, D. J., Thomson, J. A., Eggan, K., Daley, G. Q., Goldstein, L. S., & Zhang, K. (2011, Mar 3). Somatic coding mutations in human induced pluripotent stem cells. *Nature, 471*(7336), 63-67. https://doi.org/10.1038/nature09805

Grad, L. I., Rouleau, G. A., Ravits, J., & Cashman, N. R. (2017, Aug 1). Clinical Spectrum of Amyotrophic Lateral Sclerosis (ALS). *Cold Spring Harb Perspect Med, 7*(8). https://doi.org/10.1101/cshperspect.a024117

Gredal, O., Werdelin, L., Bak, S., Christensen, P. B., Boysen, G., Kristensen, M. O., Jespersen, J. H., Regeur, L., Hinge, H. H., & Jensen, T. S. (1997, Jul). A clinical trial of dextromethorphan in amyotrophic lateral sclerosis. *Acta Neurol Scand, 96*(1), 8-13. https://doi.org/10.1111/j.1600-0404.1997.tb00231.x

Gromicho, M., Pinto, S., Gisca, E., Pronto-Laborinho, A. C., Andersen, P. M., & de Carvalho, M. (2018, Oct). Frequency of C9orf72 hexanucleotide repeat expansion and SOD1 mutations in Portuguese patients with amyotrophic lateral sclerosis. *Neurobiol Aging, 70*, 325 e327-325 e315. https://doi.org/10.1016/j.neurobiolaging.2018.05.009

Gu, J., Wu, F., Xu, W., Shi, J., Hu, W., Jin, N., Qian, W., Wang, X., Iqbal, K., Gong, C. X., & Liu, F. (2017, Jun 2). TDP-43 suppresses tau expression via promoting its mRNA instability. *Nucleic Acids Res, 45*(10), 6177-6193. https://doi.org/10.1093/nar/gkx175

Guo, W., Stoklund Dittlau, K., & Van Den Bosch, L. (2020, Mar). Axonal transport defects and neurodegeneration: Molecular mechanisms and therapeutic implications. *Semin Cell Dev Biol, 99*, 133-150. https://doi.org/10.1016/j.semcdb.2019.07.010

Gurney, M. E., Pu, H., Chiu, A. Y., Dal Canto, M. C., Polchow, C. Y., Alexander, D. D., Caliendo, J., Hentati, A., Kwon, Y. W., Deng, H. X., & et al. (1994, Jun 17). Motor neuron degeneration in mice that express a human Cu,Zn superoxide dismutase mutation. *Science, 264*(5166), 1772-1775. https://doi.org/10.1126/science.8209258

Haeusler, A. R., Donnelly, C. J., & Rothstein, J. D. (2016, Jun). The expanding biology of the C9orf72 nucleotide repeat expansion in neurodegenerative disease. *Nat Rev Neurosci, 17*(6), 383-395. https://doi.org/10.1038/nrn.2016.38

Haidet-Phillips, A. M., Hester, M. E., Miranda, C. J., Meyer, K., Braun, L., Frakes, A., Song, S., Likhite, S., Murtha, M. J., Foust, K. D., Rao, M., Eagle, A., Kammesheidt, A., Christensen, A., Mendell, J. R., Burghes, A. H., & Kaspar, B. K. (2011, Aug 10). Astrocytes from familial and sporadic ALS patients are toxic to motor neurons. *Nat Biotechnol, 29*(9), 824-828. https://doi.org/10.1038/nbt.1957

Hammer, R. P., Jr., Tomiyasu, U., & Scheibel, A. B. (1979, Feb). Degeneration of the human Betz cell due to amyotrophic lateral sclerosis. *Exp Neurol, 63*(2), 336-346. https://doi.org/10.1016/0014-4886(79)90129-8

Hardiman, O., Al-Chalabi, A., Chio, A., Corr, E. M., Logroscino, G., Robberecht, W., Shaw, P. J., Simmons, Z., & van den Berg, L. H. (2017, Oct 5). Amyotrophic lateral sclerosis. *Nat Rev Dis Primers, 3*, 17071. https://doi.org/10.1038/nrdp.2017.71

Harris, J. J., Jolivet, R., & Attwell, D. (2012, Sep 6). Synaptic energy use and supply. *Neuron, 75*(5), 762-777. https://doi.org/10.1016/j.neuron.2012.08.019

Hasegawa, M., Arai, T., Nonaka, T., Kametani, F., Yoshida, M., Hashizume, Y., Beach, T. G., Buratti, E., Baralle, F., Morita, M., Nakano, I., Oda, T., Tsuchiya, K., & Akiyama,

H. (2008, Jul). Phosphorylated TDP-43 in frontotemporal lobar degeneration and amyotrophic lateral sclerosis. *Ann Neurol, 64*(1), 60-70. https://doi.org/10.1002/ana.21425

Hebron, M. L., Lonskaya, I., Sharpe, K., Weerasinghe, P. P., Algarzae, N. K., Shekoyan, A. R., & Moussa, C. E. (2013, Feb 8). Parkin ubiquitinates Tar-DNA binding protein-43 (TDP-43) and promotes its cytosolic accumulation via interaction with histone deacetylase 6 (HDAC6). *J Biol Chem, 288*(6), 4103-4115. https://doi.org/10.1074/jbc.M112.419945

Hemmings, B. A., & Restuccia, D. F. (2012, Sep 1). PI3K-PKB/Akt pathway. *Cold Spring Harb Perspect Biol, 4*(9), a011189. https://doi.org/10.1101/cshperspect.a011189

Hirano, A., Donnenfeld, H., Sasaki, S., & Nakano, I. (1984, Sep). Fine structural observations of neurofilamentous changes in amyotrophic lateral sclerosis. *J Neuropathol Exp Neurol, 43*(5), 461-470. https://doi.org/10.1097/00005072-198409000-00001

Hirano, A., Nakano, I., Kurland, L. T., Mulder, D. W., Holley, P. W., & Saccomanno, G. (1984, Sep). Fine structural study of neurofibrillary changes in a family with amyotrophic lateral sclerosis. *J Neuropathol Exp Neurol, 43*(5), 471-480. https://doi.org/10.1097/00005072-198409000-00002

Hong, C. T., Chau, K. Y., & Schapira, A. H. (2016, May 5). Meclizine-induced enhanced glycolysis is neuroprotective in Parkinson disease cell models. *Sci Rep, 6*, 25344. https://doi.org/10.1038/srep25344

Hor, J. H., Santosa, M. M., Lim, V. J. W., Ho, B. X., Taylor, A., Khong, Z. J., Ravits, J., Fan, Y., Liou, Y. C., Soh, B. S., & Ng, S. Y. (2021, Apr). ALS motor neurons exhibit hallmark metabolic defects that are rescued by SIRT3 activation. *Cell Death Differ, 28*(4), 1379-1397. https://doi.org/10.1038/s41418-020-00664-0

Horner, R. D., Kamins, K. G., Feussner, J. R., Grambow, S. C., Hoff-Lindquist, J., Harati, Y., Mitsumoto, H., Pascuzzi, R., Spencer, P. S., Tim, R., Howard, D., Smith, T. C., Ryan, M. A., Coffman, C. J., & Kasarskis, E. J. (2003, Sep 23). Occurrence of amyotrophic lateral sclerosis among Gulf War veterans. *Neurology, 61*(6), 742-749. https://doi.org/10.1212/01.wnl.0000069922.32557.ca

Houzen, H., Kano, T., Horiuchi, K., Wakita, M., Nagai, A., & Yabe, I. (2021, Jul 21). Improved Long-Term Survival with Edaravone Therapy in Patients with Amyotrophic Lateral Sclerosis: A Retrospective Single-Center Study in Japan. *Pharmaceuticals (Basel), 14*(8). https://doi.org/10.3390/ph14080705

Howe, C. L., & Mobley, W. C. (2004, Feb 5). Signaling endosome hypothesis: A cellular mechanism for long distance communication. *J Neurobiol, 58*(2), 207-216. https://doi.org/10.1002/neu.10323

Ibanez, C. F. (2007, Nov). Message in a bottle: long-range retrograde signaling in the nervous system. *Trends Cell Biol, 17*(11), 519-528. https://doi.org/10.1016/j.tcb.2007.09.003

Igaz, L. M., Kwong, L. K., Chen-Plotkin, A., Winton, M. J., Unger, T. L., Xu, Y., Neumann, M., Trojanowski, J. Q., & Lee, V. M. (2009, Mar 27). Expression of TDP-43 C-terminal Fragments in Vitro Recapitulates Pathological Features of TDP-43 Proteinopathies. *J Biol Chem, 284*(13), 8516-8524. https://doi.org/10.1074/jbc.M809462200

Igaz, L. M., Kwong, L. K., Lee, E. B., Chen-Plotkin, A., Swanson, E., Unger, T., Malunda, J., Xu, Y., Winton, M. J., Trojanowski, J. Q., & Lee, V. M. (2011, Feb). Dysregulation of the ALS-associated gene TDP-43 leads to neuronal death and degeneration in mice. *J Clin Invest, 121*(2), 726-738. https://doi.org/10.1172/JCI44867

Igaz, L. M., Kwong, L. K., Xu, Y., Truax, A. C., Uryu, K., Neumann, M., Clark, C. M., Elman, L. B., Miller, B. L., Grossman, M., McCluskey, L. F., Trojanowski, J. Q., & Lee, V. M. (2008, Jul). Enrichment of C-terminal fragments in TAR DNA-binding protein-43 cytoplasmic inclusions in brain but not in spinal cord of frontotemporal lobar degeneration and amyotrophic lateral sclerosis. *Am J Pathol, 173*(1), 182-194. https://doi.org/10.2353/ajpath.2008.080003

Iguchi, Y., Katsuno, M., Takagi, S., Ishigaki, S., Niwa, J., Hasegawa, M., Tanaka, F., & Sobue, G. (2012, Mar). Oxidative stress induced by glutathione depletion reproduces pathological modifications of TDP-43 linked to TDP-43 proteinopathies. *Neurobiol Dis, 45*(3), 862-870. https://doi.org/10.1016/j.nbd.2011.12.002

Ihara, Y., Nobukuni, K., Takata, H., & Hayabara, T. (2005, Jan). Oxidative stress and metal content in blood and cerebrospinal fluid of amyotrophic lateral sclerosis patients with and without a Cu, Zn-superoxide dismutase mutation. *Neurol Res, 27*(1), 105-108. https://doi.org/10.1179/016164105X18430

Ikenaka, K., Kawai, K., Katsuno, M., Huang, Z., Jiang, Y. M., Iguchi, Y., Kobayashi, K., Kimata, T., Waza, M., Tanaka, F., Mori, I., & Sobue, G. (2013). dnc-1/dynactin 1 knockdown disrupts transport of autophagosomes and induces motor neuron degeneration. *PLoS One, 8*(2), e54511. https://doi.org/10.1371/journal.pone.0054511

Ingre, C., Roos, P. M., Piehl, F., Kamel, F., & Fang, F. (2015). Risk factors for amyotrophic lateral sclerosis. *Clin Epidemiol, 7*, 181-193. https://doi.org/10.2147/CLEP.S37505

Inukai, Y., Nonaka, T., Arai, T., Yoshida, M., Hashizume, Y., Beach, T. G., Buratti, E., Baralle, F. E., Akiyama, H., Hisanaga, S., & Hasegawa, M. (2008, Aug 20). Abnormal phosphorylation of Ser409/410 of TDP-43 in FTLD-U and ALS. *FEBS Lett, 582*(19), 2899-2904. https://doi.org/10.1016/j.febslet.2008.07.027

Jiang, L. L., Xue, W., Hong, J. Y., Zhang, J. T., Li, M. J., Yu, S. N., He, J. H., & Hu, H. Y. (2017, Jul 21). The N-terminal dimerization is required for TDP-43 splicing activity. *Sci Rep, 7*(1), 6196. https://doi.org/10.1038/s41598-017-06263-3

Johnson, B. S., Snead, D., Lee, J. J., McCaffery, J. M., Shorter, J., & Gitler, A. D. (2009, Jul 24). TDP-43 is intrinsically aggregation-prone, and amyotrophic lateral sclerosis-linked mutations accelerate aggregation and increase toxicity. *J Biol Chem, 284*(30), 20329-20339. https://doi.org/10.1074/jbc.M109.010264

Julian, T. H., Glascow, N., Barry, A. D. F., Moll, T., Harvey, C., Klimentidis, Y. C., Newell, M., Zhang, S., Snyder, M. P., Cooper-Knock, J., & Shaw, P. J. (2021, Jun). Physical exercise is a risk factor for amyotrophic lateral sclerosis: Convergent evidence from Mendelian randomisation, transcriptomics and risk genotypes. *EBioMedicine, 68*, 103397. https://doi.org/10.1016/j.ebiom.2021.103397

Jun, K. Y., Park, J., Oh, K. W., Kim, E. M., Bae, J. S., Kim, I., & Kim, S. H. (2019, Apr). Epidemiology of ALS in Korea using nationwide big data. *J Neurol Neurosurg Psychiatry, 90*(4), 395-403. https://doi.org/10.1136/jnnp-2018-318974

Juneja, T., Pericak-Vance, M. A., Laing, N. G., Dave, S., & Siddique, T. (1997, Jan). Prognosis in familial amyotrophic lateral sclerosis: progression and survival in patients with glu100gly and ala4val mutations in Cu,Zn superoxide dismutase. *Neurology, 48*(1), 55-57. https://doi.org/10.1212/wnl.48.1.55

Kabashi, E., Valdmanis, P. N., Dion, P., Spiegelman, D., McConkey, B. J., Vande Velde, C., Bouchard, J. P., Lacomblez, L., Pochigaeva, K., Salachas, F., Pradat, P. F., Camu, W., Meininger, V., Dupre, N., & Rouleau, G. A. (2008, May). TARDBP mutations in individuals with sporadic and familial amyotrophic lateral sclerosis. *Nat Genet, 40*(5), 572-574. https://doi.org/10.1038/ng.132

Kalmar, B., Novoselov, S., Gray, A., Cheetham, M. E., Margulis, B., & Greensmith, L. (2008, Oct). Late stage treatment with arimoclomol delays disease progression and prevents protein aggregation in the SOD1 mouse model of ALS. *J Neurochem, 107*(2), 339-350. https://doi.org/10.1111/j.1471-4159.2008.05595.x

Karumbayaram, S., Novitch, B. G., Patterson, M., Umbach, J. A., Richter, L., Lindgren, A., Conway, A. E., Clark, A. T., Goldman, S. A., Plath, K., Wiedau-Pazos, M., Kornblum, H. I., & Lowry, W. E. (2009, Apr). Directed differentiation of human-induced pluripotent stem cells generates active motor neurons. *Stem Cells, 27*(4), 806-811. https://doi.org/10.1002/stem.31

Kassubek, J., Unrath, A., Huppertz, H. J., Lule, D., Ethofer, T., Sperfeld, A. D., & Ludolph, A. C. (2005, Dec). Global brain atrophy and corticospinal tract alterations in ALS, as investigated by voxel-based morphometry of 3-D MRI. *Amyotroph Lateral Scler Other Motor Neuron Disord, 6*(4), 213-220. https://doi.org/10.1080/14660820510038538

Katyal, N., & Govindarajan, R. (2017). Shortcomings in the Current Amyotrophic Lateral Sclerosis Trials and Potential Solutions for Improvement. *Front Neurol, 8*, 521. https://doi.org/10.3389/fneur.2017.00521

Kawahara, Y., & Mieda-Sato, A. (2012, Feb 28). TDP-43 promotes microRNA biogenesis as a component of the Drosha and Dicer complexes. *Proc Natl Acad Sci U S A, 109*(9), 3347-3352. https://doi.org/10.1073/pnas.1112427109

Khalfallah, Y., Kuta, R., Grasmuck, C., Prat, A., Durham, H. D., & Vande Velde, C. (2018, May 15). TDP-43 regulation of stress granule dynamics in neurodegenerative disease-relevant cell types. *Sci Rep, 8*(1), 7551. https://doi.org/10.1038/s41598-018-25767-0

Kieran, D., Kalmar, B., Dick, J. R., Riddoch-Contreras, J., Burnstock, G., & Greensmith, L. (2004, Apr). Treatment with arimoclomol, a coinducer of heat shock proteins, delays disease progression in ALS mice. *Nat Med, 10*(4), 402-405. https://doi.org/10.1038/nm1021

King, O. D., Gitler, A. D., & Shorter, J. (2012, Jun 26). The tip of the iceberg: RNA-binding proteins with prion-like domains in neurodegenerative disease. *Brain Res, 1462*, 61-80. https://doi.org/10.1016/j.brainres.2012.01.016

Kiskinis, E., Sandoe, J., Williams, L. A., Boulting, G. L., Moccia, R., Wainger, B. J., Han, S., Peng, T., Thams, S., Mikkilineni, S., Mellin, C., Merkle, F. T., Davis-Dusenbery, B. N., Ziller, M., Oakley, D., Ichida, J., Di Costanzo, S., Atwater, N., Maeder, M. L., Goodwin, M. J., Nemesh, J., Handsaker, R. E., Paull, D., Noggle, S., McCarroll, S. A., Joung, J. K., Woolf, C. J., Brown, R. H., & Eggan, K. (2014, Jun 5). Pathways disrupted in human ALS motor neurons identified through genetic correction of mutant SOD1. *Cell Stem Cell, 14*(6), 781-795. https://doi.org/10.1016/j.stem.2014.03.004

Kraemer, B. C., Schuck, T., Wheeler, J. M., Robinson, L. C., Trojanowski, J. Q., Lee, V. M., & Schellenberg, G. D. (2010, Apr). Loss of murine TDP-43 disrupts motor function and plays an essential role in embryogenesis. *Acta Neuropathol, 119*(4), 409-419. https://doi.org/10.1007/s00401-010-0659-0

Kreiter, N., Pal, A., Lojewski, X., Corcia, P., Naujock, M., Reinhardt, P., Sterneckert, J., Petri, S., Wegner, F., Storch, A., & Hermann, A. (2018, Jul). Age-dependent neurodegeneration and organelle transport deficiencies in mutant TDP43 patient-derived neurons are independent of TDP43 aggregation. *Neurobiol Dis, 115*, 167-181. https://doi.org/10.1016/j.nbd.2018.03.010

Kuo, P. H., Chiang, C. H., Wang, Y. T., Doudeva, L. G., & Yuan, H. S. (2014, Apr). The crystal structure of TDP-43 RRM1-DNA complex reveals the specific recognition for UG- and TG-rich nucleic acids. *Nucleic Acids Res, 42*(7), 4712-4722. https://doi.org/10.1093/nar/gkt1407

Kwiatkowski, T. J., Jr., Bosco, D. A., Leclerc, A. L., Tamrazian, E., Vanderburg, C. R., Russ, C., Davis, A., Gilchrist, J., Kasarskis, E. J., Munsat, T., Valdmanis, P., Rouleau, G. A., Hosler, B. A., Cortelli, P., de Jong, P. J., Yoshinaga, Y., Haines, J. L., Pericak-Vance, M. A., Yan, J., Ticozzi, N., Siddique, T., McKenna-Yasek, D., Sapp, P. C., Horvitz, H. R., Landers, J. E., & Brown, R. H., Jr. (2009, Feb 27). Mutations in the FUS/TLS gene on chromosome 16 cause familial amyotrophic lateral sclerosis. *Science, 323*(5918), 1205-1208. https://doi.org/10.1126/science.1166066

Lacomblez, L., Bensimon, G., Leigh, P. N., Guillet, P., & Meininger, V. (1996, May 25). Dose-ranging study of riluzole in amyotrophic lateral sclerosis. Amyotrophic Lateral Sclerosis/Riluzole Study Group II. *Lancet, 347*(9013), 1425-1431. https://doi.org/10.1016/s0140-6736(96)91680-3

Lagier-Tourenne, C., Polymenidou, M., & Cleveland, D. W. (2010, Apr 15). TDP-43 and FUS/TLS: emerging roles in RNA processing and neurodegeneration. *Hum Mol Genet, 19*(R1), R46-64. https://doi.org/10.1093/hmg/ddq137

Le Masson, G., Przedborski, S., & Abbott, L. F. (2014, Aug 20). A computational model of motor neuron degeneration. *Neuron, 83*(4), 975-988. https://doi.org/10.1016/j.neuron.2014.07.001

Lederer, C. W., Torrisi, A., Pantelidou, M., Santama, N., & Cavallaro, S. (2007, Jan 23). Pathways and genes differentially expressed in the motor cortex of patients with sporadic amyotrophic lateral sclerosis. *BMC Genomics, 8*, 26. https://doi.org/10.1186/1471-2164-8-26

Lee, Y. J., Kim, H. S., Seo, H. S., Na, J. O., Jang, Y. N., Han, Y. M., & Kim, H. M. (2020). Stimulation of Alpha1-Adrenergic Receptor Ameliorates Cellular Functions of Multiorgans beyond Vasomotion through PPARdelta. *PPAR Res, 2020*, 3785137. https://doi.org/10.1155/2020/3785137

Leigh, P. N., Anderton, B. H., Dodson, A., Gallo, J. M., Swash, M., & Power, D. M. (1988, Nov 11). Ubiquitin deposits in anterior horn cells in motor neurone disease. *Neurosci Lett, 93*(2-3), 197-203. https://doi.org/10.1016/0304-3940(88)90081-x

Leigh, P. N., Whitwell, H., Garofalo, O., Buller, J., Swash, M., Martin, J. E., Gallo, J. M., Weller, R. O., & Anderton, B. H. (1991, Apr). Ubiquitin-immunoreactive intraneuronal inclusions in amyotrophic lateral sclerosis. Morphology, distribution, and specificity. *Brain, 114 (Pt 2)*, 775-788. https://doi.org/10.1093/brain/114.2.775

Leighton, D. J., Newton, J., Stephenson, L. J., Colville, S., Davenport, R., Gorrie, G., Morrison, I., Swingler, R., Chandran, S., Pal, S., & Consortium, C.-M. (2019, Apr). Changing epidemiology of motor neurone disease in Scotland. *J Neurol, 266*(4), 817-825. https://doi.org/10.1007/s00415-019-09190-7

Lenaz, G. (1998, Aug 10). Role of mitochondria in oxidative stress and ageing. *Biochim Biophys Acta, 1366*(1-2), 53-67. https://doi.org/10.1016/s0005-2728(98)00120-0

Li, H. R., Chiang, W. C., Chou, P. C., Wang, W. J., & Huang, J. R. (2018, Apr 20). TAR DNA-binding protein 43 (TDP-43) liquid-liquid phase separation is mediated by just a few aromatic residues. *J Biol Chem, 293*(16), 6090-6098. https://doi.org/10.1074/jbc.AC117.001037

Li, Q., Yokoshi, M., Okada, H., & Kawahara, Y. (2015, Jan 29). The cleavage pattern of TDP-43 determines its rate of clearance and cytotoxicity. *Nat Commun, 6*, 6183. https://doi.org/10.1038/ncomms7183

Li, Y., Collins, M., An, J., Geiser, R., Tegeler, T., Tsantilas, K., Garcia, K., Pirrotte, P., & Bowser, R. (2016, Sep 15). Immunoprecipitation and mass spectrometry defines an extensive RBM45 protein-protein interaction network. *Brain Res, 1647*, 79-93. https://doi.org/10.1016/j.brainres.2016.02.047

Liguori, I., Russo, G., Curcio, F., Bulli, G., Aran, L., Della-Morte, D., Gargiulo, G., Testa, G., Cacciatore, F., Bonaduce, D., & Abete, P. (2018). Oxidative stress, aging, and diseases. *Clin Interv Aging, 13*, 757-772. https://doi.org/10.2147/CIA.S158513

Lindquist, S. (1981, Sep 24). Regulation of protein synthesis during heat shock. *Nature, 293*(5830), 311-314. https://doi.org/10.1038/293311a0

Ling, J. P., Pletnikova, O., Troncoso, J. C., & Wong, P. C. (2015, Aug 7). TDP-43 repression of nonconserved cryptic exons is compromised in ALS-FTD. *Science, 349*(6248), 650-655. https://doi.org/10.1126/science.aab0983

Ling, S. C., Albuquerque, C. P., Han, J. S., Lagier-Tourenne, C., Tokunaga, S., Zhou, H., & Cleveland, D. W. (2010, Jul 27). ALS-associated mutations in TDP-43 increase its stability and promote TDP-43 complexes with FUS/TLS. *Proc Natl Acad Sci U S A, 107*(30), 13318-13323. https://doi.org/10.1073/pnas.1008227107

Ling, S. C., Polymenidou, M., & Cleveland, D. W. (2013, Aug 7). Converging mechanisms in ALS and FTD: disrupted RNA and protein homeostasis. *Neuron, 79*(3), 416-438. https://doi.org/10.1016/j.neuron.2013.07.033

Liu, J., Zhao, W., Li, C., Wu, T., Han, L., Hu, Z., Li, X., Zhou, J., & Chen, X. (2021, Dec 30). Terazosin Stimulates Pgk1 to Remedy Gastrointestinal Disorders. *Int J Mol Sci, 23*(1). https://doi.org/10.3390/ijms23010416

Liu, R., Yang, G., Nonaka, T., Arai, T., Jia, W., & Cynader, M. S. (2013, Aug 9). Reducing TDP-43 aggregation does not prevent its cytotoxicity. *Acta Neuropathol Commun, 1*, 49. https://doi.org/10.1186/2051-5960-1-49

Liu-Yesucevitz, L., Bilgutay, A., Zhang, Y. J., Vanderweyde, T., Citro, A., Mehta, T., Zaarur, N., McKee, A., Bowser, R., Sherman, M., Petrucelli, L., & Wolozin, B. (2010, Oct 11). Tar DNA binding protein-43 (TDP-43) associates with stress granules: analysis of cultured cells and pathological brain tissue. *PLoS One, 5*(10), e13250. https://doi.org/10.1371/journal.pone.0013250

Lomen-Hoerth, C., Anderson, T., & Miller, B. (2002, Oct 8). The overlap of amyotrophic lateral sclerosis and frontotemporal dementia. *Neurology, 59*(7), 1077-1079. https://doi.org/10.1212/wnl.59.7.1077

Longinetti, E., Regodon Wallin, A., Samuelsson, K., Press, R., Zachau, A., Ronnevi, L. O., Kierkegaard, M., Andersen, P. M., Hillert, J., Fang, F., & Ingre, C. (2018, Nov). The Swedish motor neuron disease quality registry. *Amyotroph Lateral Scler Frontotemporal Degener, 19*(7-8), 528-537. https://doi.org/10.1080/21678421.2018.1497065

Lopez-Gonzalez, R., Kunckles, P., & Velasco, I. (2009). Transient recovery in a rat model of familial amyotrophic lateral sclerosis after transplantation of motor neurons derived from mouse embryonic stem cells. *Cell Transplant, 18*(10), 1171-1181. https://doi.org/10.3727/096368909X12483162197123

Lowe, J., Lennox, G., Jefferson, D., Morrell, K., McQuire, D., Gray, T., Landon, M., Doherty, F. J., & Mayer, R. J. (1988, Nov 22). A filamentous inclusion body within anterior horn neurones in motor neurone disease defined by immunocytochemical localisation of ubiquitin. *Neurosci Lett, 94*(1-2), 203-210. https://doi.org/10.1016/0304-3940(88)90296-0

Ludolph, A. C., Langen, K. J., Regard, M., Herzog, H., Kemper, B., Kuwert, T., Bottger, I. G., & Feinendegen, L. (1992, Feb). Frontal lobe function in amyotrophic lateral sclerosis: a neuropsychologic and positron emission tomography study. *Acta Neurol Scand, 85*(2), 81-89. https://doi.org/10.1111/j.1600-0404.1992.tb04003.x

Lukavsky, P. J., Daujotyte, D., Tollervey, J. R., Ule, J., Stuani, C., Buratti, E., Baralle, F. E., Damberger, F. F., & Allain, F. H. (2013, Dec). Molecular basis of UG-rich RNA recognition by the human splicing factor TDP-43. *Nat Struct Mol Biol, 20*(12), 1443-1449. https://doi.org/10.1038/nsmb.2698

Luna, J., Diagana, M., Ait Aissa, L., Tazir, M., Ali Pacha, L., Kacem, I., Gouider, R., Henning, F., Basse, A., Cisse, O., Balogou, A. A. K., Kombate, D., Agbetou, M., Houinato, D., Millogo, A., Agba, T., Belo, M., Penoty, M., Raymondeau-Moustafa, M., Hamidou, B., Couratier, P., Preux, P. M., Marin, B., & Collaboration, T. (2019, Jan). Clinical features and prognosis of amyotrophic lateral sclerosis in Africa: the TROPALS study. *J Neurol Neurosurg Psychiatry, 90*(1), 20-29. https://doi.org/10.1136/jnnp-2018-318469

Ma, X. R., Prudencio, M., Koike, Y., Vatsavayai, S. C., Kim, G., Harbinski, F., Briner, A., Rodriguez, C. M., Guo, C., Akiyama, T., Schmidt, H. B., Cummings, B. B., Wyatt, D. W., Kurylo, K., Miller, G., Mekhoubad, S., Sallee, N., Mekonnen, G., Ganser, L., Rubien, J. D., Jansen-West, K., Cook, C. N., Pickles, S., Oskarsson, B., Graff-Radford, N. R., Boeve, B. F., Knopman, D. S., Petersen, R. C., Dickson, D. W., Shorter, J., Myong, S., Green, E. M., Seeley, W. W., Petrucelli, L., & Gitler, A. D. (2022, Mar). TDP-43 represses cryptic exon inclusion in the FTD-ALS gene UNC13A. *Nature, 603*(7899), 124-130. https://doi.org/10.1038/s41586-022-04424-7

Machado, C. B., Kanning, K. C., Kreis, P., Stevenson, D., Crossley, M., Nowak, M., Iacovino, M., Kyba, M., Chambers, D., Blanc, E., & Lieberam, I. (2014, Feb). Reconstruction of phrenic neuron identity in embryonic stem cell-derived motor neurons. *Development, 141*(4), 784-794. https://doi.org/10.1242/dev.097188

Mackenzie, I. R., Bigio, E. H., Ince, P. G., Geser, F., Neumann, M., Cairns, N. J., Kwong, L. K., Forman, M. S., Ravits, J., Stewart, H., Eisen, A., McClusky, L., Kretzschmar, H. A., Monoranu, C. M., Highley, J. R., Kirby, J., Siddique, T., Shaw, P. J., Lee, V. M., & Trojanowski, J. Q. (2007, May). Pathological TDP-43 distinguishes sporadic amyotrophic lateral sclerosis from amyotrophic lateral sclerosis with SOD1 mutations. *Ann Neurol, 61*(5), 427-434. https://doi.org/10.1002/ana.21147

Mackenzie, I. R., Frick, P., & Neumann, M. (2014, Mar). The neuropathology associated with repeat expansions in the C9ORF72 gene. *Acta Neuropathol, 127*(3), 347-357. https://doi.org/10.1007/s00401-013-1232-4

Mackenzie, I. R., & Rademakers, R. (2008, Dec). The role of transactive response DNA-binding protein-43 in amyotrophic lateral sclerosis and frontotemporal dementia. *Curr Opin Neurol, 21*(6), 693-700. https://doi.org/10.1097/WCO.0b013e3283168d1d

Mackenzie, I. R., Rademakers, R., & Neumann, M. (2010, Oct). TDP-43 and FUS in amyotrophic lateral sclerosis and frontotemporal dementia. *Lancet Neurol, 9*(10), 995-1007. https://doi.org/10.1016/S1474-4422(10)70195-2

Magrane, J., Sahawneh, M. A., Przedborski, S., Estevez, A. G., & Manfredi, G. (2012, Jan 4). Mitochondrial dynamics and bioenergetic dysfunction is associated with synaptic alterations in mutant SOD1 motor neurons. *J Neurosci, 32*(1), 229-242. https://doi.org/10.1523/JNEUROSCI.1233-11.2012

Majounie, E., Renton, A. E., Mok, K., Dopper, E. G., Waite, A., Rollinson, S., Chio, A., Restagno, G., Nicolaou, N., Simon-Sanchez, J., van Swieten, J. C., Abramzon, Y., Johnson, J. O., Sendtner, M., Pamphlett, R., Orrell, R. W., Mead, S., Sidle, K. C., Houlden, H., Rohrer, J. D., Morrison, K. E., Pall, H., Talbot, K., Ansorge, O., Chromosome, A. L. S. F. T. D. C., French research network on, F. F. A., Consortium, I., Hernandez, D. G., Arepalli, S., Sabatelli, M., Mora, G., Corbo, M., Giannini, F., Calvo, A., Englund, E., Borghero, G., Floris, G. L., Remes, A. M., Laaksovirta, H., McCluskey, L., Trojanowski, J. Q., Van Deerlin, V. M., Schellenberg, G. D., Nalls, M. A., Drory, V. E., Lu, C. S., Yeh, T. H., Ishiura, H., Takahashi, Y., Tsuji, S., Le Ber, I., Brice, A., Drepper, C., Williams, N., Kirby, J., Shaw, P., Hardy, J., Tienari, P. J., Heutink, P., Morris, H. R., Pickering-Brown, S., & Traynor, B. J. (2012, Apr). Frequency of the C9orf72 hexanucleotide repeat expansion in patients with amyotrophic lateral sclerosis and frontotemporal dementia: a cross-sectional study. *Lancet Neurol, 11*(4), 323-330. https://doi.org/10.1016/S1474-4422(12)70043-1

Mandal, A., Wong, H. C., Pinter, K., Mosqueda, N., Beirl, A., Lomash, R. M., Won, S., Kindt, K. S., & Drerup, C. M. (2021, Feb 17). Retrograde Mitochondrial Transport Is Essential for Organelle Distribution and Health in Zebrafish Neurons. *J Neurosci, 41*(7), 1371-1392. https://doi.org/10.1523/JNEUROSCI.1316-20.2020

Manders, E. M. M., Verbeek, F. J., & Aten, J. A. (1993, Mar). Measurement of co-localization of objects in dual-colour confocal images. *J Microsc, 169*(3), 375-382. https://doi.org/10.1111/j.1365-2818.1993.tb03313.x

Mannen, T., Iwata, M., Toyokura, Y., & Nagashima, K. (1977, May). Preservation of a certain motoneurone group of the sacral cord in amyotrophic lateral sclerosis: its clinical significance. *J Neurol Neurosurg Psychiatry, 40*(5), 464-469. https://doi.org/10.1136/jnnp.40.5.464

Manzo, E., Lorenzini, I., Barrameda, D., O'Conner, A. G., Barrows, J. M., Starr, A., Kovalik, T., Rabichow, B. E., Lehmkuhl, E. M., Shreiner, D. D., Joardar, A., Lievens, J. C., Bowser, R., Sattler, R., & Zarnescu, D. C. (2019, Jun 10). Glycolysis upregulation is neuroprotective as a compensatory mechanism in ALS. *Elife, 8*. https://doi.org/10.7554/eLife.45114

Marcelo, A., Koppenol, R., de Almeida, L. P., Matos, C. A., & Nobrega, C. (2021, Jun 8). Stress granules, RNA-binding proteins and polyglutamine diseases: too much aggregation? *Cell Death Dis, 12*(6), 592. https://doi.org/10.1038/s41419-021-03873-8

Marchetto, M. C., Muotri, A. R., Mu, Y., Smith, A. M., Cezar, G. G., & Gage, F. H. (2008, Dec 4). Non-cell-autonomous effect of human SOD1 G37R astrocytes on motor neurons derived from human embryonic stem cells. *Cell Stem Cell, 3*(6), 649-657. https://doi.org/10.1016/j.stem.2008.10.001

Maury, Y., Come, J., Piskorowski, R. A., Salah-Mohellibi, N., Chevaleyre, V., Peschanski, M., Martinat, C., & Nedelec, S. (2015, Jan). Combinatorial analysis of developmental cues efficiently converts human pluripotent stem cells into multiple neuronal subtypes. *Nat Biotechnol, 33*(1), 89-96. https://doi.org/10.1038/nbt.3049

McDermott, C. J., & Shaw, P. J. (2008, Mar 22). Diagnosis and management of motor neurone disease. *BMJ, 336*(7645), 658-662. https://doi.org/10.1136/bmj.39493.511759.BE

McDonald, K. K., Aulas, A., Destroismaisons, L., Pickles, S., Beleac, E., Camu, W., Rouleau, G. A., & Vande Velde, C. (2011, Apr 1). TAR DNA-binding protein 43 (TDP-43) regulates stress granule dynamics via differential regulation of G3BP and TIA-1. *Hum Mol Genet, 20*(7), 1400-1410. https://doi.org/10.1093/hmg/ddr021

McGeer, P. L., & McGeer, E. G. (2002, Oct). Inflammatory processes in amyotrophic lateral sclerosis. *Muscle Nerve, 26*(4), 459-470. https://doi.org/10.1002/mus.10191

Mehta, P., Kaye, W., Raymond, J., Punjani, R., Larson, T., Cohen, J., Muravov, O., & Horton, K. (2018, Nov 23). Prevalence of Amyotrophic Lateral Sclerosis - United States, 2015. *MMWR Morb Mortal Wkly Rep, 67*(46), 1285-1289. https://doi.org/10.15585/mmwr.mm6746a1

Melamed, Z., Lopez-Erauskin, J., Baughn, M. W., Zhang, O., Drenner, K., Sun, Y., Freyermuth, F., McMahon, M. A., Beccari, M. S., Artates, J. W., Ohkubo, T., Rodriguez, M., Lin, N., Wu, D., Bennett, C. F., Rigo, F., Da Cruz, S., Ravits, J., Lagier-Tourenne, C., & Cleveland, D. W. (2019, Feb). Premature polyadenylation-mediated loss of stathmin-2 is a hallmark of TDP-43-dependent neurodegeneration. *Nat Neurosci, 22*(2), 180-190. https://doi.org/10.1038/s41593-018-0293-z

Meng, H., Yamashita, C., Shiba-Fukushima, K., Inoshita, T., Funayama, M., Sato, S., Hatta, T., Natsume, T., Umitsu, M., Takagi, J., Imai, Y., & Hattori, N. (2017, Jun 7). Loss of Parkinson's disease-associated protein CHCHD2 affects mitochondrial crista structure and destabilizes cytochrome c. *Nat Commun, 8*, 15500. https://doi.org/10.1038/ncomms15500

Messori, A., Trippoli, S., Becagli, P., & Zaccara, G. (1999, Aug). Cost effectiveness of riluzole in amyotrophic lateral sclerosis. Italian Cooperative Group for the Study of Meta-Analysis and the Osservatorio SIFO sui Farmaci. *Pharmacoeconomics, 16*(2), 153-163. https://doi.org/10.2165/00019053-199916020-00004

Meyerowitz, J., Parker, S. J., Vella, L. J., Ng, D., Price, K. A., Liddell, J. R., Caragounis, A., Li, Q. X., Masters, C. L., Nonaka, T., Hasegawa, M., Bogoyevitch, M. A., Kanninen, K. M., Crouch, P. J., & White, A. R. (2011, Aug 8). C-Jun N-terminal kinase controls TDP-43 accumulation in stress granules induced by oxidative stress. *Mol Neurodegener, 6*, 57. https://doi.org/10.1186/1750-1326-6-57

Miller, R. G., Mitchell, J. D., & Moore, D. H. (2012, Mar 14). Riluzole for amyotrophic lateral sclerosis (ALS)/motor neuron disease (MND). *Cochrane Database Syst Rev*(3), CD001447. https://doi.org/10.1002/14651858.CD001447.pub3

Misawa, H., Nakata, K., Toda, K., Matsuura, J., Oda, Y., Inoue, H., Tateno, M., & Takahashi, R. (2003, Sep). VAChT-Cre. Fast and VAChT-Cre.Slow: postnatal expression of Cre recombinase in somatomotor neurons with different onset. *Genesis, 37*(1), 44-50. https://doi.org/10.1002/gene.10224

Mitchell, J. D., & Borasio, G. D. (2007, Jun 16). Amyotrophic lateral sclerosis. *Lancet, 369*(9578), 2031-2041. https://doi.org/10.1016/S0140-6736(07)60944-1

Mitsuyama, Y., & Takamiya, S. (1979, Sep). Presenile dementia with motor neuron disease in Japan. A new entity? *Arch Neurol, 36*(9), 592-593. https://doi.org/10.1001/archneur.1979.00500450086021

Molliex, A., Temirov, J., Lee, J., Coughlin, M., Kanagaraj, A. P., Kim, H. J., Mittag, T., & Taylor, J. P. (2015, Sep 24). Phase separation by low complexity domains promotes stress granule assembly and drives pathological fibrillization. *Cell, 163*(1), 123-133. https://doi.org/10.1016/j.cell.2015.09.015

Munch, C., Rosenbohm, A., Sperfeld, A. D., Uttner, I., Reske, S., Krause, B. J., Sedlmeier, R., Meyer, T., Hanemann, C. O., Stumm, G., & Ludolph, A. C. (2005, Nov). Heterozygous R1101K mutation of the DCTN1 gene in a family with ALS and FTD. *Ann Neurol, 58*(5), 777-780. https://doi.org/10.1002/ana.20631

Munch, C., Sedlmeier, R., Meyer, T., Homberg, V., Sperfeld, A. D., Kurt, A., Prudlo, J., Peraus, G., Hanemann, C. O., Stumm, G., & Ludolph, A. C. (2004, Aug 24). Point mutations of the p150 subunit of dynactin (DCTN1) gene in ALS. *Neurology, 63*(4), 724-726. https://doi.org/10.1212/01.wnl.0000134608.83927.b1

Murphy, J. M., Henry, R. G., Langmore, S., Kramer, J. H., Miller, B. L., & Lomen-Hoerth, C. (2007, Apr). Continuum of frontal lobe impairment in amyotrophic lateral sclerosis. *Arch Neurol, 64*(4), 530-534. https://doi.org/10.1001/archneur.64.4.530

Mutihac, R., Alegre-Abarrategui, J., Gordon, D., Farrimond, L., Yamasaki-Mann, M., Talbot, K., & Wade-Martins, R. (2015, Mar). TARDBP pathogenic mutations increase cytoplasmic translocation of TDP-43 and cause reduction of endoplasmic reticulum Ca(2)(+) signaling in motor neurons. *Neurobiol Dis, 75*, 64-77. https://doi.org/10.1016/j.nbd.2014.12.010

Nagano, S., Jinno, J., Abdelhamid, R. F., Jin, Y., Shibata, M., Watanabe, S., Hirokawa, S., Nishizawa, M., Sakimura, K., Onodera, O., Okada, H., Okada, T., Saito, Y., Takahashi-Fujigasaki, J., Murayama, S., Wakatsuki, S., Mochizuki, H., & Araki, T.

(2020, Nov). TDP-43 transports ribosomal protein mRNA to regulate axonal local translation in neuronal axons. *Acta Neuropathol, 140*(5), 695-713. https://doi.org/10.1007/s00401-020-02205-y

Nakano, T., Windrem, M., Zappavigna, V., & Goldman, S. A. (2005, Jul 15). Identification of a conserved 125 base-pair Hb9 enhancer that specifies gene expression to spinal motor neurons. *Dev Biol, 283*(2), 474-485. https://doi.org/10.1016/j.ydbio.2005.04.017

Nelson, L. M., McGuire, V., Longstreth, W. T., Jr., & Matkin, C. (2000, Jan 15). Population-based case-control study of amyotrophic lateral sclerosis in western Washington State. I. Cigarette smoking and alcohol consumption. *Am J Epidemiol, 151*(2), 156-163. https://doi.org/10.1093/oxfordjournals.aje.a010183

Nelson, L. M., Topol, B., Kaye, W., Williamson, D., Horton, D. K., Mehta, P., & Wagner, T. (2018). Estimation of the Prevalence of Amyotrophic Lateral Sclerosis in the United States Using National Administrative Healthcare Data from 2002 to 2004 and Capture-Recapture Methodology. *Neuroepidemiology, 51*(3-4), 149-157. https://doi.org/10.1159/000488798

Neumann, M., Kwong, L. K., Lee, E. B., Kremmer, E., Flatley, A., Xu, Y., Forman, M. S., Troost, D., Kretzschmar, H. A., Trojanowski, J. Q., & Lee, V. M. (2009, Feb). Phosphorylation of S409/410 of TDP-43 is a consistent feature in all sporadic and familial forms of TDP-43 proteinopathies. *Acta Neuropathol, 117*(2), 137-149. https://doi.org/10.1007/s00401-008-0477-9

Neumann, M., Sampathu, D. M., Kwong, L. K., Truax, A. C., Micsenyi, M. C., Chou, T. T., Bruce, J., Schuck, T., Grossman, M., Clark, C. M., McCluskey, L. F., Miller, B. L., Masliah, E., Mackenzie, I. R., Feldman, H., Feiden, W., Kretzschmar, H. A., Trojanowski, J. Q., & Lee, V. M. (2006, Oct 6). Ubiquitinated TDP-43 in frontotemporal lobar degeneration and amyotrophic lateral sclerosis. *Science, 314*(5796), 130-133. https://doi.org/10.1126/science.1134108

Nicolas, A., Kenna, K. P., Renton, A. E., Ticozzi, N., Faghri, F., Chia, R., Dominov, J. A., Kenna, B. J., Nalls, M. A., Keagle, P., Rivera, A. M., van Rheenen, W., Murphy, N. A., van Vugt, J., Geiger, J. T., Van der Spek, R. A., Pliner, H. A., Shankaracharya, Smith, B. N., Marangi, G., Topp, S. D., Abramzon, Y., Gkazi, A. S., Eicher, J. D., Kenna, A., Consortium, I., Mora, G., Calvo, A., Mazzini, L., Riva, N., Mandrioli, J., Caponnetto, C., Battistini, S., Volanti, P., La Bella, V., Conforti, F. L., Borghero, G., Messina, S., Simone, I. L., Trojsi, F., Salvi, F., Logullo, F. O., D'Alfonso, S., Corrado, L., Capasso, M., Ferrucci, L., Genomic Translation for, A. L. S. C. C., Moreno, C. A. M., Kamalakaran, S., Goldstein, D. B., Consortium, A. L. S. S., Gitler, A. D., Harris, T., Myers, R. M., Consortium, N. A., Phatnani, H., Musunuri, R. L., Evani, U. S., Abhyankar, A., Zody, M. C., Answer, A. L. S. F., Kaye, J., Finkbeiner, S., Wyman, S. K., LeNail, A., Lima, L., Fraenkel, E., Svendsen, C. N., Thompson, L. M., Van Eyk, J. E., Berry, J. D., Miller, T. M., Kolb, S. J., Cudkowicz, M., Baxi, E., Clinical Research in, A. L. S., Related Disorders for Therapeutic Development, C., Benatar, M., Taylor, J. P., Rampersaud, E., Wu, G., Wuu, J., Consortium, S., Lauria, G., Verde, F., Fogh, I., Tiloca, C., Comi, G. P., Soraru, G., Cereda, C., French, A. L. S. C., Corcia, P., Laaksovirta, H., Myllykangas, L., Jansson, L., Valori, M., Ealing, J.,

Hamdalla, H., Rollinson, S., Pickering-Brown, S., Orrell, R. W., Sidle, K. C., Malaspina, A., Hardy, J., Singleton, A. B., Johnson, J. O., Arepalli, S., Sapp, P. C., McKenna-Yasek, D., Polak, M., Asress, S., Al-Sarraj, S., King, A., Troakes, C., Vance, C., de Belleroche, J., Baas, F., Ten Asbroek, A., Munoz-Blanco, J. L., Hernandez, D. G., Ding, J., Gibbs, J. R., Scholz, S. W., Floeter, M. K., Campbell, R. H., Landi, F., Bowser, R., Pulst, S. M., Ravits, J. M., MacGowan, D. J. L., Kirby, J., Pioro, E. P., Pamphlett, R., Broach, J., Gerhard, G., Dunckley, T. L., Brady, C. B., Kowall, N. W., Troncoso, J. C., Le Ber, I., Mouzat, K., Lumbroso, S., Heiman-Patterson, T. D., Kamel, F., Van Den Bosch, L., Baloh, R. H., Strom, T. M., Meitinger, T., Shatunov, A., Van Eijk, K. R., de Carvalho, M., Kooyman, M., Middelkoop, B., Moisse, M., McLaughlin, R. L., Van Es, M. A., Weber, M., Boylan, K. B., Van Blitterswijk, M., Rademakers, R., Morrison, K. E., Basak, A. N., Mora, J. S., Drory, V. E., Shaw, P. J., Turner, M. R., Talbot, K., Hardiman, O., Williams, K. L., Fifita, J. A., Nicholson, G. A., Blair, I. P., Rouleau, G. A., Esteban-Perez, J., Garcia-Redondo, A., Al-Chalabi, A., Project Min, E. A. L. S. S. C., Rogaeva, E., Zinman, L., Ostrow, L. W., Maragakis, N. J., Rothstein, J. D., Simmons, Z., Cooper-Knock, J., Brice, A., Goutman, S. A., Feldman, E. L., Gibson, S. B., Taroni, F., Ratti, A., Gellera, C., Van Damme, P., Robberecht, W., Fratta, P., Sabatelli, M., Lunetta, C., Ludolph, A. C., Andersen, P. M., Weishaupt, J. H., Camu, W., Trojanowski, J. Q., Van Deerlin, V. M., Brown, R. H., Jr., van den Berg, L. H., Veldink, J. H., Harms, M. B., Glass, J. D., Stone, D. J., Tienari, P., Silani, V., Chio, A., Shaw, C. E., Traynor, B. J., & Landers, J. E. (2018, Mar 21). Genome-wide Analyses Identify KIF5A as a Novel ALS Gene. *Neuron, 97*(6), 1268-1283 e1266. https://doi.org/10.1016/j.neuron.2018.02.027

Nihei, K., McKee, A. C., & Kowall, N. W. (1993). Patterns of neuronal degeneration in the motor cortex of amyotrophic lateral sclerosis patients. *Acta Neuropathol, 86*(1), 55-64. https://doi.org/10.1007/BF00454899

Nimchinsky, E. A., Young, W. G., Yeung, G., Shah, R. A., Gordon, J. W., Bloom, F. E., Morrison, J. H., & Hof, P. R. (2000, Jan 3). Differential vulnerability of oculomotor, facial, and hypoglossal nuclei in G86R superoxide dismutase transgenic mice. *J Comp Neurol, 416*(1), 112-125. https://doi.org/10.1002/(sici)1096-9861(20000103)416:1<112::aid-cne9>3.0.co;2-k

Nishimura, A. L., Zupunski, V., Troakes, C., Kathe, C., Fratta, P., Howell, M., Gallo, J. M., Hortobagyi, T., Shaw, C. E., & Rogelj, B. (2010, Jun). Nuclear import impairment causes cytoplasmic trans-activation response DNA-binding protein accumulation and is associated with frontotemporal lobar degeneration. *Brain, 133*(Pt 6), 1763-1771. https://doi.org/10.1093/brain/awq111

Nonaka, T., Suzuki, G., Tanaka, Y., Kametani, F., Hirai, S., Okado, H., Miyashita, T., Saitoe, M., Akiyama, H., Masai, H., & Hasegawa, M. (2016, Mar 11). Phosphorylation of TAR DNA-binding Protein of 43 kDa (TDP-43) by Truncated Casein Kinase 1delta Triggers Mislocalization and Accumulation of TDP-43. *J Biol Chem, 291*(11), 5473-5483. https://doi.org/10.1074/jbc.M115.695379

Okada, M., Yamashita, S., Ueyama, H., Ishizaki, M., Maeda, Y., & Ando, Y. (2018, Jun). Long-term effects of edaravone on survival of patients with amyotrophic lateral sclerosis. *eNeurologicalSci, 11*, 11-14. https://doi.org/10.1016/j.ensci.2018.05.001

Okamoto, K., Hirai, S., Yamazaki, T., Sun, X. Y., & Nakazato, Y. (1991, Aug 19). New ubiquitin-positive intraneuronal inclusions in the extra-motor cortices in patients with amyotrophic lateral sclerosis. *Neurosci Lett, 129*(2), 233-236. https://doi.org/10.1016/0304-3940(91)90469-a

Okamoto, K., Murakami, N., Kusaka, H., Yoshida, M., Hashizume, Y., Nakazato, Y., Matsubara, E., & Hirai, S. (1992, Oct). Ubiquitin-positive intraneuronal inclusions in the extramotor cortices of presenile dementia patients with motor neuron disease. *J Neurol, 239*(8), 426-430. https://doi.org/10.1007/BF00856806

Onesto, E., Colombrita, C., Gumina, V., Borghi, M. O., Dusi, S., Doretti, A., Fagiolari, G., Invernizzi, F., Moggio, M., Tiranti, V., Silani, V., & Ratti, A. (2016, May 5). Gene-specific mitochondria dysfunctions in human TARDBP and C9ORF72 fibroblasts. *Acta Neuropathol Commun, 4*(1), 47. https://doi.org/10.1186/s40478-016-0316-5

Ou, S. H., Wu, F., Harrich, D., Garcia-Martinez, L. F., & Gaynor, R. B. (1995, Jun). Cloning and characterization of a novel cellular protein, TDP-43, that binds to human immunodeficiency virus type 1 TAR DNA sequence motifs. *J Virol, 69*(6), 3584-3596. https://doi.org/10.1128/JVI.69.6.3584-3596.1995

Palese, F., Sartori, A., Verriello, L., Ros, S., Passadore, P., Manganotti, P., Barbone, F., & Pisa, F. E. (2019, Feb). Epidemiology of amyotrophic lateral sclerosis in Friuli-Venezia Giulia, North-Eastern Italy, 2002-2014: a retrospective population-based study. *Amyotroph Lateral Scler Frontotemporal Degener, 20*(1-2), 90-99. https://doi.org/10.1080/21678421.2018.1511732

Pantelidou, M., Zographos, S. E., Lederer, C. W., Kyriakides, T., Pfaffl, M. W., & Santama, N. (2007, Jun). Differential expression of molecular motors in the motor cortex of sporadic ALS. *Neurobiol Dis, 26*(3), 577-589. https://doi.org/10.1016/j.nbd.2007.02.005

Pensato, V., Tiloca, C., Corrado, L., Bertolin, C., Sardone, V., Del Bo, R., Calini, D., Mandrioli, J., Lauria, G., Mazzini, L., Querin, G., Ceroni, M., Cantello, R., Corti, S., Castellotti, B., Solda, G., Duga, S., Comi, G. P., Cereda, C., Soraru, G., D'Alfonso, S., Taroni, F., Shaw, C. E., Landers, J. E., Ticozzi, N., Ratti, A., Gellera, C., Silani, V., & Consortium, S. (2015, May). TUBA4A gene analysis in sporadic amyotrophic lateral sclerosis: identification of novel mutations. *J Neurol, 262*(5), 1376-1378. https://doi.org/10.1007/s00415-015-7739-y

Perlson, E., Maday, S., Fu, M. M., Moughamian, A. J., & Holzbaur, E. L. (2010, Jul). Retrograde axonal transport: pathways to cell death? *Trends Neurosci, 33*(7), 335-344. https://doi.org/10.1016/j.tins.2010.03.006

Petrov, D., Mansfield, C., Moussy, A., & Hermine, O. (2017). ALS Clinical Trials Review: 20 Years of Failure. Are We Any Closer to Registering a New Treatment? *Front Aging Neurosci, 9*, 68. https://doi.org/10.3389/fnagi.2017.00068

Pinarbasi, E. S., Cagatay, T., Fung, H. Y. J., Li, Y. C., Chook, Y. M., & Thomas, P. J. (2018, May 4). Active nuclear import and passive nuclear export are the primary

determinants of TDP-43 localization. *Sci Rep, 8*(1), 7083. https://doi.org/10.1038/s41598-018-25008-4

Polymenidou, M., Lagier-Tourenne, C., Hutt, K. R., Bennett, C. F., Cleveland, D. W., & Yeo, G. W. (2012, Jun 26). Misregulated RNA processing in amyotrophic lateral sclerosis. *Brain Res, 1462*, 3-15. https://doi.org/10.1016/j.brainres.2012.02.059

Polymenidou, M., Lagier-Tourenne, C., Hutt, K. R., Huelga, S. C., Moran, J., Liang, T. Y., Ling, S. C., Sun, E., Wancewicz, E., Mazur, C., Kordasiewicz, H., Sedaghat, Y., Donohue, J. P., Shiue, L., Bennett, C. F., Yeo, G. W., & Cleveland, D. W. (2011, Apr). Long pre-mRNA depletion and RNA missplicing contribute to neuronal vulnerability from loss of TDP-43. *Nat Neurosci, 14*(4), 459-468. https://doi.org/10.1038/nn.2779

Prasad, A., Bharathi, V., Sivalingam, V., Girdhar, A., & Patel, B. K. (2019). Molecular Mechanisms of TDP-43 Misfolding and Pathology in Amyotrophic Lateral Sclerosis. *Front Mol Neurosci, 12*, 25. https://doi.org/10.3389/fnmol.2019.00025

Pryor, W. A., & Squadrito, G. L. (1995, May). The chemistry of peroxynitrite: a product from the reaction of nitric oxide with superoxide. *Am J Physiol, 268*(5 Pt 1), L699-722. https://doi.org/10.1152/ajplung.1995.268.5.L699

Puls, I., Jonnakuty, C., LaMonte, B. H., Holzbaur, E. L., Tokito, M., Mann, E., Floeter, M. K., Bidus, K., Drayna, D., Oh, S. J., Brown, R. H., Jr., Ludlow, C. L., & Fischbeck, K. H. (2003, Apr). Mutant dynactin in motor neuron disease. *Nat Genet, 33*(4), 455-456. https://doi.org/10.1038/ng1123

Pupillo, E., Poloni, M., Bianchi, E., Giussani, G., Logroscino, G., Zoccolella, S., Chio, A., Calvo, A., Corbo, M., Lunetta, C., Marin, B., Mitchell, D., Hardiman, O., Rooney, J., Stevic, Z., Bandettini di Poggio, M., Filosto, M., Cotelli, M. S., Perini, M., Riva, N., Tremolizzo, L., Vitelli, E., Damiani, D., Beghi, E., & Consortiumdagger, E. (2018, Feb). Trauma and amyotrophic lateral sclerosis: a european population-based case-control study from the EURALS consortium. *Amyotroph Lateral Scler Frontotemporal Degener, 19*(1-2), 118-125. https://doi.org/10.1080/21678421.2017.1386687

Pushpakom, S., Iorio, F., Eyers, P. A., Escott, K. J., Hopper, S., Wells, A., Doig, A., Guilliams, T., Latimer, J., McNamee, C., Norris, A., Sanseau, P., Cavalla, D., & Pirmohamed, M. (2019, Jan). Drug repurposing: progress, challenges and recommendations. *Nat Rev Drug Discov, 18*(1), 41-58. https://doi.org/10.1038/nrd.2018.168

Raman, R., Allen, S. P., Goodall, E. F., Kramer, S., Ponger, L. L., Heath, P. R., Milo, M., Hollinger, H. C., Walsh, T., Highley, J. R., Olpin, S., McDermott, C. J., Shaw, P. J., & Kirby, J. (2015, Feb). Gene expression signatures in motor neurone disease fibroblasts reveal dysregulation of metabolism, hypoxia-response and RNA processing functions. *Neuropathol Appl Neurobiol, 41*(2), 201-226. https://doi.org/10.1111/nan.12147

Ratti, A., & Buratti, E. (2016, Aug). Physiological functions and pathobiology of TDP-43 and FUS/TLS proteins. *J Neurochem, 138 Suppl 1*, 95-111. https://doi.org/10.1111/jnc.13625

Reiner, A., Medina, L., Figueredo-Cardenas, G., & Anfinson, S. (1995, Feb). Brainstem motoneuron pools that are selectively resistant in amyotrophic lateral sclerosis are preferentially enriched in parvalbumin: evidence from monkey brainstem for a calcium-mediated mechanism in sporadic ALS. *Exp Neurol, 131*(2), 239-250. https://doi.org/10.1016/0014-4886(95)90046-2

Renton, A. E., Chio, A., & Traynor, B. J. (2014, Jan). State of play in amyotrophic lateral sclerosis genetics. *Nat Neurosci, 17*(1), 17-23. https://doi.org/10.1038/nn.3584

Renton, A. E., Majounie, E., Waite, A., Simon-Sanchez, J., Rollinson, S., Gibbs, J. R., Schymick, J. C., Laaksovirta, H., van Swieten, J. C., Myllykangas, L., Kalimo, H., Paetau, A., Abramzon, Y., Remes, A. M., Kaganovich, A., Scholz, S. W., Duckworth, J., Ding, J., Harmer, D. W., Hernandez, D. G., Johnson, J. O., Mok, K., Ryten, M., Trabzuni, D., Guerreiro, R. J., Orrell, R. W., Neal, J., Murray, A., Pearson, J., Jansen, I. E., Sondervan, D., Seelaar, H., Blake, D., Young, K., Halliwell, N., Callister, J. B., Toulson, G., Richardson, A., Gerhard, A., Snowden, J., Mann, D., Neary, D., Nalls, M. A., Peuralinna, T., Jansson, L., Isoviita, V. M., Kaivorinne, A. L., Holtta-Vuori, M., Ikonen, E., Sulkava, R., Benatar, M., Wuu, J., Chio, A., Restagno, G., Borghero, G., Sabatelli, M., Consortium, I., Heckerman, D., Rogaeva, E., Zinman, L., Rothstein, J. D., Sendtner, M., Drepper, C., Eichler, E. E., Alkan, C., Abdullaev, Z., Pack, S. D., Dutra, A., Pak, E., Hardy, J., Singleton, A., Williams, N. M., Heutink, P., Pickering-Brown, S., Morris, H. R., Tienari, P. J., & Traynor, B. J. (2011, Oct 20). A hexanucleotide repeat expansion in C9ORF72 is the cause of chromosome 9p21-linked ALS-FTD. *Neuron, 72*(2), 257-268. https://doi.org/10.1016/j.neuron.2011.09.010

Riviere, M., Meininger, V., Zeisser, P., & Munsat, T. (1998, Apr). An analysis of extended survival in patients with amyotrophic lateral sclerosis treated with riluzole. *Arch Neurol, 55*(4), 526-528. https://doi.org/10.1001/archneur.55.4.526

Roccatagliata, L., Bonzano, L., Mancardi, G., Canepa, C., & Caponnetto, C. (2009, Feb). Detection of motor cortex thinning and corticospinal tract involvement by quantitative MRI in amyotrophic lateral sclerosis. *Amyotroph Lateral Scler, 10*(1), 47-52. https://doi.org/10.1080/17482960802267530

Rolfe, D. F., & Brown, G. C. (1997, Jul). Cellular energy utilization and molecular origin of standard metabolic rate in mammals. *Physiol Rev, 77*(3), 731-758. https://doi.org/10.1152/physrev.1997.77.3.731

Romano, N., Catalani, A., Lattante, S., Belardo, A., Proietti, S., Bertini, L., Silvestri, F., Catalani, E., Cervia, D., Zolla, L., Sabatelli, M., Welshhans, K., & Ceci, M. (2020, Jun). ALS skin fibroblasts reveal oxidative stress and ERK1/2-mediated cytoplasmic localization of TDP-43. *Cell Signal, 70*, 109591. https://doi.org/10.1016/j.cellsig.2020.109591

Rose, L., McKim, D., Leasa, D., Nonoyama, M., Tandon, A., Bai, Y. Q., Amin, R., Katz, S., Goldstein, R., & Gershon, A. (2019). Trends in incidence, prevalence, and mortality of neuromuscular disease in Ontario, Canada: A population-based retrospective cohort study (2003-2014). *PLoS One, 14*(3), e0210574. https://doi.org/10.1371/journal.pone.0210574

Rosen, D. R., Siddique, T., Patterson, D., Figlewicz, D. A., Sapp, P., Hentati, A., Donaldson, D., Goto, J., O'Regan, J. P., Deng, H. X., & et al. (1993, Mar 4). Mutations in Cu/Zn superoxide dismutase gene are associated with familial amyotrophic lateral sclerosis. *Nature, 362*(6415), 59-62. https://doi.org/10.1038/362059a0

Rouleau, G. A., Clark, A. W., Rooke, K., Pramatarova, A., Krizus, A., Suchowersky, O., Julien, J. P., & Figlewicz, D. (1996, Jan). SOD1 mutation is associated with accumulation of neurofilaments in amyotrophic lateral sclerosis. *Ann Neurol, 39*(1), 128-131. https://doi.org/10.1002/ana.410390119

Rutherford, N. J., Zhang, Y. J., Baker, M., Gass, J. M., Finch, N. A., Xu, Y. F., Stewart, H., Kelley, B. J., Kuntz, K., Crook, R. J., Sreedharan, J., Vance, C., Sorenson, E., Lippa, C., Bigio, E. H., Geschwind, D. H., Knopman, D. S., Mitsumoto, H., Petersen, R. C., Cashman, N. R., Hutton, M., Shaw, C. E., Boylan, K. B., Boeve, B., Graff-Radford, N. R., Wszolek, Z. K., Caselli, R. J., Dickson, D. W., Mackenzie, I. R., Petrucelli, L., & Rademakers, R. (2008, Sep 19). Novel mutations in TARDBP (TDP-43) in patients with familial amyotrophic lateral sclerosis. *PLoS Genet, 4*(9), e1000193. https://doi.org/10.1371/journal.pgen.1000193

Ryberg, H., Askmark, H., & Persson, L. I. (2003, Jul). A double-blind randomized clinical trial in amyotrophic lateral sclerosis using lamotrigine: effects on CSF glutamate, aspartate, branched-chain amino acid levels and clinical parameters. *Acta Neurol Scand, 108*(1), 1-8. https://doi.org/10.1034/j.1600-0404.2003.00111.x

Sasaguri, H., Chew, J., Xu, Y. F., Gendron, T. F., Garrett, A., Lee, C. W., Jansen-West, K., Bauer, P. O., Perkerson, E. A., Tong, J., Stetler, C., & Zhang, Y. J. (2016, Sep 15). The extreme N-terminus of TDP-43 mediates the cytoplasmic aggregation of TDP-43 and associated toxicity in vivo. *Brain Res, 1647*, 57-64. https://doi.org/10.1016/j.brainres.2016.04.069

Sasaki, S., & Iwata, M. (1996a). Dendritic synapses of anterior horn neurons in amyotrophic lateral sclerosis: an ultrastructural study. *Acta Neuropathol, 91*(3), 278-283. https://doi.org/10.1007/s004010050426

Sasaki, S., & Iwata, M. (1996b, Aug). Impairment of fast axonal transport in the proximal axons of anterior horn neurons in amyotrophic lateral sclerosis. *Neurology, 47*(2), 535-540. https://doi.org/10.1212/wnl.47.2.535

Scarmeas, N., Shih, T., Stern, Y., Ottman, R., & Rowland, L. P. (2002, Sep 10). Premorbid weight, body mass, and varsity athletics in ALS. *Neurology, 59*(5), 773-775. https://doi.org/10.1212/wnl.59.5.773

Seminary, E. R., Sison, S. L., & Ebert, A. D. (2018). Modeling Protein Aggregation and the Heat Shock Response in ALS iPSC-Derived Motor Neurons. *Front Neurosci, 12*, 86. https://doi.org/10.3389/fnins.2018.00086

Sephton, C. F., Cenik, C., Kucukural, A., Dammer, E. B., Cenik, B., Han, Y., Dewey, C. M., Roth, F. P., Herz, J., Peng, J., Moore, M. J., & Yu, G. (2011, Jan 14). Identification of neuronal RNA targets of TDP-43-containing ribonucleoprotein complexes. *J Biol Chem, 286*(2), 1204-1215. https://doi.org/10.1074/jbc.M110.190884

Sephton, C. F., Good, S. K., Atkin, S., Dewey, C. M., Mayer, P., 3rd, Herz, J., & Yu, G. (2010, Feb 26). TDP-43 is a developmentally regulated protein essential for early embryonic development. *J Biol Chem, 285*(9), 6826-6834. https://doi.org/10.1074/jbc.M109.061846

Shan, X., Chiang, P. M., Price, D. L., & Wong, P. C. (2010, Sep 14). Altered distributions of Gemini of coiled bodies and mitochondria in motor neurons of TDP-43 transgenic mice. *Proc Natl Acad Sci U S A, 107*(37), 16325-16330. https://doi.org/10.1073/pnas.1003459107

Shaw, P. J., Ince, P. G., Falkous, G., & Mantle, D. (1995, Oct). Oxidative damage to protein in sporadic motor neuron disease spinal cord. *Ann Neurol, 38*(4), 691-695. https://doi.org/10.1002/ana.410380424

Shefner, J., Heiman-Patterson, T., Pioro, E. P., Wiedau-Pazos, M., Liu, S., Zhang, J., Agnese, W., & Apple, S. (2020, Feb). Long-term edaravone efficacy in amyotrophic lateral sclerosis: Post-hoc analyses of Study 19 (MCI186-19). *Muscle Nerve, 61*(2), 218-221. https://doi.org/10.1002/mus.26740

Simpson, E. P., Henry, Y. K., Henkel, J. S., Smith, R. G., & Appel, S. H. (2004, May 25). Increased lipid peroxidation in sera of ALS patients: a potential biomarker of disease burden. *Neurology, 62*(10), 1758-1765. https://doi.org/10.1212/wnl.62.10.1758

Singh, T., Jiao, Y., Ferrando, L. M., Yablonska, S., Li, F., Horoszko, E. C., Lacomis, D., Friedlander, R. M., & Carlisle, D. L. (2021, Sep 23). Neuronal mitochondrial dysfunction in sporadic amyotrophic lateral sclerosis is developmentally regulated. *Sci Rep, 11*(1), 18916. https://doi.org/10.1038/s41598-021-97928-7

Sleigh, J. N., Rossor, A. M., Fellows, A. D., Tosolini, A. P., & Schiavo, G. (2019, Dec). Axonal transport and neurological disease. *Nat Rev Neurol, 15*(12), 691-703. https://doi.org/10.1038/s41582-019-0257-2

Sleigh, J. N., Tosolini, A. P., Gordon, D., Devoy, A., Fratta, P., Fisher, E. M. C., Talbot, K., & Schiavo, G. (2020, Mar 17). Mice Carrying ALS Mutant TDP-43, but Not Mutant FUS, Display In Vivo Defects in Axonal Transport of Signaling Endosomes. *Cell Rep, 30*(11), 3655-3662 e3652. https://doi.org/10.1016/j.celrep.2020.02.078

Smith, B. N., Ticozzi, N., Fallini, C., Gkazi, A. S., Topp, S., Kenna, K. P., Scotter, E. L., Kost, J., Keagle, P., Miller, J. W., Calini, D., Vance, C., Danielson, E. W., Troakes, C., Tiloca, C., Al-Sarraj, S., Lewis, E. A., King, A., Colombrita, C., Pensato, V., Castellotti, B., de Belleroche, J., Baas, F., ten Asbroek, A. L., Sapp, P. C., McKenna-

Yasek, D., McLaughlin, R. L., Polak, M., Asress, S., Esteban-Perez, J., Munoz-Blanco, J. L., Simpson, M., Consortium, S., van Rheenen, W., Diekstra, F. P., Lauria, G., Duga, S., Corti, S., Cereda, C., Corrado, L., Soraru, G., Morrison, K. E., Williams, K. L., Nicholson, G. A., Blair, I. P., Dion, P. A., Leblond, C. S., Rouleau, G. A., Hardiman, O., Veldink, J. H., van den Berg, L. H., Al-Chalabi, A., Pall, H., Shaw, P. J., Turner, M. R., Talbot, K., Taroni, F., Garcia-Redondo, A., Wu, Z., Glass, J. D., Gellera, C., Ratti, A., Brown, R. H., Jr., Silani, V., Shaw, C. E., & Landers, J. E. (2014, Oct 22). Exome-wide rare variant analysis identifies TUBA4A mutations associated with familial ALS. *Neuron, 84*(2), 324-331. https://doi.org/10.1016/j.neuron.2014.09.027

Smith, H. L., Bourne, J. N., Cao, G., Chirillo, M. A., Ostroff, L. E., Watson, D. J., & Harris, K. M. (2016, Dec 19). Mitochondrial support of persistent presynaptic vesicle mobilization with age-dependent synaptic growth after LTP. *Elife, 5*. https://doi.org/10.7554/eLife.15275

Smith, R. G., Henry, Y. K., Mattson, M. P., & Appel, S. H. (1998, Oct). Presence of 4-hydroxynonenal in cerebrospinal fluid of patients with sporadic amyotrophic lateral sclerosis. *Ann Neurol, 44*(4), 696-699. https://doi.org/10.1002/ana.410440419

Spencer, P. S., Nunn, P. B., Hugon, J., Ludolph, A. C., Ross, S. M., Roy, D. N., & Robertson, R. C. (1987, Jul 31). Guam amyotrophic lateral sclerosis-parkinsonism-dementia linked to a plant excitant neurotoxin. *Science, 237*(4814), 517-522. https://doi.org/10.1126/science.3603037

Sreedharan, J., Blair, I. P., Tripathi, V. B., Hu, X., Vance, C., Rogelj, B., Ackerley, S., Durnall, J. C., Williams, K. L., Buratti, E., Baralle, F., de Belleroche, J., Mitchell, J. D., Leigh, P. N., Al-Chalabi, A., Miller, C. C., Nicholson, G., & Shaw, C. E. (2008, Mar 21). TDP-43 mutations in familial and sporadic amyotrophic lateral sclerosis. *Science, 319*(5870), 1668-1672. https://doi.org/10.1126/science.1154584

Stallings, N. R., Puttaparthi, K., Luther, C. M., Burns, D. K., & Elliott, J. L. (2010, Nov). Progressive motor weakness in transgenic mice expressing human TDP-43. *Neurobiol Dis, 40*(2), 404-414. https://doi.org/10.1016/j.nbd.2010.06.017

Sutedja, N. A., Veldink, J. H., Fischer, K., Kromhout, H., Heederik, D., Huisman, M. H., Wokke, J. H., & van den Berg, L. H. (2009, Oct-Dec). Exposure to chemicals and metals and risk of amyotrophic lateral sclerosis: a systematic review. *Amyotroph Lateral Scler, 10*(5-6), 302-309. https://doi.org/10.3109/17482960802455416

Suzuki, H., Lee, K., & Matsuoka, M. (2011, Apr 15). TDP-43-induced death is associated with altered regulation of BIM and Bcl-xL and attenuated by caspase-mediated TDP-43 cleavage. *J Biol Chem, 286*(15), 13171-13183. https://doi.org/10.1074/jbc.M110.197483

Swarup, V., Phaneuf, D., Bareil, C., Robertson, J., Rouleau, G. A., Kriz, J., & Julien, J. P. (2011, Sep). Pathological hallmarks of amyotrophic lateral sclerosis/frontotemporal lobar degeneration in transgenic mice produced with TDP-43 genomic fragments. *Brain, 134*(Pt 9), 2610-2626. https://doi.org/10.1093/brain/awr159

Szelechowski, M., Amoedo, N., Obre, E., Leger, C., Allard, L., Bonneu, M., Claverol, S., Lacombe, D., Oliet, S., Chevallier, S., Le Masson, G., & Rossignol, R. (2018, Mar 2). Metabolic Reprogramming in Amyotrophic Lateral Sclerosis. *Sci Rep, 8*(1), 3953. https://doi.org/10.1038/s41598-018-22318-5

Takahashi, F., Takei, K., Tsuda, K., & Palumbo, J. (2017, Oct). Post-hoc analysis of MCI186-17, the extension study to MCI186-16, the confirmatory double-blind, parallel-group, placebo-controlled study of edaravone in amyotrophic lateral sclerosis. *Amyotroph Lateral Scler Frontotemporal Degener, 18*(sup1), 32-39. https://doi.org/10.1080/21678421.2017.1361442

Takahashi, K., & Yamanaka, S. (2006, Aug 25). Induction of pluripotent stem cells from mouse embryonic and adult fibroblast cultures by defined factors. *Cell, 126*(4), 663-676. https://doi.org/10.1016/j.cell.2006.07.024

Takahashi, M., Higuchi, M., Matsuki, H., Yoshita, M., Ohsawa, T., Oie, M., & Fujii, M. (2013, Feb). Stress granules inhibit apoptosis by reducing reactive oxygen species production. *Mol Cell Biol, 33*(4), 815-829. https://doi.org/10.1128/MCB.00763-12

Tam, O. H., Rozhkov, N. V., Shaw, R., Kim, D., Hubbard, I., Fennessey, S., Propp, N., Consortium, N. A., Fagegaltier, D., Harris, B. T., Ostrow, L. W., Phatnani, H., Ravits, J., Dubnau, J., & Gale Hammell, M. (2019, Oct 29). Postmortem Cortex Samples Identify Distinct Molecular Subtypes of ALS: Retrotransposon Activation, Oxidative Stress, and Activated Glia. *Cell Rep, 29*(5), 1164-1177 e1165. https://doi.org/10.1016/j.celrep.2019.09.066

Tan, J. M., Wong, E. S., Kirkpatrick, D. S., Pletnikova, O., Ko, H. S., Tay, S. P., Ho, M. W., Troncoso, J., Gygi, S. P., Lee, M. K., Dawson, V. L., Dawson, T. M., & Lim, K. L. (2008, Feb 1). Lysine 63-linked ubiquitination promotes the formation and autophagic clearance of protein inclusions associated with neurodegenerative diseases. *Hum Mol Genet, 17*(3), 431-439. https://doi.org/10.1093/hmg/ddm320

Tan, Q., Yalamanchili, H. K., Park, J., De Maio, A., Lu, H. C., Wan, Y. W., White, J. J., Bondar, V. V., Sayegh, L. S., Liu, X., Gao, Y., Sillitoe, R. V., Orr, H. T., Liu, Z., & Zoghbi, H. Y. (2016, Dec 1). Extensive cryptic splicing upon loss of RBM17 and TDP43 in neurodegeneration models. *Hum Mol Genet, 25*(23), 5083-5093. https://doi.org/10.1093/hmg/ddw337

Tsoi, P. S., Choi, K. J., Leonard, P. G., Sizovs, A., Moosa, M. M., MacKenzie, K. R., Ferreon, J. C., & Ferreon, A. C. M. (2017, Oct 2). The N-Terminal Domain of ALS-Linked TDP-43 Assembles without Misfolding. *Angew Chem Int Ed Engl, 56*(41), 12590-12593. https://doi.org/10.1002/anie.201706769

Turgut, N., Varol SaraCoglu, G., Kat, S., Balci, K., B, G. U., Birgili, O., & Kabayel, L. (2019, Feb). An epidemiologic investigation of amyotrophic lateral sclerosis in Thrace, Turkey, 2006-2010. *Amyotroph Lateral Scler Frontotemporal Degener, 20*(1-2), 100-106. https://doi.org/10.1080/21678421.2018.1525403

Turner, M. R., Bowser, R., Bruijn, L., Dupuis, L., Ludolph, A., McGrath, M., Manfredi, G., Maragakis, N., Miller, R. G., Pullman, S. L., Rutkove, S. B., Shaw, P. J., Shefner, J.,

& Fischbeck, K. H. (2013, May). Mechanisms, models and biomarkers in amyotrophic lateral sclerosis. *Amyotroph Lateral Scler Frontotemporal Degener, 14 Suppl 1*, 19-32. https://doi.org/10.3109/21678421.2013.778554

Turner, M. R., Hardiman, O., Benatar, M., Brooks, B. R., Chio, A., de Carvalho, M., Ince, P. G., Lin, C., Miller, R. G., Mitsumoto, H., Nicholson, G., Ravits, J., Shaw, P. J., Swash, M., Talbot, K., Traynor, B. J., Van den Berg, L. H., Veldink, J. H., Vucic, S., & Kiernan, M. C. (2013, Mar). Controversies and priorities in amyotrophic lateral sclerosis. *Lancet Neurol, 12*(3), 310-322. https://doi.org/10.1016/S1474-4422(13)70036-X

Turner, M. R., Parton, M. J., Shaw, C. E., Leigh, P. N., & Al-Chalabi, A. (2003, Jul). Prolonged survival in motor neuron disease: a descriptive study of the King's database 1990-2002. *J Neurol Neurosurg Psychiatry, 74*(7), 995-997. https://doi.org/10.1136/jnnp.74.7.995

Urushitani, M., Sato, T., Bamba, H., Hisa, Y., & Tooyama, I. (2010, Mar). Synergistic effect between proteasome and autophagosome in the clearance of polyubiquitinated TDP-43. *J Neurosci Res, 88*(4), 784-797. https://doi.org/10.1002/jnr.22243

Valbuena, G. N., Rizzardini, M., Cimini, S., Siskos, A. P., Bendotti, C., Cantoni, L., & Keun, H. C. (2016, May). Metabolomic Analysis Reveals Increased Aerobic Glycolysis and Amino Acid Deficit in a Cellular Model of Amyotrophic Lateral Sclerosis. *Mol Neurobiol, 53*(4), 2222-2240. https://doi.org/10.1007/s12035-015-9165-7

Van Deerlin, V. M., Leverenz, J. B., Bekris, L. M., Bird, T. D., Yuan, W., Elman, L. B., Clay, D., Wood, E. M., Chen-Plotkin, A. S., Martinez-Lage, M., Steinbart, E., McCluskey, L., Grossman, M., Neumann, M., Wu, I. L., Yang, W. S., Kalb, R., Galasko, D. R., Montine, T. J., Trojanowski, J. Q., Lee, V. M., Schellenberg, G. D., & Yu, C. E. (2008, May). TARDBP mutations in amyotrophic lateral sclerosis with TDP-43 neuropathology: a genetic and histopathological analysis. *Lancet Neurol, 7*(5), 409-416. https://doi.org/10.1016/S1474-4422(08)70071-1

Vance, C., Rogelj, B., Hortobagyi, T., De Vos, K. J., Nishimura, A. L., Sreedharan, J., Hu, X., Smith, B., Ruddy, D., Wright, P., Ganesalingam, J., Williams, K. L., Tripathi, V., Al-Saraj, S., Al-Chalabi, A., Leigh, P. N., Blair, I. P., Nicholson, G., de Belleroche, J., Gallo, J. M., Miller, C. C., & Shaw, C. E. (2009, Feb 27). Mutations in FUS, an RNA processing protein, cause familial amyotrophic lateral sclerosis type 6. *Science, 323*(5918), 1208-1211. https://doi.org/10.1126/science.1165942

Verber, N. S., Shepheard, S. R., Sassani, M., McDonough, H. E., Moore, S. A., Alix, J. J. P., Wilkinson, I. D., Jenkins, T. M., & Shaw, P. J. (2019). Biomarkers in Motor Neuron Disease: A State of the Art Review. *Front Neurol, 10*, 291. https://doi.org/10.3389/fneur.2019.00291

Verstreken, P., Ly, C. V., Venken, K. J., Koh, T. W., Zhou, Y., & Bellen, H. J. (2005, Aug 4). Synaptic mitochondria are critical for mobilization of reserve pool vesicles at Drosophila neuromuscular junctions. *Neuron, 47*(3), 365-378. https://doi.org/10.1016/j.neuron.2005.06.018

Vianello, A., Arcaro, G., Palmieri, A., Ermani, M., Braccioni, F., Gallan, F., Soraru, G., & Pegoraro, E. (2011, Jun). Survival and quality of life after tracheostomy for acute respiratory failure in patients with amyotrophic lateral sclerosis. *J Crit Care, 26*(3), 329 e327-314. https://doi.org/10.1016/j.jcrc.2010.06.003

Wada, T., Goparaju, S. K., Tooi, N., Inoue, H., Takahashi, R., Nakatsuji, N., & Aiba, K. (2012, May). Amyotrophic lateral sclerosis model derived from human embryonic stem cells overexpressing mutant superoxide dismutase 1. *Stem Cells Transl Med, 1*(5), 396-402. https://doi.org/10.5966/sctm.2011-0061

Wainger, B. J., Macklin, E. A., Vucic, S., McIlduff, C. E., Paganoni, S., Maragakis, N. J., Bedlack, R., Goyal, N. A., Rutkove, S. B., Lange, D. J., Rivner, M. H., Goutman, S. A., Ladha, S. S., Mauricio, E. A., Baloh, R. H., Simmons, Z., Pothier, L., Kassis, S. B., La, T., Hall, M., Evora, A., Klements, D., Hurtado, A., Pereira, J. D., Koh, J., Celnik, P. A., Chaudhry, V., Gable, K., Juel, V. C., Phielipp, N., Marei, A., Rosenquist, P., Meehan, S., Oskarsson, B., Lewis, R. A., Kaur, D., Kiskinis, E., Woolf, C. J., Eggan, K., Weiss, M. D., Berry, J. D., David, W. S., Davila-Perez, P., Camprodon, J. A., Pascual-Leone, A., Kiernan, M. C., Shefner, J. M., Atassi, N., & Cudkowicz, M. E. (2021, Feb 1). Effect of Ezogabine on Cortical and Spinal Motor Neuron Excitability in Amyotrophic Lateral Sclerosis: A Randomized Clinical Trial. *JAMA Neurol, 78*(2), 186-196. https://doi.org/10.1001/jamaneurol.2020.4300

Walker, A. K., Spiller, K. J., Ge, G., Zheng, A., Xu, Y., Zhou, M., Tripathy, K., Kwong, L. K., Trojanowski, J. Q., & Lee, V. M. (2015, Nov). Functional recovery in new mouse models of ALS/FTLD after clearance of pathological cytoplasmic TDP-43. *Acta Neuropathol, 130*(5), 643-660. https://doi.org/10.1007/s00401-015-1460-x

Wang, A., Conicella, A. E., Schmidt, H. B., Martin, E. W., Rhoads, S. N., Reeb, A. N., Nourse, A., Ramirez Montero, D., Ryan, V. H., Rohatgi, R., Shewmaker, F., Naik, M. T., Mittag, T., Ayala, Y. M., & Fawzi, N. L. (2018, Mar 1). A single N-terminal phosphomimic disrupts TDP-43 polymerization, phase separation, and RNA splicing. *EMBO J, 37*(5). https://doi.org/10.15252/embj.201797452

Wang, J., Xu, G., Slunt, H. H., Gonzales, V., Coonfield, M., Fromholt, D., Copeland, N. G., Jenkins, N. A., & Borchelt, D. R. (2005, Dec). Coincident thresholds of mutant protein for paralytic disease and protein aggregation caused by restrictively expressed superoxide dismutase cDNA. *Neurobiol Dis, 20*(3), 943-952. https://doi.org/10.1016/j.nbd.2005.06.005

Wang, T., Martin, S., Nguyen, T. H., Harper, C. B., Gormal, R. S., Martinez-Marmol, R., Karunanithi, S., Coulson, E. J., Glass, N. R., Cooper-White, J. J., van Swinderen, B., & Meunier, F. A. (2016, Sep 30). Flux of signalling endosomes undergoing axonal retrograde transport is encoded by presynaptic activity and TrkB. *Nat Commun, 7*, 12976. https://doi.org/10.1038/ncomms12976

Wang, W., Li, L., Lin, W. L., Dickson, D. W., Petrucelli, L., Zhang, T., & Wang, X. (2013, Dec 1). The ALS disease-associated mutant TDP-43 impairs mitochondrial dynamics and function in motor neurons. *Hum Mol Genet, 22*(23), 4706-4719. https://doi.org/10.1093/hmg/ddt319

Wang, W., Wang, L., Lu, J., Siedlak, S. L., Fujioka, H., Liang, J., Jiang, S., Ma, X., Jiang, Z., da Rocha, E. L., Sheng, M., Choi, H., Lerou, P. H., Li, H., & Wang, X. (2016, Aug). The inhibition of TDP-43 mitochondrial localization blocks its neuronal toxicity. *Nat Med, 22*(8), 869-878. https://doi.org/10.1038/nm.4130

Watkins, J. A., Alix, J. J. P., Shaw, P. J., & Mead, R. J. (2021, Aug 17). Extensive phenotypic characterisation of a human TDP-43(Q331K) transgenic mouse model of amyotrophic lateral sclerosis (ALS). *Sci Rep, 11*(1), 16659. https://doi.org/10.1038/s41598-021-96122-z

Wegorzewska, I., Bell, S., Cairns, N. J., Miller, T. M., & Baloh, R. H. (2009, Nov 3). TDP-43 mutant transgenic mice develop features of ALS and frontotemporal lobar degeneration. *Proc Natl Acad Sci U S A, 106*(44), 18809-18814. https://doi.org/10.1073/pnas.0908767106

Westeneng, H. J., Debray, T. P. A., Visser, A. E., van Eijk, R. P. A., Rooney, J. P. K., Calvo, A., Martin, S., McDermott, C. J., Thompson, A. G., Pinto, S., Kobeleva, X., Rosenbohm, A., Stubendorff, B., Sommer, H., Middelkoop, B. M., Dekker, A. M., van Vugt, J., van Rheenen, W., Vajda, A., Heverin, M., Kazoka, M., Hollinger, H., Gromicho, M., Korner, S., Ringer, T. M., Rodiger, A., Gunkel, A., Shaw, C. E., Bredenoord, A. L., van Es, M. A., Corcia, P., Couratier, P., Weber, M., Grosskreutz, J., Ludolph, A. C., Petri, S., de Carvalho, M., Van Damme, P., Talbot, K., Turner, M. R., Shaw, P. J., Al-Chalabi, A., Chio, A., Hardiman, O., Moons, K. G. M., Veldink, J. H., & van den Berg, L. H. (2018, May). Prognosis for patients with amyotrophic lateral sclerosis: development and validation of a personalised prediction model. *Lancet Neurol, 17*(5), 423-433. https://doi.org/10.1016/S1474-4422(18)30089-9

White, M. A., Kim, E., Duffy, A., Adalbert, R., Phillips, B. U., Peters, O. M., Stephenson, J., Yang, S., Massenzio, F., Lin, Z., Andrews, S., Segonds-Pichon, A., Metterville, J., Saksida, L. M., Mead, R., Ribchester, R. R., Barhomi, Y., Serre, T., Coleman, M. P., Fallon, J. R., Bussey, T. J., Brown, R. H., Jr., & Sreedharan, J. (2018, Apr). TDP-43 gains function due to perturbed autoregulation in a Tardbp knock-in mouse model of ALS-FTD. *Nat Neurosci, 21*(4), 552-563. https://doi.org/10.1038/s41593-018-0113-5

Wichterle, H., Lieberam, I., Porter, J. A., & Jessell, T. M. (2002, Aug 9). Directed differentiation of embryonic stem cells into motor neurons. *Cell, 110*(3), 385-397. https://doi.org/10.1016/s0092-8674(02)00835-8

Wightman, G., Anderson, V. E., Martin, J., Swash, M., Anderton, B. H., Neary, D., Mann, D., Luthert, P., & Leigh, P. N. (1992, May 25). Hippocampal and neocortical ubiquitin-immunoreactive inclusions in amyotrophic lateral sclerosis with dementia. *Neurosci Lett, 139*(2), 269-274. https://doi.org/10.1016/0304-3940(92)90569-s

Williamson, M. G., Finelli, M. J., Sleigh, J. N., Reddington, A., Gordon, D., Talbot, K., Davies, K. E., & Oliver, P. L. (2019, Nov 1). Neuronal over-expression of Oxr1 is protective against ALS-associated mutant TDP-43 mislocalisation in motor neurons and neuromuscular defects in vivo. *Hum Mol Genet, 28*(21), 3584-3599. https://doi.org/10.1093/hmg/ddz190

Wils, H., Kleinberger, G., Janssens, J., Pereson, S., Joris, G., Cuijt, I., Smits, V., Ceuterick-de Groote, C., Van Broeckhoven, C., & Kumar-Singh, S. (2010, Feb 23). TDP-43 transgenic mice develop spastic paralysis and neuronal inclusions characteristic of ALS and frontotemporal lobar degeneration. *Proc Natl Acad Sci U S A, 107*(8), 3858-3863. https://doi.org/10.1073/pnas.0912417107

Winton, M. J., Igaz, L. M., Wong, M. M., Kwong, L. K., Trojanowski, J. Q., & Lee, V. M. (2008, May 9). Disturbance of nuclear and cytoplasmic TAR DNA-binding protein (TDP-43) induces disease-like redistribution, sequestration, and aggregate formation. *J Biol Chem, 283*(19), 13302-13309. https://doi.org/10.1074/jbc.M800342200

Witzel, S., Maier, A., Steinbach, R., Grosskreutz, J., Koch, J. C., Sarikidi, A., Petri, S., Gunther, R., Wolf, J., Hermann, A., Prudlo, J., Cordts, I., Lingor, P., Loscher, W. N., Kohl, Z., Hagenacker, T., Ruckes, C., Koch, B., Spittel, S., Gunther, K., Michels, S., Dorst, J., Meyer, T., Ludolph, A. C., & German Motor Neuron Disease, N. (2022, Feb 1). Safety and Effectiveness of Long-term Intravenous Administration of Edaravone for Treatment of Patients With Amyotrophic Lateral Sclerosis. *JAMA Neurol, 79*(2), 121-130. https://doi.org/10.1001/jamaneurol.2021.4893

Wouters, O. J., McKee, M., & Luyten, J. (2020, Mar 3). Estimated Research and Development Investment Needed to Bring a New Medicine to Market, 2009-2018. *JAMA, 323*(9), 844-853. https://doi.org/10.1001/jama.2020.1166

Writing, G., & Edaravone, A. L. S. S. G. (2017, Jul). Safety and efficacy of edaravone in well defined patients with amyotrophic lateral sclerosis: a randomised, double-blind, placebo-controlled trial. *Lancet Neurol, 16*(7), 505-512. https://doi.org/10.1016/S1474-4422(17)30115-1

Writing Group On Behalf Of The Edaravone Als 18 Study, G. (2017, Oct). Exploratory double-blind, parallel-group, placebo-controlled study of edaravone (MCI-186) in amyotrophic lateral sclerosis (Japan ALS severity classification: Grade 3, requiring assistance for eating, excretion or ambulation). *Amyotroph Lateral Scler Frontotemporal Degener, 18*(sup1), 40-48. https://doi.org/10.1080/21678421.2017.1361441

Wu, L. S., Cheng, W. C., Hou, S. C., Yan, Y. T., Jiang, S. T., & Shen, C. K. (2010, Jan). TDP-43, a neuro-pathosignature factor, is essential for early mouse embryogenesis. *Genesis, 48*(1), 56-62. https://doi.org/10.1002/dvg.20584

Wu, L. S., Cheng, W. C., & Shen, C. K. (2012, Aug 10). Targeted depletion of TDP-43 expression in the spinal cord motor neurons leads to the development of amyotrophic lateral sclerosis-like phenotypes in mice. *J Biol Chem, 287*(33), 27335-27344. https://doi.org/10.1074/jbc.M112.359000

Xiao, S., Sanelli, T., Chiang, H., Sun, Y., Chakrabartty, A., Keith, J., Rogaeva, E., Zinman, L., & Robertson, J. (2015, Jul). Low molecular weight species of TDP-43 generated by abnormal splicing form inclusions in amyotrophic lateral sclerosis and result in motor neuron death. *Acta Neuropathol, 130*(1), 49-61. https://doi.org/10.1007/s00401-015-1412-5

Xu, Y. F., Gendron, T. F., Zhang, Y. J., Lin, W. L., D'Alton, S., Sheng, H., Casey, M. C., Tong, J., Knight, J., Yu, X., Rademakers, R., Boylan, K., Hutton, M., McGowan, E., Dickson, D. W., Lewis, J., & Petrucelli, L. (2010, Aug 11). Wild-type human TDP-43 expression causes TDP-43 phosphorylation, mitochondrial aggregation, motor deficits, and early mortality in transgenic mice. *J Neurosci, 30*(32), 10851-10859. https://doi.org/10.1523/JNEUROSCI.1630-10.2010

Xu, Y. F., Zhang, Y. J., Lin, W. L., Cao, X., Stetler, C., Dickson, D. W., Lewis, J., & Petrucelli, L. (2011, Oct 26). Expression of mutant TDP-43 induces neuronal dysfunction in transgenic mice. *Mol Neurodegener, 6*, 73. https://doi.org/10.1186/1750-1326-6-73

Yamashita, T., Hideyama, T., Hachiga, K., Teramoto, S., Takano, J., Iwata, N., Saido, T. C., & Kwak, S. (2012). A role for calpain-dependent cleavage of TDP-43 in amyotrophic lateral sclerosis pathology. *Nat Commun, 3*, 1307. https://doi.org/10.1038/ncomms2303

Yang, C., Qiao, T., Yu, J., Wang, H., Guo, Y., Salameh, J., Metterville, J., Parsi, S., Yusuf, I., Brown, R. H., Cai, H., & Xu, Z. (2022). Low-level overexpression of wild type TDP-43 causes late-onset, progressive neurodegeneration and paralysis in mice. *PLoS One, 17*(2), e0255710. https://doi.org/10.1371/journal.pone.0255710

Yang, Y. M., Gupta, S. K., Kim, K. J., Powers, B. E., Cerqueira, A., Wainger, B. J., Ngo, H. D., Rosowski, K. A., Schein, P. A., Ackeifi, C. A., Arvanites, A. C., Davidow, L. S., Woolf, C. J., & Rubin, L. L. (2013, Jun 6). A small molecule screen in stem-cell-derived motor neurons identifies a kinase inhibitor as a candidate therapeutic for ALS. *Cell Stem Cell, 12*(6), 713-726. https://doi.org/10.1016/j.stem.2013.04.003

Yoshino, H., & Kimura, A. (2006, Dec). Investigation of the therapeutic effects of edaravone, a free radical scavenger, on amyotrophic lateral sclerosis (Phase II study). *Amyotroph Lateral Scler, 7*(4), 241-245. https://doi.org/10.1080/17482960600881870

Zala, D., Hinckelmann, M. V., Yu, H., Lyra da Cunha, M. M., Liot, G., Cordelieres, F. P., Marco, S., & Saudou, F. (2013, Jan 31). Vesicular glycolysis provides on-board energy for fast axonal transport. *Cell, 152*(3), 479-491. https://doi.org/10.1016/j.cell.2012.12.029

Zambrowicz, B. P., Imamoto, A., Fiering, S., Herzenberg, L. A., Kerr, W. G., & Soriano, P. (1997, Apr 15). Disruption of overlapping transcripts in the ROSA beta geo 26 gene trap strain leads to widespread expression of beta-galactosidase in mouse embryos and hematopoietic cells. *Proc Natl Acad Sci U S A, 94*(8), 3789-3794. https://doi.org/10.1073/pnas.94.8.3789

Zhang, S., Cooper-Knock, J., Weimer, A. K., Shi, M., Moll, T., Marshall, J. N. G., Harvey, C., Nezhad, H. G., Franklin, J., Souza, C. D. S., Ning, K., Wang, C., Li, J., Dilliott, A. A., Farhan, S., Elhaik, E., Pasniceanu, I., Livesey, M. R., Eitan, C., Hornstein, E., Kenna, K. P., Project Min, E. A. L. S. S. C., Veldink, J. H., Ferraiuolo, L., Shaw, P. J., & Snyder, M. P. (2022, Jan 11). Genome-wide identification of the genetic basis of amyotrophic lateral sclerosis. *Neuron*. https://doi.org/10.1016/j.neuron.2021.12.019

Zhang, Y. J., Caulfield, T., Xu, Y. F., Gendron, T. F., Hubbard, J., Stetler, C., Sasaguri, H., Whitelaw, E. C., Cai, S., Lee, W. C., & Petrucelli, L. (2013, Aug 1). The dual functions of the extreme N-terminus of TDP-43 in regulating its biological activity and inclusion formation. *Hum Mol Genet, 22*(15), 3112-3122. https://doi.org/10.1093/hmg/ddt166

Zhang, Y. J., Xu, Y. F., Cook, C., Gendron, T. F., Roettges, P., Link, C. D., Lin, W. L., Tong, J., Castanedes-Casey, M., Ash, P., Gass, J., Rangachari, V., Buratti, E., Baralle, F., Golde, T. E., Dickson, D. W., & Petrucelli, L. (2009, May 5). Aberrant cleavage of TDP-43 enhances aggregation and cellular toxicity. *Proc Natl Acad Sci U S A, 106*(18), 7607-7612. https://doi.org/10.1073/pnas.0900688106

Zhang, Y. J., Xu, Y. F., Dickey, C. A., Buratti, E., Baralle, F., Bailey, R., Pickering-Brown, S., Dickson, D., & Petrucelli, L. (2007, Sep 26). Progranulin mediates caspase-dependent cleavage of TAR DNA binding protein-43. *J Neurosci, 27*(39), 10530-10534. https://doi.org/10.1523/JNEUROSCI.3421-07.2007

Zhao, M., Kim, J. R., van Bruggen, R., & Park, J. (2018, Sep 30). RNA-Binding Proteins in Amyotrophic Lateral Sclerosis. *Mol Cells, 41*(9), 818-829. https://doi.org/10.14348/molcells.2018.0243

Zhou, S., Zhou, Y., Qian, S., Chang, W., Wang, L., & Fan, D. (2018, Nov). Amyotrophic lateral sclerosis in Beijing: Epidemiologic features and prognosis from 2010 to 2015. *Brain Behav, 8*(11), e01131. https://doi.org/10.1002/brb3.1131

Zuo, X., Zhou, J., Li, Y., Wu, K., Chen, Z., Luo, Z., Zhang, X., Liang, Y., Esteban, M. A., Zhou, Y., & Fu, X. D. (2021, Feb). TDP-43 aggregation induced by oxidative stress causes global mitochondrial imbalance in ALS. *Nat Struct Mol Biol, 28*(2), 132-142. https://doi.org/10.1038/s41594-020-00537-7